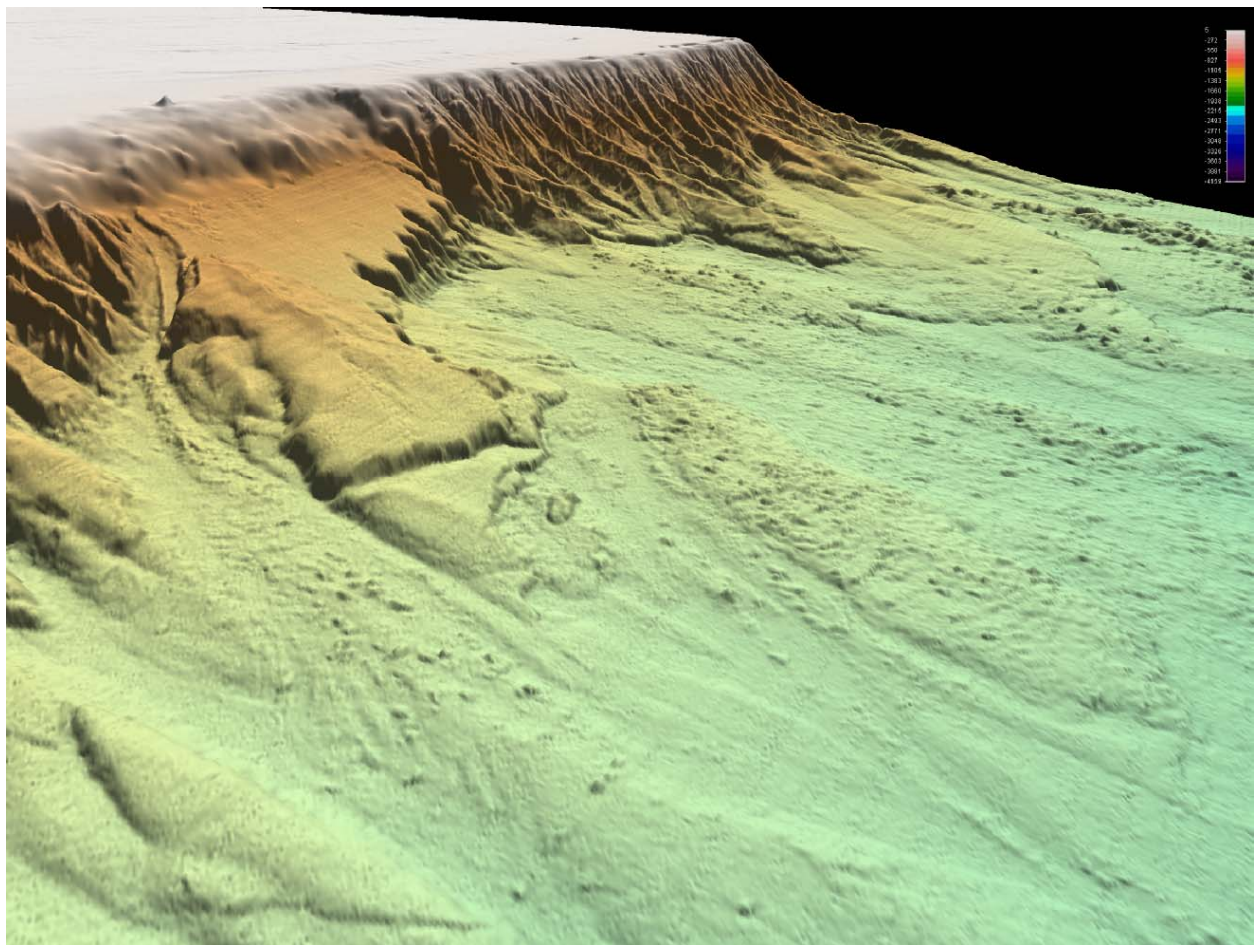


The Current State of Knowledge Regarding Potential Tsunami Sources Affecting U.S. Atlantic and Gulf Coasts

A Report to the Nuclear Regulatory Commission

By Atlantic and Gulf of Mexico Tsunami Hazard Assessment Group



The Current State of Knowledge Regarding Potential Tsunami Sources Affecting U.S. Atlantic and Gulf Coasts

A Report to the Nuclear Regulatory Commission

By Atlantic and Gulf of Mexico Tsunami Hazard Assessment Group:

Uri ten Brink¹, David Twichell¹, Eric Geist², Jason Chaytor^{1,3}, Jacques Locat⁴, Homa Lee², Brian Buczkowski¹, and Mylène Sansoucy⁴

¹ U.S. Geological Survey, Woods Hole Science Center, Woods Hole, Massachusetts, USA

² U.S. Geological Survey, Menlo Park, California, USA

³ Woods Hole Oceanographic Institution, Woods Hole, Massachusetts, USA

⁴ Department of Geology and Geological Engineering, Université Laval, Sainte-Foy, Québec, Canada

April 30, 2007

Revised September 30, 2007

NOTICE from USGS

This publication was prepared by an agency of the United States Government. Neither the United States Government nor any agency thereof, nor any of their employees, make any warranty, expressed or implied, or assumes any legal liability or responsibility for the accuracy, completeness, or usefulness of any information, apparatus, product, or process disclosed in this report, or represent that its use would not infringe privately owned rights. Reference therein to any specific commercial product, process, or service by trade name, trademark, manufacturer, or otherwise does not necessarily constitute or imply its endorsement, recommendation, or favoring by the United States Government or any agency thereof. Any views and opinions of authors expressed herein do not necessarily state or reflect those of the United States Government or any agency thereof. Although all data published on this report have been used by the USGS, no warranty, expressed or implied, is made by the USGS as to the accuracy of the data and related materials and (or) the functioning of the software. The act of distribution shall not constitute any such warranty, and no responsibility is assumed by the USGS in the use of these data, software, or related materials.

This report should be cited as:

Atlantic and Gulf of Mexico Tsunami Hazard Assessment Group, 2007, The Current State of Knowledge Regarding Potential Tsunami Sources Affecting U.S. Atlantic and Gulf Coasts - A Report to the Nuclear Regulatory Commission: U.S. Geological Survey Administrative Report.

Acknowledgements:

We thank Carolyn Ruppel (USGS) for a thorough and expedient review of this report.

Cover: Perspective view of the Currituck submarine landslide, offshore Virginia on the mid-Atlantic continental slope.

Executive Summary

The 2004 Sumatra tsunami, which took place in an area with no historical record of a similar event, has brought awareness to the possibility of tsunamis along the U.S. Atlantic and Gulf of Mexico coasts. While these rare events may not have an impact on typical tsunami probabilities used, for example, to determine flood insurance rates, they need to be considered in long-range planning, such as for the placement and hazard assessment of nuclear power plants. The U.S. Geological Survey was tasked by the Nuclear Regulatory Commission to prepare an evaluation of tsunami sources and their probability to impact the U.S. Atlantic and Gulf of Mexico coasts. This report is the first phase in this evaluation. It provides a general review of potential tsunami sources, and provides a geotechnical analysis and hydrodynamic model for one landslide offshore Virginia. The evaluation also identifies geographical areas with incomplete information and topics for further study.

The main findings of the first phase of the study include:

1. Landslides along the U.S. Atlantic margin have the potential to cause tsunamis locally. These landslides are concentrated along the New England and Long Island sections of the margin, outward of major ancient rivers in the mid-Atlantic margin and in the salt dome province offshore North Carolina. It is likely, but not established, that most landslide activity took place more than 7,000 years ago. The largest of these landslides could cause a devastating tsunami, but the presence of a wide continental shelf is expected to reduce their tsunami impact.
2. Earthquake sources that can generate trans-oceanic tsunamis, are located west of Gibraltar and in the Puerto Rico trench. The cause of large earthquakes west of Gibraltar is presently being debated, and the impact of a tsunami associated with these earthquakes has not yet been specifically established for U.S. coasts. No large historical earthquakes are known from the Puerto Rico trench; it is currently unclear whether this plate boundary is capable of storing large elastic stresses.
3. Far-field landslides, such as in the Canary Islands, are not expected to cause a devastating tsunami along the U.S. Atlantic coast.
4. Large landslides in the Gulf of Mexico are found in the submarine canyon and fan provinces extending from present (Mississippi) and former larger rivers that emptied into the Gulf. These large landslides were probably active before 7,000 years ago. In other areas, landslides

continue to be active, probably because of salt movement, but are small and may not pose a tsunami hazard. A more detailed evaluation and sampling are needed to validate these conclusions. Very little is known about the threat of landslide-generated tsunamis from the Mexican coast. Tsunamis generated by earthquakes do not appear to impact the Gulf of Mexico coast.

Contents

Chapter 1: Introduction and Background	1
Chapter 2: Distribution of Submarine Landslides along the U.S. Atlantic Continental Margin	3
Introduction	3
Setting and Previous Studies	3
Methods	5
<i>Bathymetry</i>	5
<i>GLORIA Sidescan</i>	6
<i>Seismic Reflection Profiles</i>	6
<i>Cores</i>	6
Data Analysis.....	7
Types of Submarine Mass Movements	8
Results	9
Discussion	11
Future Directions.....	13
Tables.....	13
Figures.....	15
References	25
Chapter 3: Distribution of Submarine Landslides in the Gulf of Mexico	31
Introduction	31
Setting	31
Types of Submarine Mass Movements	33
Distribution of Submarine Landslides	34
<i>Carbonate Province</i>	34
<i>Salt Province</i>	35
<i>Canyon/Fan Province</i>	36
Summary	38
Future Directions.....	38
Figures.....	39
References	43
Chapter 4: Far-field submarine landslide sources	49
Canary Islands	49
Other landslide sources along the continental margin.....	50
The mid-Atlantic ridge.....	51
Figures.....	51
References:	52
Chapter 5: Review of tsunamigenic earthquake sources that may affect the U.S. Atlantic Coast	55
Introduction	55
The Area West of Gibraltar.....	55
<i>Tectonic setting</i>	55
The debate about the source parameters of the 1755 Lisbon earthquake	56
The 1761 Earthquake and Tsunami.....	58
Summary	58
The Northeast Caribbean.....	58
<i>Tectonic Setting</i>	58

<i>The Puerto Rico Trench</i>	59
<i>The Hispaniola Trench</i>	60
Table	61
Figures.....	62
References	68
Chapter 6: Tsunamigenic earthquake sources that may affect the Gulf of Mexico	71
Introduction	71
North Panama Deformation Belt 9-12°N, 83°W-77°W.....	71
<i>Summary</i>	71
<i>Previous Tsunamis</i>	71
<i>Other Earthquakes</i>	72
<i>Relative Motion from GPS</i>	73
Northern South America Convergent Zone, 11.5°-14°N, 77°W-64°W	73
<i>Summary</i>	73
<i>Surface Deformation Offshore</i>	74
<i>Previous Tsunamis</i>	74
<i>Earthquakes</i>	74
<i>Relative Block Motion from GPS</i>	75
<i>Stress indicators</i>	75
<i>The deep structure of the convergent zone</i>	75
Figures.....	76
References	78
Chapter 7: Regional Tsunami Propagation Patterns from Caribbean Earthquakes ..	81
Method.....	81
Results	83
Table	85
Figures.....	86
References	97
Chapter 8: Geomorphology, Stability and Mobility of the Currituck Slide	99
Introduction	99
Objective	99
Approach.....	99
Geomorphological analysis	102
<i>Analysis of actual morphology</i>	102
<i>The morpo-stratigraphic model</i>	102
Stability analysis	103
Mobility analysis.....	105
<i>Geometry</i>	106
<i>Rheological parameters</i>	106
<i>Mobility and flow volume</i>	107
<i>Flow dynamics</i>	107
Discussion	108
<i>Strength parameters and pore pressures</i>	108
<i>Yield strength</i>	109
Conclusion.....	109
<i>Greek symbols</i>	110
Figures.....	111
References	127
Chapter 9: Hydrodynamic Modeling of Tsunamis from the Currituck Landslide ...	129
Introduction	129
Method	130
Initial Results	131
Effect of Variations in Failure Duration and Bottom Friction	133
Summary.....	134

Figures.....	135
References	146
Chapter 10: Summary of the Current State of Knowledge Regarding Potential Tsunami Sources Affecting U.S. Atlantic and Gulf Coasts	149
Chapter 2.....	149
Chapter 3.....	150
Chapter 4.....	151
Chapter 5.....	151
Chapter 6.....	152
Chapter 7.....	152
Chapter 8.....	152
Chapter 9.....	153
Chapter 11: Future Directions to Increase the State of Knowledge	155
Probability analysis.....	155
Understanding specific hazards	155
Data gaps.....	156

Chapter 1: Introduction and Background

The devastation caused by the 2004 Indian Ocean tsunami has brought about a heightened awareness of the dangers posed by tsunamis. Long known as a hazard in the Pacific Ocean, the 2004 event highlighted the fact the tsunamis can occur in other oceans that are less prepared for this rare phenomenon. The $M \sim 9.2$ 2004 Sumatra-Andaman earthquake was unusual from a geologic/tectonic perspective as well. This massive earthquake occurred along a highly oblique subduction zone, where the convergence rate is low ($\sim 7\text{-}14$ mm/yr). In the decades leading up to this event, highly oblique subduction zones were thought to be unlikely places for a $M \sim 9$ earthquake to occur. The 2004 Sumatra-Andaman earthquake has therefore brought about the need to reassess tsunamigenic potential for similar tectonic regimes, particularly in the Caribbean Sea, Atlantic Ocean, and the Gulf of Mexico.

As with the source area for the 2004 earthquake, where the recurrence interval for earthquakes of similar magnitude is greater than 1,000 years, many of the tsunamigenic fault zones in the Caribbean and Atlantic are characterized by low convergence rates. While these events have less impact on tsunami probability calculations for some applications (*e.g.*, FEMA flood insurance rate maps), it is critical to define the tsunami hazard at longer return times for nuclear power facilities. The Atlantic and Gulf of Mexico coasts are highly vulnerable to tsunamis when they do occur because major population centers and industrial facilities are located near the shoreline at low-lying elevations, and often in estuaries. This is in comparison to the Pacific coast where tsunamis are more frequent but the coastline is more sparsely populated and most sections have much more topographic relief.

Following the Sumatra 2004 earthquake, a major concern was raised about a similar plate tectonic geometry existing in the Puerto Rico trench with a potential impact on the U.S. East Coast. The Puerto Rico trench is a curved subduction zone where, similar to the Sumatra trench, relative plate motion is strike slip with only a small component of subduction. Tsunami hazard due to thrust earthquakes was underestimated in the Sumatra trench because of the large component of strike slip. The USGS has recently carried out extensive fieldwork in the Puerto Rico trench and is therefore in a position to provide an evaluation for this source.

Submarine landslides have also historically generated destructive tsunamis, although the extent of damaging waves generated by landslides is generally smaller. Along coastlines proximal to catastrophic submarine landslides, tsunami run-up can be significant as exemplified by the 1929

Grand Banks tsunami (Newfoundland and Nova Scotia), which likely had a significant landslide-generated component. Less is generally known about submarine landslides as tsunami triggers in comparison to their earthquake counterparts.

This report represents the combined effort of a diverse group of marine geologists, geophysicists, geotechnical engineers, and hydrodynamic modelers to evaluate tsunami sources that have the potential to impact the U.S. Atlantic and Gulf coasts. The report was commissioned by the Nuclear Regulatory Commission and was prepared between September 2006 and April 2007. The report covers the following subjects: Analysis of recently released detailed bathymetry along the Atlantic continental margin (Chapter 2), review of previous work pertaining to landslides and earthquake sources (Chapter 3-6), preliminary tsunami propagation models from Caribbean earthquake sources, which may impact U.S. coasts (Chapter 7), geotechnical analysis of the Currituck landslide offshore Virginia, and tsunami propagation models for this slide (Chapter 8-9), summary (Chapter 10), and future directions necessary to fill knowledge gaps, which were identified as a result of the preparation of this report (Chapter 11).

This report will be further updated as part of the Phase 2 research initiated in 2007.

Chapter 2: Distribution of Submarine Landslides along the U.S. Atlantic Continental Margin

Introduction

Since the 1929 earthquake near the Grand Banks offshore of Nova Scotia, Canada (Heezen and Ewing, 1952), it has been realized that submarine landslides contribute to shaping passive continental margins. However, a full appreciation of the importance of this process was delayed several decades until bathymetric, subbottom profiling, and seafloor imaging techniques were sufficiently advanced to allow systematic mapping of large portions of continental margins. We have used available multibeam bathymetry, GLORIA sidescan sonar imagery, a regional grid of high-resolution seismic profiles, and published accounts of sediment cores from the region to map the distribution and style of surficial submarine landslides along the eastern U.S. margin between the eastern end of Georges Bank and the northern end of the Blake Spur (Figure 2-1). The near-complete coverage of the U.S. Atlantic continental slope and rise by multibeam bathymetry provides a uniform data set and a more detailed and consistent view of the geomorphology of submarine landslides than had been available in the past. Here we review the distribution and style of submarine landslides on the U.S. Atlantic continental margin, and speculate on the geologic conditions that have influenced their distribution.

Setting and Previous Studies

The U.S. Atlantic continental margin rifted asynchronously from south to north during the Mesozoic (Klitgord *et al.*, 1988). Salt deposition probably was extensive during early stages of margin formation, but only in the Carolina Trough offshore of North and South Carolina did salt domes subsequently form probably due to sediment loading (Dillon *et al.*, 1982; Figure 2-1). During the early Middle Jurassic a nearly continuous carbonate platform and barrier reef system formed that stretched northward from the Bahamas to the Canadian margin (Poag, 1991). This carbonate system met its demise in the Early Cretaceous when it was buried by siliciclastic sediments shed from the continent. Deposition during the Cenozoic was

primarily siliciclastic sediments (Poag and Sevon, 1989) except during the Eocene when calcareous chalk was deposited along much of the margin (Weed *et al.*, 1974; Ryan *et al.*, 1978). Mesozoic and especially Cenozoic strata have been recovered from the floors and walls of submarine canyons along the entire Atlantic margin at depths ranging from 283-2200 m (Weed *et al.*, 1974; Ryan *et al.*, 1978; Robb, 1984). Exposures of these strata are a somewhat shallower depths off Georges Bank (283-1700 m) than south of Cape Hatteras (1,000-2,200 m). South of the study area, along the Blake Escarpment and Blake Spur, Middle Cretaceous and older limestone is exposed on this cliff face (Dillon *et al.*, 1983).

The Quaternary saw large volumes of sediment eroded from the North American continent by glacial processes being distributed unevenly along this margin (Poag and Sevon, 1989). Continental glaciers extended southward and eastward to terminal moraines that formed (but are now submerged) along the northern edge of Georges Bank and the islands that now form the southern New England and New York coasts (Oldale, 1992). Beyond the moraines, outwash plains extended south and eastward to the shelf edge. Large river systems reached the shelf edge at either end of Georges Bank (Schlee and Fritsch, 1982) and along the southern New England shelf (McMaster and Ashraf, 1973). In these areas, Quaternary sediment is 400-800 m thick under the outer shelf and upper slope (Figure 2-1). To the south, beyond the extent of glaciers, the large river systems that underlie the present Hudson, Delaware, and Chesapeake estuaries (Knebel *et al.*, 1979, Twichell *et al.*, 1977, Colman *et al.*, 1990; Uchupi *et al.*, 2001) extended across the shelf and in some cases built shelf edge deltas (Figure 2-1) and in other cases transferred sediment to deep-sea fans on the upper rise (Poag and Sevon, 1989). The thickest Quaternary deposits along the shelf edge are offshore the Virginia and Delaware coasts where the paleo- Delaware, Susquehanna, and James Rivers supplied sediment to the shelf edge (Poag and Sevon, 1989). Sediment supplied from the Hudson River system left only a thin sediment cover on the shelf and slope, and the bulk of the Quaternary sediment from this system was deposited in a deep-sea fan on the middle and lower rise. Although the Quaternary is brief, sediment accumulation rates were higher than any other time since the opening of the Atlantic Ocean (Poag and Sevon, 1989).

Regional seismic profiles show variations in aggradation of the shelf and progradation of the slope along this margin during the late Cenozoic and Quaternary. A regional seismic survey showed a mix of truncated bedding and beds that dip parallel to the gradient of the continental slope (Uchupi and Emery, 1967; Uchupi, 1970; Klitgord *et al.*, 1994). Many of the profiles across the Georges Bank and southern New England slope show reflecting horizons with dips parallel to the seafloor under the slope. The continental slope between New York and Chesapeake Bay shows reflecting horizons that are either truncated by the seafloor or a shallow unconformity that is buried by a thin veneer of more recent sediment. Offshore of Chesapeake Bay and Abermarle Sound reflecting horizons generally parallel the seafloor under the slope, and off Cape Hatteras, again they are truncated by the slope (Rona, 1969; McGregor, 1981; Uchupi and Emery, 1967). McGregor (1981) and

O'Leary (1993) have suggested that the dip strata under the continental slope may be an important factor in sea-floor stability.

Crustal faults are found throughout the syn- and post-rift sedimentary sections, as well as cutting up part way into the post-rift sedimentary units. Although most of these crustal faults are the result of rifting, and hence are restricted to the pre-Middle Jurassic time, faults that cut far into the post-rift sedimentary section are present along the shelf edge of the southern Georges Bank Basin and the Baltimore Canyon Trough (Klitgord *et al.*, 1988; Klitgord *et al.*, 1994). These faults do not appear to reach the surface, except where exposed by subsequent erosion, suggesting that they have been inactive since before the Quaternary (Klitgord *et al.*, 1994). Even so, these faults represent zones of pre-existing weakness within the geologic framework of the margin, and as such, may represent future failure planes or regions of enhanced fluid flow.

This overview of the geologic framework of the Atlantic margin provides a backdrop for the review of recent submarine landslides. While studies of individual landslides along the U.S. Atlantic margin first appeared in 1967 (Uchupi, 1967) and flourished through the 1980s (Bunn and McGregor, 1980; Cashman and Popenoe, 1985; Knebel and Carson, 1979; MacIlvaine and Ross, 1979; Malahoff *et al.*, 1980; McGregor and Bennett, 1977; McGregor and Bennett, 1979; O'Leary, 1986; Prior *et al.*, 1984; 1986), the first regional synthesis of their distribution was compiled using echo-sounder profiles and cores by Embley (1980). Subsequent regional compilations were completed by Embley and Jacobi (1986), Booth *et al.* (1988), Pratson and Laine (1989), Hance (2003), and Huhnerbach *et al.* (2004). These summaries all document the importance of submarine landslides in shaping this continental margin during the Quaternary; however one shortcoming was that these studies were based on widely-spaced echo-sounder profiles or a mix of data types. The first comprehensive survey of the U.S. Atlantic continental slope and rise was completed in 1987 using the GLORIA long-range sidescan sonar system (EEZ-SCAN87, 1991). Several reports described individual regions (O'Leary, 1993; 1996; Cashman and Popenoe, 1985; Popenoe *et al.*, 1993; Popenoe and Dillon, 1996; Schlee and Robb, 1991). Booth *et al.* (1993) provided a summary of the distribution and attributes of landslides based on this regional data set and the first tabulated information on the dimensions of these features, characteristics of the source areas, and style of failure.

Methods

Bathymetry

Data used in the compilation of the East Coast bathymetry map were acquired from several sources and vary in age, sounding density, and positional accuracy. The primary data set was acquired by the University of New Hampshire (UNH) in support of the U.S. Law of the Sea Study (Gardner *et al.*, 2006; Cartwright and Gardner, 2005) and provides near

continuous coverage of the U.S. Atlantic margin from the base of the continental slope down to the abyssal plain (~ 1,500-m and 5,000-m). These data, as supplied, included gridded bathymetric soundings and mosaiced acoustic backscatter values, both at a resolution of 100-m. To provide the best available coverage of the sections of the continental slope and rise not covered by the UNH data set several additional multibeam datasets were used. These data were collected by Woods Hole Oceanographic Institution ships R/V Knorr (14 cruises) and R/V Atlantis (13 cruises), Lamont-Doherty Earth Observatory ships R/V Ewing (11 cruises) and R/V Robert Conrad (1 cruise), and from the NOAA EEZ mapping surveys (13 cruises). The completed bathymetry is shown in Figure 2-2, areas where multibeam soundings were not available are shown in Figure 2-3, and include large sections of the continental slope offshore of Georges Bank and southern New England, smaller sections of the slope offshore of the Middle Atlantic states, and a large section of the slope and rise offshore northern Florida and southern Georgia. In these areas, sounding data from the National Ocean Service hydrographic database and the NOAA coastal relief model provided bathymetric coverage of the continental slope. The final map covers the ocean floor from the shoreline to depths greater than 5,000 m, between 43.5 and 24 degrees north latitude, were created at a horizontal pixel resolution of between 100 m and 110 m.

GLORIA Sidescan

In addition to the acoustic backscatter data from the UNH multibeam surveys, GLORIA (Geologic Long-Range Inclined Asdic) sidescan sonar data collected in 1987 were used to identify and map landslide features along the U.S. Atlantic continental margin (EEZ-SCAN 87, 1991). These data provide almost total coverage of the seafloor at a pixel resolution of 50-m, from the shelf edge out to 200 miles from shore, between 42 and 28 degrees north latitude (Figure 2-2).

Seismic Reflection Profiles

Analogue records of 3.5-kHz seismic reflection profiles, co-acquired with the GLORIA sidescan imagery, were used to determine location, geometry, and thickness of landslide features. The spatial coverage of these data can be seen in Figure 2-2. Although other data sets are available, the acquisition parameters and quality of these data are consistent over the entire area of study, and they provide a relatively clear picture of the upper sedimentary section.

Cores

Over 1400 cores have been collected from the study area, and descriptions of the cores are available from their respective core repositories as well as the National Geophysical Data Center (Figure 2-2). Of these, approximately

1,000 have been visually described, and 145 of them have had general ages assigned based on faunal content. While many of the descriptions are brief they provide a valuable summary of the overall lithology of many of the cores.

Data Analysis

Several aspects of the geomorphology of submarine landslides were more clearly resolved by the multibeam bathymetry than were revealed in previously available data sets. In particular scarps in the landslide source areas were clearly imaged in the bathymetry for the first time. Also, the detailed bathymetry of the landslide deposits allowed some to be divided into several units implying multiple failures and multiple episodes of deposition.

The thickness of landslide deposits was measured from the 3.5-kHz profiles and the average thickness of deposits identified on each profile was mapped in a GIS. The ability to resolve the thickness of landslide deposits on these profiles was variable. In some cases the thickness of the deposit was clearly imaged, in others a highly-reflective seafloor did not allow any subbottom penetration, and in other cases the base of the deposits were deeper than could be penetrated by the profiling system. Because of these limitations to the data set, the estimates of landslide volumes are minimum estimates.

The mapping of landslide-affected areas was broken into several steps. The first step was to identify scarps around and within landslide source areas. Scarps show clearly in shaded-relief and slope maps derived from the bathymetric data. The gullies that are prevalent on canyon walls and have been attributed to mass movements (Twichell and Roberts, 1982) were not mapped individually because of their huge number and small size. Next the areas affected by landslides were outlined. The shaded-relief imagery, backscatter imagery from the multibeam system (where available), and GLORIA imagery were used to map these areas. The surfaces of most landslides have a high-backscatter signature. In the southern part of the study area, offshore of the Carolinas, where the multibeam coverage was incomplete, the extent of the landslide areas was based on the GLORIA imagery alone. The final step was to merge the thickness derived from subbottom profiles with the interpretation of the sea-floor imagery to distinguish erosional and depositional sections of the landslide. The volumes of the landslide deposits probably are minimum estimates because of the inability of the 3.5-kHz profiles to resolve some of their thicknesses.

The volumes of the source areas of mapped and potential slides of various sizes and differing geologic settings (sourced in submarine canyons vs. the open slope) were calculated using techniques reported by (ten Brink *et al.*, 2006). These calculations involve the creation of interpolated smooth surfaces defining the potential pre-failure bathymetry, and subtracting the resulting grid from the post-failure bathymetry (present sea floor), resulting in an estimated volume of failed material. Identification of the source area of a particular landslide is a subjective process based on the morphology of the

slide scarp, the ability to discriminate between areas of material removal and deposition, and evidence for whether the failure was a single event or multiple events. Although the source zone volumes derived by this method may differ from calculations for areas that have undergone detailed study (*e.g.*, Currituck area, Prior *et al.*, 1986), this method provides a robust and repeatable means of estimating the volume of material removed from source areas when only bathymetry data is available.

Types of Submarine Mass Movements

Several classification schemes exist for submarine mass movements. For this report we use one presented by Locat and Lee (2002) that was adapted from the classification of subaerial mass movements proposed by the International Society for Soil Mechanics and Geotechnical Engineering (ISSMGE) Technical Committee on Landslides. While it has been observed that one type of mass movement can lead to another, here we briefly describe the end-member types.

- **Topples** – The displaced material usually is lithified rock that descends mainly through water as a coherent block that does not disintegrate during movement. Topples result in minimal lateral displacement.
- **Falls** – The displaced material mostly is lithified to semi-lithified material that is broken into smaller blocks and rubble during the failure process and descends mainly through water by falling, bouncing, and rolling. Falls also result in minimal lateral displacement.
- **Rotational slides** – The failed material undergoes rotation along a curved slip surface during displacement. This material tends to be rigid although in some cases beds within the failed mass are folded but do not undergo disintegration during translation.
- **Translational slides** – The failed material is translated along a discrete, flat slip surface. The material is rigid, and thus maintains its internal stratigraphy, however displacement can be great distances.
- **Debris flows** – Mass movements in which the failed material disintegrated during transport, and results in the deposit being a heterogeneous mix of clasts supported in a matrix of fine sediment. The clasts in debris flows vary in size and sediment texture.
- **Mudflows** – Mass movements of predominantly fine-grained material. These are similar to debris flows, but because of the more uniform texture their internal structure is not as clearly defined.
- **Turbidity currents** – Mass movements that involve the downslope movement of a relatively dilute suspension of sediment grains that are supported by the upward component of fluid turbulence.

Along the U.S. Atlantic continental margin, rotational slides, translational slides, debris flows and turbidity currents are the principal types of mass

movements that have been identified by previous authors (Booth *et al.*, 1988; 1993; Embley, 1980) as well as in this study. The deposits from turbidity currents were not mapped because this process was not considered to be a cause for landslide generated tsunamis.

Results

A total of 55 landslide areas were mapped along entire margin from eastern end of Georges Bank to the Blake Spur, from the shelf-slope break, down to the abyssal plain (Figure 2-4). This number is considerably less than the 179 that was tabulated by Booth *et al.* (1988; 1993). The reason for the difference probably is because many of the landslides that Booth *et al.* (1988) summarized were identified on widely spaced seismic lines, and when these locations are compared to the multibeam data many fall within the larger landslide complexes that now can be identified.

The types of landslides were interpreted from the morphology of the deposits as well as from their internal character as inferred mostly from high-resolution subbottom profiles. *Rotational slides*, *translational slides*, and *debris flows* were identified, and their distribution is shown in Figure 2-4. An example of one of the rotational slides offshore of Wilmington Canyon is shown in Figure 2-5a. Reflections have continuity within the deposit although they have been gently folded. The two rotational slides in this area are quite old as a thick section of younger sediment onlaps their toes (Figure 2-5a). Translational slides were identified on the multibeam bathymetry as slabs often with a toe that appears to have undergone some disintegration. No seismic profiles crossed these deposits, so their internal structure cannot be described. The headwall scarps were clearly defined and, in the observed cases, indicate a short translation distance. Debris flows were by far the most common landslide type identified. Debris flows originate from headwall scarps on the slope and upper rise, and can extend more than 200 km downslope to the distal end of the deposit. Many of the debris flows have several scarps in the source area suggesting that they consist of multiple failures rather than a single event. The area immediately downslope of the headwall scarps can have a rough surface (Figure 2-5b). Debris flow deposits commonly have mounded surfaces and amorphous internal structures (Figure 2-5c).

The general characteristics of landslides on this margin are given in Table 2-1. Landslide areas ranged from 9 to 15,241 km² with a mean of 1,880 km². The total area affected by landslides is approximately 18% of the study area. Landslides tend to be about 4 times as long as they are wide and have a mean length of 85 km. The water depth of the source area for landslides was identified as the shallowest scarp upslope of the landslide. Depths of the headwall scarps could only be measured in 33 of the 55 cases because of inadequate bathymetry on parts of the continental slope. The depth of the measured headwall scarps ranged from 92 to 3,263 m with a mean depth of 1,630 m (Table 2-1); 50% of the headwall scarps occurred on the middle and lower slope in 1,200-2,250m water depths. This range of source area depths

may change once improved bathymetry is available for the sections of the continental slope offshore of Georges Bank and southern New England that have not yet been adequately mapped (Figure 2-3). Booth *et al.* (1988; 1993) reported 900 m as the most common source depth for landslides. Again, the discrepancy is attributed to the improved view of the full extent of landslides that is provided by the multibeam bathymetric data. The relief could be measured on 45 of the headwall scarps: 75% had less than 100 m relief. The toe of the landslide deposits occurred in water depths greater than 2,126 m. Some of the landslides extended beyond the limit of the data coverage, so the maximum toe depth is unknown. The mean toe depth of those that fell entirely within the study bounds is 3,101 m.

The distribution of landslides is shown in Figure 2-4, and indicates that it is not uniform along this margin. The size of landslides is not uniform either (Figure 2-6); most cover less than 2,000 km², but one exceeds 15,000 km². Roughly 50% of the area affected by landslides and 7 of the 14 landslides that cover areas exceeding 2,000 km² are located offshore of Georges Bank and southern New England - a region that covers approximately one third of the length of the study area. Another 24% of the area affected by landslides occurs as two large ones in the Carolina Trough. The remaining 25% of all landslides are spread along the remaining half of the length of the study area (Figure 2-4).

Booth *et al.* (1993) were the first to recognize that landslides fall into two categories: (1) those with source areas on the open slope and (2) those that are sourced in submarine canyons. The landslides with open slope sources are concentrated on the southern New England margin, off the Currituck area, and in the Carolina Trough (Figure 2-7). Many of the landslides off Georges Bank appear to have a combination of canyon and the open slope sources, but existing bathymetry on this section of the slope is inadequate to fully map the source areas. Where multibeam bathymetry is available, it does show scarps on the middle to lower slope well removed from canyons which indicates that at least part of source for landslides off Georges Bank is from open slope settings. The landslides with source areas in submarine canyons are concentrated offshore of the mid-Atlantic states between Hudson and Norfolk Canyons and offshore of Cape Hatteras.

The thickness of landslide deposits could not always be determined on the profiles that were used for this analysis, but where they could be measured they ranged from 5-70 m in thickness with a mean thickness of approximately 20 m. The thickest deposits were measured on the southern New England rise, and in the Carolina Trough area (Figure 2-8). The volumes of landslide deposits range from 0.05 to 392 km³, but we recognize that in some cases these are minimum estimates because of the limited penetration of the seismic data available to us. The total volumes of some of the deposits are huge, but many appear to be comprised of several smaller deposits, and thus the deposit associated with any one failure could be considerably smaller. For example, the Currituck landslide deposit has a total volume of at least 84 km³, but it can be divided into 6 separate sections of which the largest is 38.5 km³ (Figure 2-9). Of the largest landslide complexes, two are slope-sourced landslides in the southern New England region (190

and greater than 392 km³) and two are sourced around salt domes on the open slope in the Carolina Trough area (114 and 150 km³). By contrast, the largest canyon-sourced landslide deposits have volumes less than 10 km³ (Figure 2-10).

Although numerous core and surficial sediment samples have been recovered from the slope and rise of the U.S. Atlantic margin (Figure 2-2), little information is available on the age of the landslides described herein. Of the few reliable dates that are available, most landslides are considered to be older than 10,000 yr Bp (Prior *et al.*, 1984; 1986, Popenoe *et al.*, 1993, Embley and Jacobi, 1986), and to date only one failure has been sampled that occurred more recently (Embley, 1980). Of interest, however, is that the age of material making up the landslide deposits, as defined by 30 cores, in all but one case is Quaternary (Figure 2-11). The young age of the sediment comprising the landslide deposits indicates that the failures removed only a thin surficial skin from the source area and did not cut deeply into older strata under the continental slope.

The volumes of source areas of 34 mapped and potential (*i.e.*, those areas fully expressed on the maps) slides (Figure 2-12) are given in Table 2-2. Although only a subset of the mapped and potential slides was used in these calculations, they are a representative subset that covers the full range of landslide types in the region. The largest volumes calculated are associated with the extensive slides off Georges Bank (source #3 – 112 km³) and the Currituck area (*e.g.*, source #28 – 136 km³), plus the diapir-related slides south of Cape Hatteras (*e.g.*, source #31 – 179 km³). The smallest source volumes were those found within the canyon systems, both canyon head and canyon side-wall sources, commonly having volumes of less than 1 km³ (*e.g.*, source # 4 and 6).

Discussion

Compared to previous regional studies of the distribution and size of major submarine landslides along the U.S. Atlantic margin (*e.g.*, Booth *et al.*, 1988; 1993; Embley, 1980; Embley and Jacobi, 1986; Pratson and Laine, 1989; Hance, 2003), we have benefited from the availability of high-resolution multibeam bathymetry in guiding our analysis of these features. As a result, although we report a smaller number of mass movement features, we have been able to better define the extent and thickness of individual and composite landslides, which in most cases incorporate a number of the singular features described by previous investigators.

The spatial distribution of landslides along the U.S. Atlantic margin is, in part, controlled by the underlying geology. The thickness of Quaternary sediment preserved on the outer shelf is closely associated with landslide distribution (Figure 2-13). Landslide areas are most common and tend to be largest offshore of these areas where Quaternary sediment is thickest. Nearly 60% of the area affected by landslides occurs offshore of the thick Quaternary shelf deposits of the Georges Bank, southern New England and Virginia areas. The thick Quaternary deposits presumably covered the upper

slope as well and were the source material for many of the landslides. These three areas also are regions where the older strata underlying the slope dip sub-parallel to the gradient of the present slope (Rona, 1969; Uchupi, 1970; McGregor, 1981; O'Leary, 1986). The two large landslide areas in the Carolina Trough are controlled by different geological processes. They are sourced near salt domes and the tectonic activity of the salt domes has been suggested to be the triggering mechanism for these failures (Dillon *et al.*, 1982; Cashman and Popenoe, 1985; Popenoe *et al.*, 1993). These two large salt-related landslides account for 24% of the area affected by landslides. Landslides covering the remainder of the continental margin are off sections where Quaternary deposits at the shelf edge are thin and older strata underlying the slope are nearly horizontal rather than having a dip sub-parallel to the seafloor account for only 16% of the landslide area (Figure 2-13).

From this mapping, we find that landslides along the U.S. Atlantic margin initiate predominantly in two morphologic settings, canyon (heads and sidewalls) and on the open continental slope (Figure 2-7). The canyon-sourced failures commonly have several canyons feeding a single deposit, and the deposits are smaller than those derived from the open slope. Open-slope failures originate from scarps commonly on the middle and lower slope in 800-2,200 m depths. These landslides extend farther offshore, are thicker, and have considerably larger volumes than their canyon derived counterparts.

Using the classification of Locat and Lee (2002), we find the dominant mass movement modes to be translational slides, rotational slides, and debris flows, which in most cases are now found together as part of larger, multiphase composite deposits. The dominant style of mass-wasting identified along the Atlantic margin appears to be debris flows (Figure 2-4). In part, the reason for this may be because the bulk of the sediment that makes up the mass-wasting deposits was Quaternary in age (Figure 2-11). Thus sediment in the source areas was largely unconsolidated to semi-lithified, and could not be transported large distances without undergoing disintegration. The height of scarps in most landslide source areas have less than 75 m relief indicating that in most places only the Quaternary section is being removed (Figure 2-13).

While the volumes of landslide deposits can be large (Figure 2-10), some of them, such as the Currituck landslide (Figure 2-9) appear to be composed of several smaller depositional units. In many cases the seismic data and imagery were not of adequate detail to clearly show the composite nature of landslide deposits. Analysis of landslide source areas, where good quality bathymetric data are available, commonly shows several scarps which suggests several failures contributed to the formation of many of the large landslide deposits.

We find that the open slope sourced slides are larger both in the area of failure and overall volume of per-event failed material, and as such, are the dominant means of rapid margin modification. We also find that a significant volume of material may be mobilized in landslides associated with areas of salt diapirism. Because of the large volumes of material that can fail during an individual or retrogressive open slope-sourced slide (Figure 2-10), these

are considered to have the most potential to initiate tsunami (Murty, 2003). From the modeling of source volumes (Table 2-2) of individual scarps along the margin, we see that three regions (off Georges Bank, Currituck area, and in the Carolina Trough) have had a history of, and therefore potential for, large volume failures. With the currently available data, it is difficult to determine if landslides on the southern New England slope involve large volumes of material per event, or if the region is dominated by smaller, but more numerous landslides.

Future Directions

While the recent acquisition of multibeam bathymetry from nearly the entire continental slope and rise of the eastern U.S. has greatly improved our understanding of the distribution and style of submarine mass movements, there are two areas where additional data would enhance our understanding of submarine mass movement processes.

The first is that the source areas of the landslide complexes along the Georges Bank and Southern New England margin are not adequately imaged (Figure 2-3). This region hosts the largest landslide complexes we mapped, and understanding the depth of the source area, relief and nature of the headwall scarps, stratigraphy that is being removed by failures would help explain the causes of these failures, and the volume of material removed in each failure episode.

Second, a better understanding is needed on the timing of the submarine landslides. Careful age dating is needed on cores recovered from within and adjacent to several of the landslides are needed to address this question.

Tables

Table 2-1: Characteristics of landslides on the Atlantic margin.

Dimension	Minimum	Maximum	Mean	Median
Length (km)	2.7	>291	85	51
Width (km)	2.1	151	21	12
Area (km ²)	9	15,241	1,880	424
Source depth (m)	92	3,263	1,630	1,785
Toe depth (m)	2,126	4,735	3,101	2,991
Scarp height (m)	3	1,260	256	68

Table 2-2: Area and volume of selected landslide source areas (see Figure 2-12 for location). In some cases, such as the Currituck slide, the source area is split into several smaller regions, due to the possible composite nature of these landslides.

Source #	Area (km ²)	Volume (km ³)	Downslope Length (km) ^{ad}	Cross-slope width (km) ^{bd}	Shallowest Depth (m) ^c
1	42.16	0.50	13.0	5.2	-2034
2	129.76	9.38	15.6	11.0	-2033
3	814.94	112.86	63.8	18.1	-2304
4	6.65	0.22	2.9	3.0	-2358
5	75.78	1.40	28.2	5.6	-1881
6	244.01	9.69	27.2	14.9	-2338
7	66.59	2.09	15.0	8.2	-1976
8	219.49	13.80	12.1	22.7	-749
9	226.95	0.34	7.7	43.8	-2430
10	25.71	0.72	3.7	8.7	-2131
11	47.23	0.83	11.3	6.7	-2049
12	64.61	1.94	14.0	6.7	-1972
13	84.02	4.44	11.5	10.3	-2216
14	24.77	0.31	5.1	7.3	-2108
15	30.45	0.62	10.5	7.0	-1603
16	4.86	0.06	4.2	1.8	-2095
17	108.09	21.34	28.2	5.6	-1014
18	49.24	7.58	15.5	4.2	-1503
19	25.74	3.18	13.2	3.3	-1455
20	26.90	0.75	7.3	3.5	-1049
21	30.48	0.63	10.9	4.3	-743
22	27.97	1.28	8.9	3.2	-1726
23	371.61	7.52	50.7	7.5	-1230
24	300.92	9.59	19.4	21.6	-109
25	68.42	0.50	17.7	4.2	-1070
26	1238.37	112.61	59.9	26.5	-675
27	141.04	4.46	20.0	5.7	-1897
28	577.58	135.89	38.4	16.4	-128
29	12.28	0.08	7.5	2.3	-309
30	1222.76	36.78	50.0	30.8	-2675
31	2409.77	178.91	80.8	35.1	-3508
32	650.23	23.39	60.8	14.8	-3285
33	565.38	2.19	33.8	21.9	-884
34	158.52	1.10	19.9	10.7	-1214

^a Source excavation length values listed in most cases represent the maximum length, from the shallowest part of the headwall to the deepest part of the toe, but the length changes significantly across the width of all sources.

^b The widths of all source excavations change significantly along their length. These values were measured at points where the width appeared to represent an average for the source.

^c The depth of the source can vary by 100's to 1000's of meters across their lengths and widths, so these values represent only the depth at the shallowest point of the source.

^d Because of the highly variable shape of the source excavations, using the length and width values given here will not provide an accurate value for their areas, or by extension, their volumes. For these values, use the information provided in columns 2 and 3.

Figures

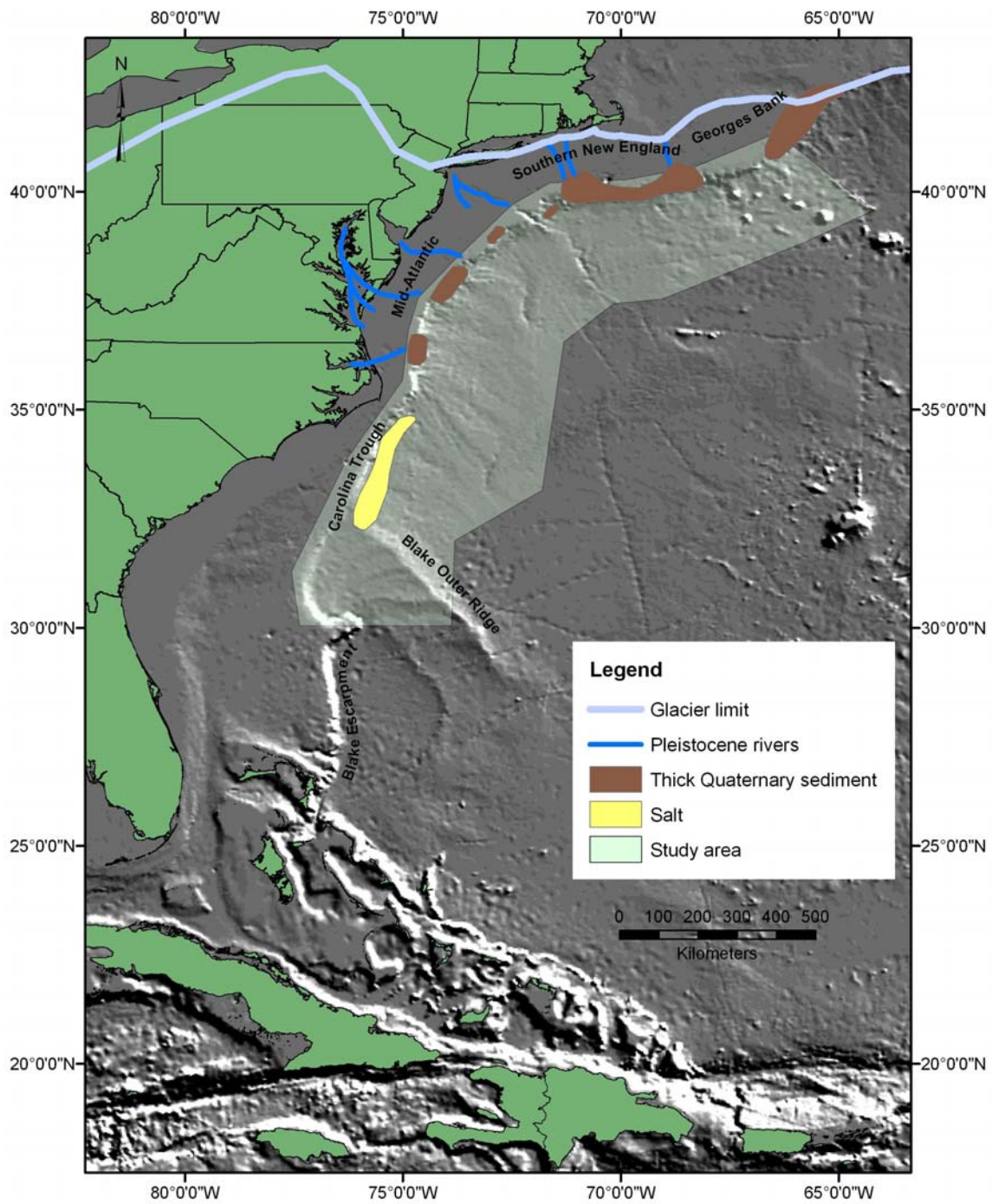


Figure 2-1: Location map showing the extent of the study area, the names of areas referenced in the text and geologic features that may influence landslide distribution along the U.S. Atlantic margin.

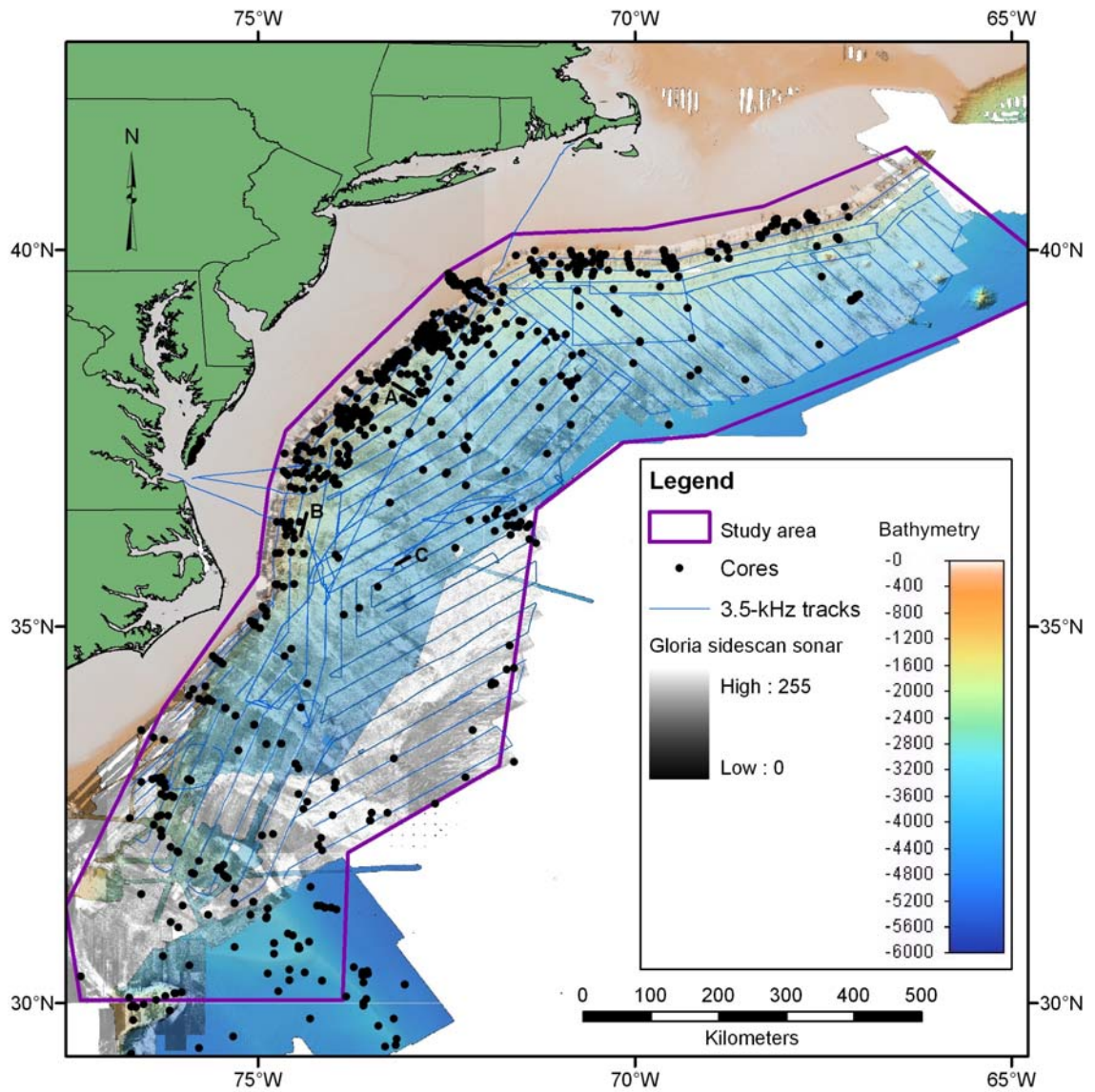


Figure 2-2: Extent of the study area and available data used in this analysis of landslides.

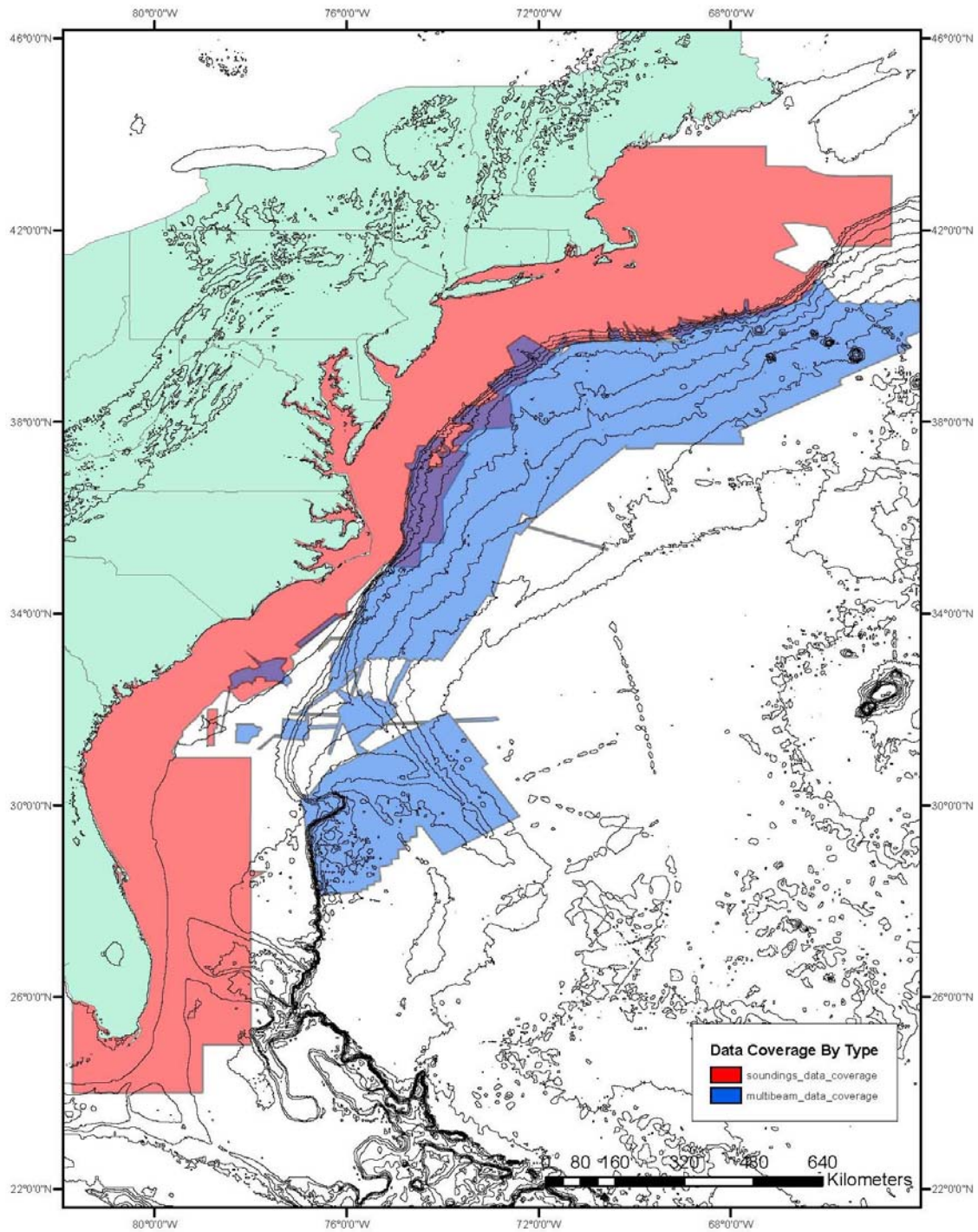


Figure 2-3: Bathymetry of the U.S. Atlantic margin with areas that were not imaged by multibeam systems highlighted.

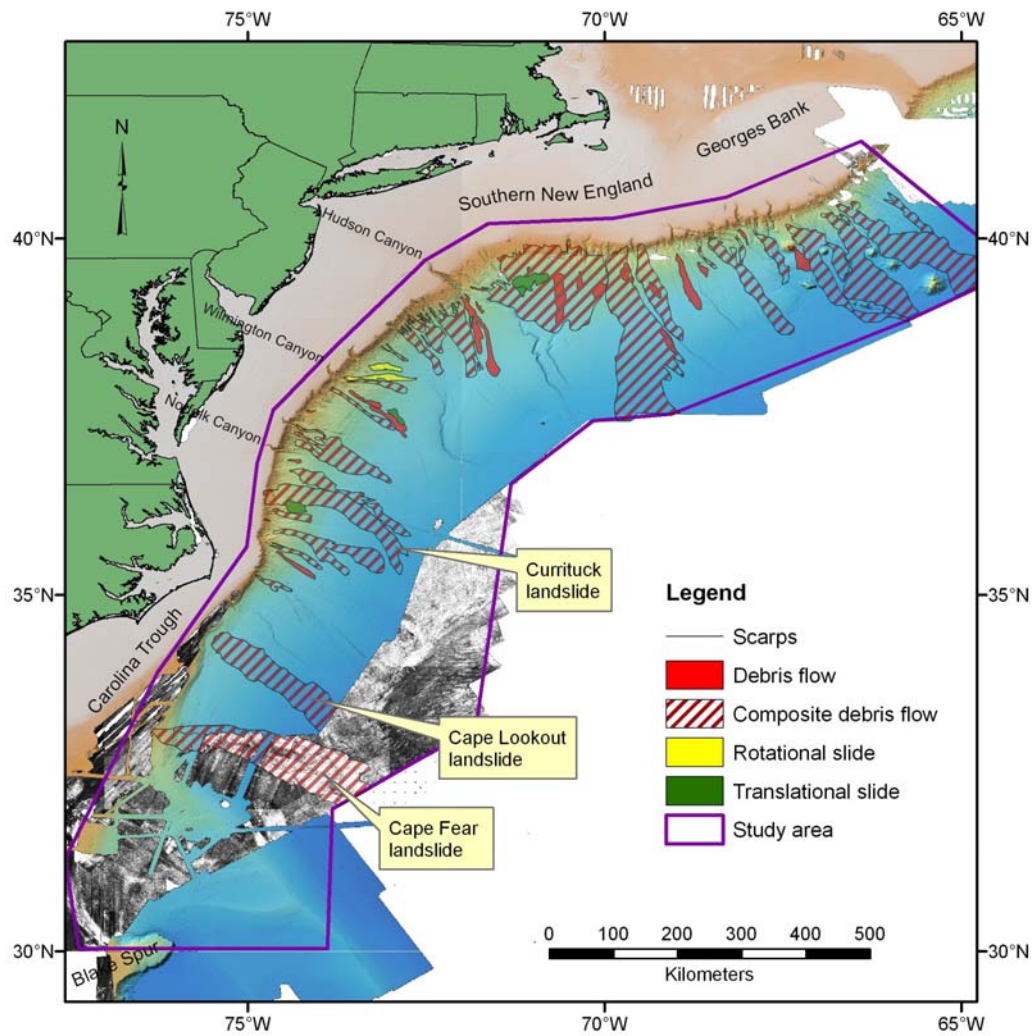


Figure 2-4: Distribution of different landslide types along the U.S. Atlantic continental slope and rise between the eastern end of Georges Bank and the Blake Spur.

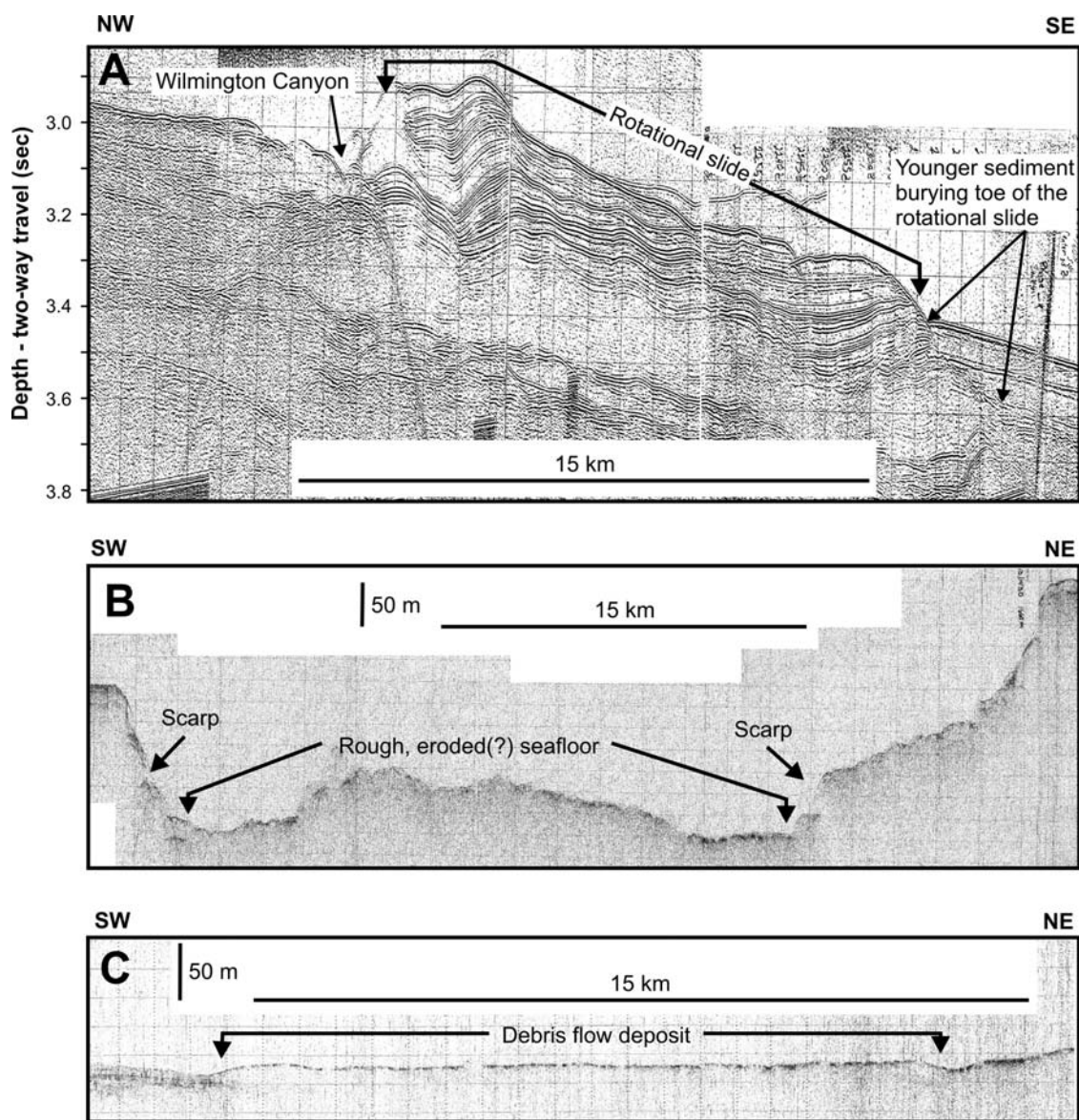


Figure 2-5: Seismic profiles showing examples of (A) airgun seismic profile showing a relatively old rotational slide near Wilmington Canyon whose toe has been buried by ~90 m of younger sediment, (B) hyperbolae on a 3.5-kHz subbottom profile below the headwall scarp of the Currituck debris flow indicating a rough eroded sea floor, and (C) a 3.5-kHz profile near the toe of the Currituck debris flow showing the external mounded appearance and internal acoustically transparent nature that is characteristic of debris flow deposits. Profile locations shown in Figure 2-2.

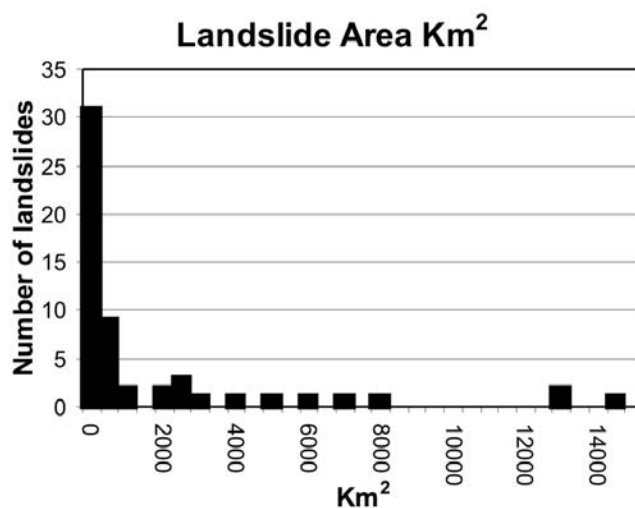


Figure 2-6: Graph showing the number landslides in increments of 500 km² area. Most of the landslides cover areas less than 2,000 km².

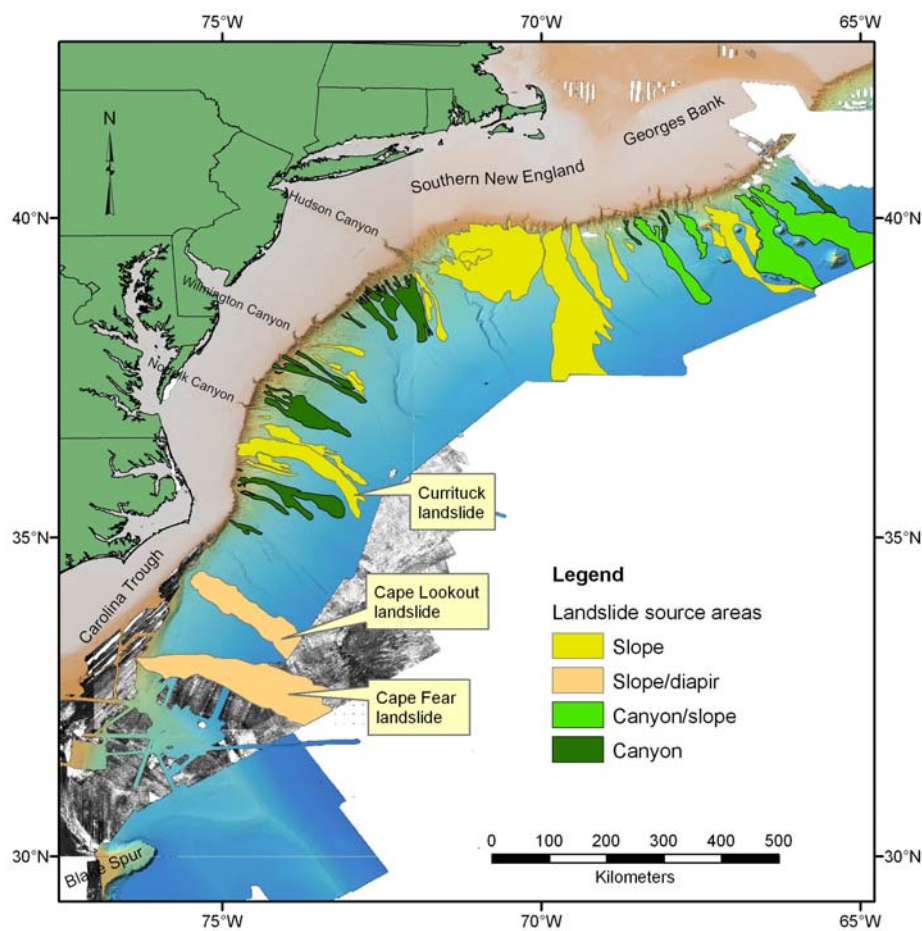


Figure 2-7: Map showing the distribution of landslides by source area. The largest landslides have open-slope source areas (in the Carolina Trough area they are associated with salt domes). The landslides off Georges Bank appear to have contributions from both canyon and open-slope sources; improved bathymetry in this area will allow assessing the importance of the two source areas. Landslides with submarine canyons as their source areas are smaller in area and shorter than the slope-sourced failures.

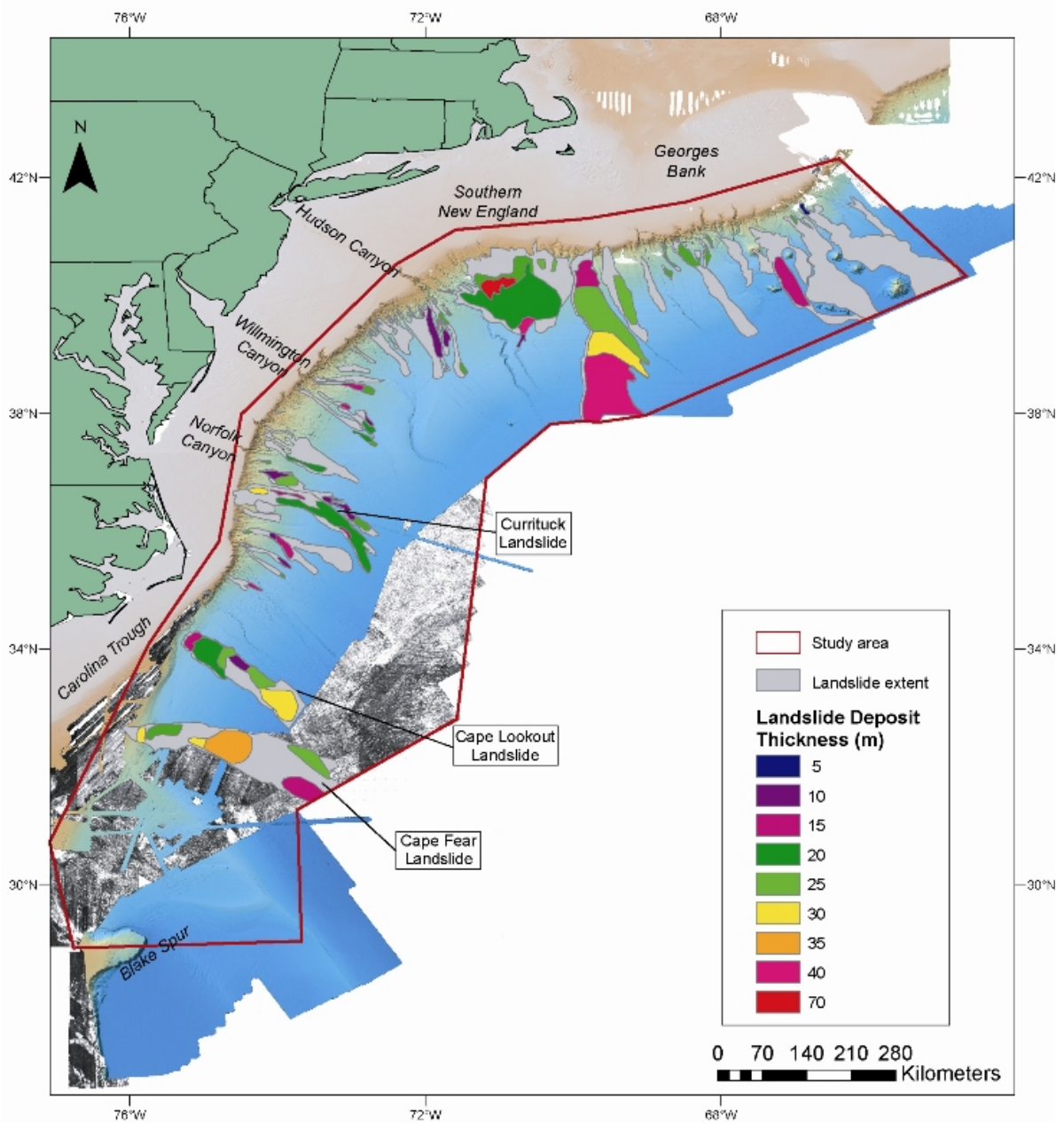


Figure 2-8: Thickness of landslide deposits mapped using 3.5-kHz profiles. Some were too thin to be resolved by these profiles and others had surface returns that attenuated the signal did not allow penetration to the base of the deposit.

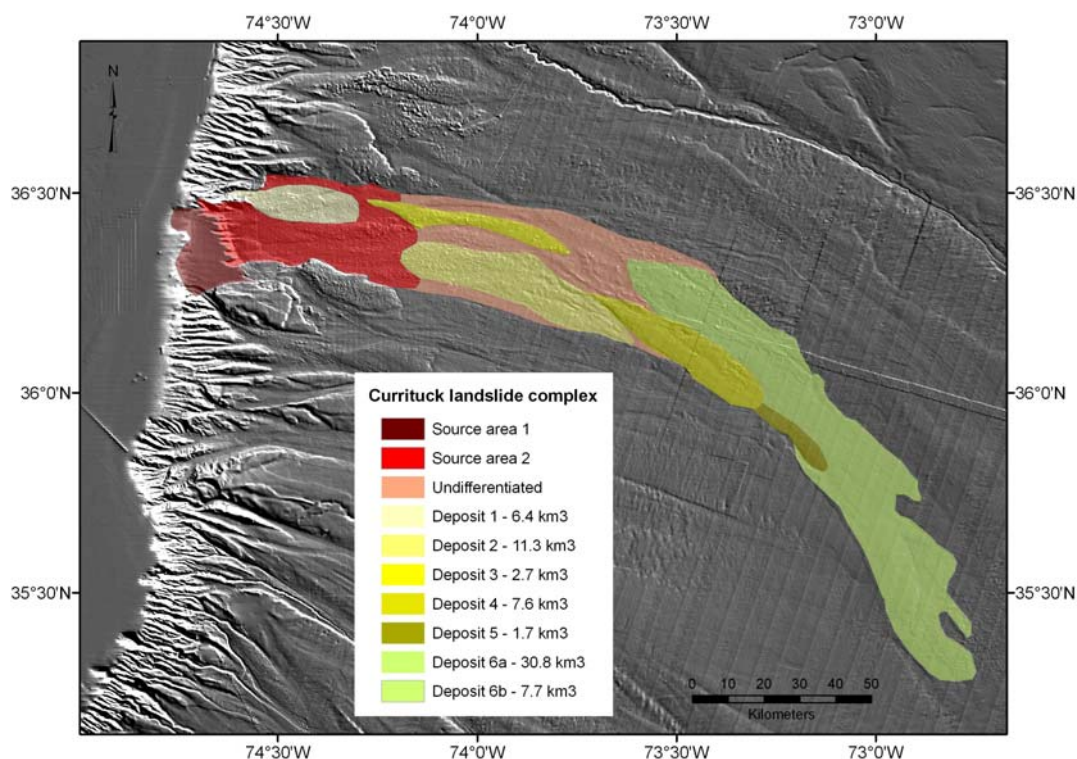


Figure 2-9: Detailed view of the Currituck landslide complex showing it has at least two headwall scarps and six deposits. While the cumulative volume of the entire complex is 84 km³, individual deposits are less than 38.5 km³.

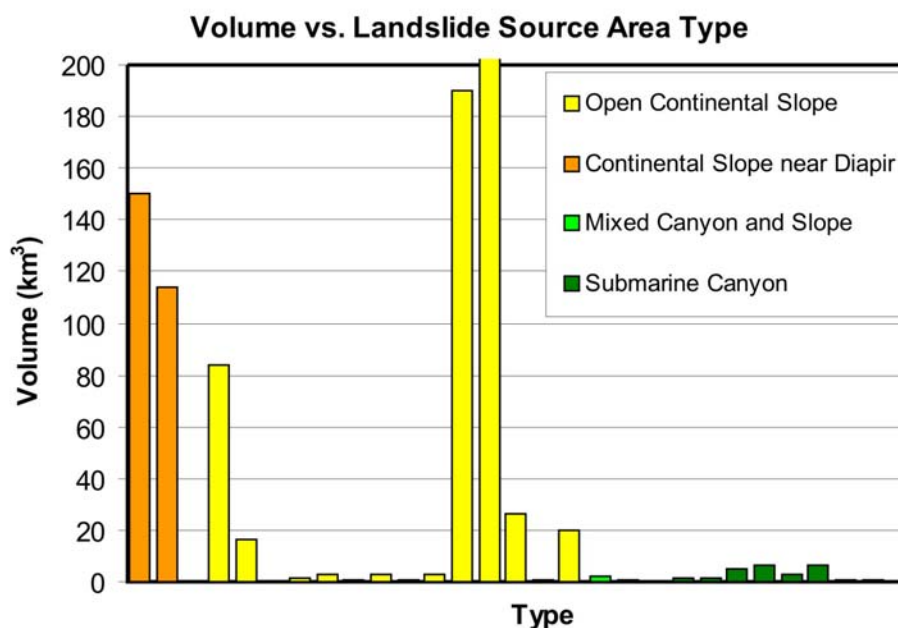


Figure 2-10: Graph showing the volume of landslides based on their source area type as noted in Figure 2-7. Landslides are grouped by geographic type. The largest landslide deposits (by volume) have sources on the open slope or on the open slope near salt domes. The graph was scaled to a maximum volume of 200 km³ to show the deposits associated with landslides derived from submarine canyons and mixed canyon and slope sources; largest landslide deposit is found on the southern New England rise and contains 392 km³.

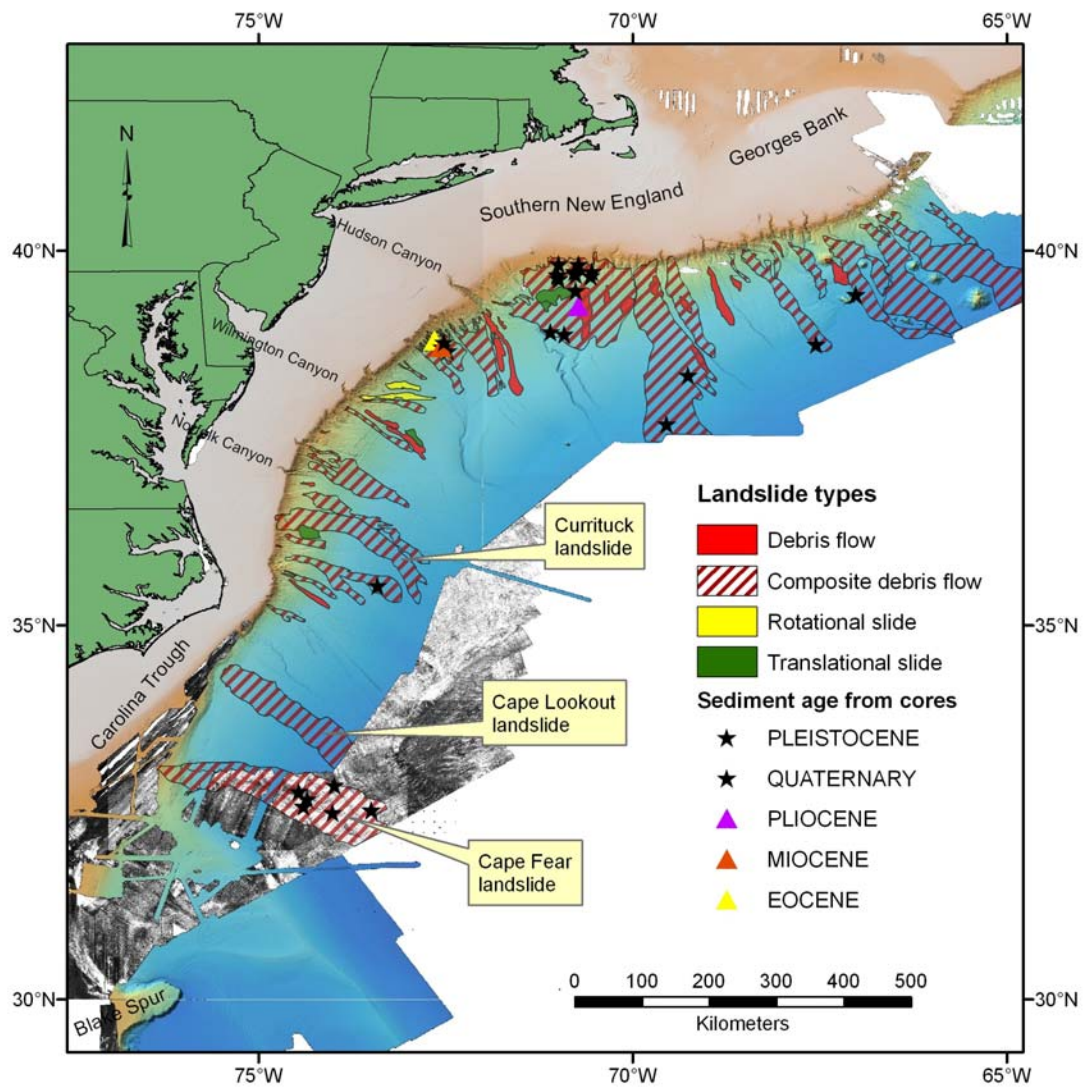


Figure 2-11: Age of cored material collected from landslide deposits. Note that of the 40 cores that recovered material from landslide deposits and that were assigned ages only 3 were not Quaternary or Pleistocene in age.

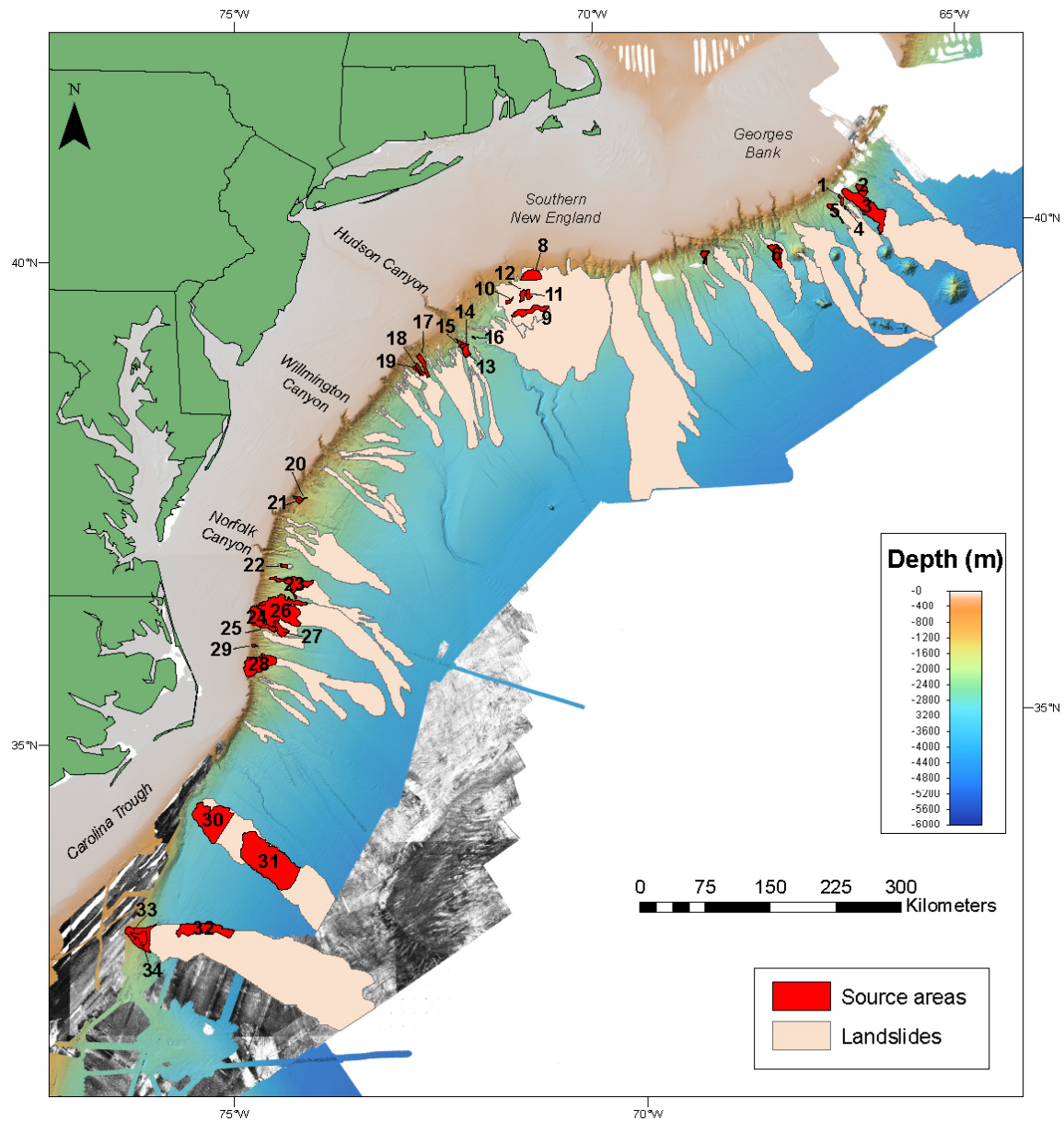


Figure 2-12: Locations of source area volume calculations that are shown in Table 2-2.

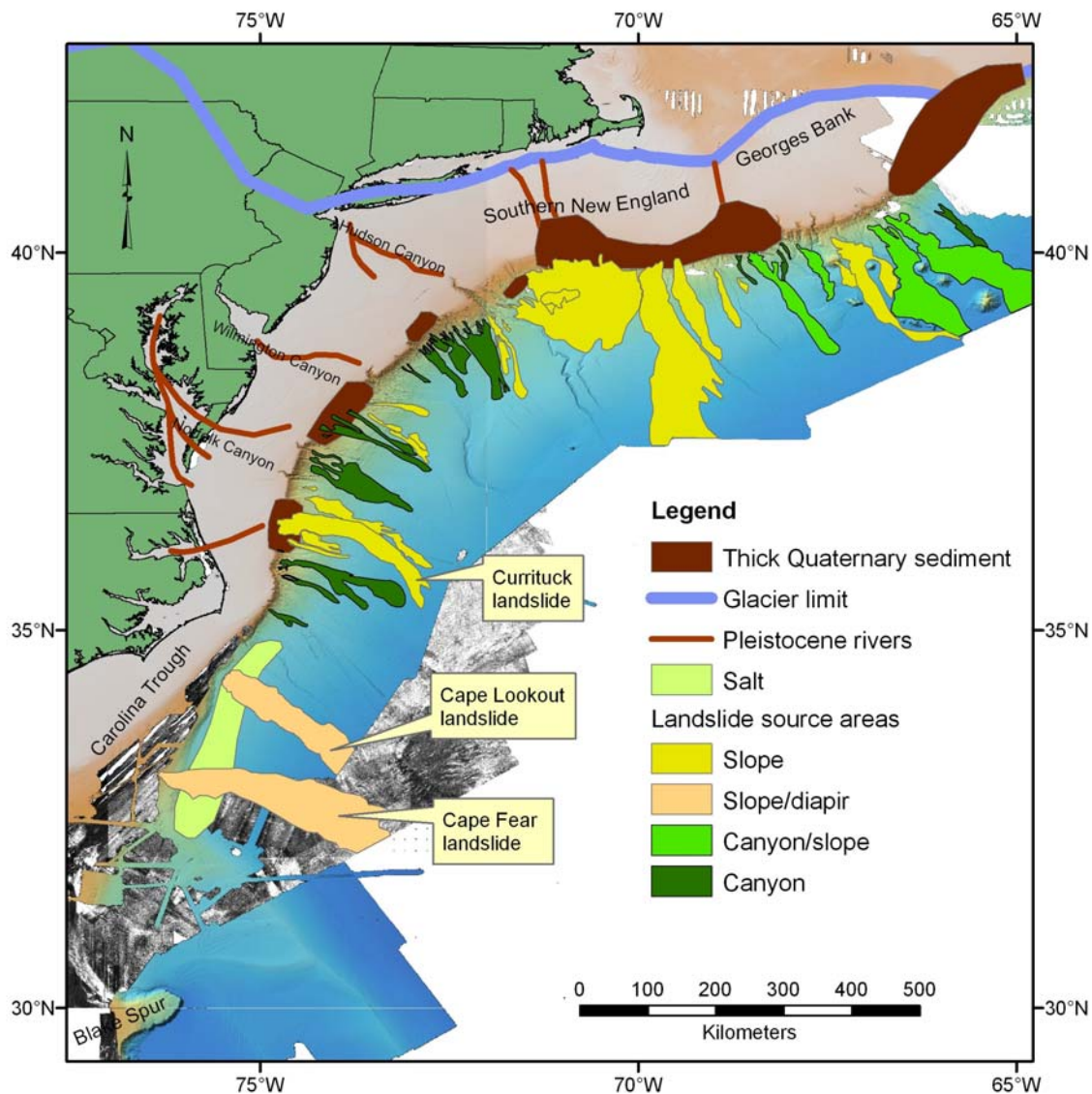


Figure 2-13: Map showing the relationship between the landslides and underlying geologic features.

References

- Booth, J.S., O'Leary, D.W., Popenoe, P., Robb, J.M., and McGregor, B.A., 1988, Map and tabulation of Quaternary mass movements along the United States-Canadian Atlantic continental slope from 32 00' to 47 00' N latitude: U.S. Geological Survey Miscellaneous Field Studies Map MF-2027.
- Booth, J.S., O'Leary, D.W., Popenoe, P., and Danforth, W.W., 1993, U.S. Atlantic continental slope landslides: Their distribution, general attributes, and implications, *in*, Schwab, W.C., Lee, H.J., and Twichell, D.C. (Editors), Submarine landslides: Selected studies in the U.S. Exclusive Economic Zone: U.S. Geological Survey Bulletin no. 2002, p. 14-22.

- Bunn, A.R., and McGregor, B.A., 1980, Morphology of the North Carolina slope, western North Atlantic, shaped by deltaic sedimentation and slumping: *Marine Geology*, v. 37, p. 253-266.
- Cartwright, D. and Gardner, J.V., 2005, U.S. Law of the Sea cruise to map the foot of the slope and 2500-m isobath of the Northeast U.S. Atlantic continental margin: Legs 4 and 5. Cruise Report, Center for Coastal and Ocean Mapping/Joint Hydrographic Center, University of New Hampshire, Durham, N.H., 30 p.
- Cashman, K.V., and Popenoe, P., 1985, Slumping and shallow faulting related to the presence of salt on the continental slope and rise off North Carolina: *Marine and Petroleum Geology*, v. 2, p. 260-271.
- Colman, S.M., Halka, J.P., Hobbs, C.H., Mixon, R.B., and Foster, D.S., 1990, Ancient channels of the Susquehanna River beneath Chesapeake Bay and the Delmarva Peninsula: *Geological Society of America Bulletin*, v. 102, p. 1268-1279.
- Dillon, W.P., Risch, J.S., Scanlon, K.M., Valentine, P.C., and Huggett, Q.J., 1993, Ancient crustal fractures control the location and size of collapsed blocks at the Blake Escarpment, East of Florida, *in*, Schwab, W.C., Lee, H.J., and Twichell, D.C. (Editors), Submarine landslides: Selected studies in the U.S. Exclusive Economic Zone: U.S. Geological Survey Bulletin no. 2002, p. 54-59.
- Dillon, W.P., Valentine, P.C., Shinn, E.A., Arthur, M., Sohl, N.F., Paull, C.K., and Newman, A.C., 1983, Geology and evolution of the Blake Escarpment: U.S. Geological Survey Professional Paper, Report P 1375, p. 114- .
- Dillon, W.P., Popenoe, P., Grow, J.A., Klitgord, K.D., Swift, B.A., Paull, C.K., and Cashman, K.V., 1982, Growth faulting and salt diapirism: Their relationship and control in the Carolina Trough, eastern North America, *in*, J.S. Watkins and C.L. Drake (Editors), Studies in continental margin geology, American Association of Petroleum Geologists Memoir 34, p. 21-46.
- EEZ-SCAN 87, 1991, Atlas of the U. S. Exclusive Economic Zone, Atlantic continental margin: U. S. Geological Survey Miscellaneous Investigations Series I-2054.
- Embley, R.W., 1980, The role of mass transport in the distribution and character of deep ocean sediments with special reference to the North Atlantic: *Marine Geology*, v. 38, p. 23-50.
- Embley, R.W. and Jacobi, R.D., 1986, Mass wasting in the western North Atlantic, *in* Vogt, P.R. and Tucholke, B.E., (Editors), The western North Atlantic region: Boulder, CO, Geological Society of America, Geology of North America, v. M, p. 479-490.
- Gardner, J.V., Mayer, L.A., and Armstrong, A.A., 2006, Mapping supports potential submission to U.N. Law of the Sea: EOS Transactions, *American Geophysical Union*, v. 87, p. 157-159.
- Hance, J. J., 2003. Development of a Database and Assessment of Seafloor Slope Stability based on Published Literature. M.S. Thesis, The University of Texas, Austin, p. 245.

- Heezen, B.C. and Ewing, M., 1952, Turbidity currents and submarine slumps, and the Grand Banks earthquake: *American Journal of Science*, v. 250, p. 849-873.
- Huhnerbach, V., Masson, D.G., partners of the COSTA-Project, 2004, Landslides in the North Atlantic and its adjacent seas: an analysis of their morphology, setting and behavior: *Marine Geology*, v. 213, p. 343-362.
- Klitgord, K.D., Hutchinson, D.R., and Schouten, H., 1988, U.S. Atlantic continental margin: structural and tectonic framework, *in*, Sheridan, R.E. and Grow, J.A., (Editors), *The Geology of North America*, Vol. I-2, *The Atlantic Continental Margin*, U.S., Geol Soc. America, Boulder, CO, p. 19-55.
- Klitgord, K. D., Poag, C. W., Schneider, C. M. and North, L., 1994. Geophysical database of the East Coast of the United States northern Atlantic margin--cross sections and gridded database (Georges Bank Basin, Long Island Platform, and Baltimore Canyon Trough), U.S. Geological Survey Open File Report 94-637.
- Knebel, H.J., 1984, Sedimentary processes on the Atlantic continental slope of the United States: *Marine Geology*, v. 61, p. 43-74.
- Knebel, H.J., and Carson, B., 1979, Small-scale slump deposits, Middle Atlantic continental slope, off eastern United States: *Marine Geology*, v. 29, p. 221-236.
- Knebel, H.J., Wood, S.A., and Spiker, E.C., 1979, Hudson River: Evidence for extensive migration on the exposed continental shelf during Pleistocene time: *Geology*, v. 7, p. 254-258.
- Locat, J., and Lee, H. J., 2002. Submarine landslides: advances and challenges. *Canadian Geotechnical Journal*, v. 39, p. 193-212.
- MacIlvaine, J.C., and Ross, D.A., 1979, Sedimentary processes on the continental slope of New England: *Journal of Sedimentary Petrology*, v. 49, p. 563-574.
- Malahoff, A., Embley, R.W., Perry, R.B., and Fefe, C., 1980, Submarine mass-wasting of sediments on the continental slope and upper rise south of Baltimore Canyon: *Earth and Planetary Science Letters*, v. 49, p. 1-7.
- McAdoo, B.G., Pratson, L.F., and Orange, D.L., 2000, Submarine landslide geomorphology, U.S. continental slope: *Marine Geology*, v. 169, p. 103-136.
- McGregor, B.A., and Bennett, R.H., 1977, Continental slope sediment instability northeast of Wilmington Canyon: *American Association of Petroleum Geologists Bulletin*, v. 61, p. 918-928.
- McGregor, B.A., and Bennett, R.H., 1979, Mass movement of sediment on the continental slope and rise seaward of the Baltimore Canyon Trough: *Marine Geology*, v. 33, p. 163-174.
- McGregor, B.A., 1981, Smooth seaward-dipping horizons – an important factor in sea-floor stability?: *Marine Geology*, v. 39, p. M89-M98.
- McMaster, R.L., and Ashraf, A., 1973, Drowned and buried valleys on the southern New England continental shelf: *Marine Geology*, v. 15, p. 249-268.
- Murty, T. S., 2003. Tsunami wave height dependence on landslide volume: *Pure and Applied Geophysics*, v. 160, p. 2147-2153.
- Oldale, R.N., 1992, Cape Cod and the Islands: The Geologic Story, Parnassus Imprints, East Orleans, MA, 208 p.

- O'Leary, D.W., 1986, The Munson-Nygren slide: A major lower-slope slide off Georges Bank: *Marine Geology*, v. 72, p. 101-114.
- O'Leary, D.W., 1993, Submarine mass movement, a formative process of passive continental margins: the Munson-Nygren landslide complex and the southeast New England landslide complex, in Schwab, W.C., Lee, H.J., and Twichell, D.C. (Editors), Submarine landslides: Selected studies in the U.S. Exclusive Economic Zone: U.S. Geological Survey Bulletin no. 2002, p. 23-39.
- O'Leary, D.W., 1996, The timing and spatial relations of submarine canyon erosion and mass movement on the New England continental slope and rise, in Gardner, J.V., Field, M.E., and Twichell, D.C. (Editors), Geology of the United States Seafloor: The view from GLORIA, Cambridge Univ. Press, Cambridge, UK, p. 47-58.
- Poag, C.W., 1991, Rise and demise of the Bahama-Grand Banks gigaplatform, northern margin of the Jurassic proto-Atlantic seaway: *Marine Geology*, v. 102, p. 63-130.
- Poag, C.W., and Sevon, W.D., 1989, A record of Appalachian denudation in postrift Mesozoic and Cenozoic sedimentary deposits of the U.S. middle Atlantic continental margin: *Geomorphology*, v. 2, p. 119-157.
- Popenoe, P., Schmuck, E. A., and Dillon, W. P., 1993. The Cape Fear Landslide: Slope failure associated with salt diapirism and gas hydrate decomposition., in Schwab, W.C., Lee, H.J., and Twichell, D.C. (Editors), Submarine landslides: Selected studies in the U.S. Exclusive Economic Zone: U.S. Geological Survey Bulletin no. 2002, p. 40-53.
- Popenoe, P., and Dillon, W.P., 1996, Characteristics of the continental slope and rise off North Carolina from GLORIA and seismic-reflection data: The interaction of downslope and contour current processes, in Gardner, J.V., Field, M.E., and Twichell, D.C. (Editors), Geology of the United States Seafloor: The view from GLORIA, Cambridge Univ. Press, Cambridge, UK, p. 59-79.
- Pratson, L.F., and Laine, E.P., 1989, The relative importance of gravity-induced versus current-controlled sedimentation during the Quaternary along the mid-east U.S. Outer continental margin revealed by 3.5 kHz echo character: *Marine Geology*, v. 89, p. 87-126.
- Prior, D.B., Doyle, E.H., and Neurauter, T., 1986, The Currituck Slide, Mid-Atlantic continental slope; revisited: *Marine Geology*, v. 73, p. 25-45.
- Prior, D.B., Coleman, J.M., and Doyle, E.H., 1984, Antiquity of the continental slope along the Middle-Atlantic margin of the United States: *Science*, v. 223, p. 926-928.
- Robb, J.M., 1984, Spring sapping on the lower continental slope, offshore New Jersey: *Geology*, v. 12, p. 278-282.
- Rona, P.A., 1969, Middle Atlantic Continental Slope of United States: Deposition and erosion: *American Association of Petroleum Geologists Bulletin*, v. 53, p. 1453-1465.
- Ryan, W.B.F., Cita, M.B., Miller, E.L., Hanselman, D., Nesterhoff, W.D., Hecker, B., and Nibbelink, M., 1978, Bedrock geology in New England submarine canyons: *Oceanologica Acta*, v. 1, p. 233-254.

- Schlee, J.S., and Fritsch, J., 1982, Seismic stratigraphy of the Georges Bank basin complex, offshore New England, *in*, Watkins, J.S., and Drake, C.L., (Editors), Studies in continental margin geology, AAPG Memoir, vol. 34, p. 223-251.
- Schlee, J.S., and Robb, J.M., 1991, Submarine processes of the middle Atlantic continental rise based on GLORIA imagery: *Geological Society of America Bulletin*, v. 103, p. 1090-1103.
- Shideler, G.L. and Swift, D.J.P., 1972, Seismic reconnaissance of post-Miocene deposits, Middle Atlantic continental shelf – Cape Henry, Virginia to Cape Hatteras, North Carolina: *Marine Geology*, v. 12, p. 165-185.
- ten Brink U.S., Geist, E.L., Andrews, B. D., 2006, Size distribution of submarine landslides and its implication to tsunami hazard in Puerto Rico. *Geophysical Research Letters*, 33, L11307, doi:10.1029/2006GL026125.
- ten Brink, U. S., Geist, E.L., Lynett, P., and Andrews, B.D., 2006, Submarine slides north of Puerto Rico, and their tsunami potential, *in*, Mercado, A., and Liu, P., (Editors), Proceedings of NSF workshop on tsunami hazard in the Caribbean: World Scientific.
- Twichell, D.C., Knebel, H.J., and Folger, D.W., 1977, Delaware River – Evidence for its former extension to Wilmington Submarine Canyon: *Science*, v. 195, p. 483-485.
- Twichell, D.C. and Roberts, D.G., 1982, Morphology, distribution, and development of submarine canyons on the U.S. Atlantic Continental Slope between Hudson and Baltimore Canyons: *Geology*, v. 10, p. 408-412.
- Uchupi, E., 1967, Slumping on the continental margin southeast of Long Island, New York: *Deep-Sea Research*, v. 14, p. 635-639.
- Uchupi, E., 1970, Atlantic continental shelf and slope of the United States – Shallow structure: U.S. Geological Survey Professional Paper 529-I, 44 p.
- Uchupi, E. and Emery, K.O., 1967, Structure of continental margin off Atlantic coast of United States: *American Association of Petroleum Geologists Bulletin*, v. 51, p. 223-234.
- Uchupi, E., Driscoll, N., Ballard, R.D., and Bolmer, S.T., 2001, Drainage of late Wisconsin glacial lakes and the morphology and late Quaternary stratigraphy of the New Jersey-southern New England continental shelf and slope: *Marine Geology*, v. 172, p. 117-145.
- Weed, E.G.A., Minard, J.P., Perry, W.J., Rhodehamel, E.C., and Robbins, E.I., 1974, Generalized pre-Pleistocene geologic map of the northern United States Atlantic continental margin: U.S. Geological Survey Miscellaneous Investigations Series I-861.

Chapter 3: Distribution of Submarine Landslides in the Gulf of Mexico

Introduction

Submarine landslides have been studied in the Gulf of Mexico for two reasons: first they can pose a hazard to offshore platforms and pipelines for hydrocarbon extraction and transportation and second, when more deeply buried they can serve either as hydrocarbon reservoirs or barriers in reservoirs depending on their composition. The threat of submarine landslides as a generator of tsunamis has not been addressed for the Gulf of Mexico region. Here we present a brief review of the literature on the distribution and style of submarine landslides that have occurred in the Gulf of Mexico during the Quaternary. This review will focus on landslides that have occurred in on the continental slope and rise in the Gulf of Mexico; with much of the discussion focused on the part of the basin within the U.S. EEZ due to the availability of a greater number of publications from this region.

Setting

The Gulf of Mexico is a small, geologically diverse ocean basin that includes three distinct geologic provinces: a carbonate province, a salt province, and canyon to deep-sea fan province (Figure 3-1a). The basement under the deep Gulf of Mexico is Upper Triassic to Lower Jurassic oceanic or transitional crust (Sawyer *et al.*, 1991). The stratigraphy of the overlying deposits records the subsequent evolution of this small ocean basin (Buffler, 1991). Three particular aspects of the basin's evolution that should be considered in an assessment of landslide activity within the basin are the Jurassic-aged salt that was deposited during the early stages of the opening of this ocean basin (Salvador, 1991a), the development and growth of extensive carbonate reef tracts during the late Jurassic and Cretaceous (Bryant *et al.*, 1991), and the siliciclastic sediment input from the North American continent during the latest Mesozoic and Cenozoic (Buffler, 1991).

Salt deposited in the late Jurassic Gulf of Mexico basin, the Louann salt, originally underlay large parts of Louisiana, southern Texas, and the area offshore of Mexico in the Bay of Campeche (Salvador, 1991a). As sediment eroded from the North American continent was deposited on this salt sheet

throughout the Mesozoic and Cenozoic, the increased load caused the salt to flow with it migrating southward from the source area into the northern Gulf of Mexico (Salvador, 1991b; Diegel *et al.*, 1995). Presently the Louann salt underlies large parts of the northern Gulf of Mexico continental shelf and continental slope. South of Louisiana and Texas, the Sigsbee Escarpment is a pronounced cliff that marks the seaward limit of the shallowest salt tongue (Bryant *et al.*, 1991). As the salt is loaded, it flows both seaward and also upward through the overlying sediment column as cylindrical salt domes. The morphology of the salt sheet varies considerably across the margin. Salt domes are most common under the continental shelf, and most of the original salt sheet between individual domes in this region has been removed in response to the sediment loading, and migrated farther seaward. Under the upper and middle continental slope the salt is shaped into a network of ridges and narrow salt sheets that are interrupted by sub circular basins, (referred to in this chapter as mini-basins) which have thin salt or no salt underlying them. Farther down slope, immediately north of the Sigsbee Escarpment, the salt is more sheet-like in appearance and has a thin sediment cover over it (Diegel *et al.*, 1995). Rates of salt movement are largely due to the confining pressure of sediment deposition. Calculated rates of salt motion range from as high as 17 cm/year to as low as only a few cms/1,000 yrs (Lowrie *et al.*, 1991).

In the southwestern corner of the Gulf, in the Bay of Campeche, the seafloor has an irregular morphology that is similar to that of the northern Gulf of Mexico slope and appears to be the result of sediment loading an underlying salt deposit (Figure 3-1a; Worzel *et al.*, 1968; Martin and Bouma, 1978).

During the Mesozoic, an extensive reef system developed around much of the margin of the Gulf of Mexico Basin by the vertical growth of reefs and carbonate shelf edge banks (Bryant *et al.*, 1969; Sohl *et al.*, 1991). This reef system is exposed along the Florida Escarpment and the Campeche Escarpment that fringe the eastern and southern margins of this basin (Figure 3-1a). These escarpments stand as much as 1,500 m above the abyssal plain floor, and have average gradients that commonly exceed 20° and locally are vertical (Jordan and Stewart, 1959; Paull *et al.*, 1990a). Reef growth ended during the Middle Cretaceous (Freeman-Lynde, 1983; Locker and Buffler, 1984; Paull *et al.*, 1990b), and subsequently the platform edges have been sculpted and steepened by a variety of erosional processes (Freeman-Lynde, 1983; Corso *et al.*, 1989; Paull *et al.*, 1991; Twichell *et al.*, 1996). The tops of the steep escarpments are in 1,500-2,500 m of water, and above these steep cliffs is a slope with a markedly gentler gradient (Figure 3-2a).

A huge volume of continental sediment has been supplied to the deep Gulf of Mexico basin from the North American continent during the Cenozoic through submarine canyons. These sediments were deposited in the central deep part of the Gulf of Mexico as a series of deep-sea fans. The oldest were deposited in the western part of the basin, and the depocenter shifted progressively eastward (Buffler, 1991). Three fan systems formed during the Pliocene and Pleistocene: Bryant Fan (Lee *et al.*, 1996; Twichell *et*

al., 2000), Mississippi Fan (Weimer, 1989), and Eastern Mississippi Fan (Weimer and Dixon, 1994). The Mississippi Fan is the largest of these three fans, and covers most of the eastern half of the deep Gulf of Mexico basin and reaches 4 km in thickness under the upper fan off the mouth of the Mississippi Canyon (Weimer, 1989; 1991). Sediment was supplied to the Mississippi Fan through the Mississippi Canyon which has retained its morphologic expression on the slope (Figure 3-1a). The canyons that supplied sediment to Bryant and Eastern Mississippi Fans have been largely erased by salt movement (Weimer and Dixon, 1994; Lee *et al.*, 1996; Twichell *et al.*, 2000).

Types of Submarine Mass Movements

Several classification schemes exist for submarine mass movements. For this report we use one presented by Locat and Lee (2002) that was adapted from the classification of subaerial mass movements proposed by the International Society for Soil Mechanics and Geotechnical Engineering (ISSMGE) Technical Committee on Landslides. While it has been observed that one type of mass movement can lead to another, here we briefly describe the end-member types.

- **Topples** – The displaced material usually is lithified rock that descends mainly through water as a coherent block that does not disintegrate during movement. Topples result in minimal lateral displacement.
- **Falls** – The displaced material mostly is lithified to semi-lithified material that is broken into smaller blocks and rubble during the failure process and descends mainly through water by falling, bouncing, and rolling. Falls also result in minimal lateral displacement.
- **Rotational slides** – The failed material undergoes rotation along a curved slip surface during displacement. This material tends to be rigid although in some cases beds within the failed mass are folded but do not undergo disintegration during translation.
- **Translational slides** – The failed material is translated along a discrete, flat slip surface. The material is rigid, and thus maintains its internal stratigraphy; however displacement can be great distances.
- **Debris flows** – Mass movements in which the failed material disintegrated during transport, and results in the deposit being a heterogeneous mix of clasts supported in a matrix of fine sediment. The clasts in debris flows vary in size and sediment texture.
- **Mudflows** – Mass movements of predominantly fine-grained material. These are similar to debris flows, but because of the more uniform texture their internal structure is not as clearly defined.
- **Turbidity currents** – Mass movements that involve the down slope movement of a relatively dilute suspension of sediment grains that are supported by the upward component of fluid turbulence.

Distribution of Submarine Landslides

Submarine landslides have occurred in each of the three provinces of the Gulf of Mexico basin although they vary in style and size among these different provinces. Landslides also have been active throughout much of the history of this basin, but this report will focus mostly on those that occurred during the Quaternary Period, up to the present.

Carbonate Province

Landslides in the carbonate provinces that fringe the eastern and southern Gulf of Mexico appear to have been derived from both the steep West Florida and Campeche Escarpments as well as from the gentler slopes above these escarpments (Figure 3-2a). On the escarpments themselves, the amount and style of erosion varies along their lengths. Landslides have removed material from the gentler slope above the Florida Escarpment as well, but this process apparently has acted on different parts of the West Florida Slope at different times. No information could be found on the processes acting on the slope above the Campeche Escarpment.

The presence of reef structures under the northern part of the Florida Escarpment suggests this part of the cliff has undergone little erosion since it originally formed during the Cretaceous (Locker and Buffler, 1984; Corso *et al.*, 1989; Twichell *et al.*, 1990). In fact, sidescan sonar imagery suggest that the only erosion along this section of the escarpment is the removal of a thin veneer of younger sediment that has accumulated as thin turbidity current or debris flow deposits at the foot of the escarpment (Figure 3-2b).

The carbonate platform edge that is exposed along the southern part of the Florida Escarpment and the Campeche Escarpment has been eroded since its initial formation and lagoonal facies are now exposed on the cliff face (Freeman-Lynde, 1983; Paull *et al.*, 1990b). The present morphology of these sections of the escarpments is quite different from the northern part of the Florida Escarpment (Figure 3-2a). Here canyons with steep sides and near-vertical headwalls, called box canyons (Paull *et al.*, 1991), incise these parts of the escarpments. These box canyons may be the result of dissolution of the limestone by discharge of acidic groundwater at the base of the escarpment in the canyon heads that resulted in collapse of the steep canyon headwalls (Paull *et al.*, 1990a). A large talus deposit has been identified in seismic profiles along the base of the Campeche Escarpment that was deposited prior to the mid-Cretaceous (Schlager *et al.*, 1984; Locker and Buffler, 1984). The full extent of this deposit is unknown because of limited seismic coverage. Breccia recovered from a DSDP hole near the base of the Campeche Escarpment (Schlager *et al.*, 1984; Halley *et al.*, 1984) presumably is the result of topples and falls from the escarpment face. The amount of material associated with an individual failure is unknown. Talus blocks up to 5-m across and rubble have been observed on the seafloor along the base of the southern part of the Florida Escarpment which suggests this cliff has recently undergone erosion (Paull *et al.*, 1990a; Twichell

et al., 1990). The talus deposits in the heads of some of the box canyons cover areas less than 15 km², and their thickness is unknown. Published information suggests that the recent falls and topples were limited to the southern part of the Florida Escarpment and perhaps the Campeche Escarpment (Twichell *et al.*, 1996), but those that have been mapped are of limited aerial extent and are concentrated in the heads of box canyons (Figure 3-2b).

Landslides on the West Florida Slope above the Florida Escarpment are sourced in Tertiary and Quaternary carbonate deposits. Mullins *et al.* (1986) mapped large collapse scars along the central part of the West Florida Slope near the latitude of Tampa, FL (Figure 3-2b). The entire slide scar is 120 km long, 30 km wide, and has 300-350 m relief. While the total volume of material removed is around 1,000 km³, there were at least 3 generations of failures with most of the sediment removal occurring prior to the middle Miocene. Presently these landslide scarps are buried and only local episodic failures have subsequently occurred along this section of the slope (Doyle and Holmes, 1985). Along the southern part of the West Florida Slope, Doyle and Holmes (1985) and Twichell *et al.* (1993) have mapped another extensive area of the slope that has undergone collapse (Figure 3-2b). Here the scarps are still exposed on the seafloor and have 50-150 m relief and are 10-70 km in length. Some of the mass-movement deposits are on the slope above the Florida Escarpment, but it is unknown how much of the failed material was transported farther and deposited at the base of the Florida Escarpment. The cross-cutting of the headwall scarps indicates that these landslides are composed of several smaller failure events (Twichell *et al.*, 1993). The age of these failures is not known, but Mullins *et al.* (1986) and Doyle and Holmes (1985) suggest periods of increased mass wasting which are probably associated with periods of higher sedimentation rates. If this is the case, then the landslides along the southern part of the West Florida Slope are most likely early Holocene or older in age (Doyle and Holmes, 1985).

Salt Province

No published information has been found on landslides in the salt province in the Bay of Campeche, so this discussion will focus on the northern Gulf of Mexico slope where good information is available on landslides. Presumably the northern Gulf is an appropriate analogue for the Bay of Campeche area (Figure 3-1a). Detailed bathymetric mapping of the salt province in the northern Gulf of Mexico shows that it has a unique morphology characterized by relatively small sub-circular basins that are 4-33 km long and have areas of 5-312 km² (Figure 3-3). These basins are bordered by narrow salt-cored ridges that stand 50-521 m above the basin floors (Pratson and Ryan, 1994).

Landslide deposits have been mapped in several of the mini-basins using GLORIA imagery (Rothwell *et al.*, 1991; Twichell *et al.*, 2000; Twichell *et al.*, 2005) as well as with high-resolution sidescan sonar, high resolution seismic profiles, and cores (Behrens, 1988; Lee and George, 2004; Orange *et al.*, 2003;

2004; Sager *et al.*, 2004, Silva *et al.*, 2004; Tripsanas *et al.*, 2004a; 2004b). The GLORIA imagery provides a regional perspective on the size and distribution of landslides, while the detailed studies provide more information on the types of failures. The GLORIA imagery identified 37 landslides in the salt province and along the base of the Sigsbee Escarpment (Figure 3-3a). The largest of these failures occurs in the northwestern Gulf of Mexico, is 114 km long, 53 km wide, covers about 2,250 km², and has been interpreted to consist of at least two debris flows (Rothwell *et al.*, 1991; McGregor *et al.*, 1993). This landslide lies offshore of the Rio Grande River system and Rothwell *et al.* (1991) suggest it is the result of failure of the shelf edge delta that formed off this river during the last lowstand of sea level.

The remaining landslides within the salt province are considerably smaller and cover areas ranging from 4-273 km² (Figure 3-3b). Most have sources on the walls of the mini-basins or on the Sigsbee Escarpment. The detailed studies indicate a wide variety of landslide types that include translational slides, rotational slides, debris flows, and creep movements (Lee and George, 2004; Orange *et al.*, 2004; Silva *et al.*, 2004). It has been suggested that triggering mechanisms for these landslides include shallow stratigraphic layers with overpressured pore waters (Orange *et al.*, 2003), salt movement (Lee and George, 2004; Tripsanas *et al.*, 2004a), oversteepening of shelf edge deltas (Tripsanas *et al.*, 2004b), and possibly gas hydrates (Twichell and Cooper, 2000).

Information is limited on the age of landslides in the salt province. The most extensive study (Tripsanas *et al.*, 2004a; b) indicates that most of the youngest landslides sampled in the salt province occurred during oxygen isotope stages 2, 3, and 4 (18,170-71,000 yr BP) when salt movement due to sediment loading was most active. One unpublished age date of a sample below a thin landslide deposit (<3 m thick) indicates that it is younger than 6,360 yr BP (H. Nelson, personal communication). Localized failure of mini-basin walls may continue to be active, but available data suggests these small failures were more prevalent during the last lowstand of sea level.

Canyon/Fan Province

Three canyon/fan systems formed during the Quaternary period; the Bryant, Mississippi, and Eastern Mississippi systems (Figure 3-1a). Of these three systems, the Mississippi is the largest and youngest (Weimer, 1989). During the latest Pleistocene, sediment was supplied to the Mississippi Fan from a point source, the Mississippi Canyon (Bryant *et al.*, 1991). Regional seismic stratigraphic analysis has been used to divide the Mississippi Fan into 17 seismic sequences (Weimer, 1989): most contain a basal chaotic unit inferred to be mass-transport deposits. The mass-transport deposits are overlain by channel-levee complexes, which are capped by a thin interval of hemipelagic sediment that represents a period of limited sediment input. Depositional style within each sequence has been attributed to changes in sea level: the mass-transport complexes were deposited during falling sea level and the initial part of the lowstand; the channel-levee complexes formed during the lowstand and the onset of the transgression; and condensed sections were

deposited during highstands (Weimer, 1989). According to this interpretation, the Holocene should have been a period of quiescence.

However, studies of the Mississippi Canyon and present surface of the Mississippi Fan indicate a different stratigraphic progression (Twichell *et al.*, 1990; Twichell *et al.*, in press) and reveal evidence of landslides at several scales. Turbidity current deposits and thin debris flow deposits associated with channel-levee development have been mapped and sampled on the distal fan (Twichell *et al.*, 1990; Twichell *et al.*, 1992; Nelson *et al.*, 1992; Schwab *et al.*, 1996). Some of these deposits have been mapped with sidescan sonar and cores and are relatively small: covering areas less than 331 km², and having volumes less than 1 km³ (Twichell *et al.*, in press). At the other extreme is a large landslide complex that covers approximately 23,000 km² of the middle and upper fan (Figure 3-4) and reaches 100 m in thickness (Walker and Massingill, 1970; Normark *et al.*, 1986; Twichell *et al.*, 1992). The total volume of this deposit cannot be accurately estimated because of inadequate seismic coverage, but, assuming an average thickness of 75 m, the volume would be 1,725 km³. Seismic profiles and GLORIA imagery suggest that this feature consists of at least two separate events (Twichell *et al.*, in press). The Mississippi Canyon appears to have the source area for these landslide deposits (Walker and Massingill, 1970; Coleman *et al.*, 1983; Goodwin and Prior, 1989; Lowrie *et al.*, 2004). Borings and seismic data from the head of Mississippi Canyon (Goodwin and Prior, 1989) indicate that there were alternating episodes of canyon filling and excavation between 19,000 and 7,500 yr BP, and Coleman *et al.* (1983) estimate total volume of sediment removed was approximately 8,600 km³. One DSDP hole through this landslide deposit penetrated thick sections of tilted beds (Normark *et al.*, 1986). This information in conjunction with the GLORIA imagery which shows a swirling pattern on the surface of the youngest part of this failure suggests it may be a translational slide that has undergone deformation but not complete disintegration as it moved (Figure 3-4).

The timing of these landslides needs to be refined to determine whether they are associated with glacial meltwater floods that discharged into the Gulf of Mexico (Laventer *et al.*, 1982; Marchitto and Wei, 1995; Aharon, 2003), or whether they occurred more recently. Available age dates indicate that this large landslide complex is younger than 11,100 yr BP, when turbidity current and debris flow transport to the distal fan ceased due to the channel being blocked by part of this landslide (Schwab *et al.*, 1996; Twichell *et al.*, in press). This large landslide is older than 7,500 yr BP, when hemipelagic sedimentation resumed in Mississippi Canyon and covered the headwall scarps of the failures (Prior *et al.*, 1989). Meltwater discharge to the Gulf of Mexico ceased about 9,000 yr BP (Marchitto and Wei, 1995; Aharon, 2003). Refining the timing of these large landslides is needed to determine if they are associated with meltwater floods or are younger than the floods and formed under conditions similar to the present.

The Bryant and Eastern Mississippi Fans may both have canyon head failures associated with them as well. The Bryant Canyon system was immediately downslope of a shelf edge delta system (Morton and Sutter, 1996), and failure of this system has been proposed as the explanation for

thick chaotic deposits in mini basins along the path of this canyon system (Lee *et al.*, 1996; Prather *et al.*, 1998; Twichell *et al.*, 2000; Tripsanas *et al.*, 2004a). Debris from the failure of the shelf edge delta was transported down the Bryant Canyon system (Lee *et al.*, 1996; Prather *et al.*, 1998), but these landslide deposits predate and are buried by the smaller landslides off the mini-basin walls that are shown in Figure 3-3 (Twichell *et al.*, 2000).

The Eastern Mississippi Fan system also has a relatively large landslide that partially buries the fan channel that supplied this fan (Figure 3-4). This landslide deposit is approximately 154 km long, as much as 22 km wide, and covers an area of 2,410 km². The volume of the deposit and its age are unknown.

Summary

Landslides occur in all three provinces (carbonate, salt, and canyon/fan) in the Gulf of Mexico. The largest failures are found in the canyon/fan province. More information is needed on the timing of the large failures that filled the Bryant Canyon and covered the upper parts of the Mississippi and Eastern Mississippi Fans (Figure 3-5). The resumption of hemipelagic sedimentation in the head of Mississippi Canyon by 7,500 yr BP (Goodwin and Prior, 1988) indicates that at least the largest of these landslide complexes had ceased being active by mid-Holocene time. Further age dating is needed to refine the timing of the landslides derived from the Mississippi Canyon area to determine if they are associated with meltwater floods discharged into the Gulf of Mexico during the early part of the Holocene or whether they were triggered by other processes at a later time.

Future Directions

The Gulf of Mexico is one of the most intensely studied ocean basins because of the energy resources it contains, but information for understanding the timing, style, and distribution of landslides is still incomplete. Little published information could be found on landslides along the Mexican margin, and this region needs to be addressed. Large sections of the margins surrounding this ocean basin have not been surveyed with multibeam techniques: acquisition of this bathymetric data set would improve our understanding of recent landslide source areas and triggering mechanisms. Published multibeam bathymetry is not available either for the Mexican margin or for the northern part of the Florida Escarpment, the West Florida Slope, or the slope in the northwestern corner of the Gulf of Mexico.

The available information on the timing of landslides in the Gulf of Mexico needs to be refined as well. Many of the available ages are based on faunal assemblages in sediment cores; accurate AMS dates of samples within and immediately above landslide deposits would greatly improve our understanding of the temporal distribution of landslides and how it varies between the three provinces.

Figures

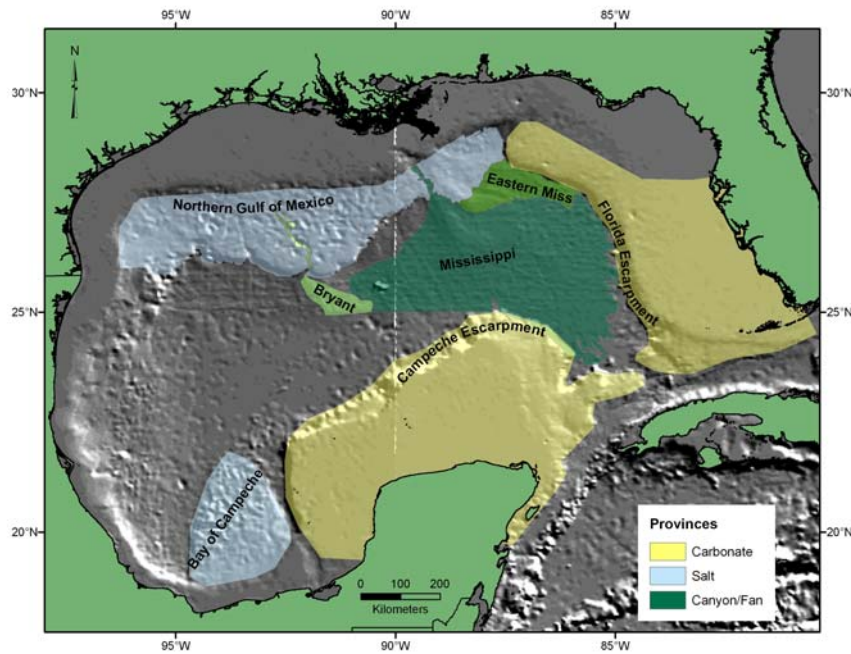


Figure 3-1a: Location map showing the extent of the carbonate, salt, and canyon/fan provinces in the Gulf of Mexico basin. The Bryant, Mississippi, and Eastern Mississippi Fans are the three youngest fans in the Gulf of Mexico, and, of these, the Mississippi is youngest.

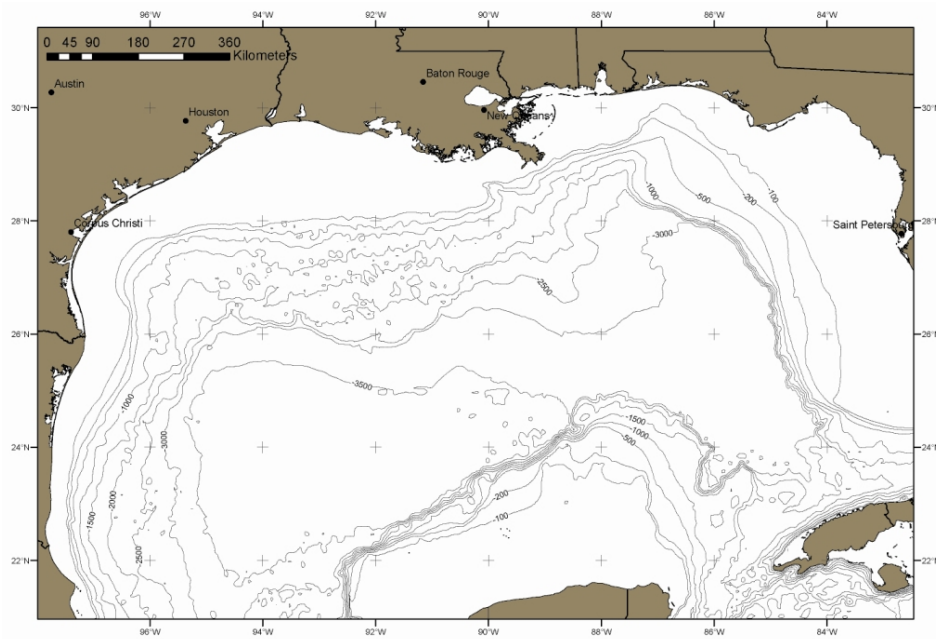


Figure 3-1b: Bathymetric map of the Gulf of Mexico.

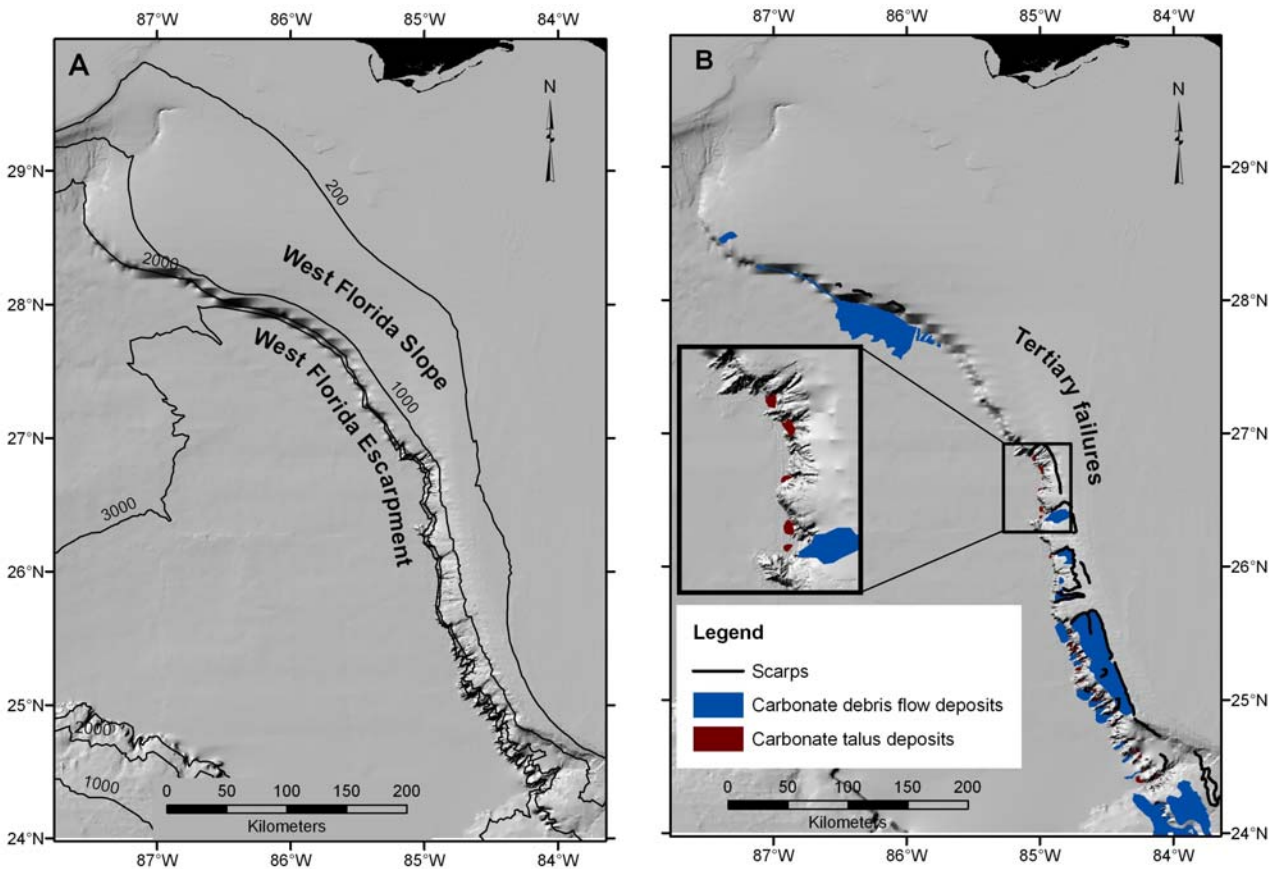


Figure 3-2: (A) Morphology of the West Florida Escarpment and the West Florida Slope, and (B) the extent and distribution of carbonate debris flow deposits and talus deposits derived from this part of the carbonate province. “Tertiary failures” marks the general location of older landslides mapped by Mullins *et al.* (1986) that now have been completely buried. Inset box shows a detailed view of some of the carbonate talus deposits. Equivalent information is not available for the slope above the Campeche Escarpment.

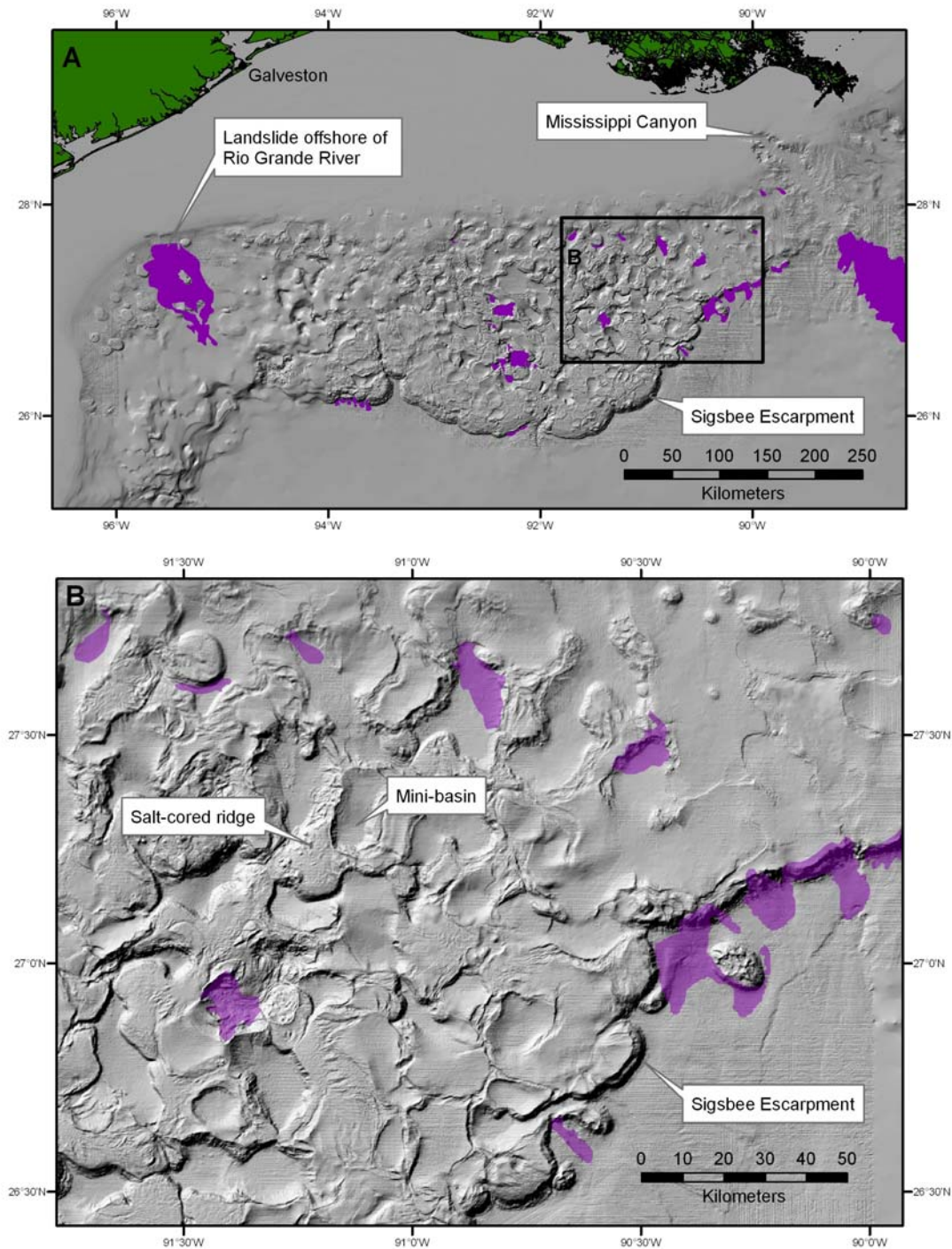


Figure 3-3: (A) Shaded relief image of a large part of the northern Gulf of Mexico salt deformation province west of Mississippi Canyon showing the irregular morphology of this continental slope and the distribution of landslides (purple areas), and (B) an enlarged view of part of this region showing the relation of landslides (purple areas) to the mini basins and the Sigsbee Escarpment.

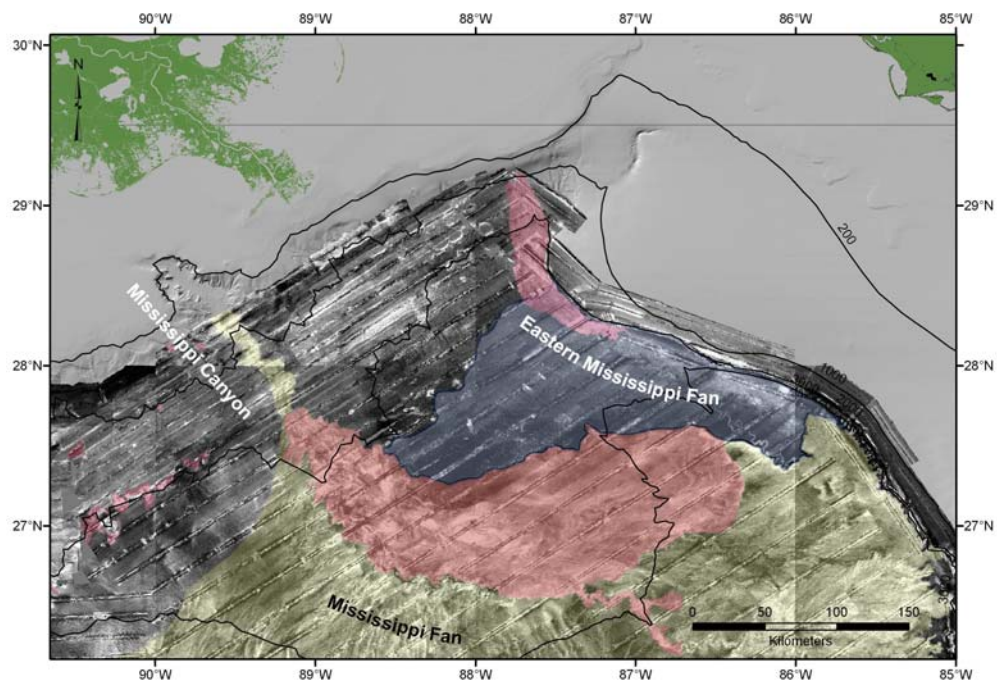


Figure 3-4: GLORIA sidescan sonar imagery showing part of the Mississippi Fan (yellow) and Eastern Mississippi Fan (blue) and two large landslide areas (red) that spread across the upper parts of these two fans. The landslide on the upper Mississippi Fan was sourced from the Mississippi Canyon region (Coleman *et al.*, 1983) and is the largest Quaternary landslide found in the Gulf of Mexico.

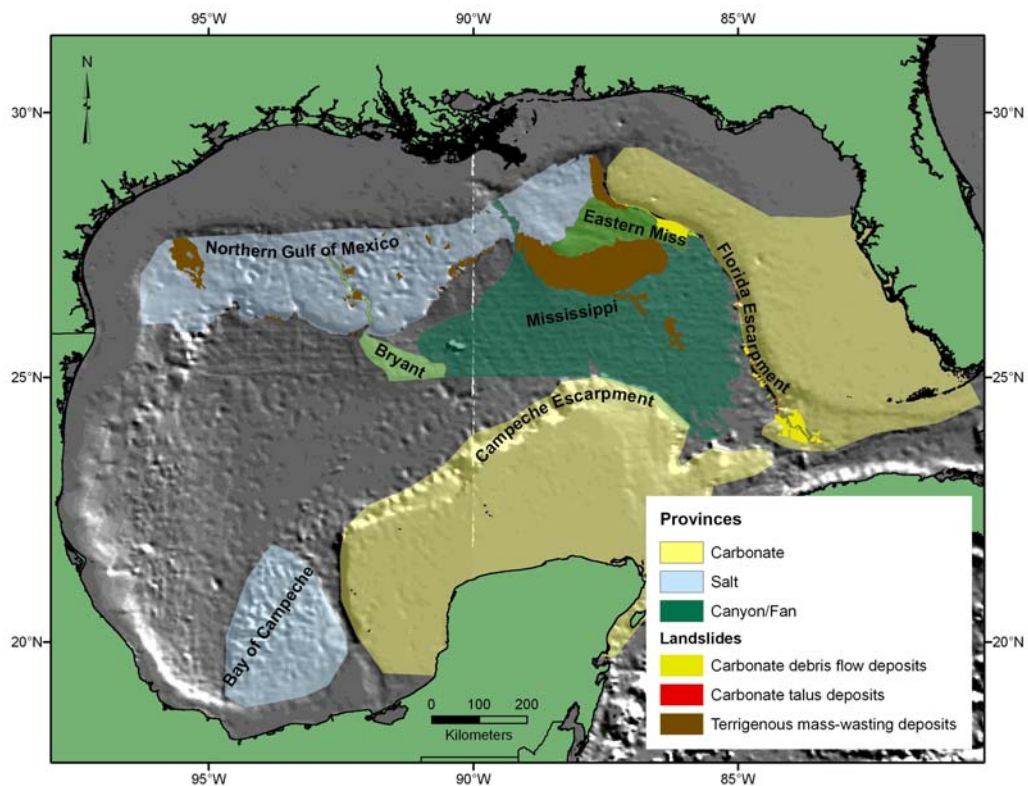


Figure 3-5: Summary map showing the size, distribution, and composition of landslides in the three provinces. Carbonate talus deposits are too small to show at this scale.

References

- Aharon, P., 2003, Meltwater flooding events in the Gulf of Mexico revisited: Implications for rapid climate changes during the last deglaciation: *Paleoceanography*, v. 18, 1079, doi: 10.1029/2002PA000840.
- Behrens, W.E., 1988, Geology of a continental slope oil seep, northern Gulf of Mexico: *American Association of Petroleum Geologists Bulletin*, v. 72, p. 105-114.
- Bryant, W.R., Meyerhoff, A.A., Brown, N.K., Furrer, M.A., Pyle, T.E., and Antoine, J.W., 1969, Escarpments, reef trends, and diapiric structures, eastern Gulf of Mexico: *American Association of Petroleum Geologists Bulletin*, v. 53, p. 2506-2542.
- Bryant, W.R., Lugo, J., Cordova, C., and Slavador, A., 1991, Physiography and bathymetry, in Salvador, A. (Editor), *The Geology of North America*, Vol. J, Gulf of Mexico Basin: Geological Society of America, Boulder, CO, p. 13-30.
- Buffler, R.T., 1991, Seismic stratigraphy of the deep Gulf of Mexico basin and adjacent margins, in Salvador, A. (Editor), *The Geology of North America*, Vol. J, Gulf of Mexico Basin: Geological Society of America, Boulder, CO, p. 353-387.
- Coleman, J.M., Prior, D.B., and Lindsay, J.F., 1983, Deltaic influences on shelf edge instability processes, in Stanley, D.J., and Moore, G.T. (Editors), *The shelfbreak: Critical interface on continental margins*: Society of Economic Paleontologists and Mineralogists Special Publication 33, p. 121-137.
- Corso, W., Austin, J.A., and Buffler, R.T., 1989, The early Cretaceous platform off northwest Florida: Controls on morphologic development of carbonate margins: *Marine Geology*, v. 86, p. 1-14.
- Diegel, F.A., Karlo, J.F., Schuster, D.C., Shoup, R.C., and Tauvers, P.R., 1995, Cenozoic structural evolution and tectono-stratigraphic framework of the northern Gulf Coast continental margin, in Jackson, M.P.A., Roberts, D.G., and Snelson, S. (Editors), *Salt tectonics: A global perspective*: AAPG Memoir 65, p. 109-151.
- Doyle, L.J., and Holmes, C.W., 1985, Shallow structure, stratigraphy, and carbonate sedimentary processes of West Florida Continental Slope: *American Association of Petroleum Geologists Bulletin*, v. 69, p. 1133-1144.
- Freeman-Lynde, R.P., 1983, Cretaceous and Tertiary samples dredged from the Florida Escarpment, eastern Gulf of Mexico: *Transactions Gulf Coast Association of Geological Societies*, v. 33, p. 91-99.
- Goodwin, R.H., and Prior, D.B., 1989, Geometry and depositional sequences of the Mississippi Canyon, Gulf of Mexico: *Journal of Sedimentary Petrology*, v. 59, p. 318-329.
- Halley, R.B., Pierson, B.J., and Schlager, W., 1984, Alternative diagenetic models for Cretaceous talus deposits, Deep Sea Drilling Project site 536, Gulf of Mexico, in, Buffler, R.T., Schlager, W. *et al.*, Initial Reports of the Deep Sea Drilling Project v. 77, Washington DC, U.S. Government Printing Office, p. 397-408.

- Jordan, G.F., and Stewart, H.B., 1959, Continental slope off southwest Florida: *American Association of Petroleum Geologists Bulletin*, v. 43, p. 974-991.
- Laventer, A., Williams, D.F., and Kennett, J.P., 1982, Dynamics of the Laurentide Ice Sheet during the last deglaciation: Evidence from the Gulf of Mexico: *Earth and Planetary Science Letters*, v. 59, p. 11-17.
- Lee, G.W., Watkins, J.S., and Bryant, W.R., 1996, Bryant Canyon fan system: An unconfined large river-sourced system in the northwestern Gulf of Mexico: *American Association of Petroleum Geologists Bulletin*, v. 80, p. 340-358.
- Lee, E.Y.D., and George, R.A., 2004, High-resolution geological AUV survey results across a portion of the eastern Sigsbee Escarpment: *American Association of Petroleum Geologists Bulletin*, v. 88, p. 747-764.
- Locat, J., and Lee, H. J., 2002, Submarine landslides: advances and challenges: *Canadian Geotechnical Journal*, v. 39, p. 193-212.
- Locker, S.D. and Buffler, R.T., 1984, Comparison of Lower Cretaceous carbonate shelf margins, northern Campeche Escarpment and northern Florida Escarpment, Gulf of Mexico, in Bally, P.W. (Editor), *Seismic Expression of Structural Styles – A Picture and Work Atlas*, American Association of Petroleum Geologists Studies in Geology Series, No. 15, v. 2, p. 123-128.
- Lowrie, A., Lutken, C.B., and McGee, T.M., 2004, Multiple outer shelf deltas and downslope massive mass-wastings characterize the Mississippi Canyon, northern Gulf of Mexico: *Transactions Gulf Coast Association of Geological Societies*, v. 54, p. 383-392.
- Lowrie, A., Yu, Z., and Lerche, I., 1991, Hydrocarbon trap types and deformation styles modeled using quantified rates of salt movement, Louisiana margin: *Transactions-Gulf Coast Association of Geological Societies*, v. 41, p. 445-459.
- Marchitto, T.M., and Wei, K., 1995, History of Laurentide meltwater flow to the Gulf of Mexico during the last deglaciation, as revealed by reworked calcareous nannofossils: *Geology*, v. 23, p. 779-782.
- Martin, R.G., and Bouma, A.H., 1978, Physiography of Gulf of Mexico, in Bouma, A.H., Moore, G.T., and Coleman, J.M., eds., *Framework, facies, and oil-trapping characteristics of the upper continental margin*: American Association of Petroleum Geologists Studies in Geology no. 7, p. 3-19.
- McGregor, B.A., Rothwell, R.G., Kenyon, N.H., and Twichell, D.C., 1993, Salt tectonics and slope failure in an area of salt domes in the northwestern Gulf of Mexico, in Schwab, W.C., Lee, H.J., and Twichell, D.C. (Editors), *Submarine Landslides: Selected Studies in the U.S. Exclusive Economic Zone*: U.S. Geological Survey Bulletin, 2002, p. 92-96.
- Morton, R.A., and Suter, J.R., 1996, Sequence stratigraphy and composition of Late Quaternary shelf-margin deltas, northern Gulf of Mexico: *American Association of Petroleum Geologists Bulletin*, v. 80, p. 505-530.
- Mullins, H.T., Gardulski, A.F., and Hine, A.C., 1986, Catastrophic collapse of the West Florida carbonate platform margin: *Geology*, v. 14, p. 167-170.
- Nelson, C.H., Twichell, D.C., Schwab, W.C., Lee, H.J., and Kenyon, N.H.,

- 1992, Late Pleistocene turbidite sand beds and chaotic silt beds in the channelized distal outer fan lobes of Mississippi Fan: *Geology*, v. 20, p. 693-696.
- Normark, W.R., Meyer, A.H., Cremer, M., Droz, L., O'Connell, S., Pickering, K.T., Stelting, C.E., Stow, D.A.V., Brooks, G.R., Mazzullo, J., Roberts, H., and Thayer, P., 1986, Summary of drilling results for the Mississippi Fan and considerations for application to other turbidite systems, in Bouma, A.H., Coleman, J.M., Meyer, A.W., *et al.* (Editors), Initial Reports of the Deep Sea Drilling Project: U.S. Government Printing Office, Washington, D.C., v. 96, p. 425-436.
- Orange, D.L., Saffer, D., Jeanjean, P., Khafaji, Z.A., Humphrey, G., and Riley, G., 2003, Measurements and modeling of the shallow pore pressure regime at the Sigsbee Escarpment: Successful prediction of overpressure and ground-truthing with borehole measurements: *The Leading Edge*, v. 22, p. 906-913.
- Orange, D.L., Angell, M.M., Brand, J.R., Thomson, J., Buddin, T., Williams, M., Hart, W., Berger, W.J., 2004, Geologic and shallow salt tectonic setting of the Mad Dog and Atlantis fields: Relationship between salt, faults, and seafloor geomorphology: *The Leading Edge*, v. 23, p. 354-365.
- Paull, C.K., Spiess, F.N., Curray, J.R., and Twichell, D.C., 1990a, Origin of Florida Canyon and the role of spring sapping on the formation of submarine box canyons: *Geological Society of America Bulletin*, v. 102, p. 502-515.
- Paull, C.K., Freeman-Lynde, R.P., Bralower, T.J., Gardemal, J.M., Neumann, A.C., D'Argenio, B., and Marsella, E., 1990b, Geology of the strata exposed on the Florida Escarpment: *Marine Geology*, v. 91, p. 177-194.
- Paull, C.K., Twichell, D.C., Spiess, F.N., and Curray, J.R., 1991, Morphological development of the Florida Escarpment: Observations on the generation of time transgressive unconformities in carbonate terrains: *Marine Geology*, v. 101, p. 181-201.
- Prather, B.E., Booth, J.R., Steffens, G.S., and Craig, P.A., 1998, Classification, lithologic calibration, and stratigraphic succession of seismic facies of intraslope basins, deep-water Gulf of Mexico: *American Association of Petroleum Geologists Bulletin*, v. 82, p. 701-728.
- Pratson, L.F., and Ryan, W.B.F., 1994, Pliocene to Recent infilling and subsidence of intraslope basins offshore Louisiana: *American Association of Petroleum Geologists Bulletin*, v. 78, p. 1483-1506.
- Rothwell, R.G., Kenyon, N.H., and McGregor, B.A., 1991, Sedimentary features of the south Texas continental slope as revealed by side-scan sonar and high-resolution seismic data: *American Association of Petroleum Geologists Bulletin*, v. 75, p. 298-312.
- Sager, W.W., and MacDonald, I.R., and Hou, R., 2004; Side-scan sonar imaging of hydrocarbon seeps on the Louisiana continental slope: *American Association of Petroleum Geologists Bulletin*, v. 88, p. 725-746.
- Salvador, A., 1991a, Triassic-Jurassic: in Salvador, A. (Editor), The Geology of North America, Vol. J., The Gulf of Mexico Basin, Geological Society of America, Boulder, CO, p. 131-180.

- Salvador, A., 1991b, Origin and development of the Gulf of Mexico basin: *in* Salvador, A. (Editor), *The Geology of North America*, Vol. J., *The Gulf of Mexico Basin*, Geological Society of America, Boulder, CO, p. 389-444.
- Sawyer, D.S., Buffler, R.T., and Pilger, R.H., 1991, The crust under the Gulf of Mexico basin, *in* Salvador, A. (Editor), *The Geology of North America*, Vol. J, *Gulf of Mexico Basin*: Geological Society of America, Boulder, CO, p. 53-72.
- Schlager, W., Buffler, R.T., and Scientific Party of DSDP Leg 77, 1984, DSDP Leg 77; Early history of the Gulf of Mexico: *Geological Society of America Bulletin*, v. 95, p. 226-236.
- Schwab, W.C., Lee, H.J., Twichell, D.C., Locat, J., Nelson, C.H., McArthur, W.G., and Kenyon, N.H., 1996, Sediment mass-flow processes on a depositional lobe, outer Mississippi Fan: *Journal of Sedimentary Research*, v. 66, p. 916-927.
- Silva, A.J., Baxter, C.D.P., LaRosa, P.T., and Bryant, W.R., 2004, Investigation of mass wasting on the continental slope and rise: *Marine Geology*, v. 203, p. 355-366.
- Sohl, N., Martinez, E., Salmeron-Urena, P., and Soto-Jaramillo, F., 1991, Upper Cretaceous, *in* Salvador, A. (Editor), *The Geology of North America*, Vol. J., *The Gulf of Mexico Basin*, Geological Society of America, Boulder, CO, p. 205-244.
- Tripsanas, E.K., Bryant, W.R., and Phaneuf, B.A., 2004, Slope-instability processes caused by salt movements in a complex deep-water environment, Bryant Canyon area, northwest Gulf of Mexico: *American Association of Petroleum Geologists Bulletin*, v. 88, p. 801-824.
- Tripsanas, E.K., Bryant, W.R., and Phaneuf, B.A., 2004, Depositional processes of uniform mud deposits (unifites), Hedberg Basin, northwest Gulf of Mexico: New perspectives: *American Association of Petroleum Geologists Bulletin*, v. 88, p. 825-840.
- Twichell, D.C., Parson, L.M., and Paull, C.K., 1990, Variations in the styles of erosion along the Florida Escarpment, eastern Gulf of Mexico: *Marine and Petroleum Geology*, v. 7, p. 253-266.
- Twichell, D.C., Kenyon, N.H., Parson, L.M., and McGregor, B.A., 1991, Depositional patterns of the Mississippi Fan surface: Evidence from GLORIA II and high-resolution seismic profiles, *in* Weimer, P., and Link, M.H. (Editors), *Seismic Facies and Sedimentary Processes of Submarine Fans and Turbidite Systems*, Springer-Verlag, New York, p. 349-363.
- Twichell, D.C., Schwab, W.C., Nelson, C.H., Lee, H.J., and Kenyon, N.H., 1992, Characteristics of a sandy depositional lobe on the outer Mississippi Fan from SeaMARC IA sidescan sonar images: *Geology*, v. 20, p. 689-692.
- Twichell, D.C., Valentine, P.C., and Parson, L.M., 1993, Slope failure of carbonate sediment on the West Florida Slope, *in*, Schwab, W.C., Lee, H.J., and Twichell, D.C. (Editors), *Submarine landslides: Selected studies in the U.S. Exclusive Economic Zone*, U. S. Geological Survey Bulletin 2002, p. 69-78.

- Twichell, D.C., Dillon, W.P., Paull, C.K., and Kenyon, N.H., 1996, Morphology of carbonate escarpments as an indicator of erosional processes, *in* Gardner, J. V. Field, M.E., and Twichell, D.C. (Editors), *Geology of the United States' Seafloor: The view from GLORIA*, Cambridge University Press, p. 97-107.
- Twichell, D.C., and Cooper, A.K., 2000, Relation between sea floor failures and gas hydrates in the Gulf of Mexico; a regional comparison: *American Association of Petroleum Geologists Annual Convention, v. 9*, p. A150.
- Twichell, D.C., Nelson, C.H., and Damuth, J.E., 2000, Late-stage development of the Bryant Canyon turbidite pathway on the Louisiana continental slope, *in* Weimer, P., Slatt, R.M., Coleman, J., Rosen, N.C., Nelson, H., Bouma, A.H., Styzen, M.J., and Lawrence, D.T. (Editors), *Deep-Water Reservoirs of the World: Proceedings of the Gulf Coast Section SEPM*, p. 1032-1044, CD-ROM.
- Twichell, D.C., Cross, V.A., Paskevich, V.F., Hutchinson, D.R., Winters, W.J., and Hart, P.E., 2005, GIS of selected geophysical and core data in the northern Gulf of Mexico continental slope collected by the U.S. Geological Survey: U.S. Geological Survey Open-File Report 2005-1071, 1 DVD-ROM.
- Twichell, D.C., Nelson, C.H., Kenyon, N. and Schwab, W., in press, The influence of external processes on the latest Pleistocene and Holocene evolution of the Mississippi Fan, *in*, Kneller, B., McCaffrey, W., Martinsen, O., and Posamentier, H. (Editors), *External Controls on Deep Water Depositional Systems: Climate, sea-level, and Sediment Flux*, SEPM Special Publication.
- Walker, J.R., and Massingill, J.V., 1970, Slump features on the Mississippi Fan, northeastern Gulf of Mexico: *Geological Society of America Bulletin, v. 81*, p. 3101-3108.
- Weimer, P., 1989, Sequence stratigraphy of the Mississippi Fan (Plio-Pleistocene), Gulf of Mexico: *Geo-Marine Letters, v. 9*, p. 185-272.
- Weimer, P., 1991, Seismic facies, characteristics, and variations in channel evolution, Mississippi Fan (Plio-Pleistocene), Gulf of Mexico, *in* Weimer, P., and Link, M.H. (Editors), *Seismic Facies and Sedimentary Processes of Submarine Fans and Turbidite Systems*, Springer-Verlag, New York, p. 323-347.
- Weimer, P. and Dixon, B.T., 1994, Regional sequence stratigraphic setting of the Mississippi Fan complex, northern deep Gulf of Mexico: Implications for evolution of the northern Gulf basin margin, *in* Weimer, P., Bouma, A.H., and Perkins, B.F. (Editors), *Submarine fans and turbidite systems: Sequence stratigraphy, reservoir architecture and production characteristics*, GCSEPM Foundation 15th Annual Research Conference, p. 373-381.
- Worzel, J.L., Leyden, R., and Ewing, M., 1968, Newly discovered diapirs in the Gulf of Mexico: *American Association of Petroleum Geologists Bulletin, v. 52*, p. 1194-1203.

Chapter 4: Far-field submarine landslide sources

Numerous debris deposits from subaerial and submarine landslide have been identified along the Canadian, European and African coasts of the Atlantic Ocean (*e.g.*, Canals *et al.*, 2004; Piper and McCall, 2003; Weaver and Mienert, 2003).

Canary Islands

Perhaps the most publicized hazard is that of a possible collapse of Cumbre Vieja, a volcano on the Canary island of La Palma (Ward and Day, 2001). As envisioned by Ward and Day (2001), a flank collapse of the volcano may drop a rock volume of up to 500 km³ into the surrounding ocean. The ensuing submarine slide, which was assumed to propagate at a speed of 100 m/s, will generate a strong tsunami with amplitudes of 25 m in Florida. In addition, they claimed that the collapse of Cumbre Vieja is imminent.

In our opinion, the danger to the U.S. Atlantic coast from the possible collapse of Cumbre Vieja is exaggerated. Mader (2001) pointed out that Ward and Day's (2001) assumption of linear propagation of shallow water waves is incorrect, because it only describes the geometrical spreading of the wave and neglects dispersion effects. A more rigorous hydrodynamic modeling by Gisler *et al.* (2006), confirms Mader's criticism. Their simulations show significant wave dispersion and predict amplitude decay proportional to r^{-1} for a 3-dimensional model and $r^{-1.85}$ for a 2-D model. (r is distance). Their predicted wave amplitude for Florida is between 1-77 cm. They use slightly smaller volume, 375 km³, than Ward and Day (2001), but a much higher slide speed, that is much closer to the phase speed for tsunamis in the deep ocean (4,000 m of water). The amplitude in Ward and Day (2001) model scales proportionally with rock volume times slide speed. Hence, the much smaller predicted amplitude of Gisler *et al.* (2006) for the Florida coast cannot be attributed to the smaller slide volume. Moreover, typical speeds of landslides are thought to be 20-80 m/s, slower than assumed by either model (ten Brink *et al.*, 2006a, and references therein).

Masson *et al.* (2002) have identified at least 14 landslides with volumes ranging between 50-500 km³ taking place within the last 1.3 m.y., or an average of 1 slide per 10⁵ yr. However, volcanoclastic turbidites that are correlated with the two most recent landslides in the Canary Islands shows stacked sub-units within the turbidite bed, which may indicate multiple stages of landslide failures, not a single catastrophic collapse (Wynn and Masson,

2003). Therefore, the recurrence interval may be shorter than 10^5 yr but the landslide volumes are also smaller.

Other landslide sources along the continental margin

Many submarine landslides have been discovered along the glaciated margins of northern Europe and Canada (Canals *et al.*, 2004; Piper and McCall, 2003; Weaver and Mienert, 2003, Leynaud *et al.*, submitted).

The largest of these landslides is the Storegga landslide (Figure 4-1), which caused a tsunami that impacted the coasts of Norway (runup of ≤ 13 m), the Faeroes islands (>14 m), Shetland islands (>20 m), Scotland and northern England (3-6 m), and Iceland (Bondevik *et al.*, 2005). The impacted areas are all within 600 km of the slide. The runup observations were fit with a retrogressive slide source with a relatively low slide speed (25-30 m/s) (Bondevik *et al.*, 2005). The Storegga slide is a composite failure with 7 slides occurring during the past 0.5 m.y., when the ice sheet started advancing across the continental shelf (Solheim *et al.*, 2005, and ref. within). The latest and largest landslide, which also caused the tsunami, is dated at 8150 yr BP. The total volume of the latest slide is 2,500-3,000 km³, the area of the slide scar is 27,000 km² and the length of the headwall is 290 km. The repeated failures within the same area are explained by excess pore pressure in the sediments due to rapid loading from glacial deposits, followed by triggering by earthquakes (Bryn *et al.*, 2005).

Several scarps, disturbances in glacial sediments, and debris flow were also identified along the Scotia margin, immediately NE of the U.S. border (Piper and McCall, 2003). A very large failure event in the eastern Scotian margin at 0.15 m.y. has released perhaps 10 times the volume of sediments released during the 1929 Grand Banks landslide (Piper and Ingram, 2003). Increased deposition and perhaps slope failure on the Scotian margin occurred at 0.5 m.y. when the glacial advance reached close to the shelf edge (Piper *et al.*, 2003). Deposition rate on the slope decreased about 8,000 years ago by a factor of 20-50 as deglaciation came to an end (Piper *et al.*, 2003). Among the 23 dated slope failures in the Grand Banks and the Scotia shelf, only two postdate the Holocene, one of them being the 1929 Grand Banks failure (Piper *et al.*, 2003).

Other submarine landslides were identified along the northern European margin (Kenyon, 1987), and the Puerto Rico trench (ten Brink *et al.*, 2006a, b), but to our knowledge, none of them are associated with very large deposit volumes. The Puerto Rico landslide scarps are generally in deep ($>3,000$ m) water, but are located on steep carbonate slopes, and have the characteristics of rock falls (ten Brink *et al.*, 2006a). Hence, the initial slide acceleration of falling competent blocks may be higher than along most other margins described above, although this is only a conjecture.

The mid-Atlantic ridge

The mid-Atlantic ridge is one of the few tectonic features in the Atlantic Ocean, which is associated with frequent earthquake activity. Two magnitude 7+ earthquakes took place on the ridge between latitudes 10°-50° during the last 34 years. High seafloor slope angles and relatively fractured basaltic and gabbroic rocks are often encountered along both the rift valley and the transform valley, and they may be susceptible to landslides. A scarp and debris field at a depth of 2700 – 3100 m were found at latitude 26°27'N in an area of steep slopes (14-23°) (Tucholke, 1992). The estimated slide volume is 19km³ and the slide took place within the past 0.45 m.y. (Tucholke, 1992). Massive slumps of gabbroic bedrock on steep slopes (~30°) were observed at the intersection between the Kane Transform and the ridge at 23°38'N (Gao, 2006). However, about 3/4 of the ridge length between 10°-45°N are not yet surveyed in detail (Marine Geoscience Data Center, www.marine-geo.org).

The Azores are a group of volcanic islands on the triple junction between the North American, Eurasian and African plates at 37°-39°N. The rate of volcanic activity in the Azores is lower than in the Canary Islands and the slope angles and height of the volcanic islands are also smaller. A devastating earthquake on October 22nd, 1522 induced several landslides over San Miguel Island. 5,000 lives were lost by the subaerial slide, which involved a volume of about 6,75x10⁶ m³ and a small tsunami has occurred. (http://www.acri.fr/retina/Deliverables/D48_M42.htm)

Figures

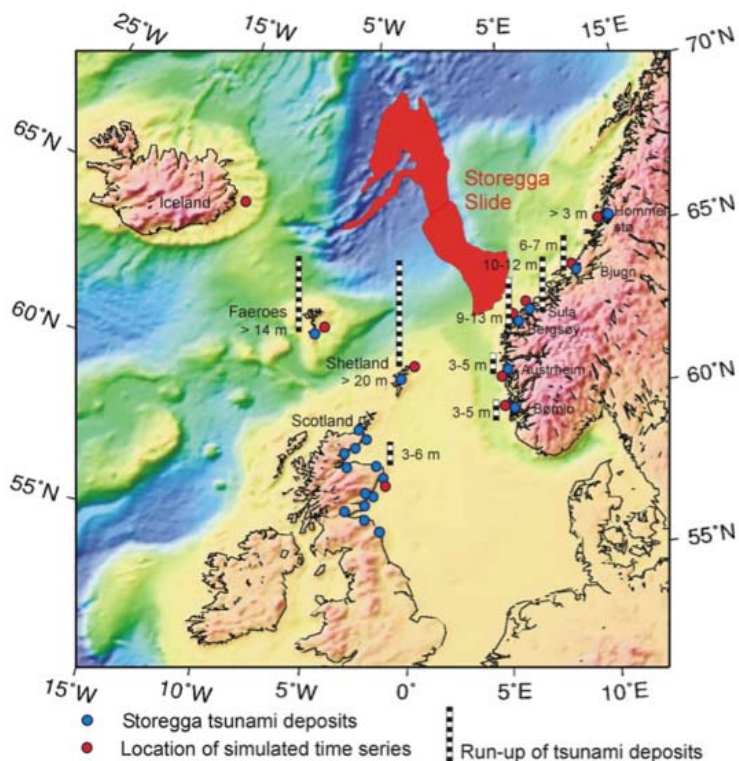


Figure 4-1: Location map of the Storegga Slide.

References:

- Bondevik, S., Lovholt, F., Harbitz, C. B., Mangerud, J., Dawson, A., and Svendsen, J. I., 2005, The Storegga Slide tsunami; comparing field observations with numerical simulations: *Marine and Petroleum Geology*, v. 22, p. 195-208.
- Bryn, P., Berg, K., Forsberg, C. F., Solheim, A., and Kvalstad, T. J., 2005, Explaining the Storegga Slide, *Marine and Petroleum Geology*, 22, p. 11-19.
- Canals, M., *et al.*, 2004, Slope failure dynamics and impacts from seafloor and shallow sub-seafloor geophysical data; case studies from the COSTA project: *Marine Geology*, v. 213, p. 9-72.
- Gao, D., 2006, Gravitational sliding on the Mid-Atlantic Ridge at the Kane Transform; implications for submarine basin-slope degradation and deformation: *AAPG Bulletin*, v. 90, p. 159-176.
- Gisler, G., Weaver, R., and Gittings, M. L., 2006, SAGE calculations of the tsunami threat from La Palma, *Science of Tsunami Hazards*, 24, p. 288-301.
- Kenyon, N. H., 1987, Mass-wasting features on the continental slope of Northwest Europe: *Marine Geology*, v. 74, p. 57-77.
- Leynaud, D., Mienert, J., and Vanneste, M., *submitted*, Submarine mass movements on glaciated and non-glaciated European continental margins: Triggering mechanisms and preconditions to failure: *Marine Geology*.
- Mader, C. L., 2001, Modeling the La Palma landslide tsunami: *Science of Tsunami Hazards*, v. 19, p. 160.
- Masson, D. G., Watts, A. B., Gee, M. J. R., Urgeles, R., Mitchell, N. C., Le Bas, T. P., and Canals, M., 2002, Slope failures on the flanks of the western Canary Islands: *Earth-Science Reviews*, v. 57, p. 1-35.
- Piper, D. J. W., and Ingram, S., 2003, Major Quaternary failures on the East Scotian Rise, Current Research: Geological Survey of Canada, 7 p.
- Piper, D. J. W., and McCall, C., 2003, A synthesis of the distribution of submarine mass movements on the eastern Canadian margin, *in* Locat, J., and Meinert, J. (Editors), Submarine mass Movements and Their Consequences, Kluwer, Dordrecht, p. 291-298.
- Piper, D. J. W., Mosher, D. C., Gauley, B.-J., Kimberley, J., and Campbell, D. C., 2003, The chronology and recurrence of submarine mass movements on the continental slope off southeastern Canada, *in* Locat, J., and Meinert, J. (Editors), Submarine mass Movements and Their Consequences, Kluwer, Dordrecht, p. 299-306.
- Solheim, A., Berg, K., Forsberg, C. F., and Bryn, P., 2005, The Storegga Slide Complex; repetitive large scale sliding with similar cause and development: *Marine and Petroleum Geology*, v. 22, p. 97-107.
- ten Brink, U. S., Geist, E. L., and Andrews, B. D. 2006a, Size distribution of submarine landslides and its implication to tsunami probability in Puerto Rico, *Geophys. Res. Lett.*, v. 33, L11307, doi:10.1029/2006GL026125.
- ten Brink, U. S., Geist, E. L., Lynett, P., and Andrews, B., 2006b, Submarine slides north of Puerto Rico and their tsunami potential, *in* Mercado, A.,

- and Liu, P. L.-F. (Editors), Caribbean Tsunami Hazard, World Scientific, Singapore, p. 67-90.
- Tucholke, B. E., 1992, Massive submarine rockslide in the rift-valley wall of the Mid-Atlantic Ridge: *Geology*, v. 20, p. 129-132.
- Ward, S. N., and Day, S., 2001, Cumbre Vieja Volcano; potential collapse and tsunami at La Palma, Canary Islands: *Geophysical Research Letters*, v. 28, p. 3397-3400.
- Weaver, P. P. W., and Mienert, J., 2003, European margin sediment dynamics side-scan sonar and seismic images, Springer, New York, 310 pp.
- Wynn, R. B., and Masson, D. G., 2003, Canary Island landslides and tsunami generation: can we use turbidite deposits to interpret landslide processes?, *in* Locat, J., and Meinert, J. (Editors), Submarine mass Movements and Their Consequences, Kluwer, Dordrecht, p. 325-332.

Chapter 5: Review of tsunamigenic earthquake sources that may affect the U.S. Atlantic Coast

Introduction

Earthquake-generated tsunamis generally originate by the sudden vertical movement of a large area of the seafloor during a large magnitude ($M > 6.5$) earthquake. Such movement is generated by reverse or thrust faulting, most often in subduction zones. The Atlantic Ocean basin is generally devoid of subduction zones or potential sources of large reverse faults. The two exceptions are the Hispaniola-Puerto Rico-Lesser Antilles subduction zone, where the Atlantic tectonic plate subducts under the Caribbean plate, and the enigmatic zone of large earthquakes west of Gibraltar. Following is a review of these two earthquake source areas and an evaluation of their tsunamigenic potential.

The Area West of Gibraltar

Tectonic setting

The Africa-Eurasia plate boundary extends from the Azores Triple Junction in the west to the area SW of the Iberian Peninsula (Figure 5-1). Relative plate motion is slow (4 mm/y, HS3-Nuvel 1a) and the motion is strike-slip with slight divergence at the western end near the Azores and convergence near its eastern end SW of the Iberian Peninsula (*e.g.*, Argus *et al.*, 1989). The juxtaposition of two old (>100 m.y.) and dense plates along the eastern end of the plate boundary, does not allow for subduction to develop (*e.g.*, Grimison and Chen, 1986). Instead, a zone of diffuse compressive deformation has developed with Gorringe Bank and other lesser banks and seamounts separated by abyssal plains (Hayward *et al.*, 1999). The plate boundary continues eastward to the collision zone along the Algerian coast, but the geometry of this section has never been clearly established.

Faccenna *et al.* (2004) proposed a different explanation for the tectonics of the area west of Gibraltar. In their model, the Western Mediterranean Subduction Zone had fragmented during the Miocene into two narrow subduction zones that are moving progressively east (the Calabrian Arc,

southern Italy) and west (the Gibraltar Arc). The outward retreat of the subduction zones is producing the backarc extension of the Tyrrhenian and Alboran Seas and thrusting at their fronts. The thrust front of the Gibraltar Arc is presently 350 km west of Gibraltar (Thiebot and Gutscher, 2006).

The debate about the source parameters of the 1755 Lisbon earthquake

Four large tsunamigenic earthquakes have occurred in the Atlantic Ocean west of Gibraltar in the last 300 years, the 1722 (Baptista and Lemos, 2000), 1755 (Lisbon), 1761 (Baptista *et al.*, 1998) and the $M_w=7.8$ 1969 (Johnston, 1996) earthquakes. However, there is no simple tectonic model for this area that explains the generation of these earthquakes.

Johnston (1996) assumed that Gorringe Bank was the source of the November 1, 1755 Lisbon Earthquake. Gorringe Bank (Figure 5-1) is a major morphologic feature rising from a depth of 4000 m to 25 m bsl. The $M=7.9$ 1969 earthquake occurred on a fault parallel to the Gorringe escarpment, but 90 km to the SE (Johnston, 1996). The strike directions of the escarpment and the earthquake was 45° - 50° and slip of the 1969 earthquake was to the NW.

Johnston proposed the following fault and slip parameters for the 1755 Lisbon earthquake:

Length = 200 km, width = 80 km, dip = 40° , strike = 62° , slip = 332°, displacement = 12 m, density = 3330 kg/m^3 (mostly oceanic lithosphere, shear modulus $\mu = 6.5 \times 10^{11} \text{ dyne/cm}^2$. The much higher than normal shear modulus represents a high stress drop because the fault is thought to penetrate the oceanic mantle lithosphere to a depth of 50 km.

Curiously, Johnston's (1996) isoseismal map for the 1755 Lisbon earthquake (Figure 5-2) is not compatible with a thrust fault oriented at 62° , and is more compatible with fault location and orientation discussed below.

Gracia *et al.* (2003) used multibeam bathymetry and high-resolution seismic reflection data to map the region near Cape St. Vincente (SW corner of the Iberian Peninsula, see Figure 5-3). They proposed that the 1755 Lisbon earthquake occurred on two other thrust faults (Marques de Pombal fault and Horseshoe-San Vincente fault). These faults have an average strike of $\sim 20^\circ$ and their suggested slip direction was to the northwest.

Gutscher *et al.* (2006) favored the model of thrusting and subduction of the eastern Atlantic under the Alboran Sea the source of the 1755 Lisbon earthquake (Figure 5-4). A simplified fault plane was (Figure 5-5) used by Gutscher *et al.* (2006) to perform tsunami waveform modeling of a shallow east dipping subduction source. The initial displacement of the seafloor (Figure 5-5, which they consider equal to the initial displacement of the sea surface) was calculated using the elastic half-space approach (Okada, 1985). The principal fault plane was represented by a series of rectangular sub-planes extending from 6.5 km depth eastwards to a maximum depth of 24 km (Figure 5-4, Table 5-1). Their fault dip increases progressively from 2.5° , to 5° to 7.5° . They also tested a model with a frontal fault splay, extending

from the seafloor to 6.5 km depth, where it joins the principal fault plane (Figure 5-5).

The average dimensions of Gutscher's fault plane are: N - S length = 180 km; total E - W width = 210 km. Moment magnitudes were calculated for two uniform co-seismic slips, 20 and 10 m using the following parameters:

Moment $M_0 = \mu SD$, Moment magnitude $M_w = 2/3 \log M_0 - 6.03$; shear modulus $\mu = 3 \times 10^{10}$ Pa; rupture area $S = 37,800 \text{ km}^2$;

If slip $D = 20 \text{ m} \rightarrow M_0 = 2.27 \times 10^{22} \text{ Nm}$; $M_w = 8.80$

If slip $D = 10 \text{ m} \rightarrow M_0 = 1.13 \times 10^{22} \text{ Nm}$; $M_w = 8.64$

It should be noted that using uniform slip will underestimate the amplitude of the generated tsunami in comparison to a more realistic distribution slip mode (*e.g.*, from a crack-like rupture) (Geist and Dmowska, 1999).

Gutcher *et al.* (2006) also proposed a recurrence interval of 1,000–2,000 years based on paleo-tsunami evidence from Cadiz, the periodicity of turbidites in the Horseshoe abyssal plain, and the suggested westward rate of motion of the Gibraltar block, 5-10 mm/y.

Baptista *et al.*, (1998) fit tsunami travel times to different coastal observations by backward ray tracing inversion with a grid search for the best location. The optimal location is a composite rupture along the SW Iberian coast with strikes of 160° and 135° (Figure 5-6b), but no parameters were specified. The travel time fit is superior to that from the source proposed by Gutscher *et al.*, 2006 (see table 2 in Gutscher *et al.*, 2006), but there was no attempt to identify the causative tectonic source of the tsunami.

To date, there has not been an attempt to fit cross-ocean tsunami reports of the 1755 Lisbon earthquake to any of the above sources. Lockridge *et al.*, 2002 compiled a list of reports on the effect of the 1755 Lisbon tsunami in the Caribbean: Antigua, Saba, St. Martin at the northeast corner of the Caribbean had the highest flooding, but flooding was also reported from Santiago de Cuba and Samana Bay, Dominican Republic, in the north to Barbados in the south. If we assume that the highest runup was in the direction of fault slip, then the slip azimuth from the Gulf of Cadiz to Saba is 263° , and if the fault strike is perpendicular to slip then the fault strike was 173° . This fault strike is compatible with the fault strikes proposed by Baptista *et al.* (1998) and Gutscher *et al.* (2006) and is incompatible with the sources proposed at Goringe Bank (Johnston, 1996) and the Marques de Pombal and Horseshoe-San Vincente faults (Gracia *et al.*, 2003).

There are also reports about flooding in Bonavista, north of St. Johns, Newfoundland as a result of the 1755 Lisbon earthquake (*e.g.*, Ruffman, <http://www.sthjournal.org/tsabst/rlisbon.pdf>, Feb. 24, 2006), but there are no reports of flooding anywhere else between Cuba and

Newfoundland, despite the presence at that time of population centers in low-lying areas of the eastern U.S. and Canada.

The 1761 Earthquake and Tsunami

Two other large earthquakes (probably $M > 7$) have struck the Iberian Peninsula during the 18th century. The first occurred on December 27, 1722 (Baptista and Lemos, 2000) and the second on March 31, 1761. The 1761 earthquake was felt across the Iberian Peninsula, Madeira, Agadir (Morocco), southern England, Ireland and the Netherlands (Baptista *et al.*, 2006). The earthquake generated a tsunami that was observed in Lisbon, Portugal, Cadiz, Spain, Cornwall, England, the south coast of Ireland, Terceira in the Azores, Barbados and Antigua (Baptista *et al.*, 2006, and references therein). Baptista *et al.* (2006) located the earthquake and tsunami source at 13°N 34.5°W (south of Ampere seamount) using the intersection between regions defined by back-tracking of tsunami travel time, and the intensity of the earthquake in the Iberian Peninsula (Figure 5-7). Their location contradicts previously suggested locations that the earthquake took place close to reported sea quakes (no. 1, 2, and 3, in figure 5-7), or at Gorringer Bank (marked by X in Figure 5-7).

Summary

The proposed 1755 Lisbon earthquake sources by Gutscher *et al.*, (2006) and Baptista *et al.*, (1998) (and mimicked in the isoseismals shown by Johnston, 1996) appear to be the best available. Faccenna *et al.* (2004) and Thiebot and Gutscher (2006) may indeed be correct to propose a short eastward dipping subduction zone within the Atlantic basin in the Gulf of Cadiz.

In the future, we propose running a propagation model to evaluate the impact of tsunamigenic earthquakes from this hypothesized subduction zone on the Caribbean and U.S. Atlantic coast, using the following simple source parameters:

Location (South corner of surface fault expression): 34°35'N 9°45'W (Gutscher's solution), or 35°25'N 9°55'W (Baptista's solution). N - S length = 180 km; total E - W width = 210 km, strike - 170°, dip - 5° (with perhaps a splay), rake 90° Slip - 10 or 20 m.

The Northeast Caribbean

Tectonic Setting

The Greater Antilles volcanic arc, which extends from Cuba to the Virgin Islands (Figure 5-8), was formed during the Cretaceous and Early Tertiary as the North American plate was subducting southwesterly beneath the Caribbean plate (Pindell and Barrett, 1990). Beginning at 49 Ma, relative plate motion changed to a more easterly direction (~250°), resulting in a more oblique subduction, a large component of left-lateral strike-slip, and the

cessation of arc volcanism. This relative plate motion has been fairly stable ever since as evident from the opening of Cayman Trough between Cuba and Honduras (ten Brink *et al.*, 2002 and references therein). Presently, a typical old oceanic crust of 90-110 m.y. in age subducts under Puerto Rico and the Virgin Islands, whereas the descending plate adjacent to the Hispaniola trench is a thick crust of an unknown origin, which underlies the Bahamas platform (Freeman-Lynde and Ryan, 1987). Thrust earthquakes at a shallow angle (20°) under northern Hispaniola (Dolan and Wald, 1998) indicate that subduction process is likely to be active there.

The Puerto Rico Trench

The geometry of the Puerto Rico trench with respect to relative plate motion is similar to the Sumatra-Andaman trench, where the 26 December 2004 Indian Ocean tsunami took place (Figure 5-8). Specifically, the Puerto Rico trench is curved, and the convergence angle between the subducting NOAM plate and the overlying Caribbean plate is increasingly more oblique to the west (Figure 5-2). By inference, it was suggested that perhaps the Puerto Rico Trench is capable of generating a mega-tsunami that will affect the Atlantic coast of the U.S. While more detailed modeling studies need to be carried out, it is worth pointing out some fundamental differences between the two trenches. Slip during the $M=9.3$ earthquake in Sumatra was sub-perpendicular to the trench, despite the highly oblique convergence angle. This indicates that additional deformation should take place in the overriding plate within the forearc and arc regions. Using numerical modeling of static stress changes, ten Brink and Lin (2004) recently showed that slip during earthquakes in the Puerto Rico Trench is highly oblique and almost parallel to the convergence direction (Figure 5-9). This finding matches evidence from GPS (Calais *et al.*, 2003) and earthquake focal mechanisms (Figure 5-9) in the area, all indicating little deformation of the overlying plate due to subduction. Therefore, only a small component of thrust motion is expected during large earthquakes, because most of the motion during a subduction earthquake will be parallel to the trench.

There is no historical record of large earthquakes along the Puerto Rico trench, although McCann (2004) proposed that the 1787 earthquake had magnitude 8 and was located north of Puerto Rico. The largest instrumentally recorded earthquake in the area is the 1943 $M_w=7.3$ northwest of Puerto Rico (*e.g.*, Dolan and Wald, 1998). Although plate secular motion from GPS is limited by the paucity of landmass, available data indicate a relative displacement of 19 ± 2 mm/y with respect to the North American plate oriented at an angle of 70° (Figure 5-9).

Using focal mechanisms for small to medium earthquakes ($M_w=5.3-6$) in the past 30 years and arguments discussed in ten Brink and Lin (2004), we propose the following rupture parameters: slip direction of N60E along an inclined interface with dip of 20° . The downdip length of the interface is unknown. Ten Brink and Lin (2004) assumed a length of 102 km extending from depth of 5 to 40 km. The worst-case scenario for an earthquake

rupture along the Puerto Rico Trench is a single rupture of a 675 km segment between 68°W (north of eastern Dominican Republic) and 62°W. For an assumed 10 m slip and shear modulus $\mu = 3 \times 10^{10}$ Pa, the rupture area $S = 68,850 \text{ km}^2$, the moment is $M_0 = 2.06 \times 10^{22}$ Nm, and the moment magnitude is $M_w = 8.85$.

However, it should be emphasized that such a large earthquake has never been documented along the Puerto Rico trench, and the downdip length of the fault rupture is unknown. There is also significant uncertainty in scaling average slip with respect to the rupture dimensions (Geist et al., 2007). In addition, the subducting plate is 90-110 m.y. old (ten Brink, 2005). Subduction zones consuming a 100 m.y. old oceanic lithosphere at a long-term convergence rate of 20 mm/y are typically associated with earthquakes $< M=8$ (e.g., Ruff and Kanamori, 1980), although other studies (e.g., Bird and Kagan, 2004) suggest little correlation between maximum earthquake magnitude and various subduction parameters. Most important, ten Brink and Lin proposed that slip during an earthquake is expected to be sub-parallel to the trench. The relatively small component of thrusting relative to strike-slip during the earthquake slip will generate a smaller tsunami compared to a pure thrust event.

The Hispaniola Trench

According to GPS measurements, slightly oblique convergence under Hispaniola is partitioned between 5.2 ± 2 mm/y of reverse motion on the subduction interface and 12.8 ± 2.5 mm/y and 9.0 ± 9.0 mm/y left-lateral strike-slip on the Septentrional and Enriquillo Faults, respectively, which traverse the arc (Calais et al., 2002) (Figure 5-9a, Enriquillo Fault is located along the southwest side of Hispaniola beyond the map). A series of $M_s = 7.0-8.1$ earthquakes ($M_w = 6.8-7.6$; D. Wald, pers. Comm., 2003) with mostly thrust motion took place in the eastern half of northern Hispaniola between 1946 and 1953 (Kelleher et al., 1973) (Figure 5-9), presumably on a shallow dipping ($\sim 20^\circ$) subduction interface (Dolan and Wald, 1998) (Figure 5-9). Slip in these events was slightly oblique with average slip azimuth of 23° (D. Wald, pers. Comm., 2003). One of the events in 1946 was accompanied by a destructive local tsunami.

In contrast to the Puerto Rico trench, slip on the Hispaniola segment of the trench farther west, is sub-perpendicular to the trench, hence, a larger vertical motion is expected for a given magnitude of slip. In contrast to the Puerto Rico trench, where a normal thickness oceanic crust is subducting, the crust entering the Hispaniola trench is very thick (e.g., Freeman-Lynde and Ryan, 1987), and will likely allow more stress to accumulate, and therefore larger earthquakes to occur.

The Hispaniola segment may extend from 68°W to the Windward Passage 525 km to the west, where it meets the eastern end of Cayman Trough (Figure 5-8). Earthquake focal mechanisms indicate a dip of 20° (Dolan and Wald, 1998), and slip direction of N23E. The average strike of the Hispaniola segment is N95E-N102E. The downdip fault length is assumed to be 117 km assuming that rupture extend between depths of 0 -

40 km. The relocated region of the 1946-1953 aftershocks define a 95 km long downdip zone (Dolan and Wald, 1998).

Assuming a complete rupture of the Hispaniola trench with 10 m slip yields a rupture area $S = 61,425 \text{ km}^2$; moment $M_0 = 1.84 \times 10^{22} \text{ Nm}$, and moment magnitude $M_w = 8.81$. The easternmost 200 km long section of the subduction zone has ruptured in a series of earthquakes between 1946-1953. It is unclear, whether the western part of the subduction zone would rupture in a single earthquake and how far west the rupture would extend.

Modeling is needed to determine if the U.S. Atlantic coast would be protected from tsunamis generated in this subduction zone by the Bahamas banks which are near sea level and act as obstructions to tsunami wave propagation.

Table

Table 5-1: Source parameters of rectangular fault plane segments (given in UTM29 coordinates in m)

Segment	Dip	X seg	Y seg	X seg	Y seg
<i>Splay</i>	30	516047	3825131	485098	3984165
<i>Plane1</i>	2.5	521937	3826277	490988	3985311
<i>Plane2</i>	5.0	588938	3839316	557989	3998350
<i>Plane3</i>	7.5	655750	3852318	624801	4011352

Segment	Strike (°)	Rake (°)	Slip (m)	Width (m)	Length (m)
<i>Splay</i>	-11,0125	90	10/20	6000	162017
<i>Plane1</i>	-11,0125	90	10/20	68258	162017
<i>Plane2</i>	-11,0125	90	10/20	68065	174017
<i>Plane3</i>	-11,0125	90	10/20	68065	198017

Figures

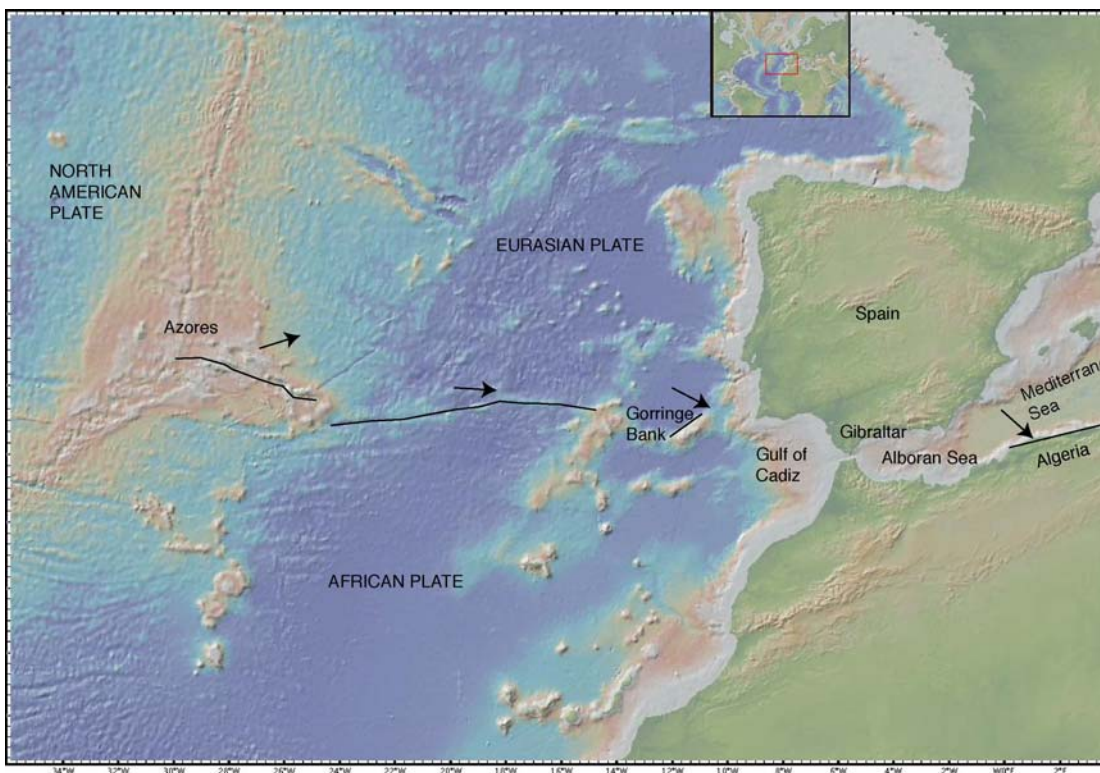


Figure 5-1: Topography and bathymetry map of the Eurasian-African plate boundary. Eurasian plate motion relative to Africa from NUVEL1A model. The rate of relative motion is 4 mm/y.

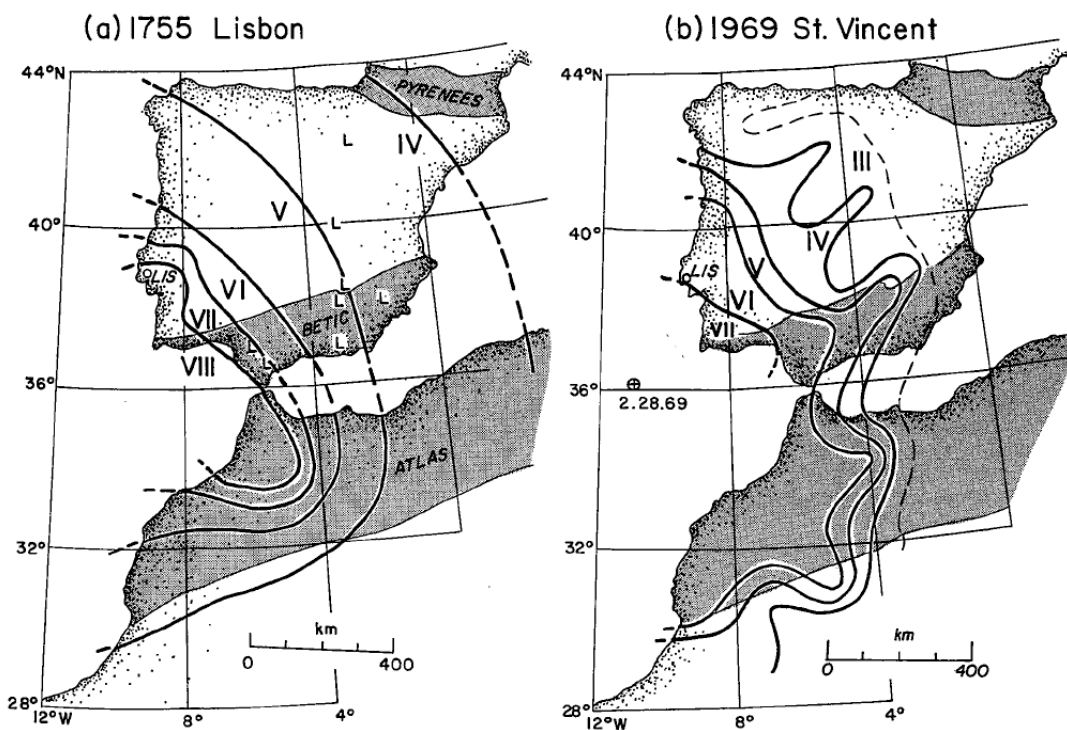


Figure 5-2: Isoseismal comparison of the (a) 1755 Lisbon and (b) 1969 St. Vincent (M 7.8) earthquakes (from Johnston, 1996).

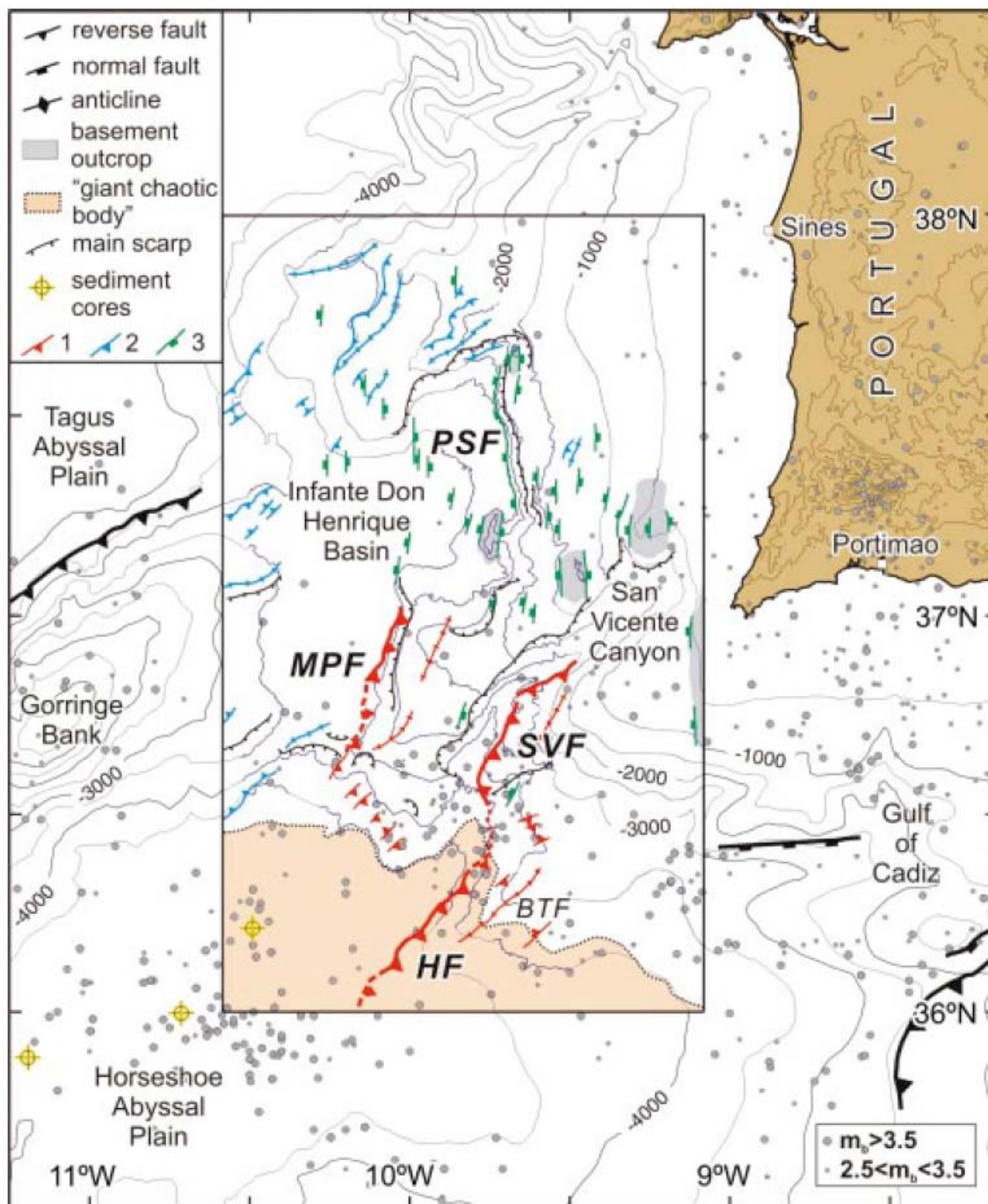


Figure 5-3: Interpretative structural map of the southwest Iberian margin based on multichannel seismic data and multibeam bathymetry, where available (from Gracia *et al.*, 2003). Earthquake epicenters are for the period 1965-1999. 1 - Red: Active faults, dashed where buried. 2 - Blue: Structures showing Miocene deformation. 3 - Green: Mesozoic extensional faults. MPF - Marques de Pombal fault. SVF - San Vicente Fault, HF - Horseshoe fault. Bathymetric contour - 500 m. Topographic contour - 100 m.

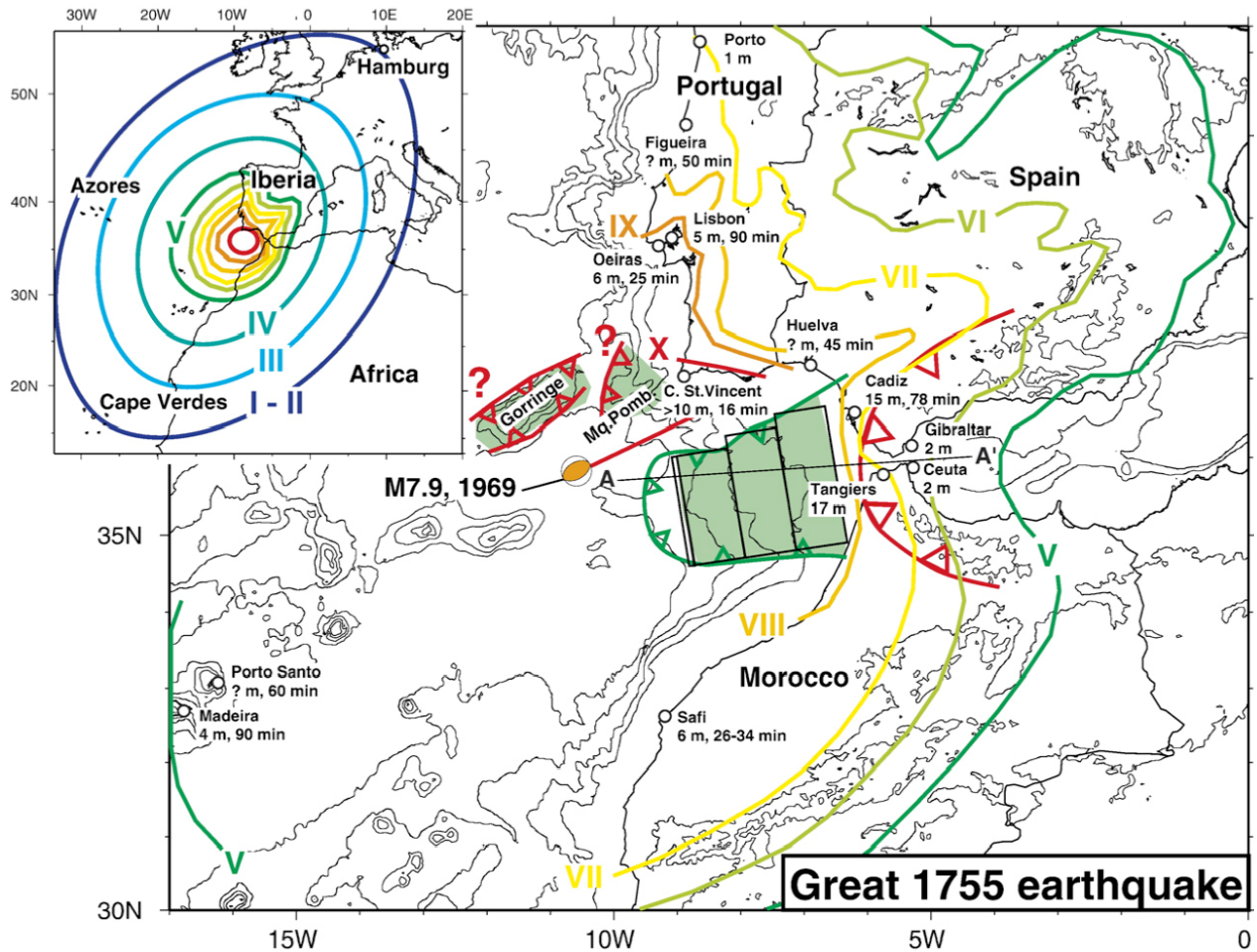


Figure 5-4: Map of the region west of Gibraltar (from Gutscher *et al.*, 2006 and references therein) showing the extent of the shallow east-dipping fault plane (green bars), the Betic arc (red bars), Gorringe, and the Bank and Marques de Pombal thrusts and the locations of the 1969 and the 1761 earthquakes. Also shown are the isoseismals from the 1755 Lisbon earthquake and historically reported tsunami arrival times and amplitudes.

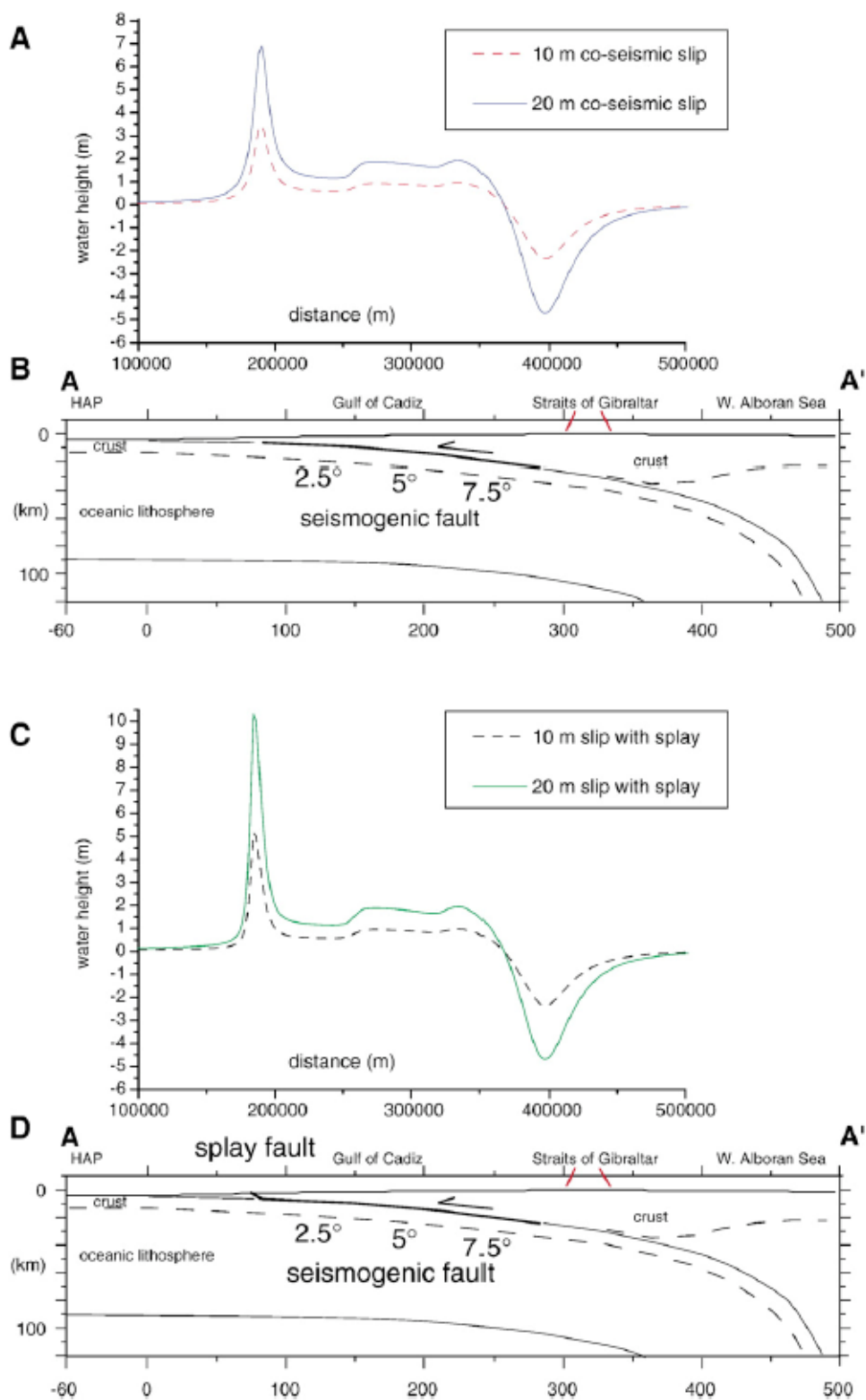


Figure 5-5: Cross-section through the thrust fault plane (A-A' in Figure 5-4), showing the geometry of the sources tested by Gutscher *et al.* (2006), with (C, D) and without (A, B) a fault splay, and the initial water height, associated with each (from Gutscher *et al.*, 2006). The initial water height was assumed to be equal to the initial seafloor displacement. Distance axis in A, C is from model coordinates. Note that using more realistic slip distribution will yield different initial wave profile (Geist and Dmowka, 1999).

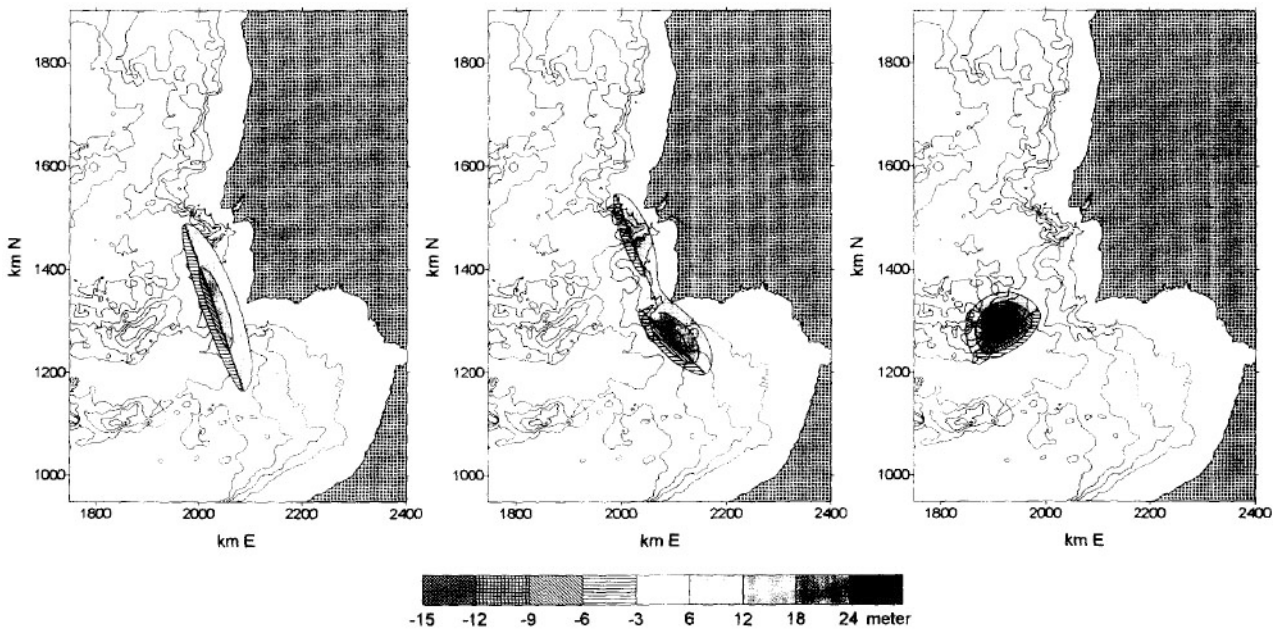


Figure 5-6: Initial displacement for shallow water simulations of the 1755 Lisbon earthquake (from Baptista *et al.*, 1998). (a) Source with strike 160° . (b) Composite source with strikes of 160° and 135° which best fits the observed tsunami travel times and amplitudes (c) Source mimicking the 1969 earthquake source with a strike of 55° , which does not fit the observations.

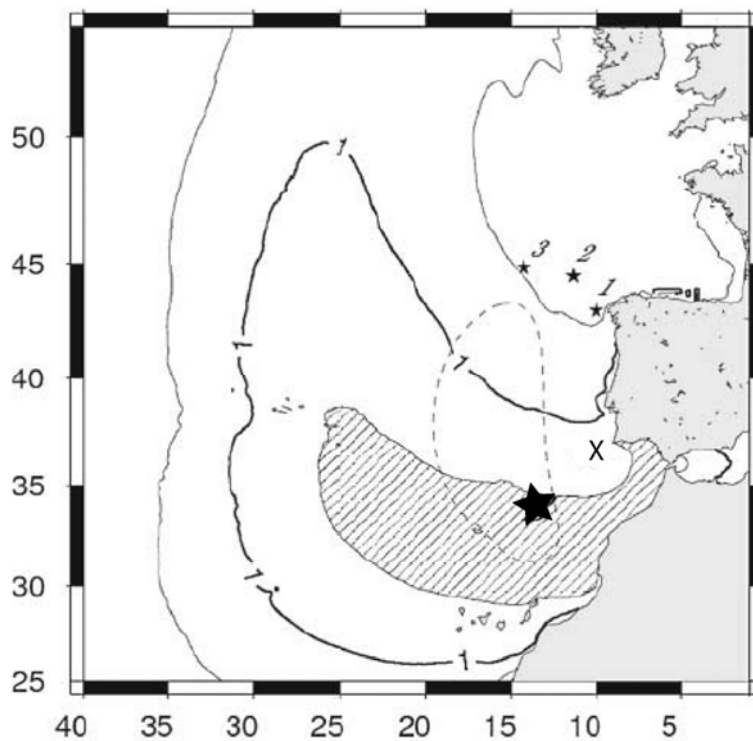


Figure 5-7: Probable location of the 31 March 1761 earthquake and tsunami (from Baptista *et al.*, 2006). Contours – average misfit (in hours) of backward tsunami ray tracing, with striped area being < 0.5 hr. Dashed line – Enclosed area where the averaged intensity errors are minimized assuming the MSK attenuation law. Stars – locations of reported sea quakes. X- Goringe Bank.

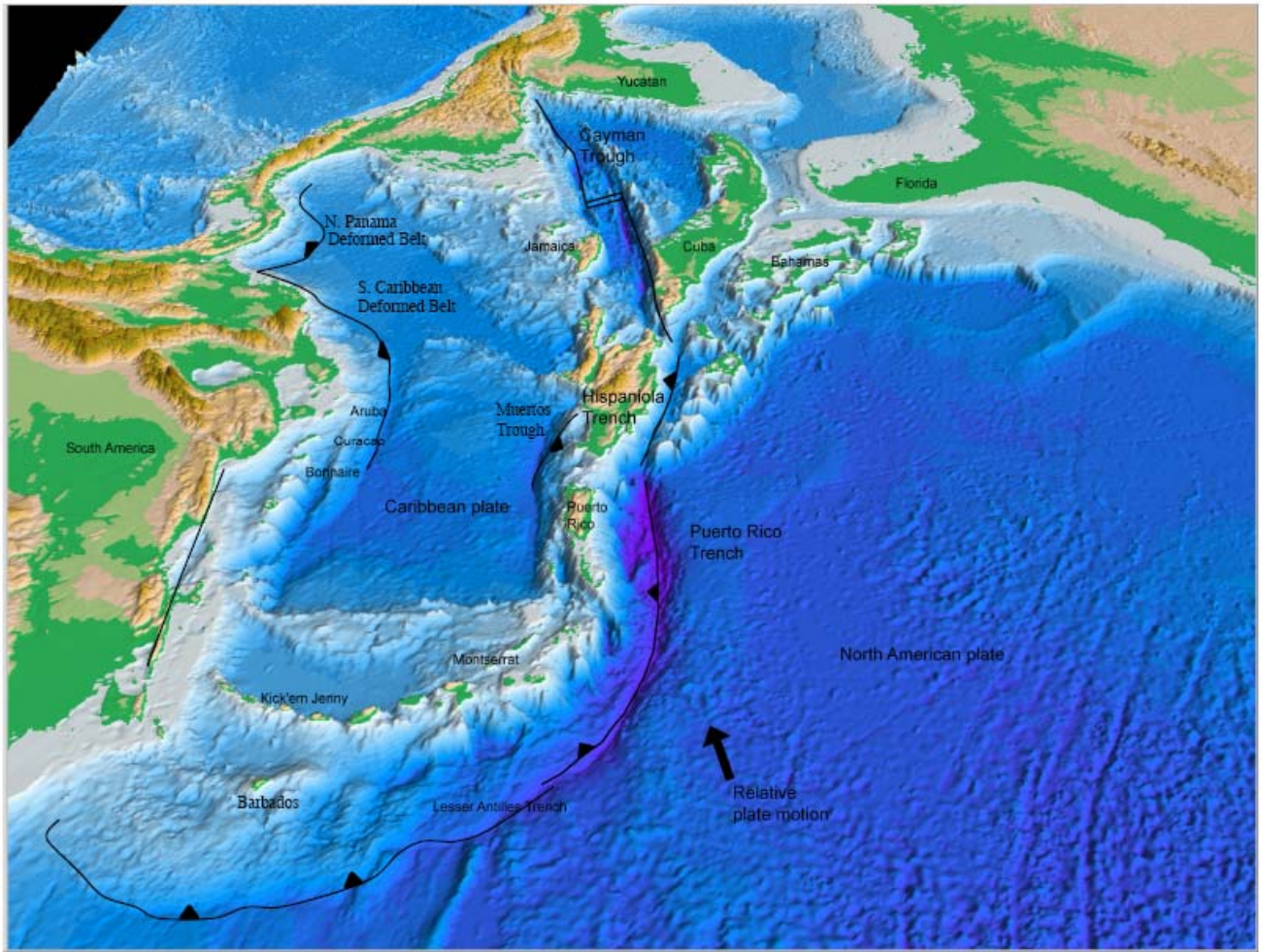


Figure 5-8: Perspective view of the tectonic elements in the Caribbean plate and seafloor topography.

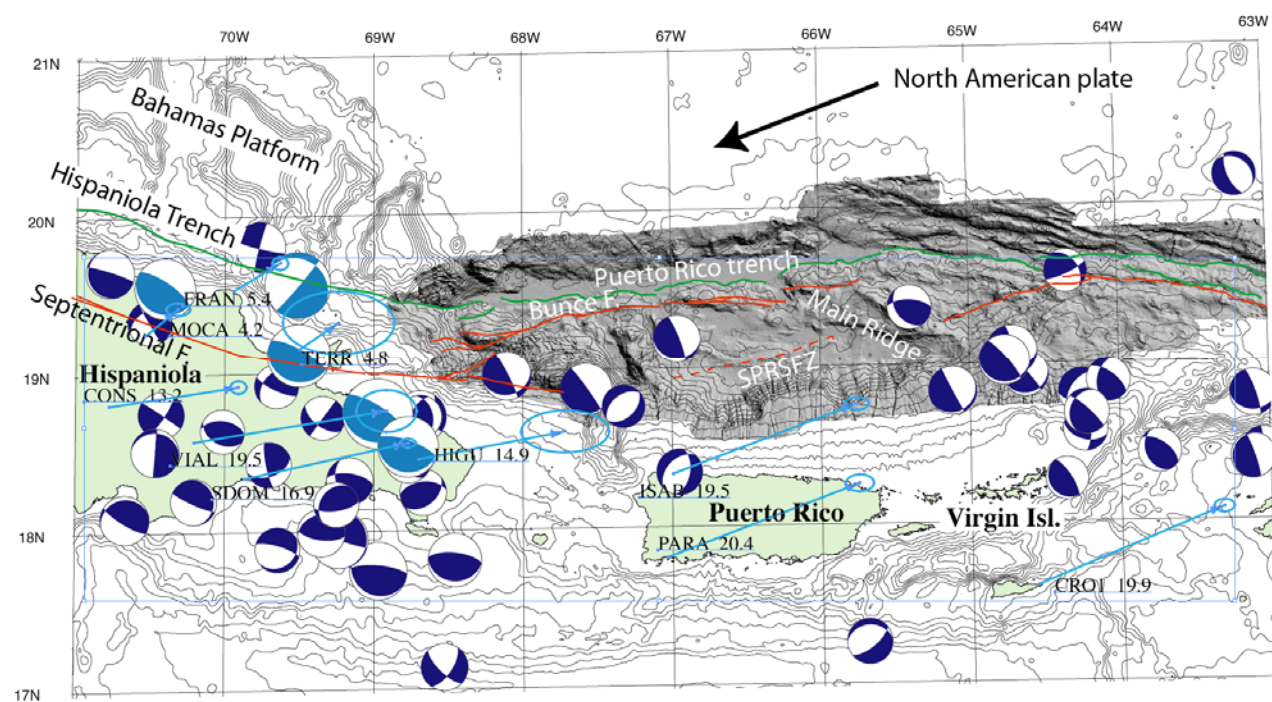


Figure 5-9: Bathymetry map of the northern Caribbean with a shaded relief map obtained from detailed multibeam bathymetry survey (ten Brink and Lin, 2004, and references therein). Solid green line – Frontal thrust of the subduction zone. Solid red line – Interpreted strike-slip faults. Blue beach balls – Focal plane solutions (lower hemisphere) of moderate earthquakes between 1977-2002 from the Harvard CMT catalog. Light blue beach balls – Same for historical earthquake sequence. Arrows – Velocity vectors relative to stable North America accompanied by rate (in mm/y) and station name, and error ellipse.

References

- Argus, D. F., Gordon, R. G., DeMets, C., and Stein, S., 1989, Closure of the Africa-Eurasia-North America plate motion circuit and tectonics of the Gloria Fault: *Journal of Geophysical Research*, v. 94, p. 5585-5602.
- Baptista, M. A., Miranda, J. M., and Luis, J. F., 2006, In search of the 31 March 1761 earthquake and tsunami source: *Bulletin of the Seismological Society of America*, v. 96, p. 713-721.
- Baptista, M. A., and Lemos, C., 2000, The source of the 1722 Algarve earthquake, inferred from hydrodynamic modeling of the associated tsunami, European Geophysical Society, 25th general assembly, Nice, France, April 25-29, 2000.
- Baptista, M. A., Miranda, P. M. A., Miranda, J. M., and Mendes Victor, L., 1998, Constraints on source of the 1755 Lisbon tsunami inferred from numerical modelling of historical data on the source of the 1775 Lisbon tsunami: *Journal of Geodynamics*, v. 25, p. 159-174.
- Bird, P., and Kagan, Y. Y., 2004, Plate-tectonic analysis of shallow seismicity: apparent boundary width, beta-value, corner magnitude, coupled lithosphere thickness, and coupling in 7 tectonic settings: *Bull. Seismol. Soc. Am.*, v. 94, p. 2380-2399.
- Calais, E., Mazabraud, Y., Mercier de Lepinay, B., Mann, P., Mattioli, G. S., and Jansma, P. E., 2002, Strain partitioning and fault slip rates in the

- northeastern Caribbean from GPS measurements: *Geophysical Research Letters*, v. 29, 1856, doi:1810.1029/2002GL015397.
- Dolan, J. F., and Wald, D. J., 1998, The 1943-1953 north-central Caribbean earthquakes: Active tectonic setting, seismic hazards, and implications for Caribbean-North America plate motions: *Geological Society of America Special publications*, v. 326, p. 143-170.
- Faccenna, C., Piromallo, C., Crespo-Blanc, A., Jolivet, L., and Rossetti, F., 2004, Lateral slab deformation and the origin of the western Mediterranean arcs: *Tectonics*, v. 23, no.1, p. 21.
- Freeman-Lynde, R. P., and Ryan, W. B. F., 1987, Subsidence history of the Bahama Escarpment and the nature of the crust underlying the Bahamas: *Earth and Planetary Science Letters*, v. 84, p. 457-470.
- Geist, E. L., 1999, Local tsunamis and earthquake source parameters: *Adv. Geophys.*, v. 39, p. 117-209.
- Geist, E. L., and Dmowska, R., 1999, Local tsunamis and distributed slip at the source: *Pure Appl. Geophys.*, v. 154, p. 485-512.
- Geist, E. L., Titov, V. V., Arcas, D., Pollitz, F. F., and Bilek, S. L., 2007, Implications of the December 26, 2004 Sumatra-Andaman earthquake on tsunami forecast and assessment models for great subduction zone earthquakes: *Bull. Seismol. Soc. Am.*, v. 97, p. S249-S270.
- Gracia, E., et al., 2003, Mapping active faults offshore Portugal (36 degrees N-38 degrees N); implications for seismic hazard assessment along the Southwest Iberian margin: *Geology*, v. 31, p. 83-86.
- Grimison, N. L., and Chen, W.-P., 1986, The Azores-Gibraltar plate boundary; focal mechanisms, depths of earthquakes, and their tectonic implications: *Journal of Geophysical Research*, v. 91, p. 2029-2047.
- Gutscher, M. A., Baptista, M. A., and Miranda, J. M., 2006, The Gibraltar Arc seismogenic zone; Part 2, Constraints on a shallow east dipping fault plane source for the 1755 Lisbon earthquake provided by tsunami modeling and seismic intensity: *Tectonophysics*, v. 426, p. 153-166.
- Hayward, N., Watts, A. B., Westbrook, G. K., and Collier, J. S., 1999, A seismic reflection and GLORIA study of compressional deformation in the Gorringe Bank region, eastern North Atlantic: *Geophysical Journal International*, v. 138, p. 831-850.
- Johnston, A. C., 1996, Seismic movement assessment of earthquakes in stable continental regions; III, New Madrid 1811-1812, Charleston 1886 and Lisbon 1755: *Geophysical Journal International*, v. 126, p. 314-344.
- Lander, J. F., Whiteside, L. S., and Lockridge, P. A., 2002, A brief history of tsunamis in the Caribbean Sea: *Science of Tsunami Hazards*, v. 20, p. 57-94.
- McCann, W. R., Feldman, L., and McCann, M., *in press*, Catalog of felt earthquakes for Puerto Rico and neighbouring islands 1492-1899 with additional information for some 20th century earthquakes: *Tectonophysics*.
- Okada, Y., 1985, Surface deformation due to shear and tensile faults in a half-space: *Bulletin of the Seismological Society of America*, v. 75, p. 1135-1154.
- Pindell, J. L., and Barrett, S. F., 1990, Geological evolution of the Caribbean region; a plate tectonic perspective, edited by Dengo, G., and Case, J. E.: Geol. Soc. Am., Boulder.

- Ruff, L., and Kanamori, H., 1980, Seismicity and the subduction process: *Physics of the Earth and Planetary Interiors*, v. 23, p. 240-252.
- ten Brink, U. S., Coleman, D. F., and Dillon, W. P., 2002, The nature of the crust under Cayman Trough from gravity: *Marine and Petroleum Geology*, v. 19, p. 971-987.
- ten Brink, U. S., and Lin, J., 2004, Stress interaction between subduction earthquakes and forearc strike-slip faults: modeling and application to the northern Caribbean plate boundary: *J. Geophys. Res.*, v. 109, B12310, 12310.11029/12004JB003031.
- Thiebot, E., and Gutscher, M. A., 2006, The Gibraltar Arc seismogenic zone; Part 1, Constraints on a shallow east dipping fault plane source for the 1755 Lisbon earthquake provided by seismic data, gravity and thermal modeling: *Tectonophysics*, v. 426, p. 135-152.

Chapter 6: Tsunamigenic earthquake sources that may affect the Gulf of Mexico

Introduction

Earthquake-generated tsunamis generally originate by the sudden vertical movement of a large area of the seafloor during an earthquake. Such movement is generated by reverse faulting, most often in subduction zones. The Gulf of Mexico basin is devoid of subduction zones or potential sources of large reverse faults. However, the Caribbean basin contains two convergence zones whose rupture may affect the Gulf of Mexico, the North Panama Deformation Belt and the Northern South America Convergent Zone. Hydrodynamic modeling is needed to evaluate the role of the Yucatan straits (between Cuba and the Yucatan Peninsula) in modifying the propagation of tsunamis into the Gulf of Mexico. Initial results are given in the Chapter 6 addendum. The following is a review of these convergent zones.

North Panama Deformation Belt 9-12°N, 83°W-77°W

Summary

The largest segment of the North Panama Deformation Belt is oriented between 60°-77°. The 1882 Panama earthquake appears to have ruptured at least 3/4 of the available length of the convergence zone, and was estimated to have a magnitude of 8 (Mendoza and Nishenko, 1989). While there was significant tsunami damage locally, there were no reports from the Gulf of Mexico of a tsunami from this earthquake (Mendoza and Nishenko, 1989). The low convergent rate (7-11 mm/y, (Trenkamp, *et al.*, 2002)) across the North Panama Deformation Belt supports long recurrence interval for large earthquakes.

Previous Tsunamis

A tsunami flooded San Blas islands and the northern coast of Panama (Figure 6-1) and killed 65 people on 09/07/1882 following an offshore earthquake at about 10°N, 78°W (Mendoza and Nishenko, 1989). Mendoza and Nishenko (1989) isoseismal map (Figure 6-2) suggests that rupture

occurred along almost the entire segment between longitude 80.3°W-77.8°W. Eyewitnesses report water withdrawal before flooding. The tide gauge in Colon at the northern end of Panama Canal reported a level change of only 62 cm. The Jamaica-Panama underwater cable broke (perhaps indicating a submarine slide). The authors estimated the earthquake to be $\sim M=8$, an increase from previous estimates (Mendoza and Nishenko, 1989).

Plafker and Ward (1992) reported an $M_s=7.5$ earthquake on 04/22/1991 at 9.74N 83.1W (on land), which caused uplift along 135 km of the Caribbean coast in southern Costa Rica. This earthquake was reported by the Harvard CMT catalog with location: 10.10N, 82.77W, depth: 15 km, and $M_w=7.6$. It also caused a damaging tsunami, which was recorded by a tide gauge in St. Croix (Lander, *et al.*, 2002). Plafker and Ward (1992) best fit parameters of the ruptured fault from seismic and geodetic data are: thrust fault, striking between 105-120°, dipping at 30°, fault dimensions: 40 km wide and 80 km long, Their estimated recurrence time on this fault is 200-1100 y.

The parameters for this earthquake are given as:

<i>ref.</i>	<i>strike</i>	<i>dip</i>	<i>rake</i>
1	103°	25°	58° (oblique thrust and left-lateral)
2	123° (91°-138°)	32° (16°-39°)	89° (69°-96°)
3	107±5°	21°±10°	56°±11°

where reference 1: the Harvard CMT catalog, reference 2: Tajima and Kikuchi (1995), and reference 3: Goes, *et al.* (1993).

Other Earthquakes

Within the central and eastern sections of this deformation belt, the USGS catalog lists 10 focal plane solutions, 6 of them, normal mechanisms, 4 reverse mechanisms. Their magnitudes range between 5.4-6.3. The parameters for the 4 reverse focal mechanisms are:

<i>lat</i>	<i>long</i>	<i>strike</i>	<i>dip</i>	<i>rake</i>	
9.7	79.7	238	70	31	(LL+ compression facing NW)
10.2	80.0	35	45	57	(compression+LL facing SE)
10.3	79.7	72	54	56	(compression+LL facing ESE)
9.0	77.4	75	26	20	(LL+compression facing ESE);

The USGS catalog lists the following earthquakes with reverse mechanism along the westernmost section (Costa Rica):

<i>lat</i>	<i>long</i>	<i>strike</i>	<i>dip</i>	<i>rake</i>	
9.88	-82.34	138	21	105	(compression+RL facing SW)
9.54	-82.64	151	9	108	(compression+RL facing SW)
9.65	-82.47	155	34	135	(compression+RL facing SW)
9.643	-82.3	346	34	134	(compression+RL facing ENE)

9.91	-82.1	320	32	126	(compression+RL facing ENE)
9.69	-82.46	313	26	94	(compression facing NE)
10.1	-83.07	143	46	112	(compression+RL facing SW)

Relative Motion from GPS

The relative motion between Isla San Andres (east of Nicaragua), which is considered representative of Caribbean plate motion, and Panama is 11 mm/y in azimuth 180° (Kellogg, *et al.*, 1995). Others suggest a rate of relative motion of 7 ± 2 mm/y in direction southwest between Isla San Andres and Costa Rica and westernmost Panama (Trenkamp, *et al.*, 2002).

Northern South America Convergent Zone, 11.5°-14°N, 77°W-64°W

Summary

It is difficult to evaluate the potential tsunami hazard from the convergence zone along the north coast of South America. Although there is shortening in the SE direction between the Caribbean and South American plates, much of the shortening is probably absorbed by deformation inland within and at the boundaries of the North Andes and Maracaibo blocks (Figures 6-1, 6-3). The amount of offshore deformation is not well known. There have been only two moderate earthquakes with reverse mechanisms during the past 40 years in the offshore areas. Shallow compressional deformation is more intense west of Aruba than to the east and reaches a maximum around longitude 75°W. There is no Holocene deformation west of 76.5°W on the north/south oriented subduction segment. The shape of the subduction zone under the northwest corner of South America is in dispute, with pieces of Nazca plate entering from the west and Caribbean plate perhaps also entering from the west as well as from the north. Some workers suggest that the Caribbean plate has a dip of 17°, but the lack of seismicity does not enable a good definition of the slab. There are no historical tsunamis associated with the convergent zone.

East of 68°W, 80% of the 2 cm/y motion between Caribbean and South American plates is confined to an 80-km narrow shear zone centered around the El Pilar strike-slip fault. The expected recurrence rate there is 150-200 y with slip magnitude of 3 - 4 m. There have been several devastating tsunamis associated with the El-Pilar fault in the past 500 years, but in our opinion, those are due to local compression or submarine landslides along the strike-slip fault. Between the El-Pilar fault and Aruba, the deformation zone widens but shows signs of extension, not compression.

As a worse case scenario (probably highly unlikely), we suggest thrust faulting along a 550 km long segment of the convergent zone between 72.5°-76.5°W oriented at N53°W with a dip of 17° and an unknown downdip length and slip. Another thrust fault could exist north of Oca fault (Figure 6-1), but motion there should be fairly oblique.

Surface Deformation Offshore

NE-facing normal faults are found around Aruba, Bonaire, and Curacao (Taboada, *et al.*, 2000). Seismic reflection profiles perpendicular to the margin show an apron of undeformed sediments migrating northward across an older deformed belt (*ibid.*). The deformation zone is narrow (~45 km) and shows mild compression north of Bonaire, and the sediments of the Venezuela basin entering the trench appear sagged, as if under tension. Deformation is getting more intense and its frontal edge is steeper north of Aruba and Guajira peninsula (~71.5°W). Deformation reaches maximum intensity along the NW corner of the convergence zone, and becomes less intense farther south (Ladd, *et al.*, 1984). No deformation is observed in offshore Holocene sediments of western Columbia (from Cartagena all the way south. (Duque-Caro, 1984)

Previous Tsunamis

01/17/1929 – A tsunami destroyed Cumana, Venezuela (South of Isla Margarita) following an Ms=6.9 earthquake (Lander, *et al.*, 2002). All other historical tsunamis appear to concentrate in the Gulf of Cariaco, Isla Margarita, and the Gulf of Paria, (Lander, *et al.*, 2002)) where the Pilar fault has a strike slip motion.

Earthquakes

Only four earthquakes are listed in the Harvard CMT catalog between 1976 and 2007 offshore NW South America. All four earthquakes were located east of 72.8°W and show normal fault mechanisms. Two earthquake with reverse mechanisms were quoted by Perez *et al.*, (1997):

03/12/1968	13.15°N	72.3°W	depth 58 km	Mb=5.3
04/28/1978	11.99°N	72.54°W	depth 62 km	Mb=5.2

Earthquakes around Aruba, Bonaire, and Curacao, show right-lateral strike slip.

Seismicity is shallower than 50 km deep between the northern edge of the deformation zone and the coast (200 km east of 73.5W) (Figure 6-3). The slab has a sharp corner at 73.5°W-75°W (Colmenares and Zoback, 2003).

Large historic earthquakes occurred along the coast on the El Pilar strike-slip fault system which connects to the Bocono fault system which continues inland to the southwest (McCann and Pennington, 1990). The Oca fault, a westerly continuation of the El Pilar fault (Figure 6-1) has not been active historically (Figure 6-3). There is a disagreement whether the Caribbean actually subducts under northern South America, because of lack of shallow seismicity (McCann and Pennington, 1990).

Relative Block Motion from GPS

The relative motion between the Caribbean plate (as measured on San Andres Island) and stable South America is 20 mm/y in direction 104° (Corredor, 2003). Perez, *et al.* (2001) and Weber, *et al.* (2001) showed that east of 68°W, 80% of the motion between Caribbean and South American plates is confined to an 80-km narrow shear zone centered around the El Pilar strike-slip fault. The expected recurrence rate of earthquakes there is estimated to be 150-200 y with a slip magnitude of 3-4 m (Perez, *et al.*, 2001). The deformation zone widens to the west. The region south of Aruba and north of Bonoco fault (the Falcon Basin) moves at 15 mm/y at N82°E, implying a very small component of N-S compression (Perez, *et al.*, 2001).

The relative block motion Caribbean (San Andres) – North Andes Block (as represented by the Bogota, Columbia station) is 14 ± 2 mm/y in southeast direction (Trenkamp, *et al.*, 2002). However 2/3 of this motion may be taken by internal deformation of the north Andean block on shore, as evidenced by the fact that relative motion between the Caribbean and the stable South America plate is 20 mm/y, while the relative motion between Cartagena, Columbia, and stable South America is 14 mm/y at almost the same direction (Trenkamp, *et al.*, 2002). Trenkamp, *et al.*, (2002) suggested that the North Andes block escapes to the NE along the Bonoco Fault at a rate of 6 mm/y.

Stress indicators

Colmenares and Zoback (2003) show evidence for maximum horizontal compression in a southeast direction on land west of Maracaibo basin, and SW shortening, SE opening (*i.e.*, strike slip motion) in the Falcon Basin south of Aruba (Figure 6-3).

The deep structure of the convergent zone

The Caribbean subduction zone under western Columbia is suggested to be very steep. However, the shape of subduction zones under South America is in dispute, with various authors proposing that pieces of Nazca plate enter from west and the Caribbean plate perhaps entering from west as well as from north (Malave and Suarez, 1995; van der Hilst and Mann, 1994). van der Hilst and Mann (1994) proposed an average dip of 17° for Caribbean under northwest S. America.

Figures

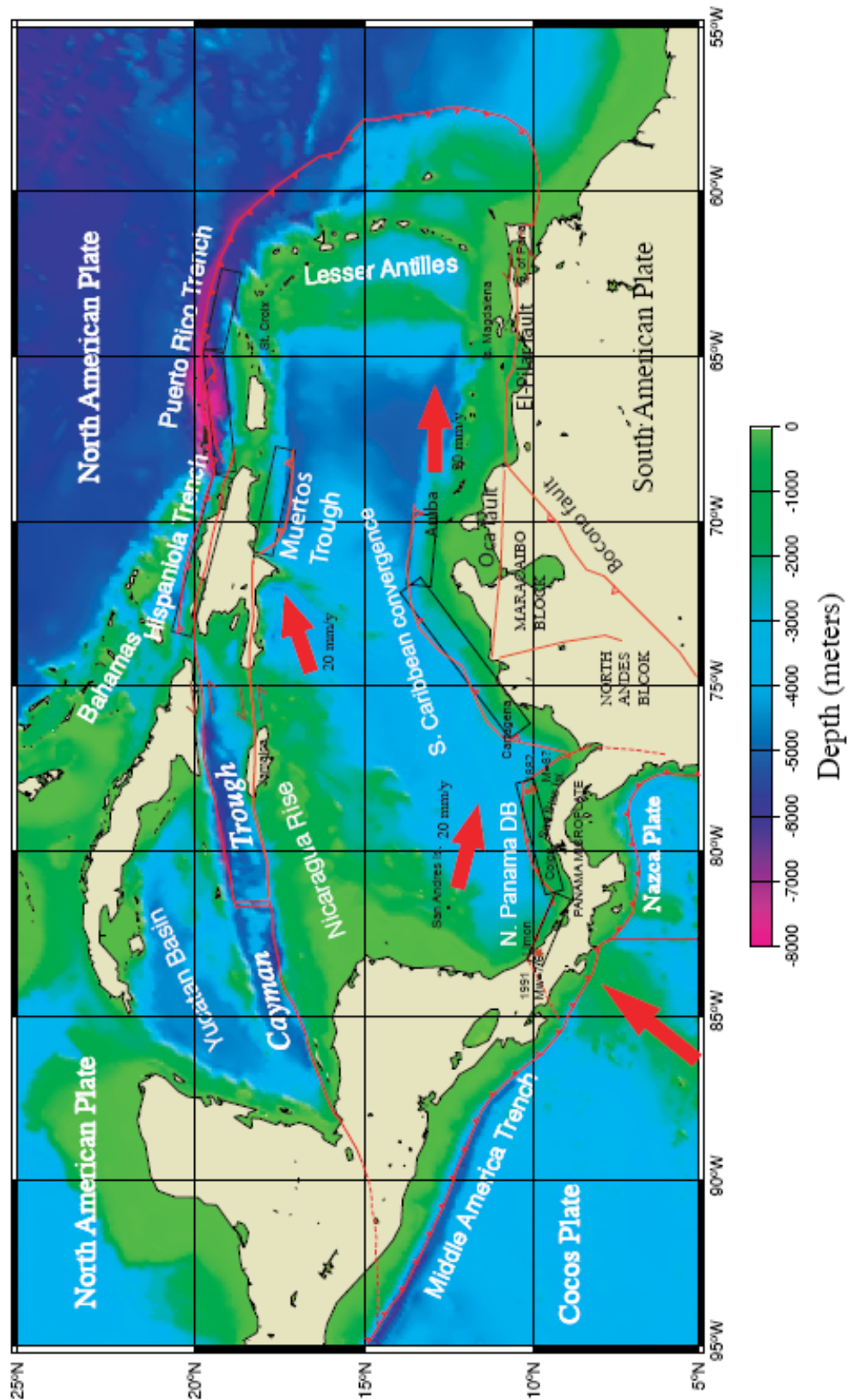


Figure 6-1: The Caribbean plate boundary and its tectonic elements.

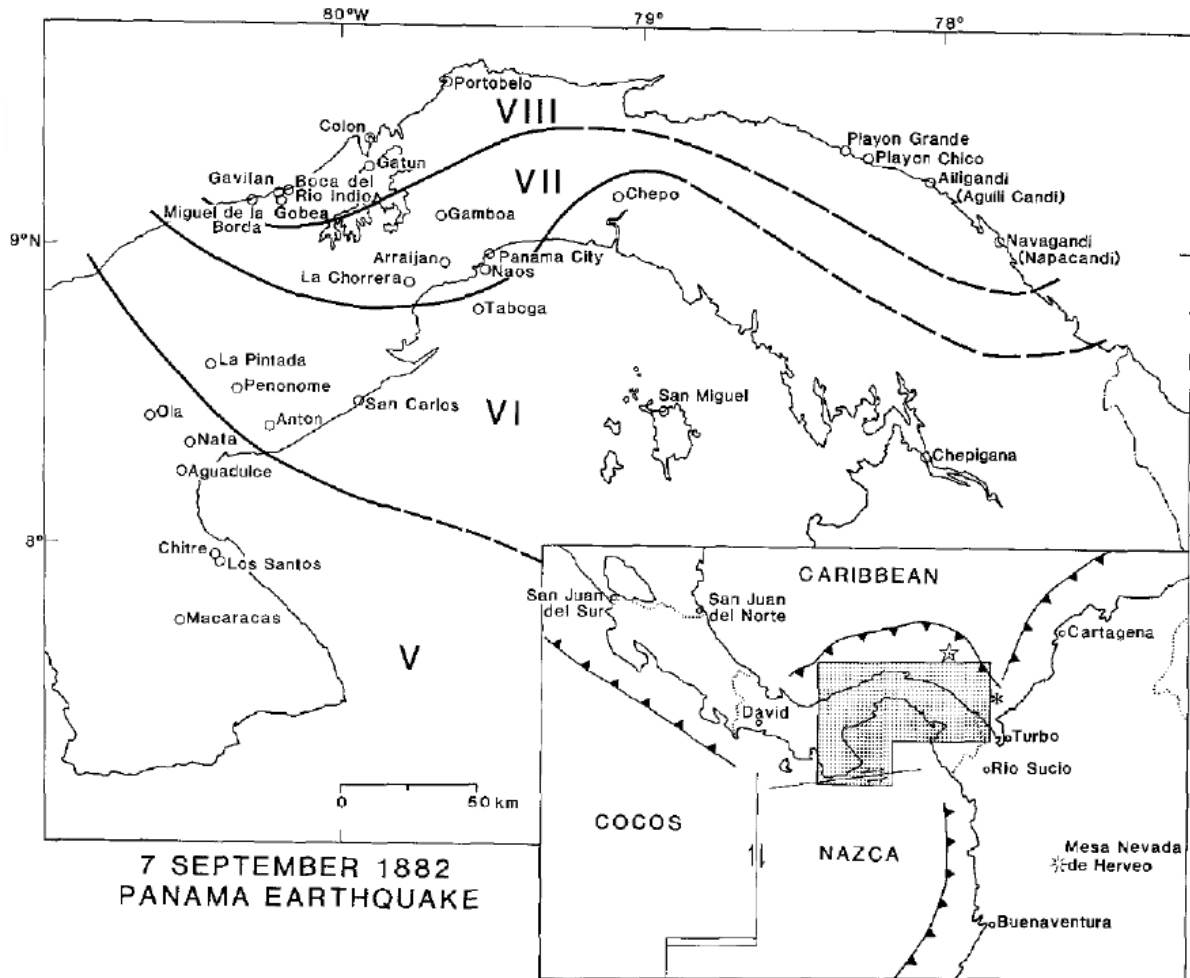


Figure 6-2: Iseisma map of the 1882 earthquake in the North Panama Deformation Belt (from Mendoza and Nishenko, 1989). The star in the inset is their preferred epicenter.

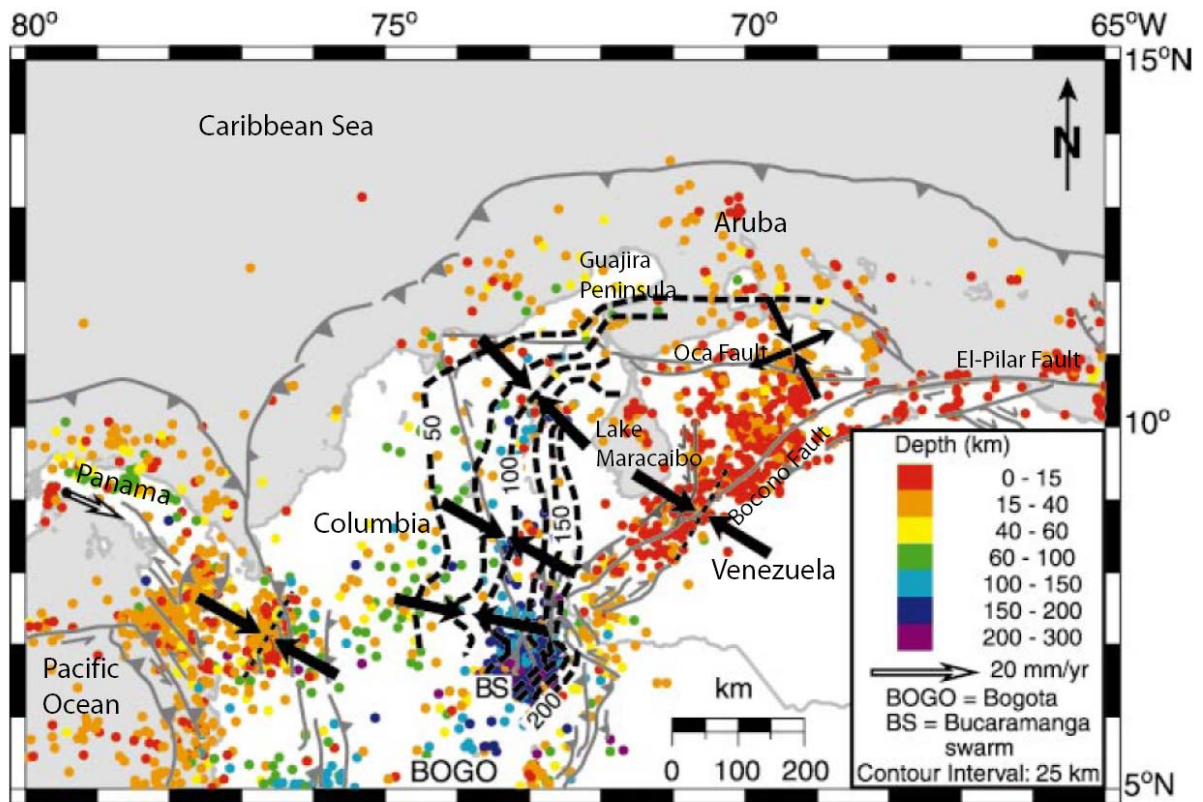


Figure 6-3: Depth of seismicity and generalized stress directions (from Colmenares and Zoback, 2003). Contour lines depths in km to top surface of inclined seismic zones.

References

- Colmenares, L., and Zoback, M. D., 2003, Stress field and seismotectonics of northern South America: *Geology*, v. 31, p. 721-724.
- Corredor, F., 2003, Seismic strain rates and distributed continental deformation in the Northern Andes and three-dimensional seismotectonics of northwestern South America: *Tectonophysics*, v. 372, p. 147-166.
- Duque-Caro, H., 1984, Structural style, diapirism, and accretionary episodes of the Sinu-San Jacinto terrane, southwestern Caribbean borderland: *Memoir - Geological Society of America*, v. 162, p. 303-316.
- Goes, S. D. B., Velasco, A. A., Schwartz, S. Y., and Lay, T., 1993, The April 22, 1991, Valle de la Estrella, Costa Rica (M (sub w) = 7.7) earthquake and its tectonic implications; a broadband seismic study: *Journal of Geophysical Research*, v. 98, p. 8127-8142.
- Kellogg, J. N., Vega, V., Stallings, T. C., Aiken, C. L. V., and Kellogg, J. N., 1995, Tectonic development of Panama, Costa Rica, and the Colombian Andes; constraints from Global Positioning System geodetic studies and gravity: *Special Paper - Geological Society of America*, v. 295, p. 75-90.

- Ladd, J. W., Truchan, M., Talwani, M., Stoffa, P. L., Buhl, P., Houtz, R., Mauffret, A., and Westbrook, G. K., 1984, Seismic reflection profiles across the southern margin of the Caribbean: *Memoir - Geological Society of America*, v. 162, p. 153-159.
- Lander, J. F., Whiteside, L. S., and Lockridge, P. A., 2002, A brief history of tsunamis in the Caribbean Sea: *Science of Tsunami Hazards*, v. 20, p. 57-94.
- Malave, G., and Suarez, G., 1995, Intermediate-depth seismicity in northern Colombia and western Venezuela and its relationship to Caribbean Plate subduction: *Tectonics*, v. 14, p. 617-628.
- McCann, W. R., and Pennington, W. D., 1990, Seismicity, large earthquakes, and the margin of the Caribbean Plate, Geol. Soc. Am. Boulder CO United States (USA).
- Mendoza, C., and Nishenko, S. P., 1989, The North Panama earthquake of 7 September 1882; evidence for active underthrusting: *Bulletin of the Seismological Society of America*, v. 79, p. 1264-1269.
- Perez, O. J., Bilham, R., Bendick, R., Velandia, J. R., Hernandez, N., Moncayo, C., Hoyer, M., and Kozuch, M., 2001, Velocity field across the southern Caribbean plate boundary and estimates of Caribbean/South-American plate motion using GPS geodesy 1994-2000: *Geophysical Research Letters*, v. 28, p. 2987-2990.
- Perez, O. J., Jaimes, M. A., and Garciacaro, E., 1997, Microseismicity evidence for subduction of the Caribbean Plate beneath the South American Plate in northwestern Venezuela: *Journal of Geophysical Research*, v. 102, p. 17,875-817,882.
- Plafker, G., and Ward S. N., 1992, Backarc thrust faulting and tectonic uplift along the Caribbean Sea coast during the April 22, 1991 Costa Rica earthquake: *Tectonics*, v. 11, p. 709-718.
- Reed, D. L., and Silver, E. A., 1995, Sediment dispersal and accretionary growth of the North Panama deformed belt: *Special Paper - Geological Society of America*, v. 295, p. 213-223.
- Taboada, A., Rivera, L. A., Fuenzalida, A., Cisternas, A., Philip, H., Bijwaard, H., Olaya, J., and Rivera, C., 2000, Geodynamics of the Northern Andes; subductions and intracontinental deformation (Colombia): *Tectonics*, v. 19, p. 787-813.
- Tajima, F., and Kikuchi, M., 1995, Tectonic implications of the seismic ruptures associated with the 1983 and 1991 Costa Rica earthquakes: *Special Paper - Geological Society of America*, v. 295, p. 327-340.
- Trenkamp, R., Kellogg, J. N., Freymueller, J. T., and Mora, H. P., 2002, Wide plate margin deformation, southern Central America and northwestern South America, CASA GPS observations: *Journal of South American Earth Sciences*, v. 15, p. 157-171.
- van der Hilst, R., and Mann, P., 1994, Tectonic implications of tomographic images of subducted lithosphere beneath northwestern South America: *Geology*, v. 22, p. 451-454.
- Weber, J. C., *et al.*, 2001, GPS estimate of relative motion between the Caribbean and South American plates, and geologic implications for Trinidad and Venezuela: *Geology*, v. 29, p. 75-78.

Chapter 7: Regional Tsunami Propagation Patterns from Caribbean Earthquakes

Tsunami propagation from large-magnitude earthquakes in the Caribbean is calculated to estimate deep ocean tsunami amplitudes offshore U.S. Atlantic and Gulf coasts. Sources for the tsunami calculations are discussed previously in Chapter 6: Tsunamigenic earthquake sources that may affect the Gulf of Mexico, and Chapter 5: Review of tsunamigenic earthquake sources that may affect the U.S. Atlantic Coast. This is a preliminary effort for the purpose of determining the relative severity among tsunamis from different sources and complements recent work by Knight (2006). A range of tsunami amplitudes is determined based on natural variations in slip distribution patterns expected for large magnitude earthquakes along plate boundaries in the Caribbean. This work predicts maximum wave amplitudes in 250 m of water at the shelf edge and does not predict runup nor propagation characteristics across the continental shelf.

Method

Large magnitude earthquakes in the Caribbean (Figure 6-1) were specified by determining a maximum rupture length along the following plate boundary segments (using classification scheme by Bird, 2003): (1) west Cayman oceanic transform fault (OTF), also known as Swan Island Fault, (2) east Cayman (OTF), also known as Oriente Fault, (3) northern Puerto Rico/Lesser Antilles subduction zone (SUB), (4) north Panama deformation belt, classified by Bird (2003) as an oceanic convergent boundary (OCB), and (5) the north coast of South America convergence zone classified by Bird (2003) as a subduction zone (SUB) (termed the north Venezuela subduction zone below). This classification scheme will be used to assess the probability of earthquakes along these fault zones in a later study.

Other faults in the Caribbean that can generate destructive local tsunamis, but unlikely to generate far-field tsunamis such as thrust faulting in the Muertos Trough and normal faulting in the Mona Passage were not modeled in this study. For the transform faults, the moment magnitude was estimated from rupture length using the Wells and Coppersmith (1994) empirical relationships. From this relationship and an estimate of the fault width (seismogenic thickness) from Bird and Kagan (2004), an average slip was assigned to each fault, assuming a shear modulus of 35 GPa. Fault dip and rake were estimated from analysis of past focal mechanisms from the

Global CMT database (<http://www.globalcmt.org/>). For the subduction boundary faults, geometric parameters were taken from regional studies described previously in the report and in prior publications (*e.g.*, ten Brink and Lin, 2004). Scaling of average slip from rupture length was taken from compiled databases of source parameters for subduction interplate thrust earthquakes (Lay *et al.*, 1982; Geist, 2002). Uncertainty caused by variations in slip distribution patterns is assessed by computing 100 different slip distributions that all have nearly the same average slip and slip spectrum (Herrero and Bernard, 1994; Geist, 2002; Geist *et al.*, 2007). A summary of the range of magnitude and average slip for each fault is given in Table 7-1.

Initial conditions for the propagation model are specified by the coseismic displacement of the seafloor. This includes primarily the vertical component of displacement. In addition, horizontal displacement in regions of steep bathymetric gradient will also contribute to vertical displacement of the water column in a manner described by Tanioka and Satake (1996). Since this component of the initial wavefield depends on the bathymetric gradient field near the source region, it is relatively incoherent compared to the primary component of the initial wavefield from vertical coseismic displacement. The transform faults (OTF) are much less efficient at generating tsunami waves (Figure 7-1a, b) than the thrust faults along subduction zones (SUB) and oceanic convergent boundaries (OCB) (Figure 7-1c, d, e).

Tsunami propagation was modeled using the linear long-wave equation, numerically implemented with a leap-frog, finite-difference algorithm. Only deep-ocean tsunami propagation is modeled, where linear theory is most applicable. Propagation across the continental shelf (specified by water depth less than 250 m) and runup are not modeled. As a very rough approximation, runup is approximately 3 times the tsunami amplitude at 250 m water depth, accounting for shoaling and runup amplification (Shuto, 1991; Satake, 1995, 2002), but not including energy dissipation from geometric spreading, bottom friction, and non-linear attenuation that is evident in the simulations of the Currituck landslide tsunami offshore Virginia, USA (Chapter 9). It is unclear whether the latter two dissipation mechanisms are as significant for far-field seismogenic tsunamis as they are for landslide tsunamis. Radiation boundary conditions are specified at the open-ocean boundaries, whereas reflection boundary conditions are specified at the 250 m isobath. The spatial grid size for the simulations is 2 arc-minutes and the time step is 8 s, which satisfies the Courant-Friedrichs-Lewy stability criterion (Satake, 2002). Total propagation time for each simulation is 4.4-6.6 hours, which is sufficient to capture the first few waves at the 250 m isobath within the model domain.

Results

For each fault, results from the simulation are shown in Figure 7-1 through Figure 7-4. Figure 7-1 shows the maximum tsunami amplitude in the open ocean for one of the 100 simulations for each source. Figures 7-2 and 7-3 shows the range of peak offshore tsunami amplitudes from all 100 simulations at the 250 m isobath for a latitudinal profile in the Gulf of Mexico (Figure 7-2) and a longitudinal profile along the Atlantic coast, respectively (Figure 7-3). Figure 7-4 shows the range in tsunami amplitudes as a time series (*i.e.*, marigrams) for selected offshore locations in the Gulf of Mexico and Atlantic. Tsunami characteristic for coastal regions will be different, because of nearshore propagation and runup effects.

In terms of overall severity, large earthquakes along the northern Puerto Rico subduction zone generate the largest tsunamis propagating toward the U.S. Atlantic coast, of the cases studied (Figure 7-1c). For the Gulf Coast, the largest tsunamis are generated by large earthquakes along the north Venezuela subduction zone. The absolute tsunami amplitudes are highly dependent, however, on the magnitude specified for each of these fault zones. (Distributions of earthquake magnitudes for these fault zones will be discussed in a future study. In general, these results are consistent with the findings of Knight (2006), where the far-field tsunamis generated from earthquakes located beneath the Caribbean Sea are higher along the Gulf coast than the Atlantic coast because of dissipation through the Greater Antilles islands. Conversely, tsunamis generated from earthquakes north of the Greater Antilles are higher along the Atlantic coast than the Gulf coast.

Profiles of peak offshore tsunami amplitudes along the Atlantic coast (Figure 7-3) indicate regions of focusing from variations in bathymetry. A prominent increase in tsunami amplitude between approximately 32-24°N is caused by focusing of the tsunami by the Blake Ridge (see Figure 2-1 from Chapter 2). Bathymetric ridges often act as waveguides if the ray path of the wave is within a critical angle of obliquity with respect to the orientation of the ridge (Mei, 1989; Satake *et al.*, 1992). There is also higher peak offshore tsunami amplitudes at the higher latitudes (>39°N) caused simply by the change in the orientation of the Atlantic shelf edge to a more E-W orientation.

Similarly in the Gulf of Mexico (Figure 7-2), tsunami amplitudes are higher where the shelf edge is approximately normal to the incidence of tsunami waves propagating from the south (*i.e.*, between ~83-85°W and ~87.5-88.5°W). The range in tsunami amplitudes caused by variations in slip distribution patterns is dependent on the propagation path distance from the source to the shelf edge. This distance dependence of the resulting tsunami amplitude variability is also evident on the synthetic marigrams (graph of tsunami amplitude as a function of time) (Figure 7-4). In addition, for most cases except for the northern Puerto Rico subduction zone scenario tsunami, the onset of the tsunami at the 6 marigram stations can be characterized as emergent (*i.e.*, initial tsunami waves are smaller than later ones), primarily because of obstructed propagation paths. In general, spectral characteristics

of tsunami marigrams is dependent on source characteristics, propagation path, and site response (Rabinovich, 1997).

To determine the tsunami characteristic along the coast from these sources, a more refined hydrodynamic model needs to be employed. For example, the Method of Splitting Tsunami (MOST) model (Titov and Synolakis, 1996; Titov and González, 1997; Titov and Synolakis, 1998) is specifically designed to determine propagation and runup characteristics for regional and far-field tsunamis. Source characterizations similar to what is being used for the tsunami forecasting system (Titov *et al.*, 2005) should be adequate for determining tsunami characteristics along the U.S. Atlantic and Gulf coasts.

Table

Table 7-1: Source parameters and range of average slip and moment magnitudes of earthquakes from which tsunami simulations were computed.

Fault #*	Name	Type†	Length (km)	Width (km)	strike (°)	dip (°)	rake (°)	Avg. Slip-low (m)	Avg. Slip-high (m)	M _w (low)	M _w (high)
1	W. Cayman	OTF	746	15	N73E	83N	185	10.6	12.4	8.3	8.35
2	E. Cayman	OTF	915	15	N77E	80S	175	12.1	14.2	8.4	8.45
3a	Hispaniola	SUB	525	50	N98E	20S	70	8.2	9.4	8.8	8.84
3b	Puerto Rico	SUB	385	50	N83E	20S	23				
3c	Virgin Islands	SUB	485	50	N102E	20S	42				
4a	W. Northern Panama	OCB	200	40	N113E	30S	90	3.7	4.3	8.24	8.28
4b	E. Northern Panama	OCB	350	40	N75E	35S	90				
5a	W. Southern Caribbean	SUB	550	50	N53E	17S	90	4.7	5.4	8.46	8.5
5b	E. Southern Caribbean	SUB	200	50	N95E	17S	90				

*Faults with same numeral are treated as one tsunami source.

†See Bird (2003).

Figures

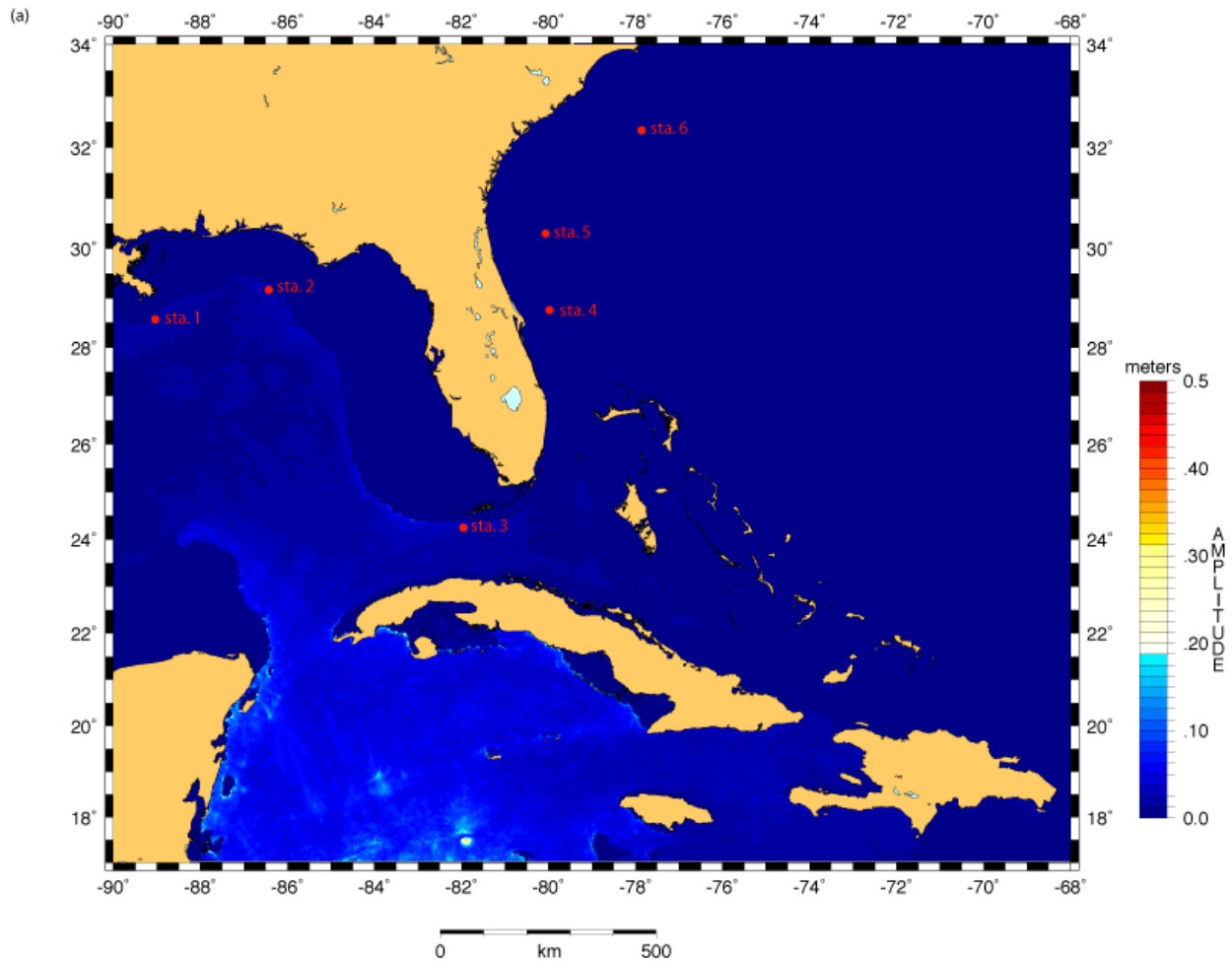
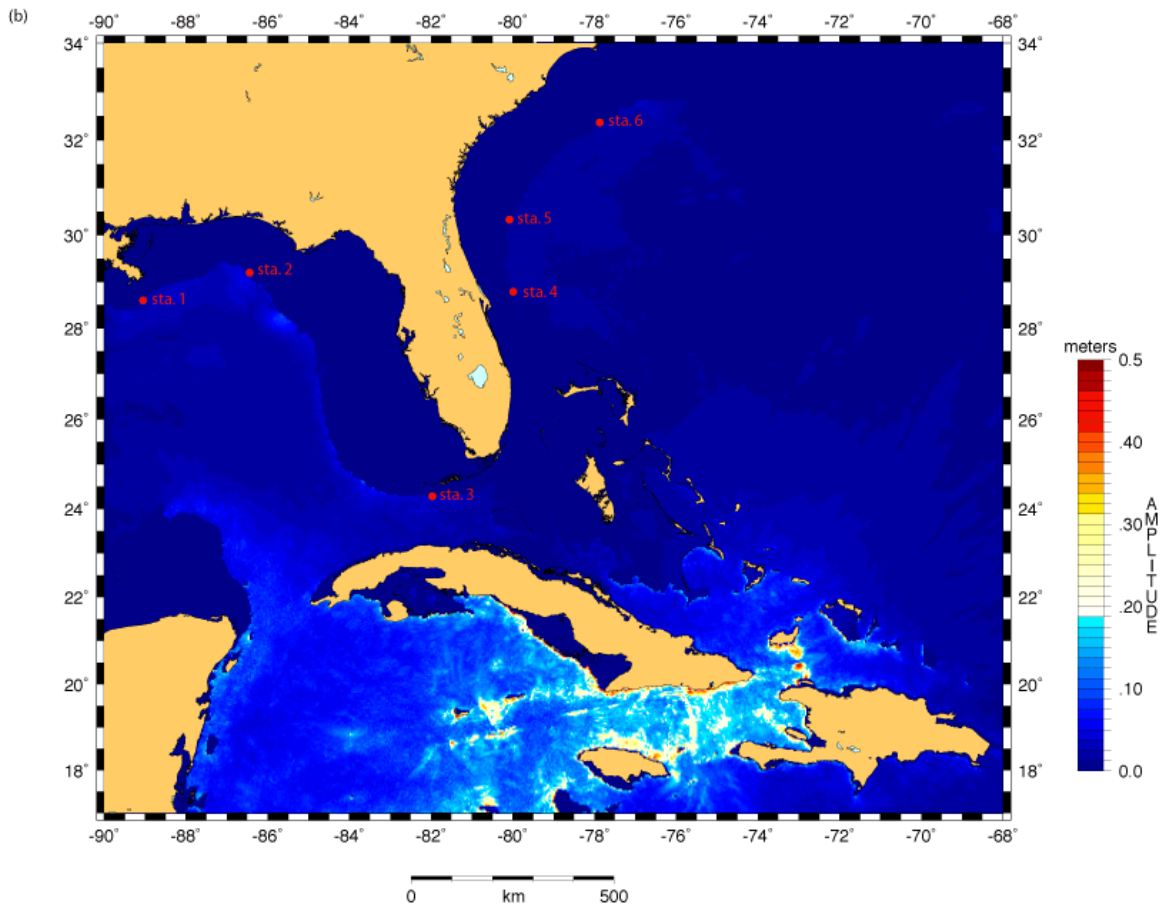
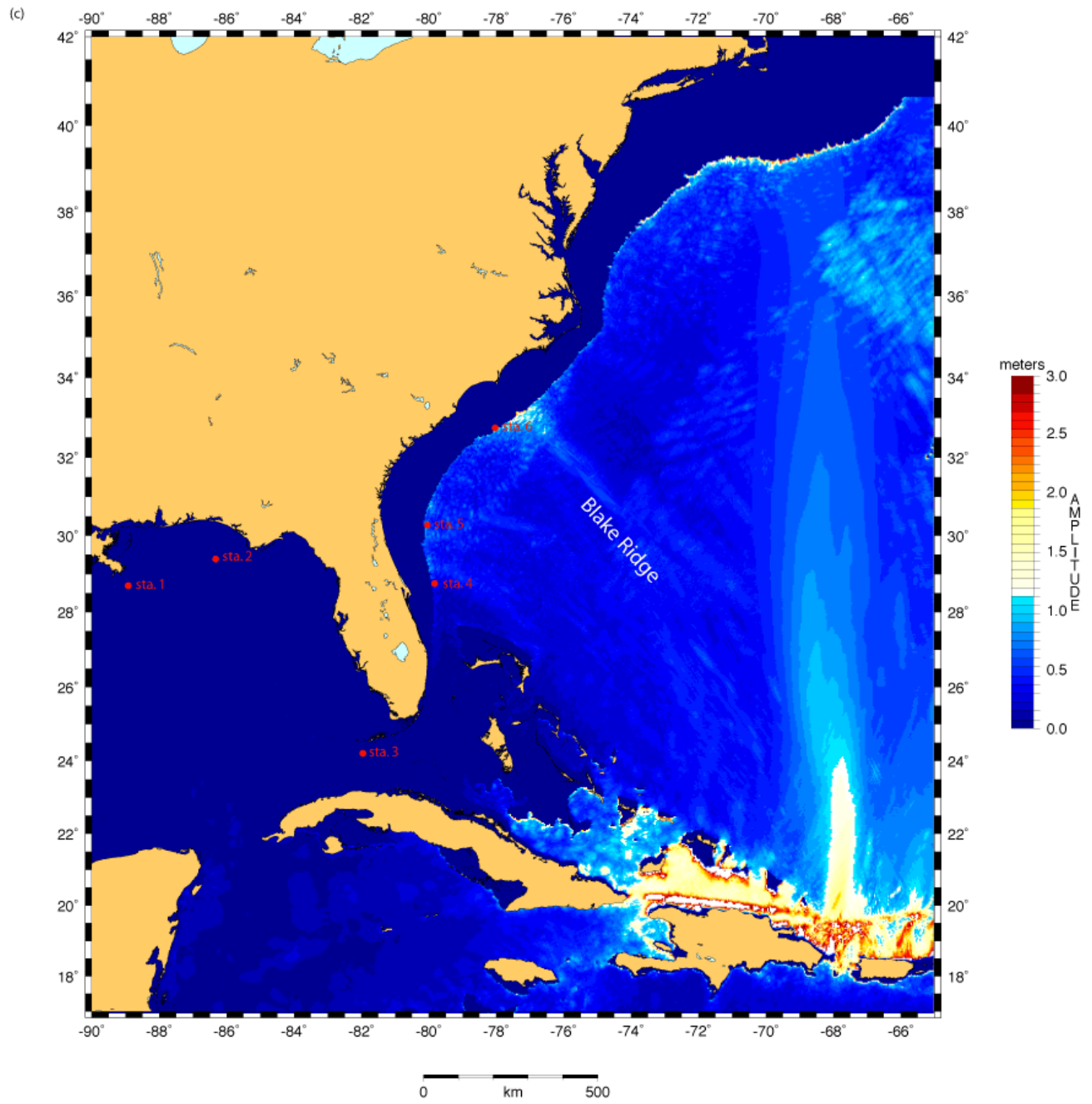
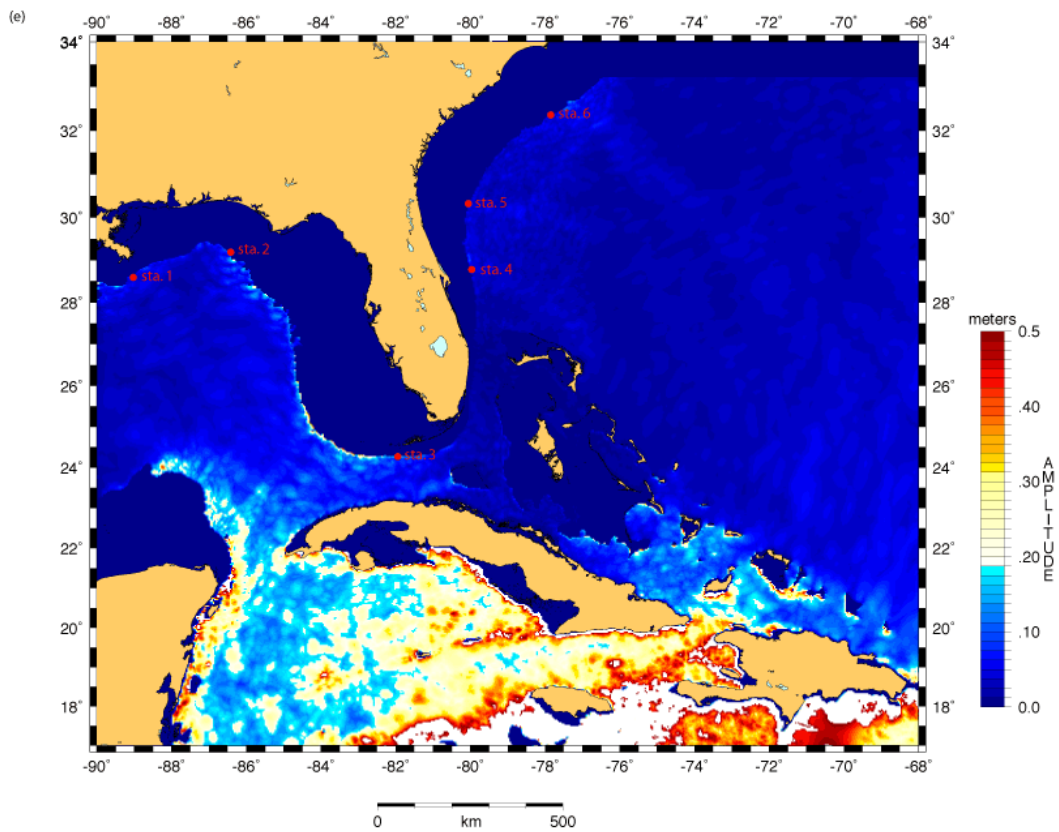
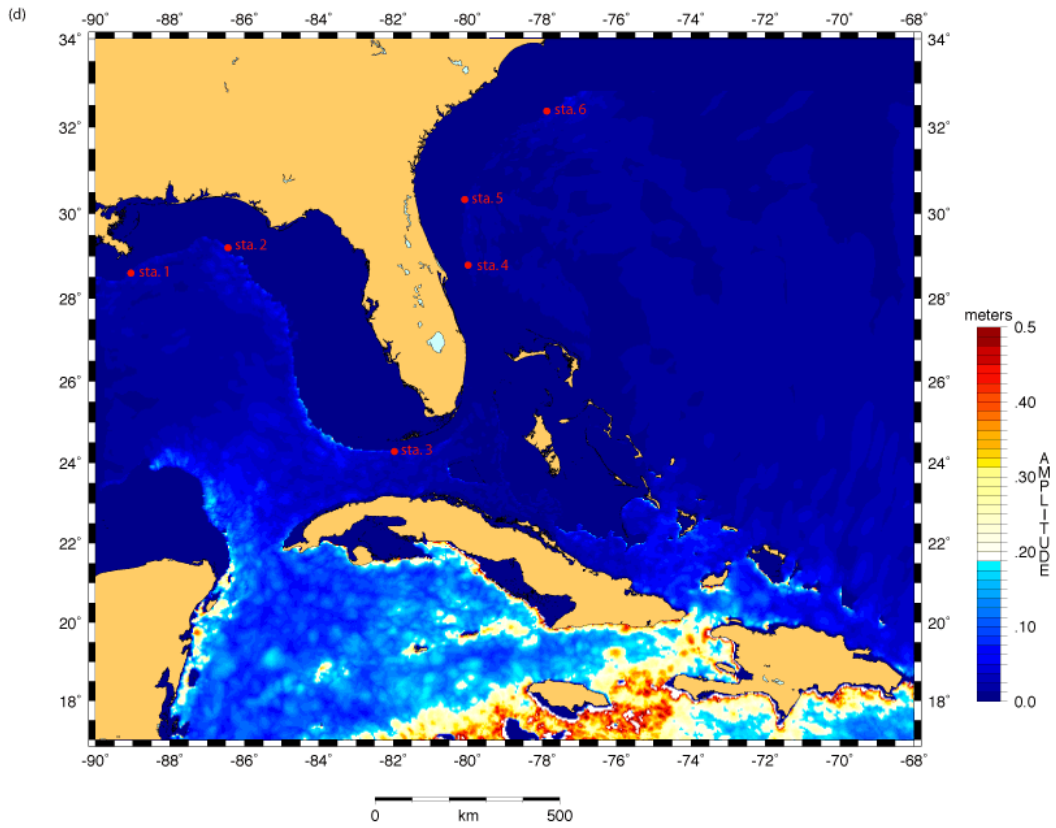


Figure 7-1: One simulation of maximum open-ocean tsunami amplitude over 4.4 hours of propagation time for each of the faults in the Caribbean: (a) W. Cayman OTF, (b) E. Cayman OTF, (c) N. Puerto Rico/Lesser Antilles SUB, (d) N. Panama OCB, (e) N. Venezuela SUB. Note change in amplitude scale for (c). Red dots indicate locations where synthetic marigrams are shown in Figure 7-4.







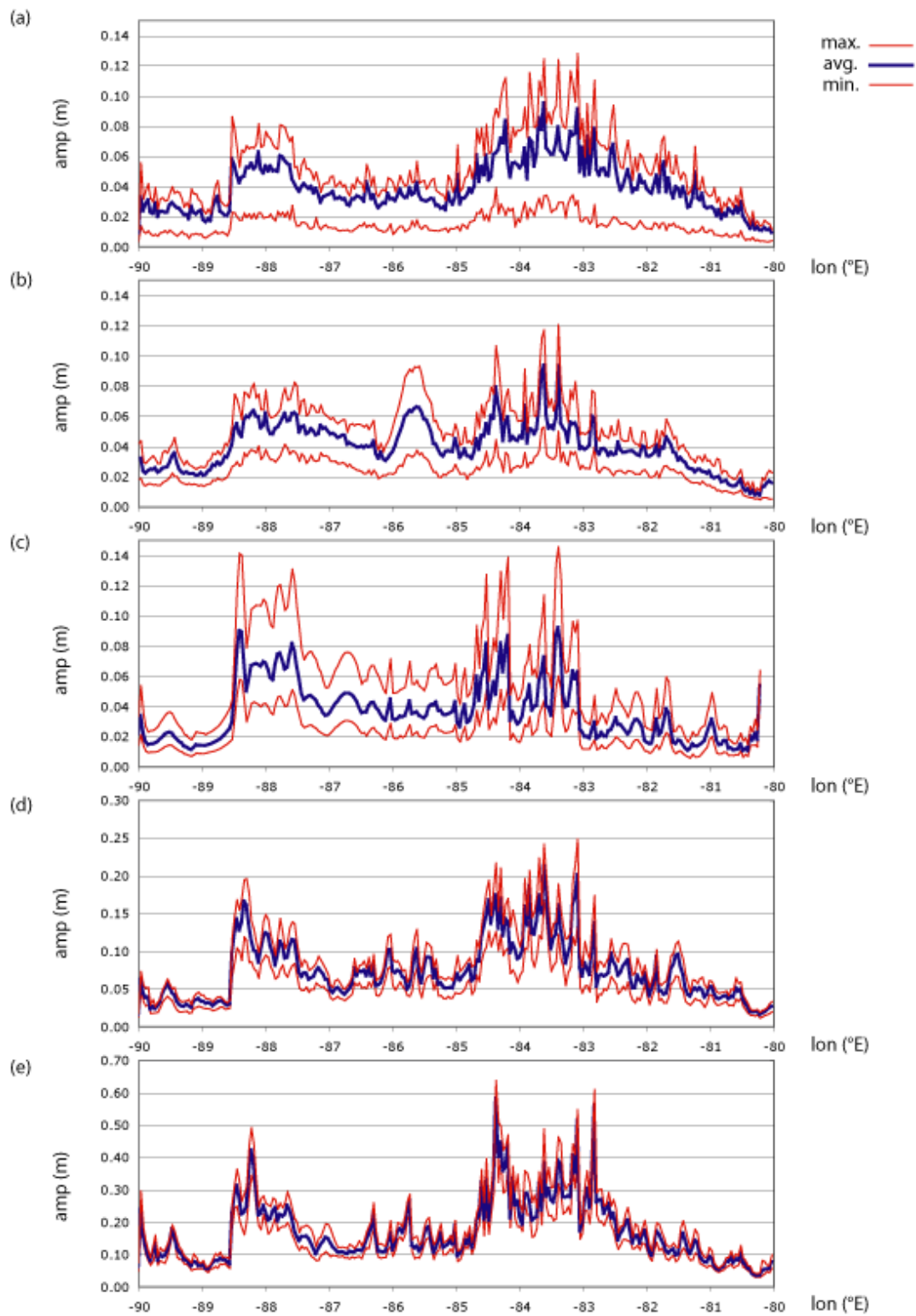


Figure 7-2: Peak offshore tsunami amplitude at the 250 isobath for 100 realizations of earthquakes on faults in the Caribbean: (a) W. Cayman OTF, (b) E. Cayman OTF, (c) N. Puerto Rico/Lesser Antilles SUB, (d) N. Panama OCB, (e) N. Venezuela SUB. Blue line shows average values; red lines extrema values. Results plotted along a latitudinal profile for the Gulf of Mexico coast. Note change in amplitude scale for (d) and (e).

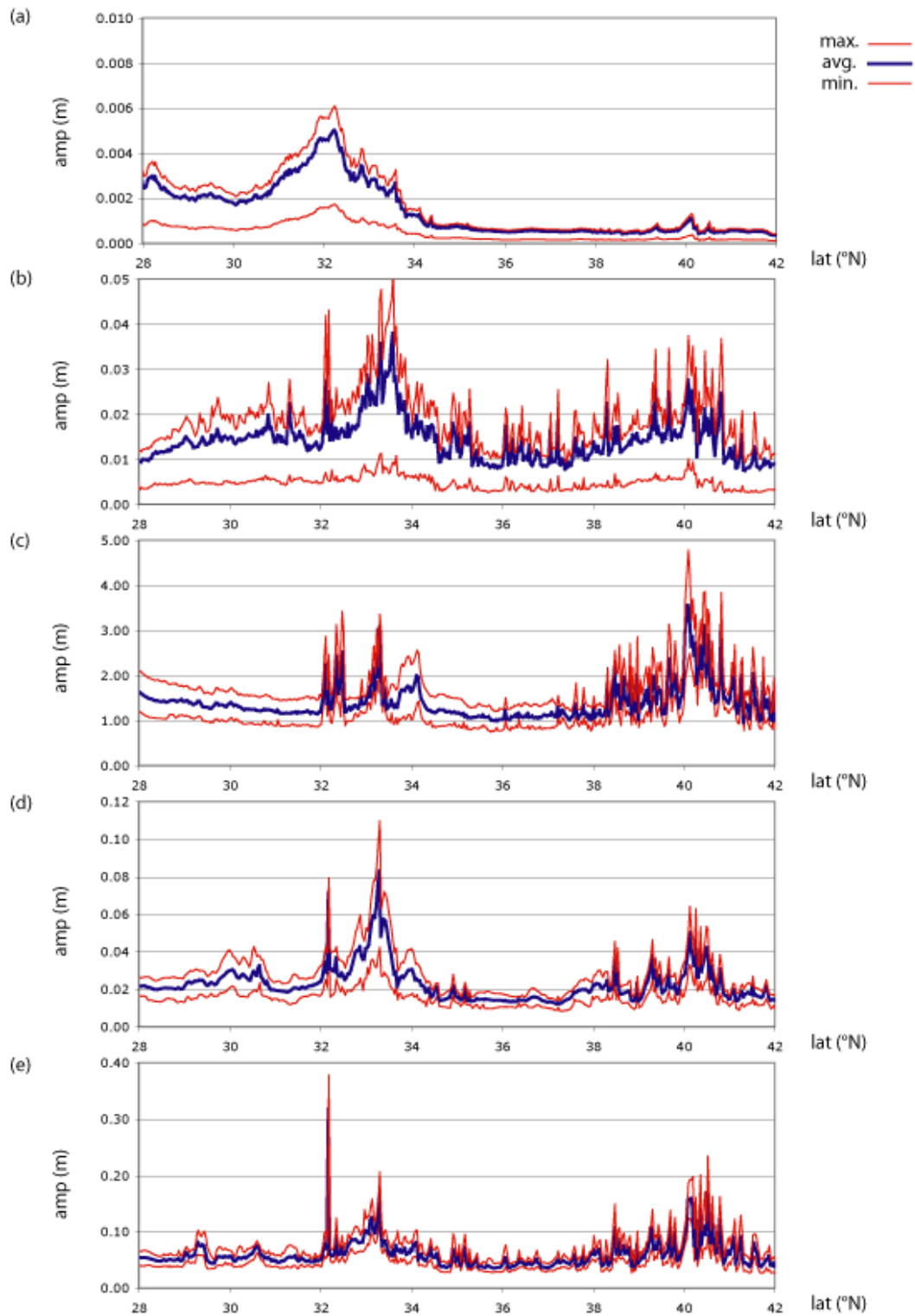


Figure 7-3: Peak offshore tsunami amplitude at the 250 isobath for 100 realizations of earthquakes on faults in the Caribbean: (a) W. Cayman OTF, (b) E. Cayman OTF, (c) N. Puerto Rico/Lesser Antilles SUB, (d) N. Panama OCB, (e) N. Venezuela SUB. Blue line shows average values; red lines extrema values. Results plotted along a longitudinal profile for the Atlantic coast. Note change in amplitude scale for each case.

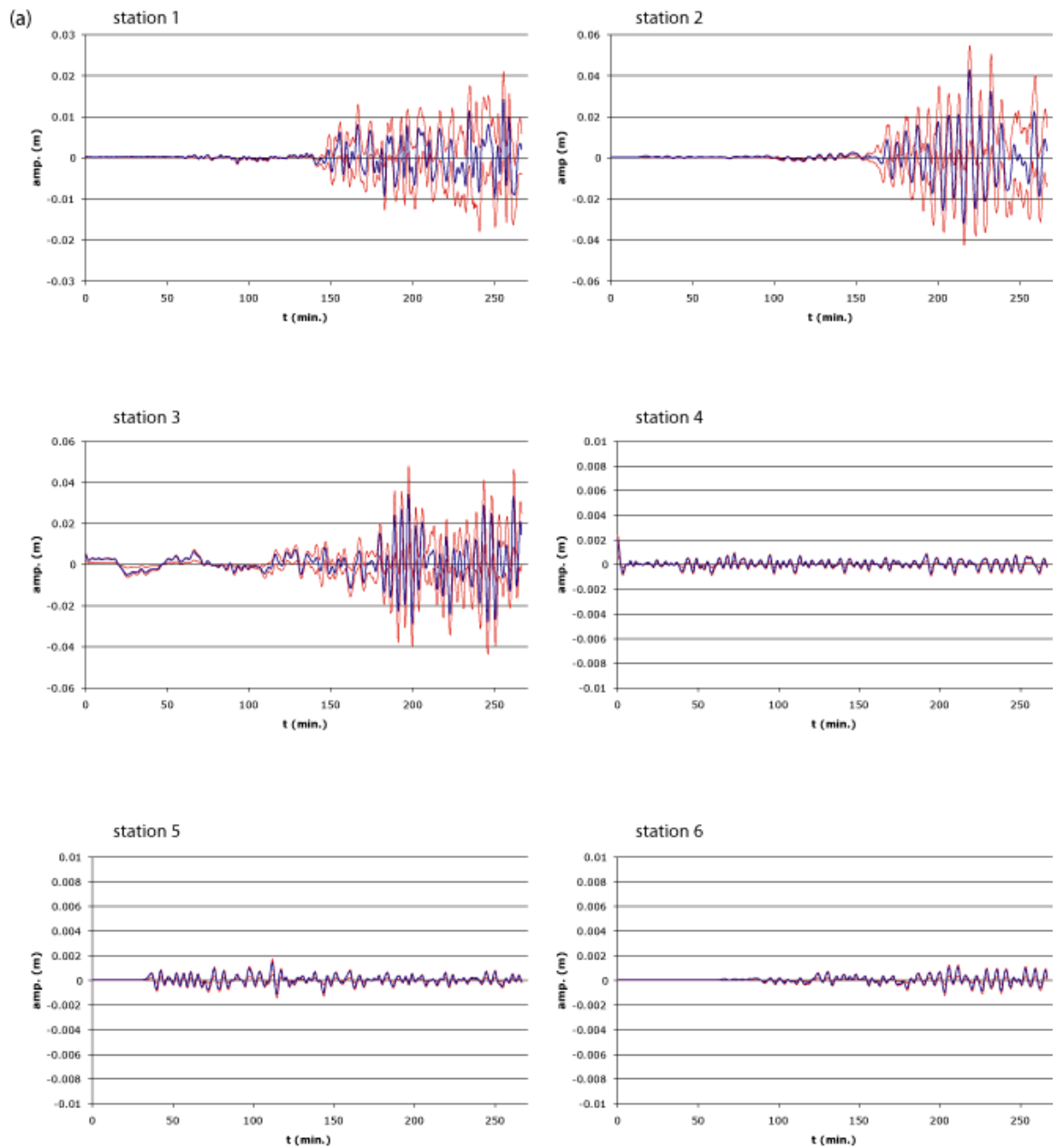
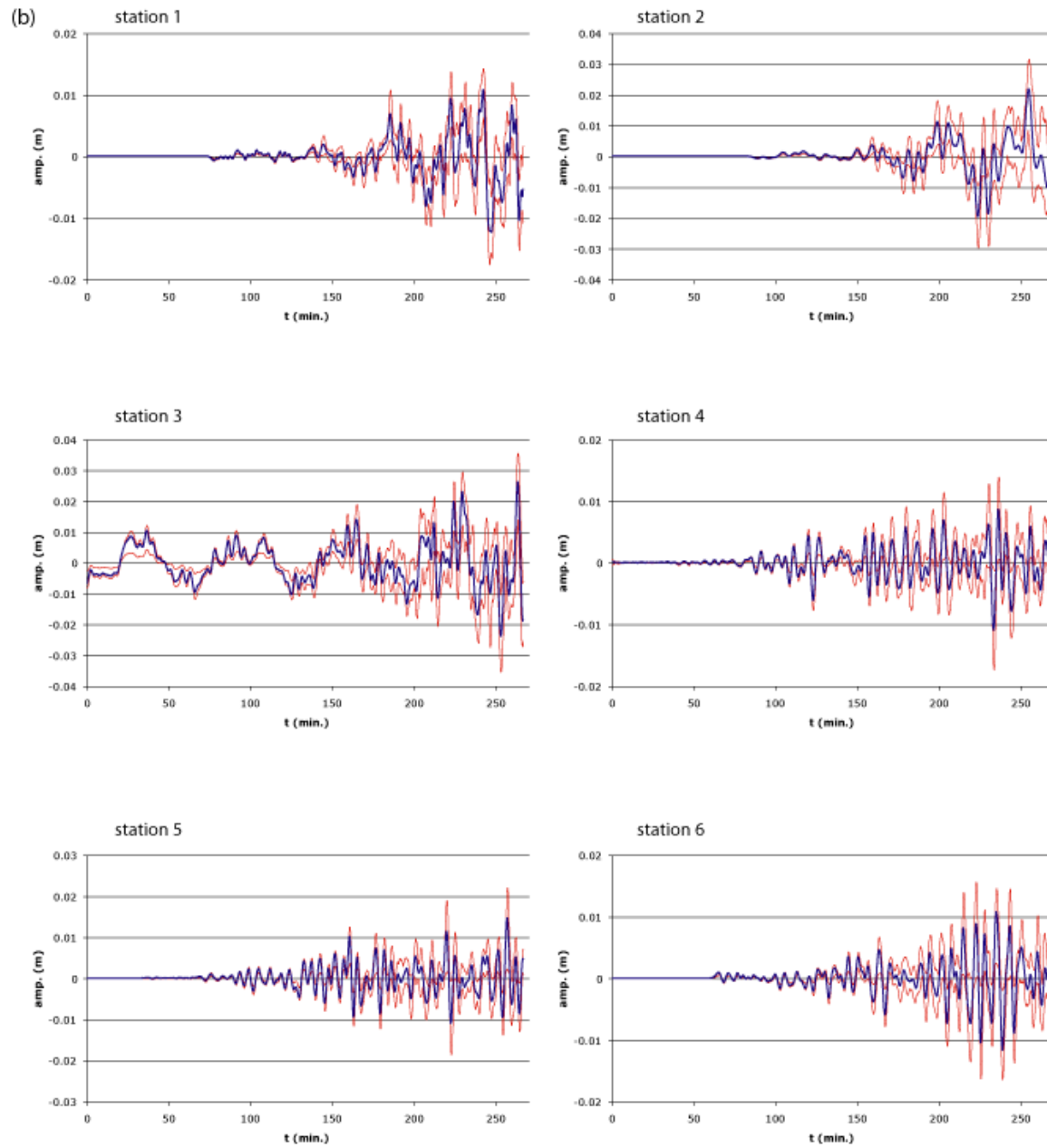
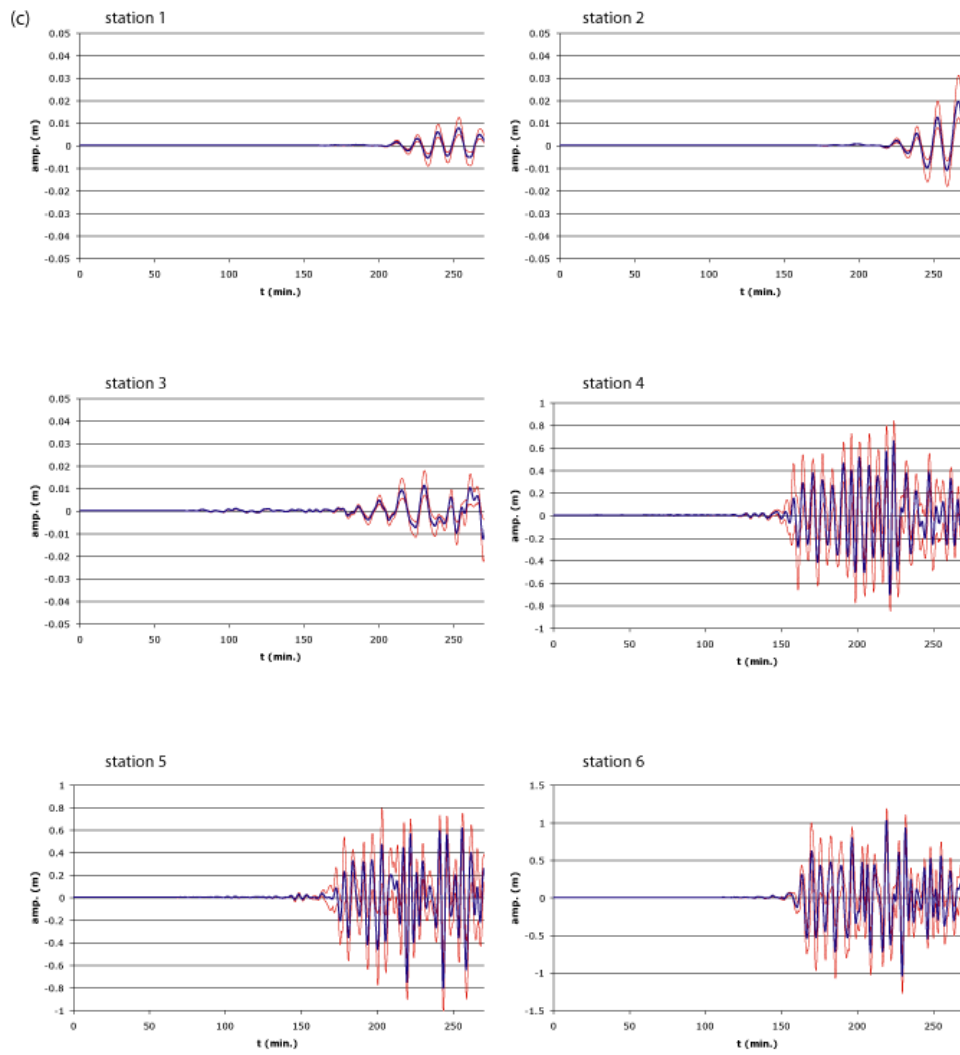
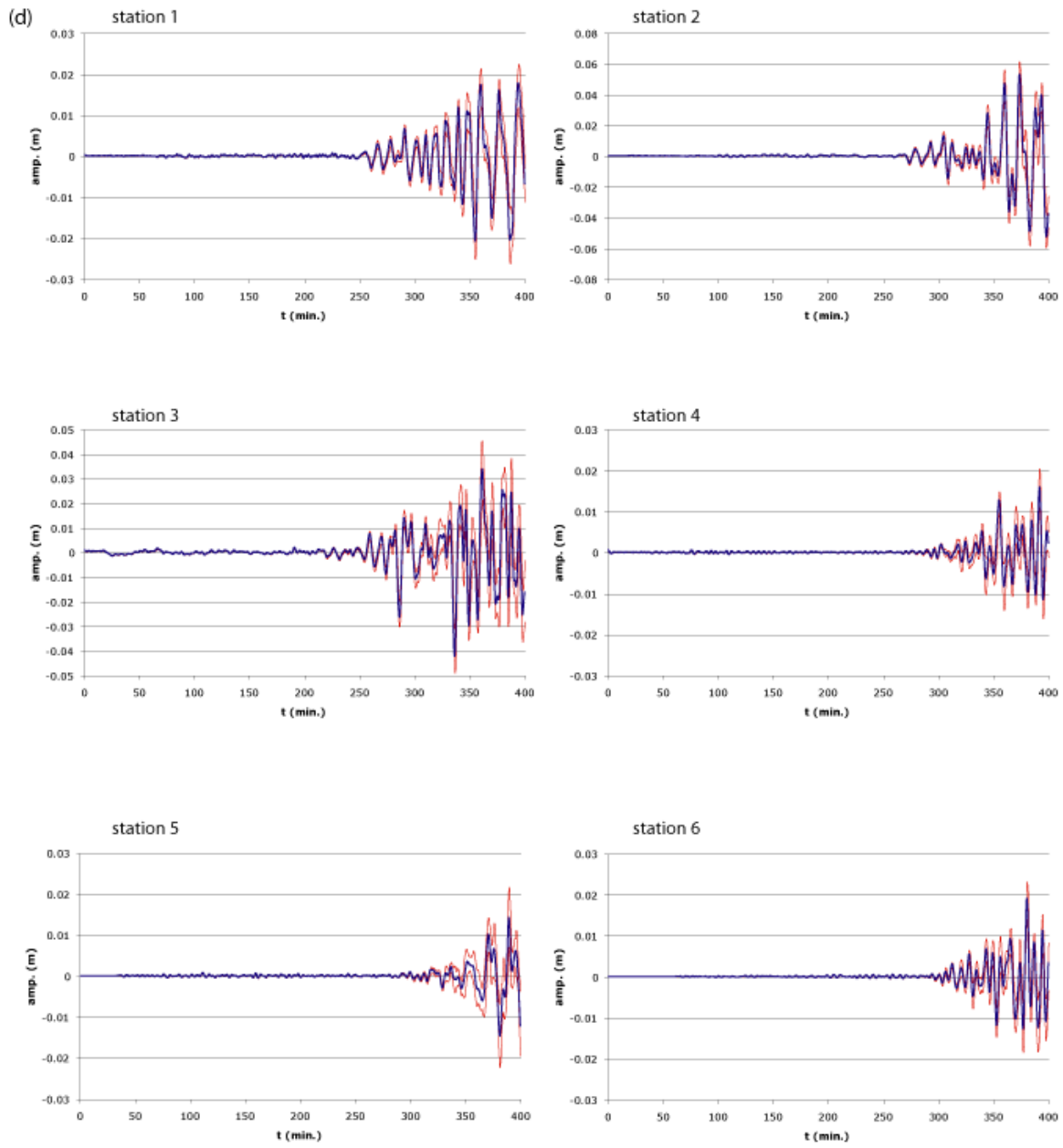
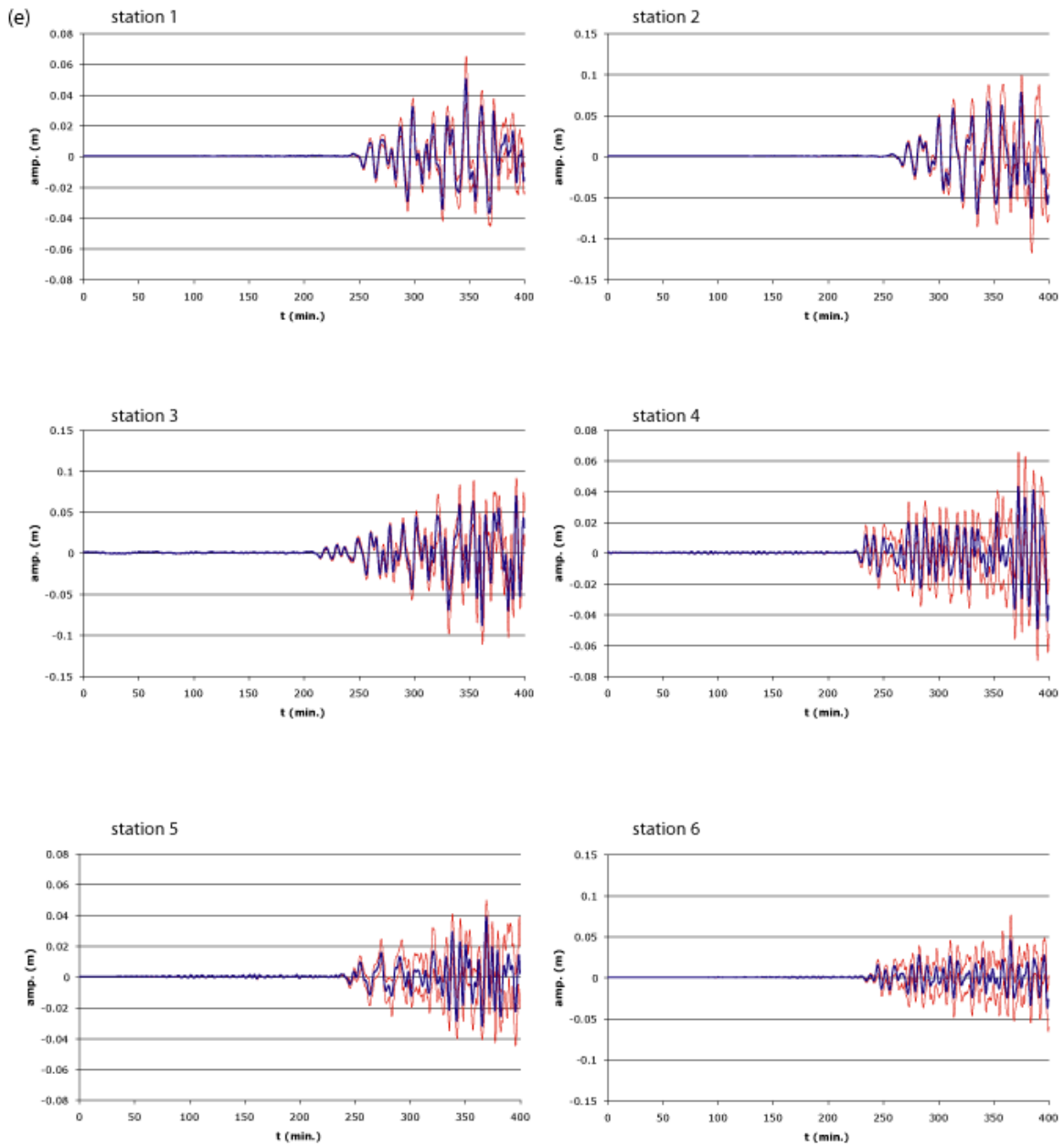


Figure 7-4: Range in synthetic marigrams (tsunami amplitude as a function of time) for six locations shown in Table 7-1. Results shown for each of the faults in the Caribbean: (a) W. Cayman OTF, (b) E. Cayman OTF, (c) N. Puerto Rico/Lesser Antilles SUB, (d) N. Panama OCB, (e) N. Venezuela SUB. Blue line shows average values; red lines extrema values. Note changes in amplitude scale.









References

- Bird, P., 2003, An updated digital model of plate boundaries: *Geochemistry, Geophysics, Geosystems*, v. 4, doi:10.1029/2001GC000252.
- Bird, P., and Kagan, Y. Y., 2004, Plate-tectonic analysis of shallow seismicity: apparent boundary width, beta-value, corner magnitude, coupled lithosphere thickness, and coupling in 7 tectonic settings: *Bull. Seismol. Soc. Am.*, v. 94, 2380-2399.
- Geist, E. L., 2002, Complex earthquake rupture and local tsunamis, *J. Geophys. Res.*, v. 107, doi:10.1029/2000JB000139.
- Geist, E. L., Titov, V. V., Arcas, D., Pollitz, F. F., and Bilek, S. L., 2007, Implications of the December 26, 2004 Sumatra-Andaman earthquake on tsunami forecast and assessment models for great subduction zone earthquakes: *Bull. Seismol. Soc. Am.*, v. 97, p. S249-S270.
- Herrero, A., and Bernard, P., 1994, A kinematic self-similar rupture process for earthquakes: *Bull. Seismol. Soc. Am.*, v. 84, p. 1216-1228.
- Knight, W., 2006, Model predictions of Gulf and southern Atlantic coast tsunami impacts from a distribution of sources: *Science of Tsunami Hazards*, v. 24, p. 304-312.
- Lay, T., Kanamori, H., and Ruff, L. J., 1982, The asperity model and the nature of large subduction zone earthquakes: *Earthquake Prediction Research*, vol. 1, p. 3-71.
- Mei, C. C., 1989, *The Applied Dynamics of Ocean Surface Waves*, World Scientific, Singapore, 740 p.
- Rabinovich, A. B., 1997, Spectral analysis of tsunami waves: Separation of source and topography effects: *J. Geophys. Res.*, v. 102, p. 663-612,676.
- Satake, K., 1995, Linear and nonlinear computations of the 1992 Nicaragua earthquake tsunami: *Pure Appl. Geophys.*, v. 144, p. 455-470.
- Satake, K., 2002, Tsunamis, in Lee, W. H. K., *et al.* (Editors), *International Handbook of Earthquake and Engineering Seismology, Part A*, Academic Press, San Diego, p. 437-451.
- Satake, K., Yoshida, Y., and Abe, K., 1992, Tsunami from the Mariana earthquake of April 5, 1990: Its abnormal propagation and implications for tsunami potential from outer-rise earthquakes: *Geophys. Res. Lett.*, v. 19, p. 301-304.
- Shuto, N., 1991, Numerical simulation of tsunamis--Its present and near future: *Natural Hazards*, v. 4, p. 171-191.
- Tanioka, Y., and Satake, K., 1996, Tsunami generation by horizontal displacement of ocean bottom: *Geophys. Res. Lett.*, v. 23, p. 861-865.
- ten Brink, U. S., and Lin, J., 2004, Stress interaction between subduction earthquakes and forearc strike-slip faults: Modeling and application to the northern Caribbean plate boundary: *J. Geophys. Res.*, v. 109, B12310, doi:10.1029/2004JB003031.
- Titov, V. V., and Synolakis, C. E., 1996, Numerical modeling of 3-D long wave runup using VTCS-3, in Yeh, H., *et al.* (Editor), *Long wave runup models*: World Scientific Publishing Co., Singapore, p. 242-248.

- Titov, V. V., and González, F. I., 1997, Implementation and testing of the Method of Splitting Tsunami (MOST) model, Technical Memorandum, , NOAA, 11 p.
- Titov, V. V., and Synolakis, C. E., 1998, Numerical modeling of tidal wave runup: *Journal of Waterway, Port, Coastal, and Ocean Engineering*, v. 124, p. 157-171.
- Titov, V. V., González, F. I., Bernard, E. N., Ebel, J. E., Mofjeld, H. O., Newman, J. C., and Venturato, A. J., 2005, Real-time tsunami forecasting: Challenges and solutions: *Natural Hazards*, v. 35, p. 40-58.
- Wells, D. L., and Coppersmith, K. J., 1994, New empirical relationships among magnitude, rupture length, rupture width, rupture area, and surface displacement: *Bull. Seismol. Soc. Am.*, v. 84, p. 974-1002.

Chapter 8: Geomorphology, Stability and Mobility of the Currituck Slide

Introduction

The USGS has been tasked by the Nuclear Regulatory Commission to perform an evaluation of the risk of damaging tsunamis impacting the U.S. East and Gulf coasts. Experience with tsunamis has shown that they can be caused by either movement on offshore faults (seismogenic tsunamis) or by large submarine landslides (landslide tsunamis). Tsunami magnitude depends strongly upon the size of the slide and how the landslide moves as it fails and flows. This chapter is part of an overall effort to consider various geoscientific aspects of tsunamigenic mass movements and uses the case of the Currituck slide (Figure 8-1) to showcase the methodology. In addition, this work, coupled with that described in Chapter 9, provides insight into the potential tsunami impact of some of the past slides that have been mapped.

Objective

The objective of this component of the study is to provide models of landslide motion for one landslide: selected for this case study to be Currituck slide (Figure 8-1). The models and their input parameters are based on engineering judgement and existing geophysical, mapping, and sediment core data. The following models are required:

1. A morpho-stratigraphic model of the excavation zone of the slide area.
2. A depositional model in the run-out zone.

The approach to obtain these models is presented below; the models are intended to provide input information for tsunami modellers who will predict the magnitude and areal extent of the tsunamis that would have been generated by the landslides.

Approach

The approach used follows these steps (Figure 8-2): (1) morphological analysis, (2) estimation of geotechnical properties of the sediment or rock for

limit equilibrium analysis of slope failure conditions, (3) post-failure flow dynamics (analysis of the run-out characteristics of the failed mass). At the end this analysis we provide some conclusion on:

1. The geometry of the slide prior to failure.
2. The potential triggering mechanism and potential initial mass movement sequences.
3. A validation of the initial estimation of the volume from the mobility analysis and consideration of run out characteristics of the slide.
4. From the mobility analysis, provide some data on initial velocity and acceleration of the failed mass.

The geomorphological analysis follows from seismic and multibeam surveys (Chapter 2) and also the analysis provided by Prior *et al.* (1986). The stratigraphy used herein is based on the description by Prior *et al.* (1986) on the nature of the sediments in the area. From the sediment type, we estimated geotechnical properties based on the work of Dugan *et al.* (2003) at the ODP site 1073.

We used the slope stability package, SlopeW, to assess the limit equilibrium state of the slope under ambient and seismic loading and for various conditions of pore pressure. It is assumed here that the material failure behavior follows a Mohr-Coulomb failure criterion such as:

$$\tau = c' + (\sigma - u) \tan \phi' \quad (1)$$

where τ = the shear strength mobilized along the failure plane, c' = the cohesion, σ = the total stress, u = the pore pressure and ϕ' = the friction angle.

For post-failure analysis of the failed mass, we used a 1D-flow dynamics model, BING, presented by Imran *et al.* (2001a) which has been developed for the study of debris flows. BING can be used with various rheological models: Bingham, Herschel-Bulkley and bi-linear.

The bi-linear model has been proposed by Locat (1997) to describe the rheology of clayey silt or silt mixtures, which often present a pseudo-plastic behavior. A similar approach was followed by O'Brien and Julien (1988), also for coarse silt mixtures. In our analysis, we use both bi-linear and Bingham flow models. The bi-linear model assumes that the initial phase of the flow is Newtonian (Figure 4 in Locat *et al.* 2003b) and evolves, after reaching a threshold shear rate value (γ_o), into a Bingham type flow. The constitutive equation proposed by Locat (1997) for bi-linear flow is expressed by:

$$\tau = \tau_{ya} + \mu_{dh} \gamma - \frac{\tau_{ya} \gamma_o}{\gamma + \gamma_o}, \quad (2)$$

where τ is the flow shear resistance, τ_{ya} the yield strength, μ_{dh} the viscosity, γ the shear strain rate, and γ_o the shear strain rate at the transition from a Newtonian to a Bingham behavior.

In BING (Imran *et al.*, 2001b), Equation 2 is re-written

$$\frac{\tau}{\tau_{ya}} = 1 + \frac{\gamma}{\gamma_r} - \frac{1}{1 + r \frac{\gamma}{\gamma_r}}, \quad (3)$$

where γ_r , is the strain rate defined as

$$\gamma_r = \frac{\tau_{ya}}{\mu_{dh}} \quad (4)$$

and r the ratio of the strain rates,

$$r = \frac{\gamma_r}{\gamma_o} \quad (5)$$

One of the main parameters used in this analysis, the yield strength, τ_{ya} , can be estimated from field observations of the failed mass in the accumulation zone or measured directly on samples. Direct measurements could not be conducted in this case because no samples were available. The values related to the viscosity, *i.e.* the strain rate, γ_r , and the ratio of strain rates, r , will be estimated from a parametric analysis to find the best values which fit the observed geometric characteristics in the run-out zone. The value of γ_r can also be estimated from rheological testing results, which show that the value of γ_r is about 1,000 for clays (Locat 1997, Locat and Lee 2002, Lee *et al.* 2007) but can be as low as 10 for sand (Jeong *et al.* 2007).

The Herschel Bulkley model corresponds to the following expression:

$$\tau = \tau_{ya} + K\gamma^n \quad (6)$$

where

$$K = \frac{\tau_{ya}}{\gamma_r^n} \quad (7)$$

and is equivalent to a Bingham model when the exponent 'n' equals 1. For the mobility analysis both models (Bingham and Bilinear) are used.

Geomorphological analysis

Analysis of actual morphology

The slopes of the study area can be grouped into three categories. The first category is for slopes generated by sediment accumulation near the shelf edge resulting in prograding clinoforms with surface slopes varying between 4 and 10°. The second category is for slopes formed by erosional processes associated with submarine canyon development. In this case, slope angles can be as high as 30°. The third category is for slopes resulting from mass failures along failure planes that are more or less controlled by the bedding underlying the continental slope. The flat surface at the center of the Currituck slide is an excellent example of this category (Figure 8-3). If one is looking for rough strength estimates of the sediments on the continental slope, the eroded slope (category 2) would provide the best indications on the strength parameters: the friction angle in particular. The deeper scarp that forms the lower part of that surface is also dissected by erosion, which probably was generated after failure (Figure 8-4). In any case, the slope angles in these gullies are similar to those in other canyons on adjacent sections of the continental slope (*i.e.* an angle as high as 30°). From these considerations, the actual flat surface of the exposed failure plane developed in sediment that was at least normally consolidated so that such a failure could only take place by the generation of high pore pressures. These high pore pressures can be the result of one or a combination of the following processes: (1) groundwater seepage forces generated by either rapid deltaic accumulation or flow through the underlying aquifer, (2) gas hydrates, and (3) earthquakes. Erosion at the base of the continental slope alone could not generate this type of failure.

The initial geomorphology of the Currituck slide has been detailed by Prior *et al.* (1986) who describe slide morphologies for conditions before and after the event (Figure 8-3b). The actual topography of the slide is also provided by a profile generated from the multibeam data along the axis of the failed area showing the various scarps and variations in slope angles along the profile (Figure 8-4). Prior *et al.* (1986) noted the presence of step-like features in the lower escarpment that are well imaged with the multibeam data (Figure 8-5). These steps indicate the strong influence of the layering of geological formations on this slide.

With the use of the multibeam bathymetry, it is possible to recognize up to three potential failure planes (Figure 8-6). A key question here is whether they represent different events or if they were created as part of a single event. The mobility analysis presented below suggests that it must have been a single event.

The morpho-stratigraphic model

Having established the morphology of the existing slide area, the next step is to determine the morphology prior to the slide, *i.e.* establish a morpho-

stratigraphic model of the slide prior to failure. At this step, the critical point is to estimate the initial volume, *i.e.* to come up with a pre-existing surface before failure. This is done by analysing the detailed morphology of the upper part of the slide and comparing it to the surrounding morphology.

Prior *et al.* (1986) estimated the volume of sediment that was removed to be about 128 km³ (Figure 8-3b, and point (a) in Figure 8-22). The main difficulty here is to evaluate the original shape of the continental slope before the slide. It seems that some relict sediments of the former delta are preserved along the southern shoulder of the landslide scarp (Figure 8-7) indicating that the delta covered a larger area than failed. The morphology of the slide area is rich in various instability features (*e.g.* scarps, failure plane, etc.). The position of the base of the footprint of the delta has been taken by extrapolating the pre-slide surface suggested by Prior *et al.* (1986) which gives the position of the footprint of the delta as shown in Figure 8-8 (see also in Figure 8-9) so that the length of the center line of the slide is about 30 km..

Using the cross section shown in Figure 8-9 and the available bathymetry, we have estimated that the volume involved is about 108 km³ and 57 km³ for slide 1 and 2, respectively, for a total of 165 km³ (this value corresponds to (b) in Figure 8-22).

The morphostratigraphic model shown in Figure 8-9 was constructed considering the following elements:

1. The slide took place at a time close to the minimum sea level (Prior *et al.*, 1986).
2. The delta, having a topset slope of about 1°, extended as far as 5 km seaward of the present shelf break, *i.e.* at a depth of 200m.
3. The pre-slide surface topography is assumed to be parallel to the bedding plane and extended until it intersected the present sea floor, *i.e.* at about 30 km from the actual shelf edge, as suggested by Prior *et al.* (1986).

From this re-construction, it appears that the maximum thickness of the mass involved in the slide is about 750 m (H in Figure 8-9) at the base of the lower scarp. When we look at the actual slide morphology (Figures 8-4 to 8-8) and the actual slope angles, the clean surface exposed just above the lower scarp indicates that the failure developed rapidly, much like what has been modelled for the Storegga slide (Figure 8-10) (Bryn *et al.*, 2005). The main similarity between the Storegga and the Currituck slides is the control of the bedding planes on the position of the failure plane (as also pointed out by Prior *et al.* 1986, Figure 8-3b). The conditions leading to the initial failure are analyzed in the following section.

Stability analysis

The slope stability analysis has been carried out here not to show the location of the potential failure plane, since this is fairly well known, but to explore under which conditions a failure could take place. The equilibrium analysis

considers that the forces acting on a slope are in equilibrium when the resisting forces equal the gravitational forces so that the ratio of these forces, called the Factor of Safety (F), are at unity ($F = 1$).

All the results are shown in 2D diagrams that present the modelled slope with the origin taken 5 km upslope from the actual edge of the delta, and the datum is placed at a depth of 2200 m below present sea level (*e.g.*, Figure 8-11). In order to see the stratigraphic model in greater detail, the elevation is exaggerated by a factor of 3. On each of these figures (*e.g.* Figure 8-11a, where $F = 1.485$), there is a dot above the ground that represents the position of the center of the circular failure surface that gives the lowest factor of safety.

A first trial was carried out using a simple slope profile and the potential failure plane geometry for slide 1 with the lower scarp having a slope angle of 30° (Figure 8-11a). This analysis shows that high pore pressures (approaching 90% of lithostatic, Figure 8-11b) are required in order to approach a factor safety of unity, and that it is only after a pore pressure ratio greater than 0.5 that we see a significant decrease in the factor of safety. The same is also true for the effect of the seismic acceleration ratio (α) (Figure 8-11c). Here, a combination of a pore pressure ratio of only 0.5 and an α value of 0.28 would be sufficient to reduce the factor of safety to unity. Therefore, there must have been conditions that produced both high pore pressure on a given bedding plane (*e.g.* rapid sediment accumulation or dissociation of gas hydrates) and also a significant seismic acceleration to generate the conditions that led to the total collapse of the Currituck slide area.

For a more detailed analysis of the Currituck failure, we adapted the stratigraphic model of Prior *et al.* (1986) and used geotechnical parameters derived from stratigraphic information (Figure 8-12). We also assumed that we could use the closest ODP drill site (1073) south of Hudson Canyon for estimating other geotechnical properties (Dugan *et al.* 2003 and 2005; properties identified in Figure 8-12). Since it has been postulated by Prior *et al.* 1986 that the failure could have been triggered by excess pore pressure resulting from sediment accumulation, we included this parameter in our analysis. In the absence of direct *in situ* measurements, we consider that the high pore pressure modelled by Dugan *et al.* (2005) for sediment in the Hudson Canyon area may be applicable here as well for the purpose of a parametric analysis. A similar approach has been tested on the Hudson Apron by Locat *et al.* (2003a).

Bunn and McGregor (1980), along with Prior *et al.* (1986), considered that deltaic sedimentation on the shelf may have increased the instability of the outer shelf and slope. Therefore, we look at the loading effect of a prograding delta on the underlying stratigraphic formations. As we try to keep the base of the slope at the same position, moving the delta edge seaward 20 km increases the slope angle near the shelf edge from 4° to about 16° (Figure 8-13). A direct effect of this geometric change is an increase in the volume of the slide source zone due to the delta advance. This has been simulated in Figures 8-13 and 8-14 with the results shown in Figure 8-15 for slide 1 and in Figures 8-16 and 8-17 for slide 2. In this case, slide 2 has been considered a separate event from slide 1. The overall observation is that for

realistic positions of the delta edge, in terms of slope angle and volume, *i.e.* less than 10 km, the impact of moving the delta edge is greater for slide 1 than for slide 2. Interestingly, even for a delta advancing more than 10 km, significant pore pressures are still required for the material to fail. The simulation in Figures 8-15 and 8-17 suggests that the actual impact of delta advance, considered only as a new load, is not particularly significant. A simple explanation may be related to the fact that the actual stress increase from delta progradation only affects a rather small portion of the failure plane. It is also important to point out here that the effect of pore pressure increase, in the underlying formations, due to delta progradation, has not been considered.

From the above analysis we used a delta advance of 5 km to simulate the effect of seismic acceleration on the factor of safety and for various conditions of the pore pressure ratio (Figure 8-18). Results indicate that even by taking into account added volume and a more complex stratigraphy, high pore pressure or a significant earthquake is necessary to generate failure ($F = 1$).

As we look at the morphology of the continental slope, both inside the Currituck slide area and to either side, it is apparent that the scarp is quite steep and high (up to 350 m). The steepness and height of the scarp indicate that the overall strength of the sediments making up this part of the slope are likely to be at least normally consolidated and do not show signs of high *in situ* pore pressures. If the triggering of the Currituck slide was linked to the presence of high pore pressures, they clearly do not exist anymore, and if they ever existed over a long term (*e.g.* through a groundwater flow regime), they must have been generated after the development of strength in the sediments. So, delta construction could have led to increased pore pressures in what otherwise would have been normally consolidated sediment.

Prior *et al.* (1986) suggest the slide took place more than 16,600 yr ago during a period of low sea level so that at that time there could have been significant changes in the groundwater flow system that may be connected to the continent. Since the slide could have also been triggered by an earthquake, it is likely that local less stable conditions around the delta were such that sliding could only take place in this part of the slope.

In any case, a very large volume of sediment was mobilized by the Currituck slide. In the next section, we will investigate the link between the run-out distance of the slide debris as a function of the volume, in the starting zone, to see whether or not the slide occurred as one event.

Mobility analysis

The preliminary geomorphological and stability analyses of the Currituck slide clearly indicate that the slide took place under conditions that dislodged a large volume of sediment at a pace that was fast enough to almost completely clear the failure surface above the lower scarp (see Figures 8-4 to 8-6 in particular). The multibeam map of the slide area has been analyzed in detail (Chapter 2) and six lobes were identified (Figure 8-19) for which it has

been possible, in most cases, to estimate volume and average thickness. The farthest distance reached by the debris was 220 km from the shelf edge and 150 km from the toe of the source area. These observations are key elements for the analysis of the mobility of the Currituck slide and provide geomorphological boundary conditions for the back analysis of the flow properties.

The bathymetry of the area inside the flow path (axis) and outside (flank) was derived from the multibeam bathymetry, and for the purpose of modelling, we derived a smooth profile obtained mostly from the flank profile (Figure 8-20). The slope angle along this profile varies from about 8° on the upper slope to less than 0.5° on the continental rise.

Geometry

For the mobility analysis we need to define the geometry of the slide and the properties of the flowing material. BING requires a flow path, which is provided by the bathymetry (Figure 8-20). We also need to know the vertical cross section of the slide so that we can supply the length of the failing mass and its thickness. For simplicity, BING uses a half ellipse for the initial shape of the slide (see insert in Figure 8-20) which is very close to a long rectangle in our case because of the large width to height ratio. The initial geometry of the flowing mass is computed from volume estimates based on the geometry identified in Figures 8-8 and 8-9. Here we consider that the length of the failed area is about 30,000 m (30 km), and the width about 20 km. For example, if the initial thickness (H_i) in the starting zone is 250m (see insert in Figure 8-20) we get a volume of 150 km^3 . So, for the computed values of Prior *et al.* (1986) at 128 km^3 and herein at 165 km^3 , the values of H_i are 213 and 275m respectively.

Rheological parameters

To obtain a field calibrated value for the yield strength (τ_c , in kPa), we use the following equation provided by Hampton (1972):

$$\tau_c = H_c \gamma' \sin \beta \quad (8)$$

Where H_c , in meters, is the critical height or thickness, γ' the buoyant unit weight in kN/m^3 (taken here at 8 kN/m^3 , not to be confused with strain rate) and β the slope angle. Using Eq. [8] and considering the potential slope angle and thickness of the debris, it is possible to construct a nomogram that will help select the appropriate yield strength. Results are shown in Figure 8-21. Considering that the slope angle in the depositional zone is between 0.2° and 0.4° , we can see that for a range in critical height (or thickness) between 20 and 50 m, the yield strength could vary between 2 and 4 kPa.

Mobility and flow volume

Using BING with the Bilinear model we then computed the relationship between the mobilized flow volume and the run-out distance of a flow over the topography given in Figure 8-20. The computation was done to cover the range in yield strength, *i.e.* between 2 and 4 kPa. Results are shown in Figure 8-22. On that figure, we also point out four specific volumes: slides 1 and 2 of Prior *et al.* (1986), the total volume of Prior *et al.* (1986, as in Figure 8-22) and our estimate (b in Figure 8-22). On Figure 8-22, we also indicate the maximum run-out distance observed from the multibeam map of Figure 8-19.

A major element to point out here is that if the slides are taken separately, they cannot generate the observed mobility. Therefore, the various features observed in the starting zone (failure area) were apparently created more or less at the same time, indicating that, for post-failure analysis (and likely for tsunami generation), the total volume must be used.

From this point on, we analyse the mobility of the Currituck slide using a single volume of 150 km³ and a yield strength of 2 kPa.

Flow dynamics

In order to provide some insight into the tsunamigenic potential of the Currituck slide, we use BING to look at the velocity and acceleration profiles of the failing mass. It is relevant here to point out that BING, like all other flow models, assumes that the failed mass has instantaneously reached the flow properties required for modelling, *i.e.* there is no transition in terms of displacements between failure and post-failure. As noted by Imran *et al.* (2001b) this will yield an initial high acceleration. Still, the observed values can be used or modified according to a flow transition model so that the initial acceleration can be modified. For the flow dynamics, we used two models (Bingham and Bi-linear) to help describe the flow behavior.

First, the velocity distribution as a function of distance from the toe of the slide is shown in Figure 8-23a for both Bingham and Bilinear models. As indicated by Imran *et al.* (2001b), the Bilinear model tends to provide higher peak velocities than the Bingham because the Bilinear model uses a very low yield strength in the first phase of the flow. With the parameters identified above, a peak velocity of 43 and 32 m/s were computed for the Bilinear and Bingham models respectively. The stretching of the failed mass is shown in Figure 8-23b for data computed using the Bingham model. The thickness varies from a maximum of 250 m, in the starting zone, to less than 50m in the distal part for the depositional zone.

As we look at the change in velocity and acceleration with time (Figure 8-24) we can see that results from both models differ in the first few minutes of the event, but otherwise are quite similar. The peak velocity (or 0 acceleration) is reached at about the same time in both cases (about 7min). Since the Bilinear model has a higher peak velocity, the deceleration is also more rapid and reaches much lower values than with the Bingham model,

but the timing of the maximum deceleration is about the same in both cases, *i.e.* at about 10 min (Figure 8-24b). After only 20 minutes, the deceleration proceeds very slowly until the end of the event. The initial high acceleration, expected after the above comments, is at about 12 m/s^2 , *i.e.* more than the gravitational acceleration.

The above mobility was mostly considered for the frontal element. It is possible to extract the data to look at the behavior of a given element as is shown in Figure 8-25 for frontal, middle and back elements. We can see that, for the first 10 minutes of the event, the absolute velocity decreases as we move away from the front (Figure 8-25a). It is interesting to note that all three elements decelerate to about 0 (or reach maximum velocity) at about the same time (*i.e.* 7 minutes).

Discussion

The analysis of the stability and mobility of the Currituck slide has been carried out assuming various properties that were, in some cases, derived from field observations. The results are very much inference due to assumptions that had to be made as to strength parameters, pore pressure conditions, earthquake acceleration and yield strength.

Strength parameters and pore pressures

Strength parameters were primarily derived from the known nature of the sediments involved in the slide. We feel that these are appropriate, particularly the friction angle. The cohesion is more difficult to establish, but considering the size of the slope, even a value of 100 kPa would have little impact on the mobilized shear strength, as it is illustrated in Figure 8-26.

Choosing the appropriate pore pressure is much more difficult and can only be ascertained by *in situ* measurements. Our approach does however illustrate how much pore pressure was required to generate a failure. Our analysis also indicates that high pore pressures have to be developed rapidly to generate a failure on such low slope angles. The slopes in the various canyons and even on the lower scarp indicate that the strength of the sediment is quite high and that high pore pressure could not result from sediment accumulation, since it is at least normally consolidated if not over-consolidated. So, remaining causes for pore pressure increases may be those linked to rapid delta construction, post-depositional (*i.e.* after the formation and consolidation of the sediments) groundwater seepage, or earthquake. It could also be a combination of all of these. The fact that only the portion covered by the delta has been involved in the large mass failure points to a link with the presence of the delta that may have locally induced some high pore pressures that could be further increased by an earthquake.

An earthquake of a given magnitude will have more impact on the stability of a slope if the slope is underwater. The reason is that the total stresses are always considered in the computation while for the strength of the sediment we use buoyant conditions.

Yield strength

For the mobility analysis, the yield strength is one of the main parameters and it can be estimated from the geomorphology of the debris in the run-out zone. A key assumption here is that we consider that the debris has been deposited all at once. To that effect, the analysis of seismic information and availability of cores may prove essential to evaluate this assumption.

Conclusion

From the above analysis we can conclude that:

1. The Currituck slide took place as a single event.
2. It involved a volume of sediment between 165 km^3 and 128 km^3 .
3. It was triggered by a catastrophic event that must have required a sudden increase in pore pressure, likely due to an earthquake.
4. The mobilized yield strength was of the order of 2,000 Pa.
5. The peak velocity may have been between 30 and 40 m/s.
6. Most of the acceleration phase was completed within less than 10 minutes.
7. The acceleration of the flowing mass is not uniformly distributed with the shallowest elements having a lower acceleration than the frontal element.

List of symbols and abbreviations used in this chapter:

c' : cohesion, kPa
 c_v : coefficient of volumetric compression
 E : energy
 F : factor of safety
 G : gravitational acceleration, m/s^2
 H_c : critical height, m
 H_i : initial thickness, m
 H_f : final thickness, m
 I_L : liquidity index
 L_R : Run-out distance, m
 r : ratio of strain rates
 r_u : pore pressure ratio ($u/\gamma H$)
 St : sensitivity (ratio of intact to remoulded strength)
 u : pore pressure, kPa
 V : volume, m^3 , km^3

Greek symbols:

α : coefficient of seismic acceleration (fraction of g)
 β : slope angle, degree
 γ : unit weight (kN/m^3), strain rate, s^{-1}
 γ' : buoyant unit weight, kN/m^3
 γ_r : reference strain rate, s^{-1}
 ϕ' : friction angle, degree
 τ : shear strength, kPa, or flow resistance, (Pa)
 τ_c : critical yield strength, Pa
 τ_{ya} : yield strength considering a Bingham fluid, Pa
 η : plastic viscosity, Pa.s
 σ : total stress, kPa

Figures



Figure 8-1: Location of the Currick Slide.

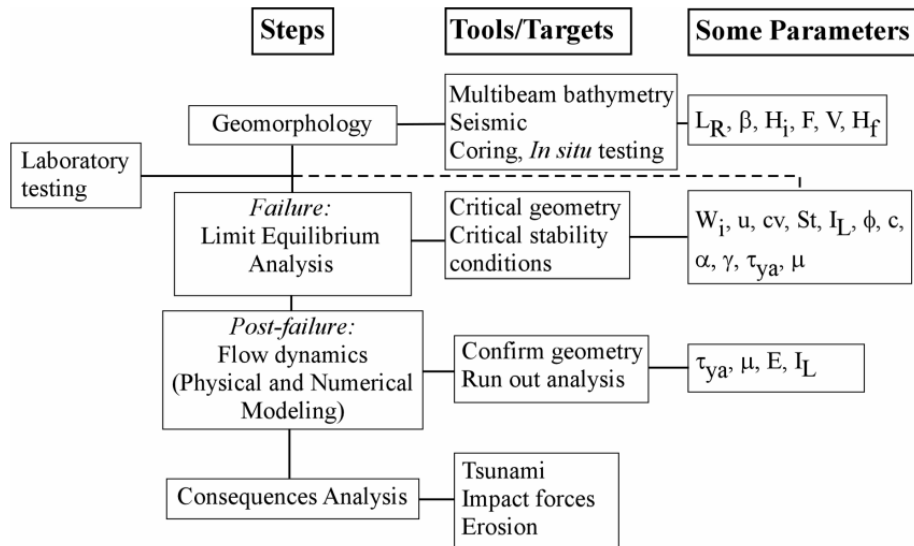


Figure 8-2: Approach used in the analysis of submarine mass movements and their consequences. The part dealing with consequence analysis is not included in this report (Locat and Lee, 2005).

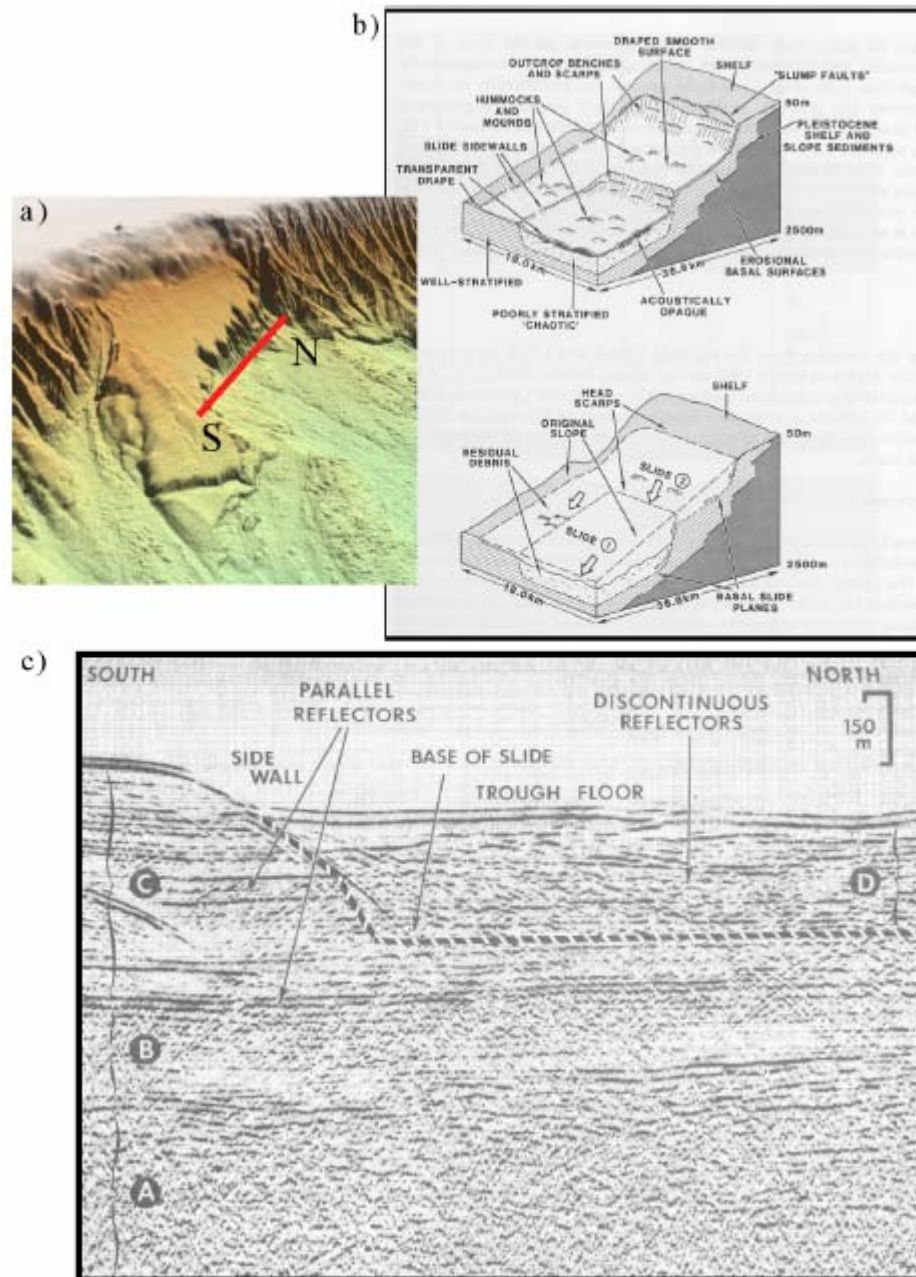


Figure 8-3: Seismic and morphological data from Prior *et al.* (1986). Trace of the seismic line is shown over the multibeam image.

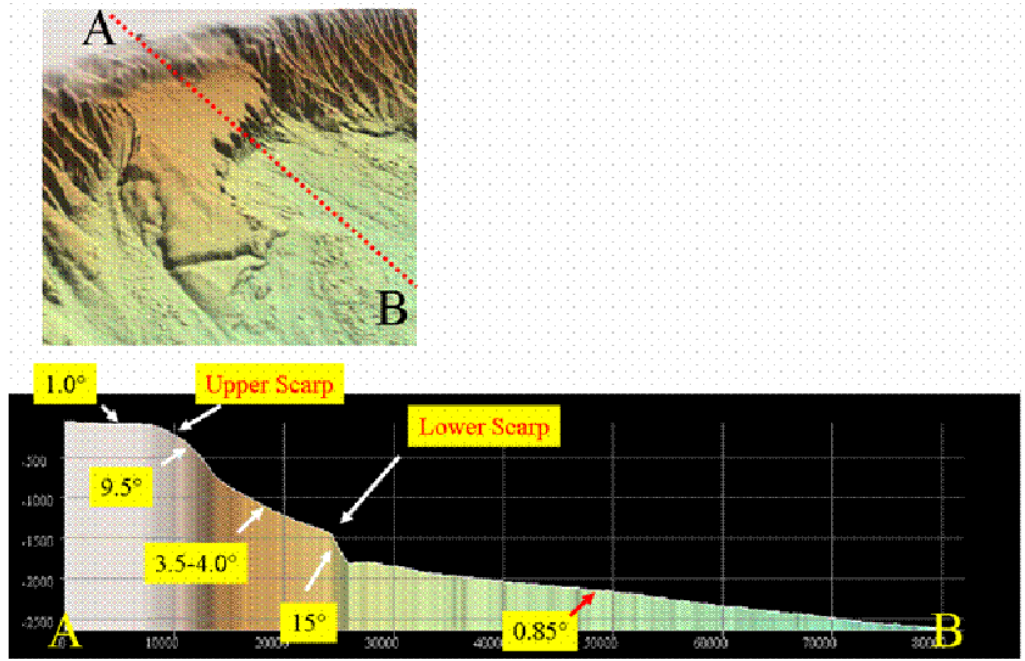


Figure 8-4: General slope profile along actual center line of Currituck slide showing the various escarpments.

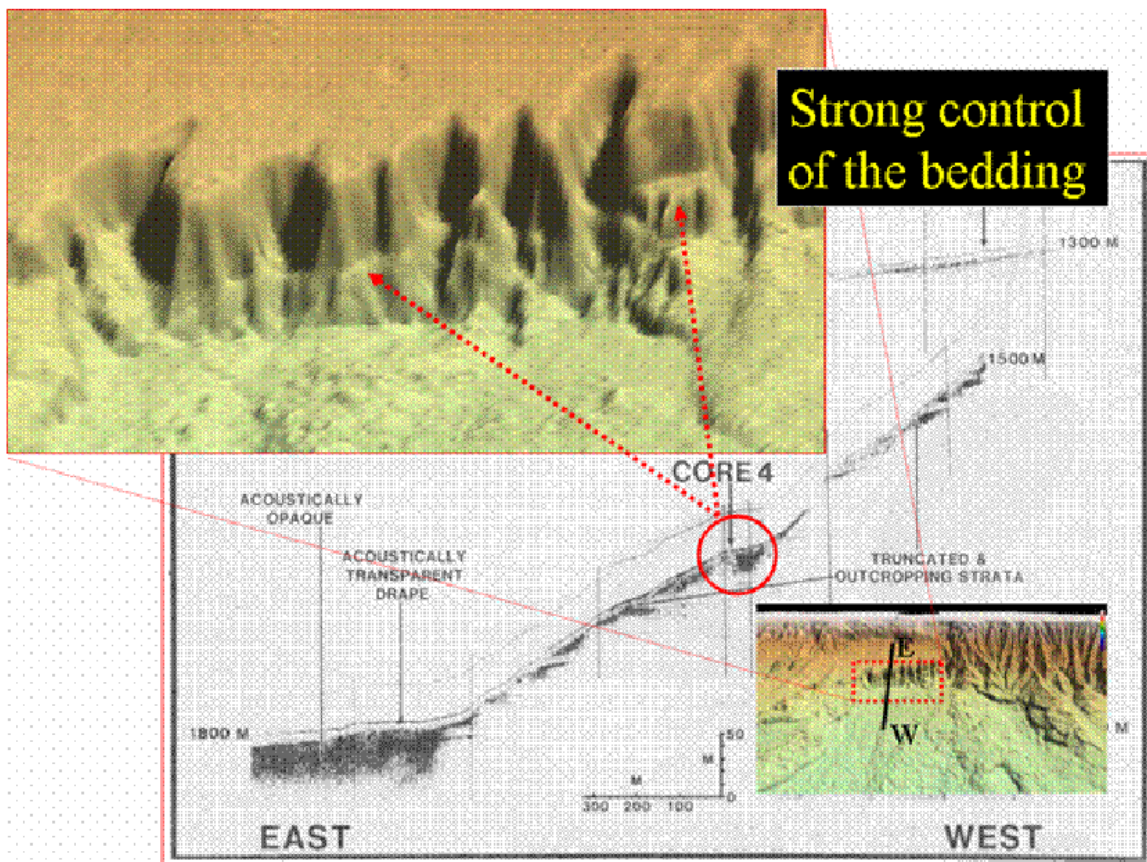


Figure 8-5: Stratigraphic control on the lower escarpment geomorphology (seismic line is from Prior *et al.*, 1986).

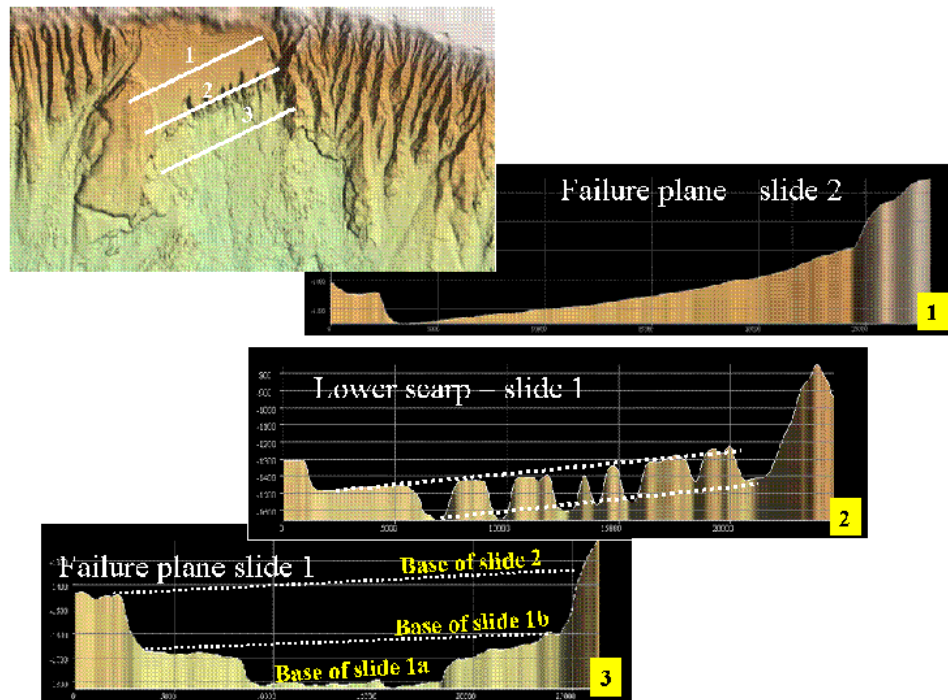


Figure 8-6: Topographic profiles across the upper head of the Currituck slide showing three potential failure planes.

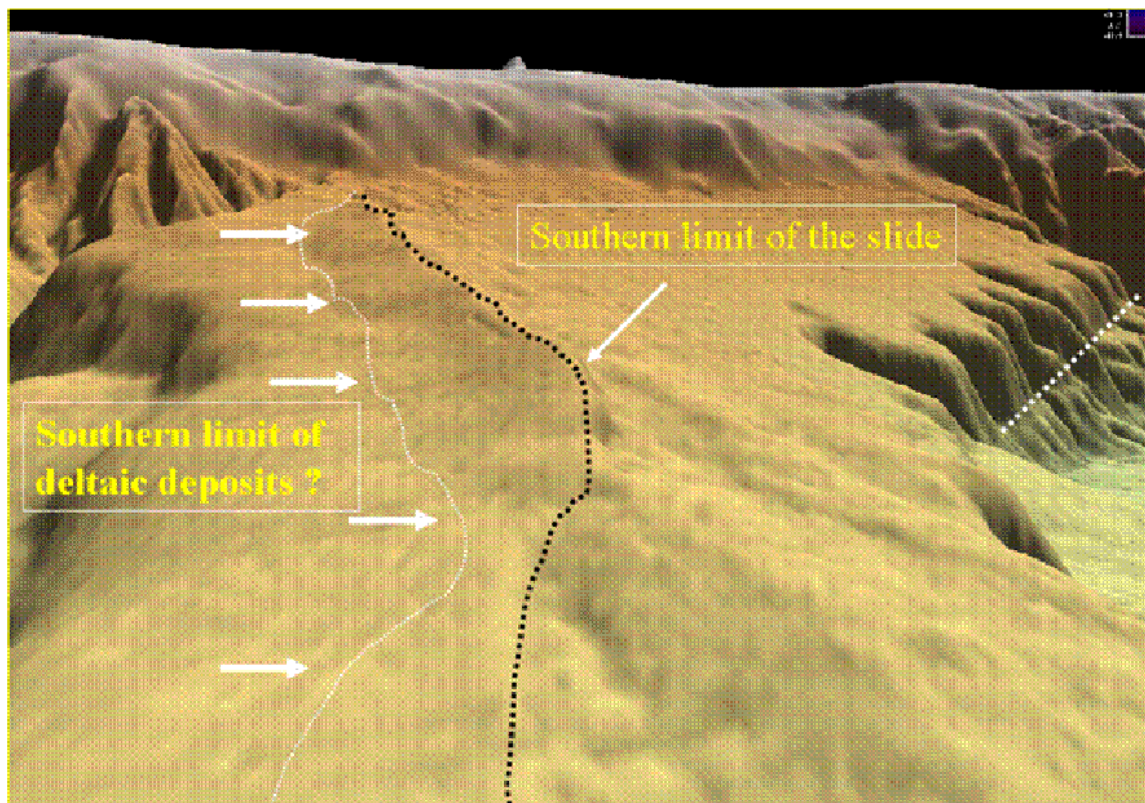


Figure 8-7: Possible limit of the southern toe of the initial deltaic morphology and position of the southern escarpment.

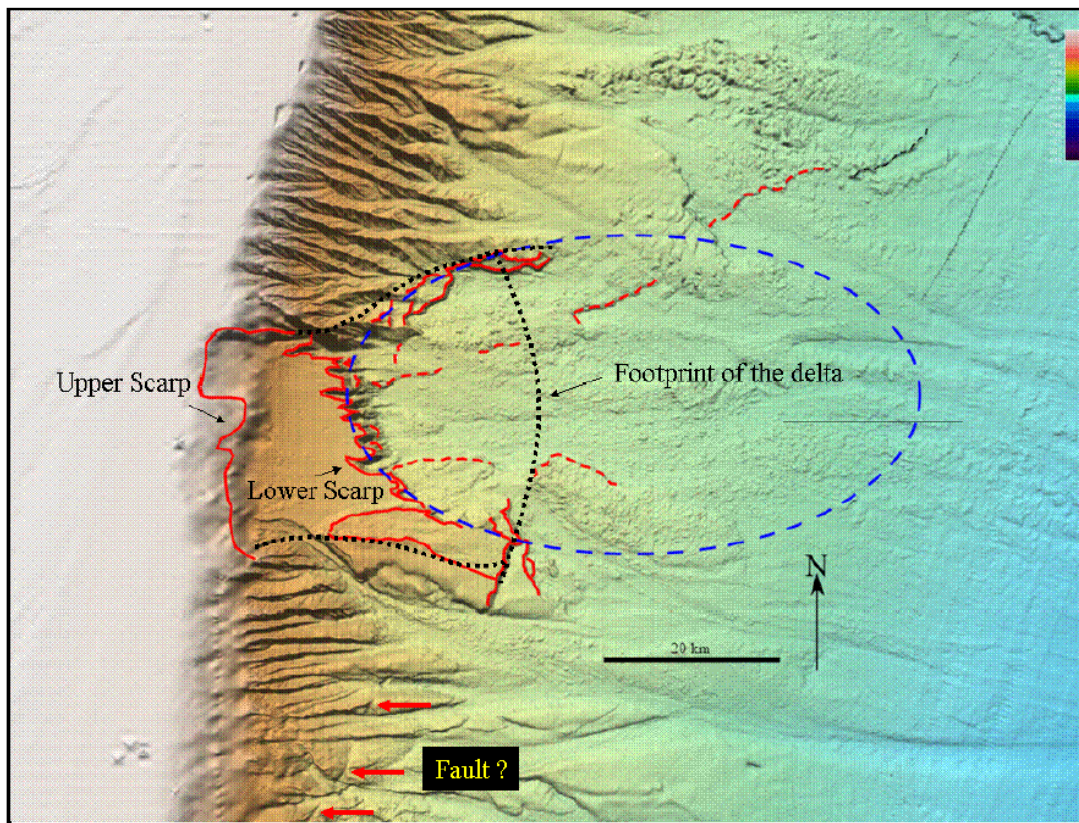


Figure 8-8: Possible position of the base of the slope (black dashed line), used for the following computation. Dashed ellipse (blue line) would delineate the first phase of the lower failure plane.

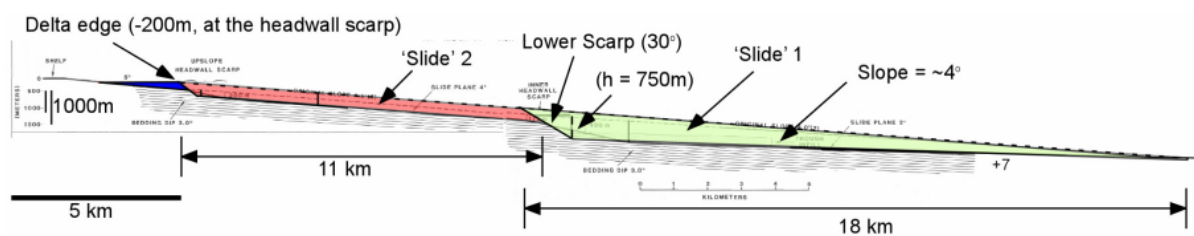
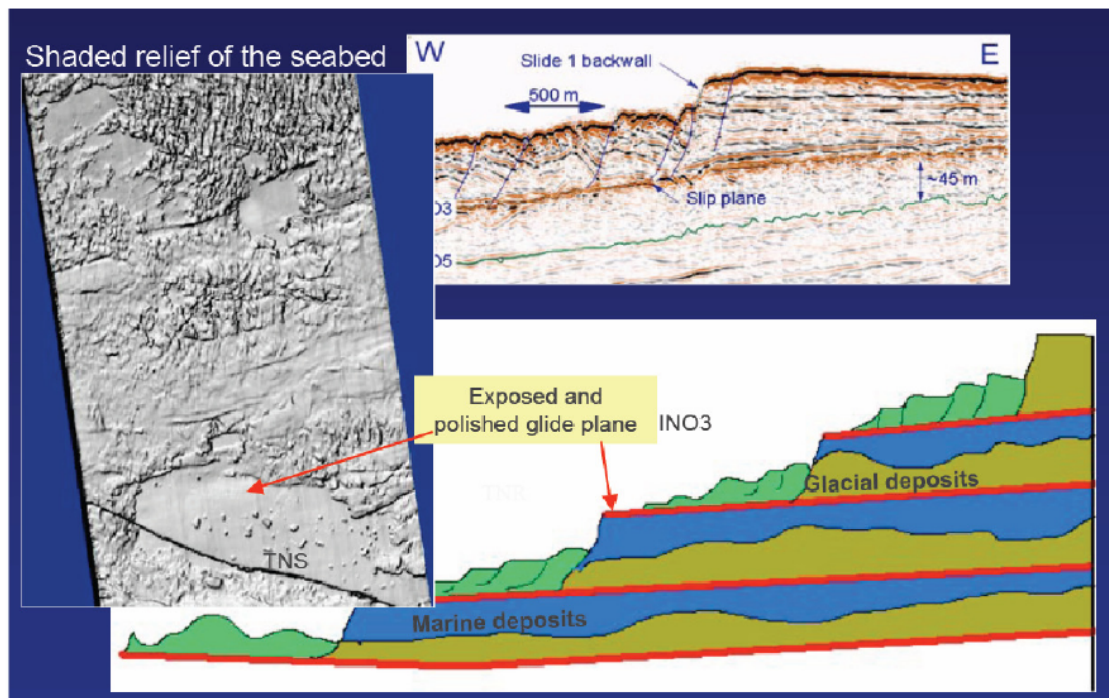
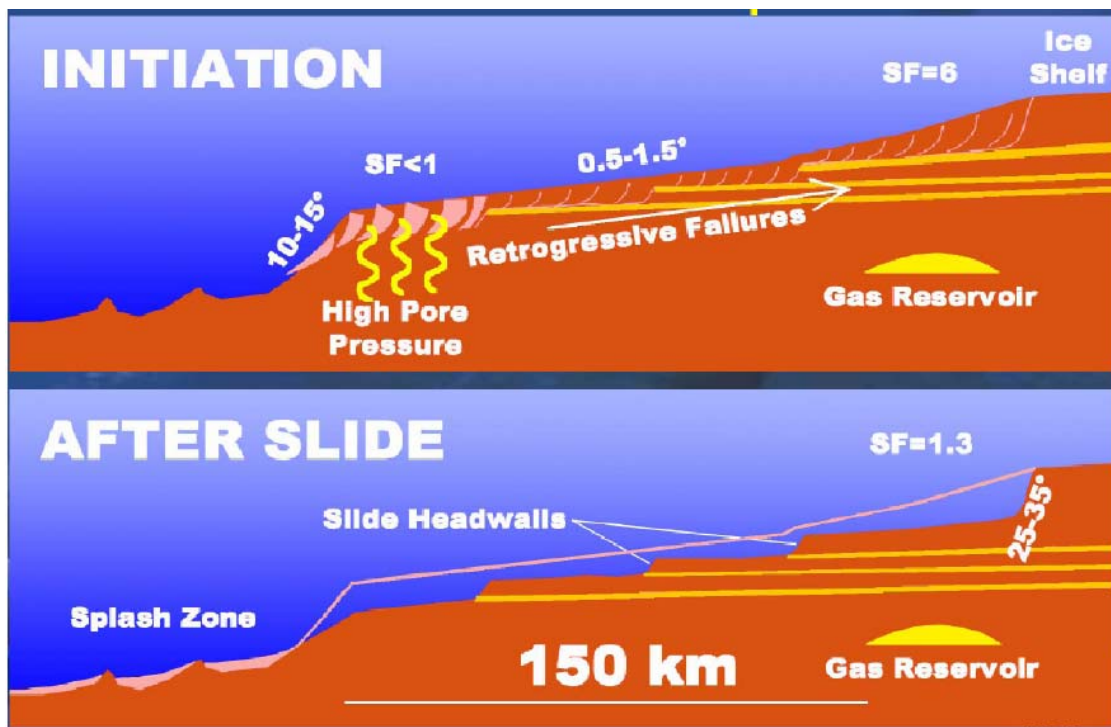


Figure 8-9: Adaptation of the model of Prior, *et al.* (1986) based on recent bathymetry data. Note that the delta has advanced about 2.5 km over the shelf. The model also considers an scarp slope of 30°. The surface of the delta is at -200m.



(a)



(b)

Figure 8-10: (a) Morphology of the Storegga slide in the upper part and (b) a schematic view of the failure planes and potential triggering factors (source: Norsk Hydro).

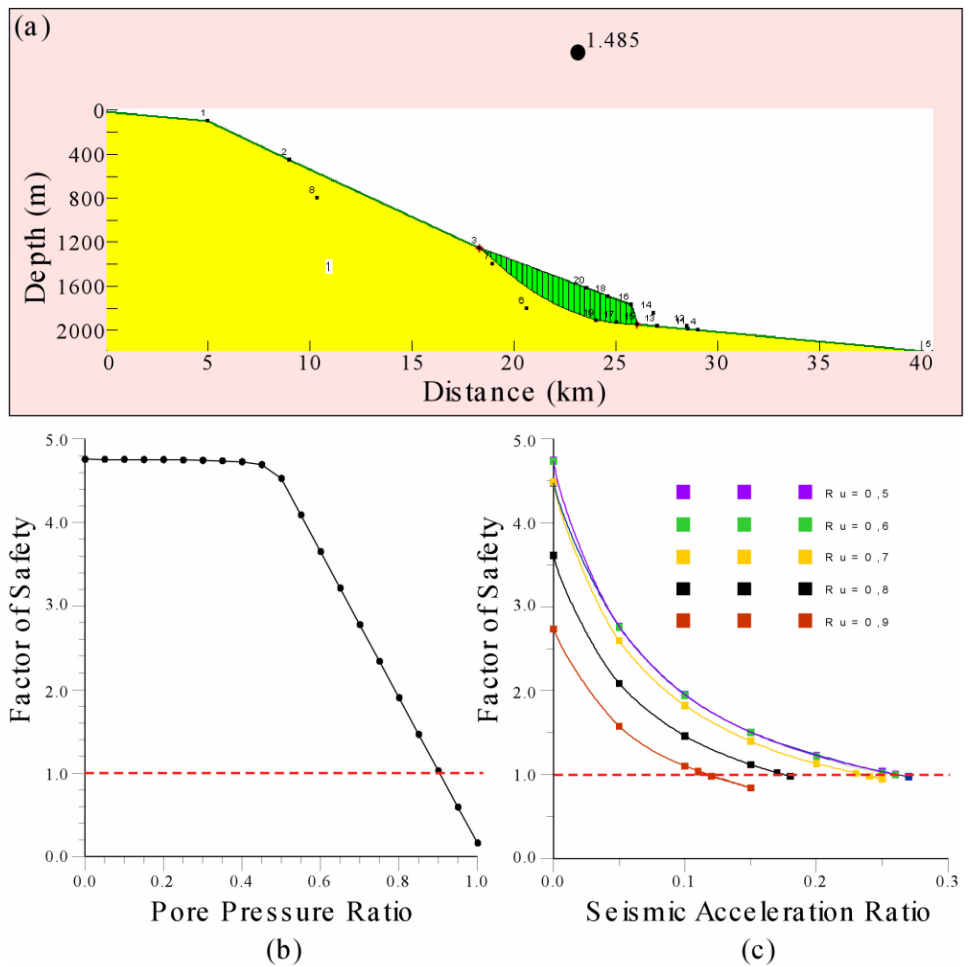


Figure 8-11: (a) Simple slope model for slide 1 and (b) effect of pore pressure ratio (r_u) on the factor of safety without seismic acceleration and (c) effect of seismic acceleration ratio on factor of safety when considering various pore pressure ratios.

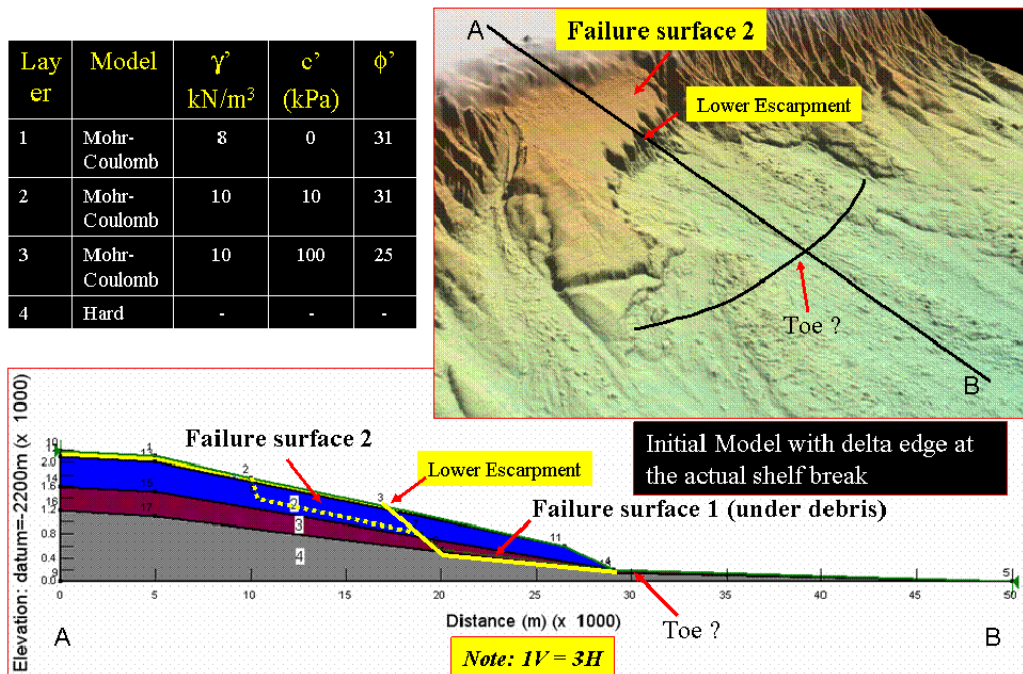


Figure 8-12: Geotechnical properties and failure planes used for the stability analysis with SLOPEW.

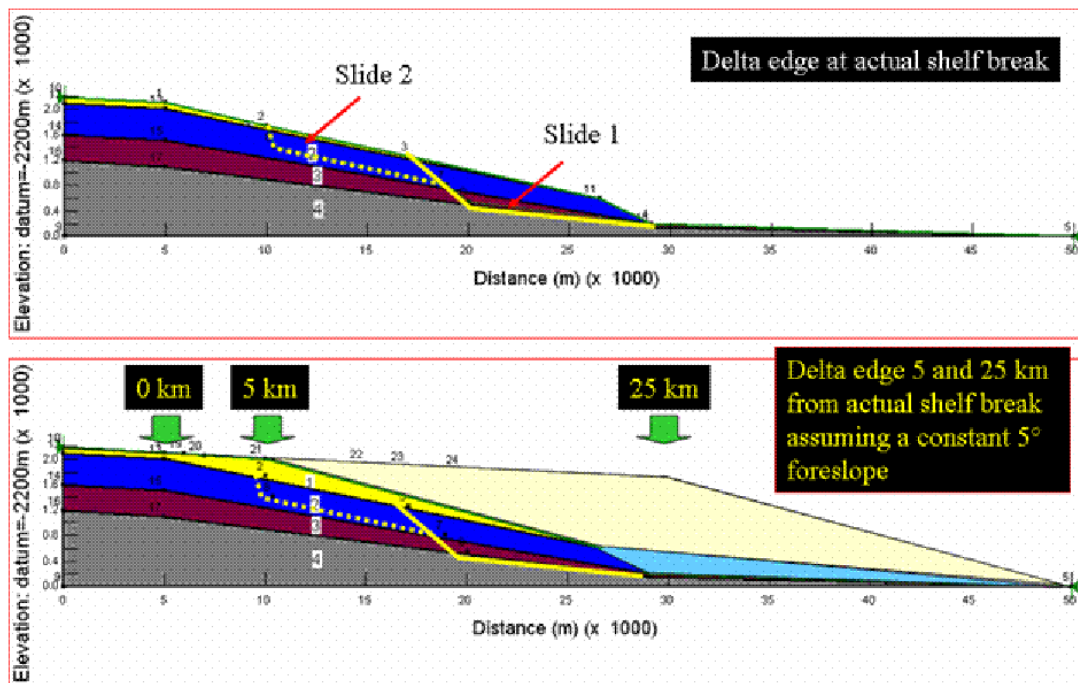


Figure 8-13: Position of the failure plane and the location of the delta edge at 0, 5 and 25 km from shelf edge.

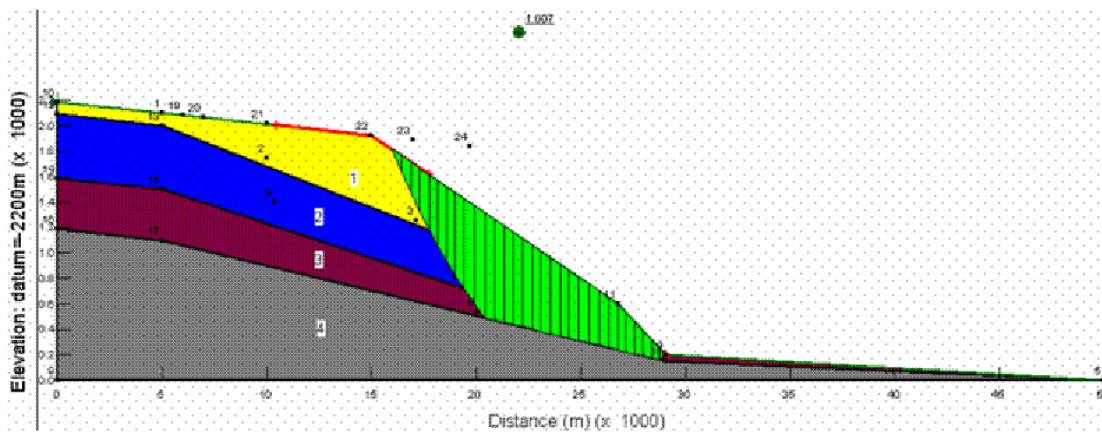


Figure 8-14: Example of slope geometry considered for testing morphology of initial slide (slide 1) with a delta edge at about 25 km.

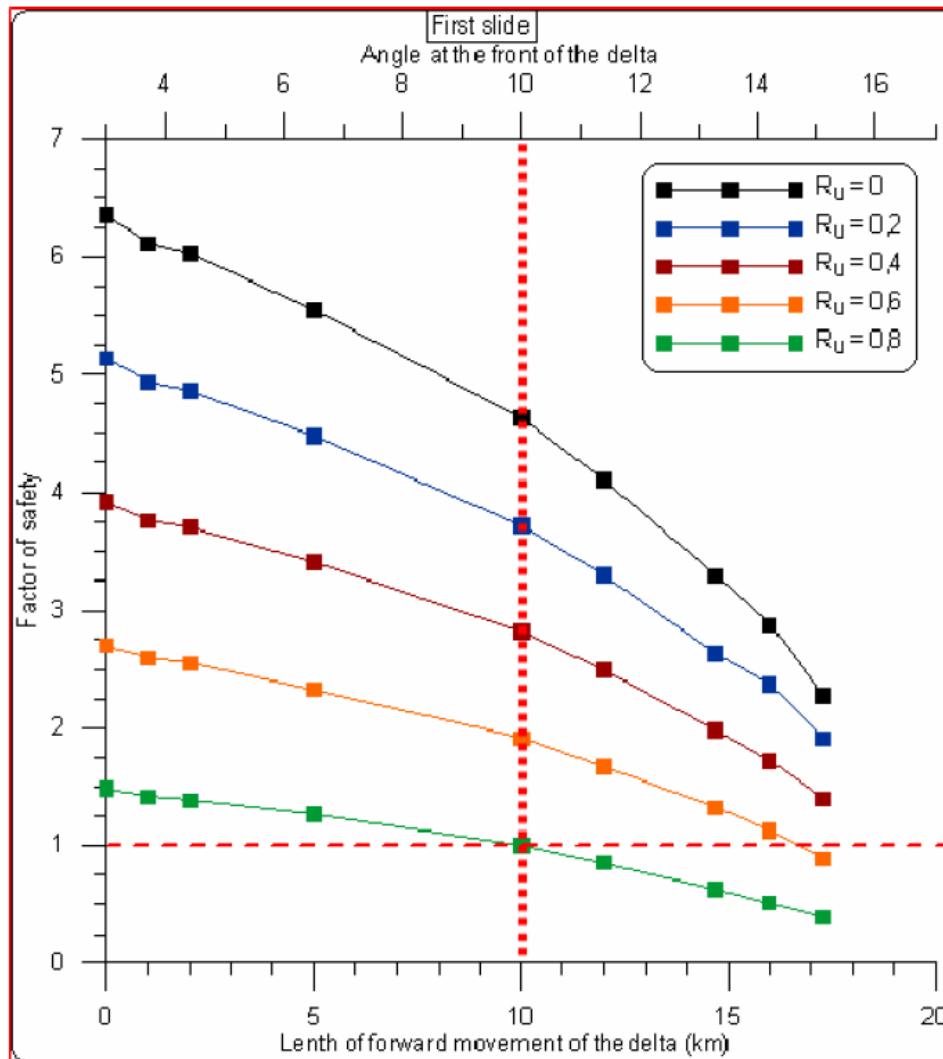


Figure 8-15: Effect of the position of the delta edge on the factor of safety of the slope for different pore pressure ratios.

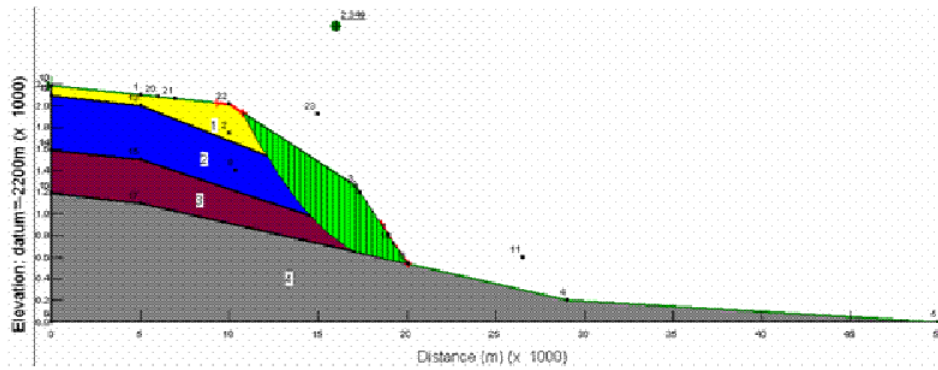


Figure 8-16: Example of a model used for simulating stability conditions for slide 2.

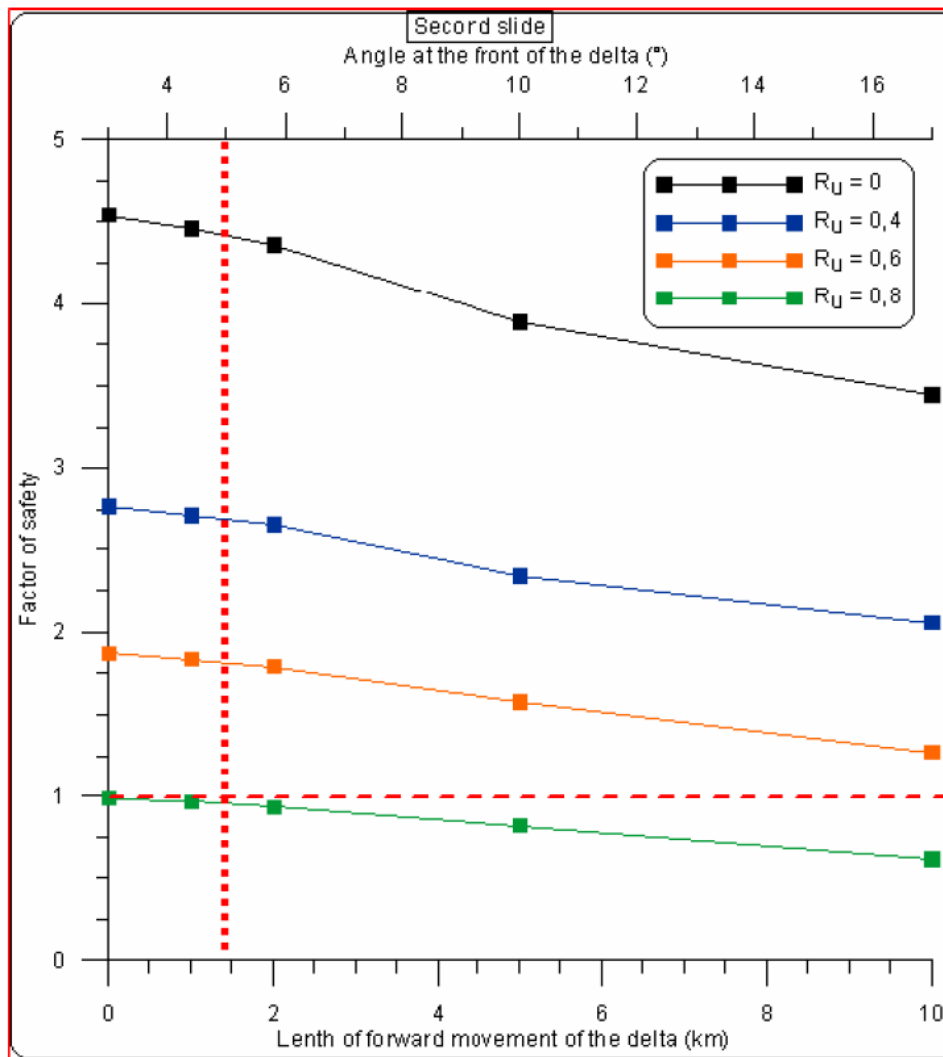


Figure 8-17: Effect of delta front position on stability conditions for slide 2.

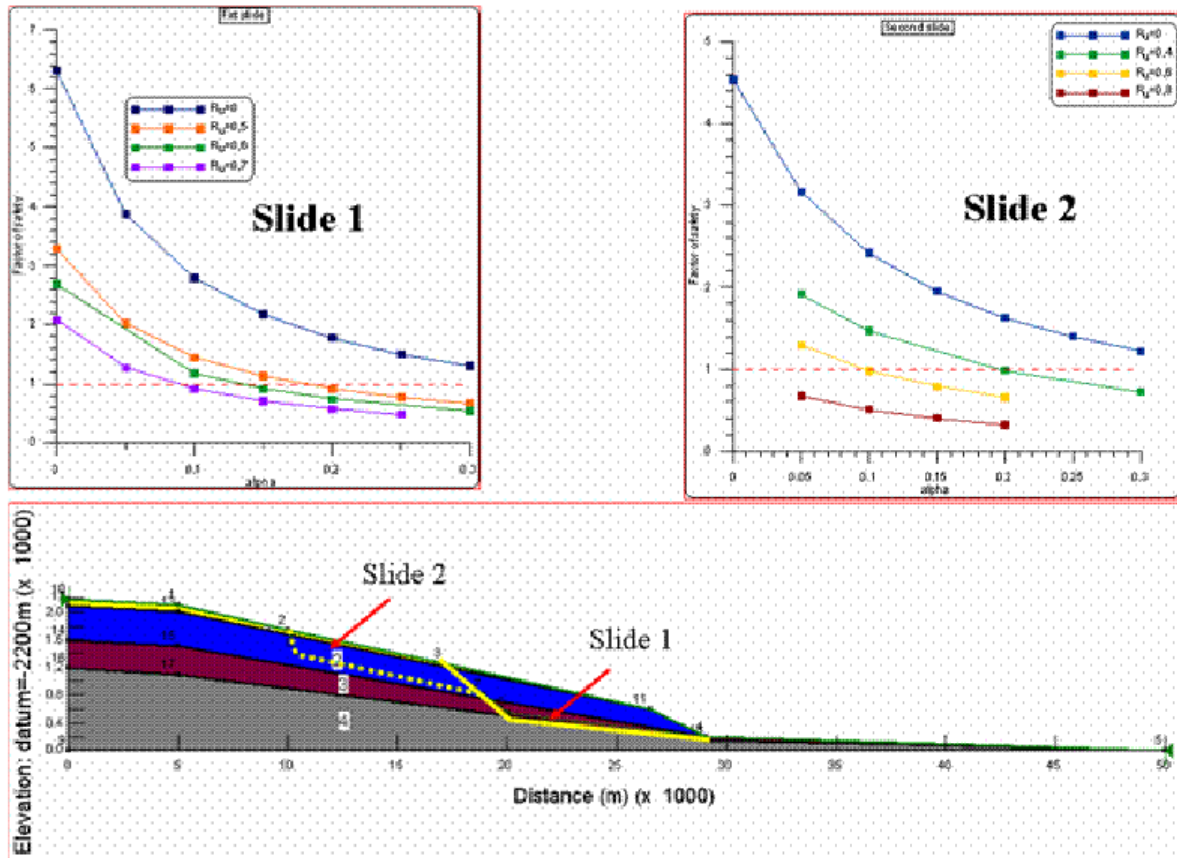


Figure 8-18: Effect of earthquake acceleration on stability conditions for slide 1 and 2 as a function of the pore pressure ratio.

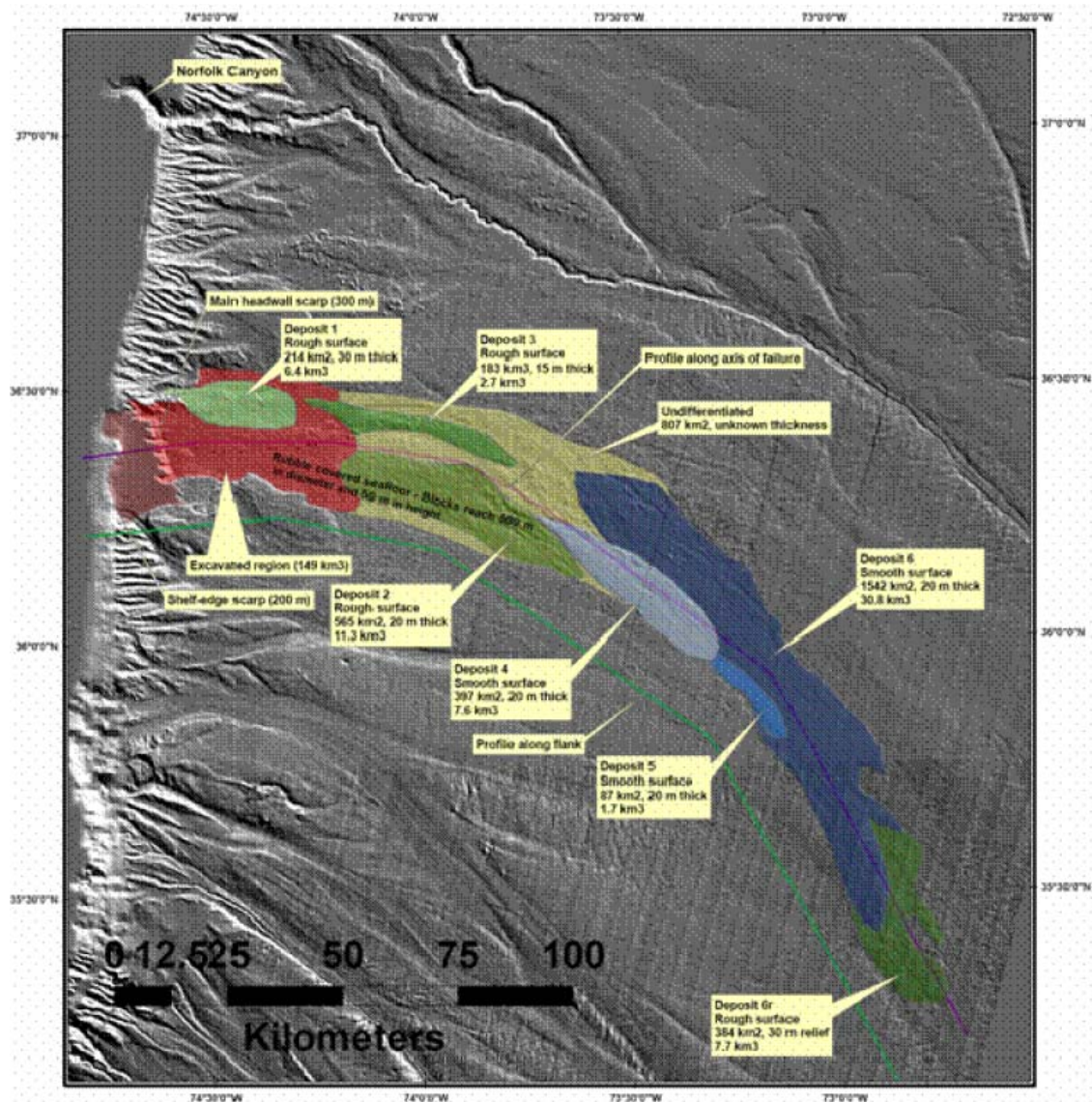


Figure 8-19: Morphological analysis of the Currituck slide from coupling seismic and multibeam data (Chapter 2)

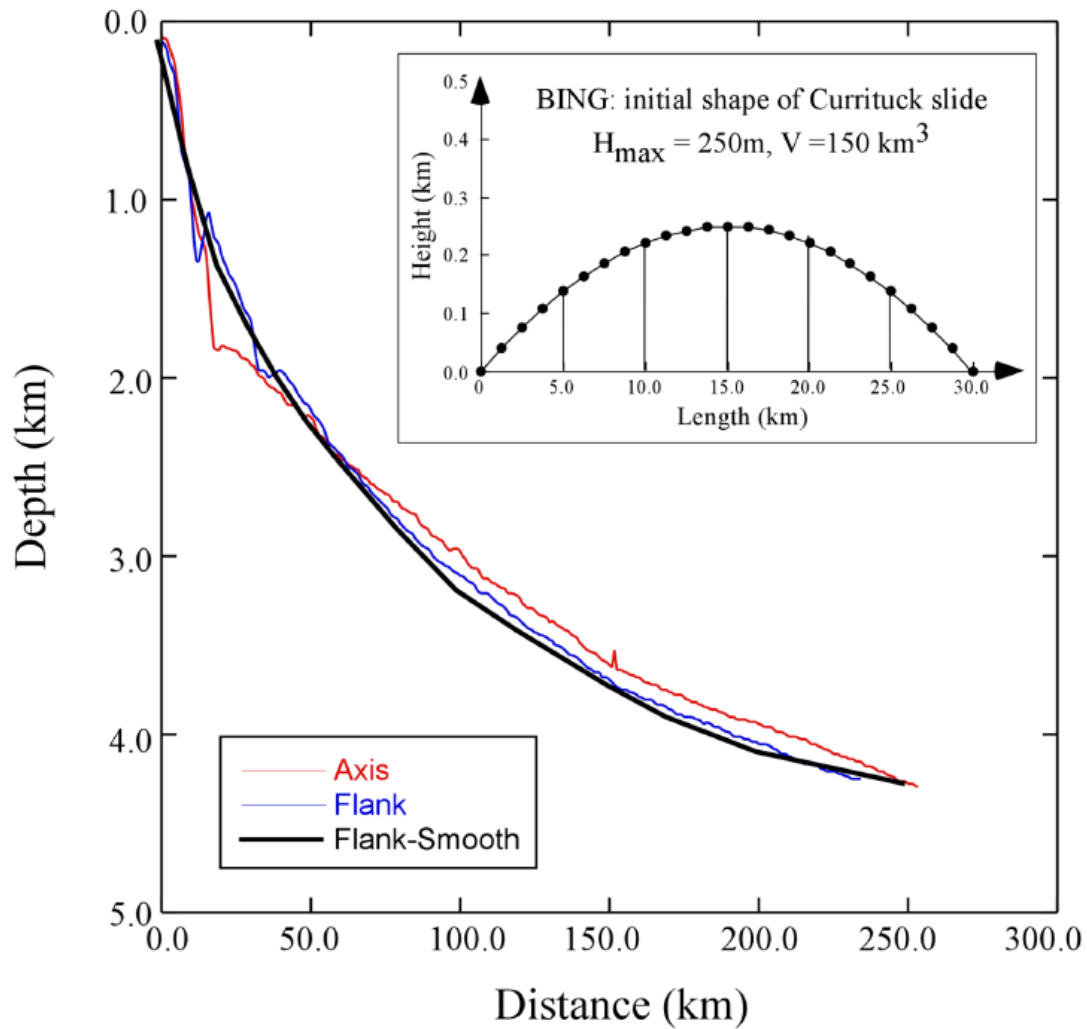


Figure 8-20: Flank and axis bathymetry profiles (Chapter 2) and the smooth profile used for mobility simulation using BING. Insert shows the initial shape of the flowing material use in modeling with BING (note the scale difference).

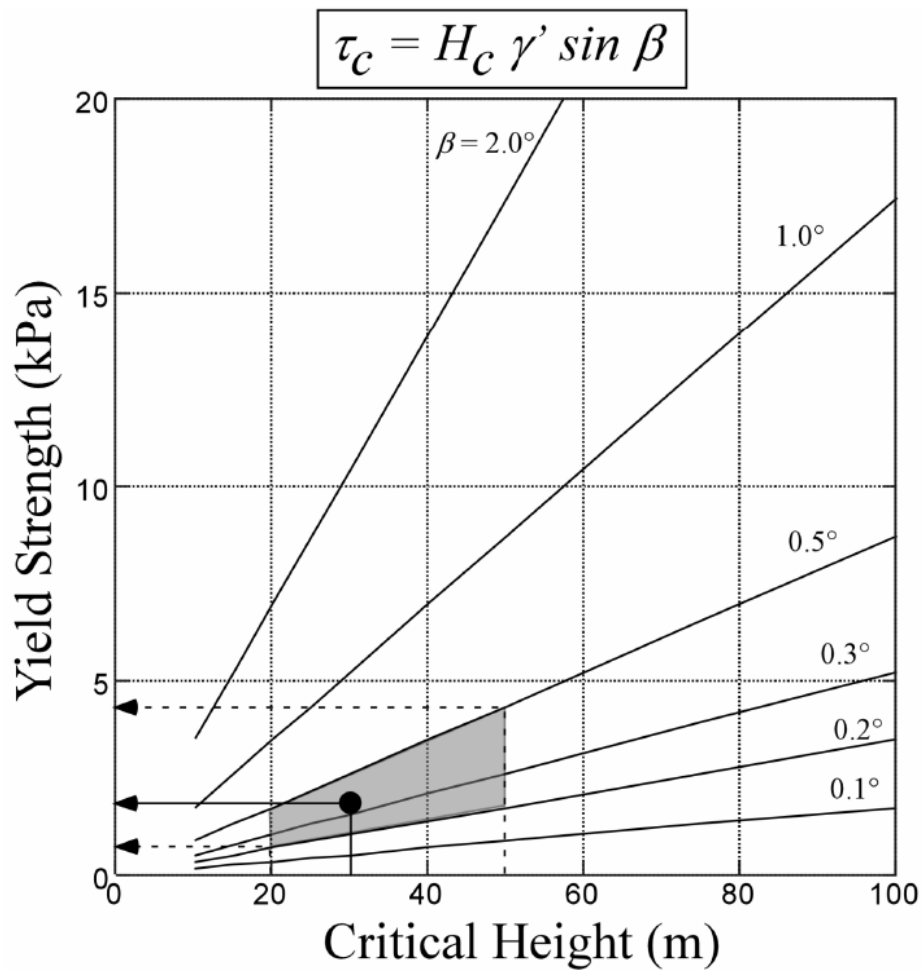


Figure 8-21: Yield strength as a function of the critical height in the depositional zone. The colored box is for a range of reported thickness for the various depositional lobes. Black dot is for a height of 30 m and a yield strength of 2.0 kPa.

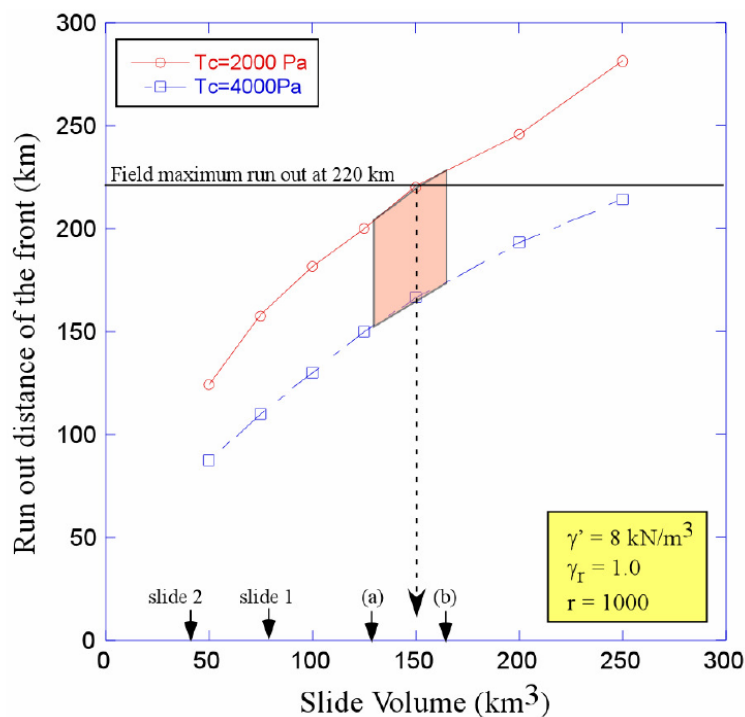


Figure 8-22: Initial volume and run out distance for two values of the yield strength. Volume at (a) is from Prior *et al.* (1986) and is taken at 128 km³. Slide 1, and volume (b) is from herein computation at 165 km³. Slide 1 and slide 2 are from models shown in Figure 8-13. Field maximum run out is taken from Figure 8-19.

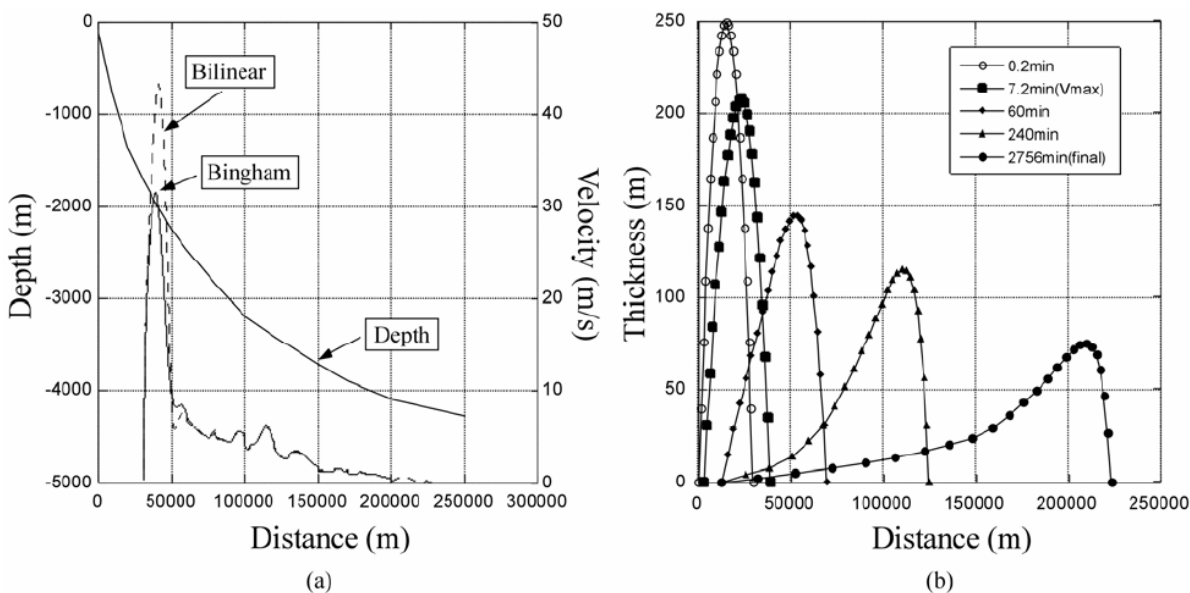


Figure 8-23: Mobility analysis for Currituck slide (a) using both Bingham and Bilinear models to illustrate the velocity distribution as a function of distance and (b) with the shape change at various times using the Bingham parameters.

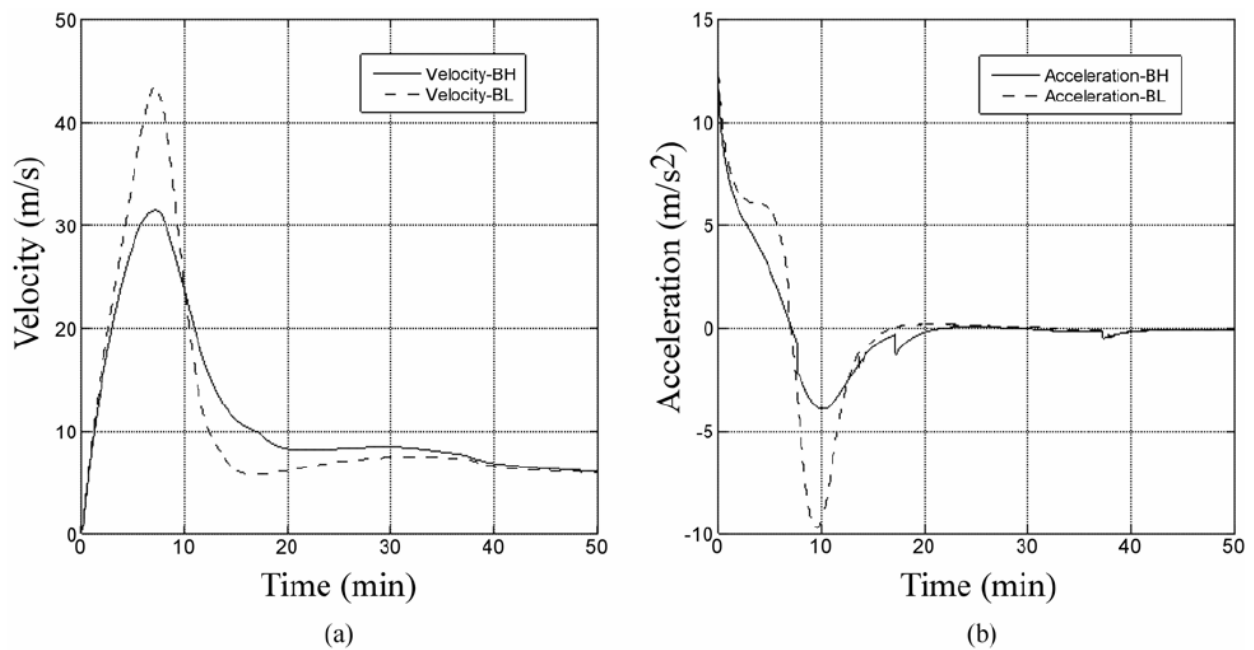


Figure 8-24: (a) Velocity and (b) acceleration profile as a function of time using both Bingham and Bilinear models (BH: Bingham; BL: Bilinear).

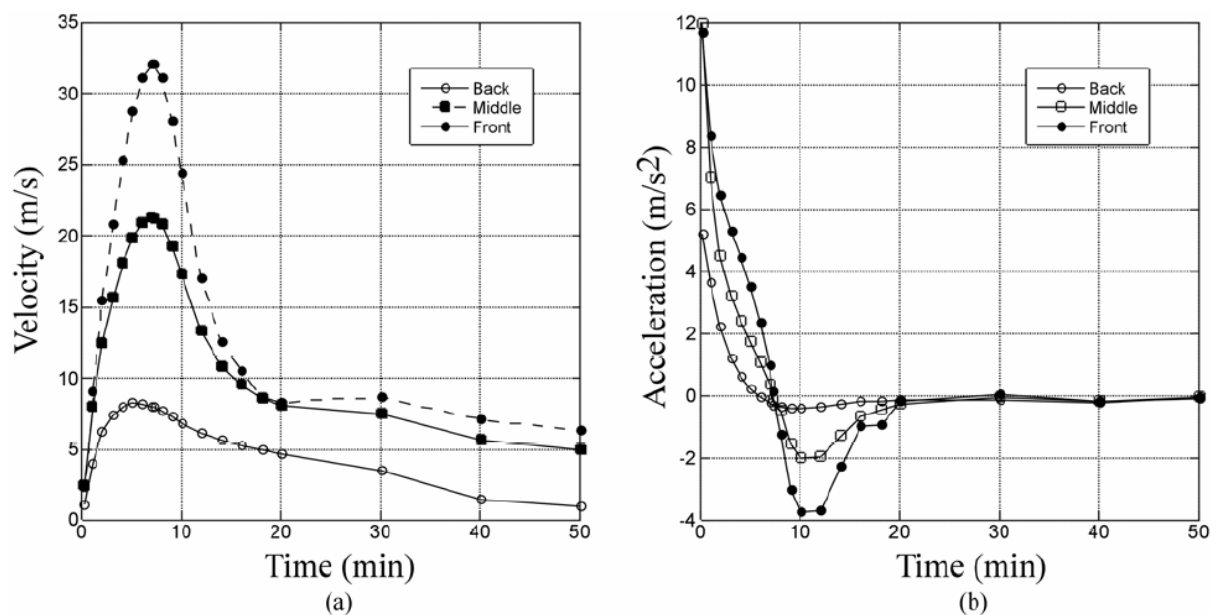


Figure 8-25: Use of the Bingham model results to show (a) the velocity profiles and (b) the acceleration profiles as a function of time for the frontal, middle and back elements.

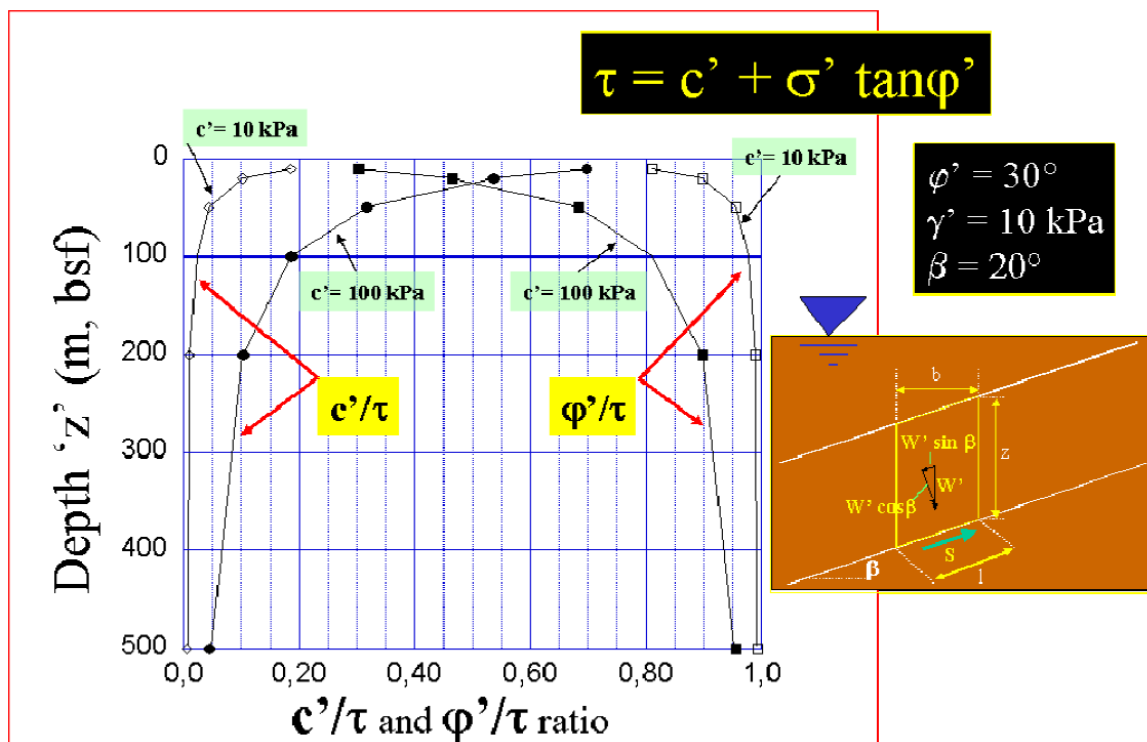


Figure 8-26: Relative contribution of the cohesion on the shear strength mobilized on a failure plane, considering an infinite slope approach (inclined at 20°).

References

- Bryn, P., Berg, K., Forsberg, C.F., Solheim, A., and Kvalstad, T.J., 2005, Explaining the Storegga Slide: *Marine and Petroleum Geology*, v. 22, p. 11-19.
- Bunn, A.R., and McGregor, B.A., 1980, Morphology of the North Carolina continental slope, Western North Atlantic, shaped by deltaic sedimentation and slumping: *Marine Geology*, v. 37, p. 253-266.
- Dugan, B., and Flemings, P.B., 2005, Overpressure and fluid flow in the New Jersey continental slope: implications for failure and cold seeps: *Science*, v. 289, p. 288-291.
- Dugan, B., Flemings, P.B., Olgaard, D.L., and Gooch, M.J., 2003, Consolidation, effective stress, and fluid pressure of sediments from ODP site 1073, U.S. mid-Atlantic continental slope: *Earth and Planetary Science Letters*, v. 215, p. 13-26.
- Hampton, M.A., 1972, The role of subaqueous debris flows in generating turbidity currents, *Journal of Sedimentary Petrology*, v. 42, p. 775-793.
- Imran, J., Harff, P., and Parker, G., 2001a, A numerical model of submarine debris flow with graphical user interface: *Computers and Geosciences*, v. 27, p. 717-729.
- Imran, J., Parker, G., Locat, J., and Lee, H., 2001b, A 1-D numerical model of muddy subaqueous and subaerial debris flows: *Journal of Hydraulic Engineering*, v. 127, p. 959-958.
- Jeong, S.W., Locat, J., and Leroueil, S., 2007, Rheological properties of fine-grained sediments in modelling submarine mass movements: the role of

- texture. In: Proceedings of the 3rd International Symposium on Submarine Mass Movements and Their Consequences, Santorini (accepted).
- Lee, H.J., Locat, J., Desgagnés, P., Parson, J., McAdoo, B., Orange, D., Puig, P., Wong, F., Dartnell, P., and Boulanger, É., 2007, Chapter 6: Submarine Mass Movements *in* Nittrouer *et al.* (Editors), Continental-margin Sedimentation: Transport to Sequence.
- Locat, J., 1997, Normalized rheological behaviour of fine muds and their low properties in a pseudoplastic regime. ASCE, First Conference on Debris Flows Hazards Mitigation, Mechanics, Prediction and assessment, p. 260-269.
- Locat, J., Desgagnés, P., Leroueil, S., and Lee, H.J., 2003a, Stability of the Hudson Apron slope off New Jersey *in* Locat, J., and Mienert, J. (Editors), Submarine mass Movements and Their Consequences, Kluwer series on Natural and Technological Hazards, v. 19, p. 257-270.
- Locat, J., and Lee, H.J., 2002. Submarine landslides: advances and challenges: *Canadian geotechnical Journal*, v. 39, p. 193-212.
- Locat, J., and Lee, J., 2005, Chapter 9: Subaqueous Debris Flows *in* Mathias and Hungr (Editors), Debris-flows Hazards and Related Phenomena, Springer, p. 203-245.
- Locat, J., Lee, H.J., Locat, P., and Imran, J., 2003b, Numerical analysis of the mobility of the Palos Verdes debris avalanche: *Marine Geology*, v. 203, p. 269-280.
- O'Brien, J.S., and Julien, P.Y., 1988, Laboratory analysis of mudflow properties: *Journal of Hydraulics Engineering, A.S.C.E.*, v. 114, p. 877-887.
- Prior, D.P., Doyle, E.H., and Neurauter, T., 1986, The Currituck Slide, Mid Atlantic continental slope-revisited: *Marine Geology*, v. 73, p. 25-4.

Chapter 9: Hydrodynamic Modeling of Tsunamis from the Currituck Landslide

Introduction

Preliminary hydrodynamic modeling of the tsunami generated by the Currituck landslide was conducted for the purpose of determining the range of possible nearshore wave heights directly shoreward from the landslide. The broad continental shelf off the U.S. Atlantic and Gulf coasts likely has a significant effect on tsunami propagation (cf., Shibata, 1983). It should be noted, however, that the continental shelf shoreward of the Currituck landslide is one of the narrowest along the U.S. Atlantic shelf. The geometry and kinematics of the landslide are based on Chapter 8. In particular, we model waves using the Slide 1, Slide 2, and composite slide (Slide 1 + Slide 2) descriptions from that section, varying the duration of slide movement in the excavation region. We also determine how different hydrodynamic parameters, such as bottom friction and non-linearity in the momentum equations, affect nearshore wave height estimates.

The model used for this study is the Cornell University Long and Intermediate Wave Modeling Package (COULWAVE) developed by Profs. Patrick J. Lynett (Texas A&M Univ.) and Philip L.-F. Liu (Cornell Univ.). The advantage of this modeling package is that it includes many different levels of approximation and parameters associated with the hydrodynamic equations for the propagation and runup of long and intermediate waves. It also provides a kinematic characterization of landslide movement, involving both regions of excavation and deposition, although in a smoothed form to make the hydrodynamic simulation stable. In this study, results from Chapter 8 are used to constrain the kinematic parameters for tsunami source implemented in COULWAVE. A variety of other models have been implemented to study the landslide tsunami problem (Jiang and LeBlond, 1992, 1993, 1994; Rubino *et al.*, 1998; Grilli and Watts, 1999; Heinrich *et al.*, 2001; Ward, 2001; Satake *et al.*, 2002; Todorovska *et al.*, 2002; Rabinovich *et al.*, 2003; Trifunac *et al.*, 2003; Løvholt *et al.*, 2005). In particular, work by Jiang and LeBlond (1994) explicitly model mudflow dynamics coupled with the overlying water column, using a viscous rheology for the landslide and the non-linear, shallow-water wave equations for the tsunami. In this study, the advantage of using COULWAVE is that there is no constraint on the particular rheology assumed for the tsunami generation model and that higher order hydrodynamic equations are used to accurately model the

evolution of the tsunami wavefield. The disadvantage is that the coupled system of landslide and water motion is not explicitly modeled.

Method

The COULWAVE package models the propagation and runup of long and intermediate length waves, using fully nonlinear and dispersive wave theory (*i.e.*, the nonlinear Bousinesq equations) as described in a number of papers (Lynett and Liu, 2002; Lynett *et al.*, 2002; Lynett and Liu, 2005; Lynett, 2006). Because this wave-modeling package is computationally intensive, there are also options to use different approximations, such as weakly nonlinear, linear, and non-dispersive forms of the wave equations. Although the objective is to determine the characteristics of the local tsunami, dispersion, which is typically only significant for transoceanic tsunamis, is likely to be important here because of the small lateral dimensions of the source (in comparison to seismogenic tsunamis) and because of the broad, shallow continental shelf (Carrier, 1971; Shibata, 1983). Because of the time constraint on this project and based on a series of initial sensitivity tests, the weakly nonlinear “extended” equations (termed WNL-EXT in Lynett and Liu, 2002) were used for the multiple simulations of the Currituck landslide tsunami. Other aspects of COULWAVE such as multi-layer flow (Lynett and Liu, 2004) and implementation on parallel processors (Sitanggang and Lynett, 2005) were not used in this study.

The WNL-EXT form of the wave equations described by Lynett and Liu (2002) are derived from the fully nonlinear form by assuming that the wavelength is much greater than the water depth and that the wave amplitude and vertical seafloor displacement are much smaller than the water depth. Specifically, for the non-dimensional parameters

$$\varepsilon = \frac{a_0}{h_0}, \quad \mu = \frac{h_0}{l_0}, \quad \delta = \frac{\Delta h}{h_0},$$

where a_0 is a characteristic amplitude, h_0 characteristic water depth, l_0 characteristic slide length, and Δh is the change in seafloor depth,

$$O(\varepsilon) = O(\delta) = O(\mu^2) \ll 1.$$

In addition, the conventional form of the linear dispersion relation is “extended” to an arbitrary depth (Nwogu, 1993; Chen and Liu, 1995) which improves the accuracy for modeling intermediate-depth waves.

These equations are numerically implemented using a finite-difference algorithm, and an iterative, high-order predictor-corrector scheme (Wei *et al.*, 1995; Lynett and Liu, 2002). The open ocean boundaries accommodate radiation of wave energy through a sponge layer, whereas runup on land boundaries is accommodated using a moving-boundary algorithm (Lynett *et al.*, 2002). A high resolution DEM for the region encompassing the failed region of the Currituck slide and extending to shore was developed for the

tsunami model (Figure 9-1). Although the grid spacing for the DEM is 200m, it was necessary to use a coarse grid spacing ($\Delta x = 2$ km) for the tsunami wave modeling, because of the computation cost associated with COULWAVE. The time step used in the finite-difference scheme was 2.47 s, which is much less than required by the Courant-Friedrichs-Lewy stability criterion. It is recommended that refined wave modeling of the region encompass a broader area to account for the effects of edge waves (Lynett and Liu, 2005) and use a finer grid spacing, especially for modeling runup and overland flow.

The results of preliminary sensitivity tests on many of the parameters specified by COULWAVE (*e.g.*, non-linearity, bottom friction, time and grid interval, energy dissipation from wave breaking) suggest that bottom friction and linear vs. non-linear formulation have the greatest effect on the results. The linear assumption overestimates nearshore tsunami amplitudes, in comparison to the more accurate nonlinear representations (Figure 9-2). The linear theory also under estimates the maximum amplitude in the source region, consistent with results described by Lynett and Liu (2002). For the out-going wave in deep water (right side Figure 9-2), there is little difference between the linear and nonlinear formulations. There is also little difference for this case study between the weakly nonlinear and fully nonlinear formulations (Figure 9-2). Because of the marked increase in computational time, extensive tests using smaller grid sizes ($\Delta x < 2$ km) were not performed, although a smaller grid spacing may increase the accuracy of the results.

The landslide source for tsunami waves is parameterized by its geometry and duration of vertical displacement. The geometry is specified by a width of slope that fails, down slope lengths for the regions of excavation and deposition, and a parameter that affects the thickness of slide masses (Lynett and Liu, 2002). Because tsunami generation is principally affected by vertical motion of the seafloor, the time history is parameterized by an overall duration of the vertical component of slide movement. Since our focus is the back-going wave propagating to the local shoreline (Figure 9-3), this is interpreted as the duration of excavation during landslide movement termed “failure duration”. The out-going wave, propagating in the direction of slide movement, quickly moves out of the model domain (Figure 9-3). Both the spatial and temporal descriptions of slide movement are smoothed to ensure stability in the numerical model. The resulting volumes of the regions of excavation and deposition are approximately conserved.

Initial Results

Tsunami simulations are computed for three landslide geometries discussed in Chapter 8 this report: Slide 1 (down slope sub-event, volume=108 km³), Slide 2 (up slope sub-event, volume=57 km³), and a composite of Slides 1 and 2 (volume=128-165 km³). As indicated in that section, it is difficult to determine whether Slides 1 and 2 occurred as separate tsunami-generating events (relative to the phase speed of tsunami waves), although it is likely that these events occurred simultaneously during failure (*i.e.*, the composite slide). Evolution of the tsunami wavefield is calculated for a propagation time of

100 minutes, which is approximately the time it takes the first waves to reach the nearest shoreline (Currituck barrier island) at the western edge of the model domain. Results are presented in the form of (1) maps of maximum wave amplitude throughout the model domain during the entire propagation time, (2) profiles of maximum wave amplitude along a slope-parallel transect aligned in the middle (axis) of the slide, and (3) time series of wave amplitude (marigram) at a nearshore location (20 km offshore) broadside from the landslide. For (3), the water depth for the nearshore location is 22 m. Initial results for each slide scenario are described using a failure duration (*i.e.*, duration of vertical displacement in the excavation region) of 10 min and a bottom friction coefficient of $f = 2.5 \times 10^{-3}$ that is typical for the continental shelf (Soulsby, 1983). Tsunami energy dissipation from bottom turbulence is primarily important for propagation across the shallow continental shelf. The effect of variations in each of these parameters is described in the next section.

For Slide 1, the peak in tsunami amplitude is landward of the generation region and is caused by shoaling amplification of the back-going wave from the source region to the continental shelf edge (Figure 9-4a, b). A secondary peak seaward of source region is caused by the downslope directivity of the out-going tsunami. Significant off-axis tsunami energy for the back-going wave is evident in Figure 9-4a that would affect coastal sites at azimuths oblique to the landslide (outside the model domain). The initial drawdown of the tsunami at the nearshore station starts approximately 65 minutes after landslide initiation and lasts approximately 15 minutes before the initial elevation wave arrives (Figure 9-4c). Drawdown after the first wave is expected to be larger in magnitude for the later arrivals. It is unclear when tsunami amplitudes start to decrease from the model domain size and propagation duration used in this study.

The excavation area for Slide 2 is at shallow water depths and therefore the back-going tsunami is less affected by shoaling amplification compared to Slide 1. Because of this and because the volume of Slide 2 is smaller than that for Slide 1, the peak amplitudes are significantly less (Figure 9-5a, b). Note that the seaward peak in tsunami amplitude over the deposition region (Figure 9-5a) is slightly off the center axis profiled in Figure 9-5b. The drawdown at the nearshore station occurs slightly earlier for Slide 2 (Figure 9-5c) compared to Slide 1 (Figure 9-4c), but is otherwise similar.

For the composite scenario where Slide 1 and Slide 2 occur as a single tsunami generating event, the amplitudes near the source are much larger than for each individual slide (Figure 9-6a, b). The nearshore tsunami amplitudes for the composite slide, however, are only slightly greater than for Slide 1. The initial drawdown phase for the composite slide is less pronounced (Figure 9-6c) than for either Slide 1 or Slide 2.

Effect of Variations in Failure Duration and Bottom Friction

For each slide scenario, three different values of failure duration in the excavation region are used to determine the effect on the tsunami wavefield. In general, landslide duration is inversely proportional to the height of the generated tsunami waves, holding landslide volume constant. Two duration values are chosen according to the characteristic times from the mobility analysis of the Currituck landslide described in the previous section. The first value is the time of the maximum in slide deceleration (approximately 10 min). The second value is the time for acceleration to approach 0 after the deceleration phase starts (approximately 20 min). It is thought that the former value better accounts for the initial high acceleration of failure, whereas the latter value represents the overall total duration of slide movement in the excavation region. We also examine a very short duration time (7.2 min.) to examine the effect on tsunami amplitudes of a slide that is much more mobile than expected from the mobility analysis (*e.g.*, from low basal shear stress).

Results shown in Figure 9-7 indicate that failure duration has a dramatic effect on maximum tsunami amplitudes over the source region (bottom friction held constant at $f = 2.5 \times 10^{-3}$). Because tsunami waves are leaving the source region at a phase speed of \sqrt{gh} (long wavelength limit), slower process times will result in smaller initial tsunami amplitudes. This effect is also evident for the out-going tsunami (right side of model domain), which is significantly affected by downslope landslide speed (Godorovska *et al.*, 2002; Trifunac *et al.*, 2002). This effect is much less significant at nearshore water depths for the back-going tsunami of interest (Figure 9-7), suggesting that landslide volume is a more significant source parameter than failure duration.

Bottom friction is parameterized in COULWAVE by the friction coefficient f . Shear stress (τ) at the bottom boundary is given by

$$\tau = \frac{1}{2} \rho f |\mathbf{u}_b| \mathbf{u}_b,$$

where ρ is fluid density and \mathbf{u}_b is the horizontal velocity field near the sea floor. Increasing the bottom friction coefficient will lead to greater dissipation of tsunami energy during propagation. The friction coefficient is related to two other parameters that describe the hydraulic roughness of the bottom boundary layer: Chézy coefficient (C) and Manning's roughness coefficient (n)

$$f = \frac{g}{C^2},$$

$$f = \frac{gn^2}{(h+a)^{1/3}},$$

where g is the gravitational acceleration, h is the water depth and a is the tsunami amplitude. Estimates of f for continental shelf environments range

between approximately $1.6 - 6.1 \times 10^{-3}$, depending on the bottom type and the presence of bed forms (Soulsby, 1983). In addition, estimates of f for shoaling waves and runup are considerably higher $> 10^{-2}$ (Mei, 1989; Satake, 1995).

Results of using different bottom friction coefficients for the composite slide scenario are shown in Figure 9-8 (failure duration held constant at 10 min.). Above the source region, there is a slight decrease in maximum tsunami amplitude. During propagation of the back-going tsunami across the continental shelf, however, higher bottom friction results in greater energy dissipation and significantly smaller tsunami amplitude estimates. Conversely, for the out-going tsunami, the effect is minimal because of the much greater water depths along the continental slope.

Bivariate analysis of the effect failure duration and bottom friction have on maximum nearshore tsunami wave height are presented for each of the slide scenarios in Figures 9-9, 9-10, and 9-11. In each case, bottom friction has more of an effect on maximum nearshore tsunami wave height than failure duration, for the ranges tested. The curvature in the contours of maximum wave height indicates that rupture duration is a more significant effect for low values of bottom friction ($f \sim 10^{-3}$). For high values of bottom friction ($f \sim 10^{-2}$), maximum nearshore wave height is less sensitive to variations in failure duration.

Summary

Preliminary simulations of potential waves generated from the Currituck landslide yield a wide range in estimated near-shore wave heights. The primary source parameters that affect near-shore wave heights are the overall volume of the landslide and the duration of vertical movement in the excavation region that generates the back-going, leading depression wave. The mobility analysis, presented earlier in this report, is key in constraining the failure duration parameter. Reasonable variations in failure duration have less of an effect on nearshore wave height estimates than the primary source parameter: landslide volume. Other source parameters of the landslide tsunami such as water depth in the excavation region, slide thickness, and down-slope length also have a significant effect on the wave characteristics. The primary hydrodynamic parameter that affects estimates of near-shore wave height is bottom friction along the continental shelf and nearshore region. Improvements to future models would incorporate different coefficients for bottom friction in the shelf and near-shore region. It is also shown, that an assumption of linearity in the momentum equations over estimates the near-shore wave heights.

Modeling of tsunamis generated from landslides off the continental slope needs further refinement, primarily in the form of small spatial grid size and a larger region of examination. The latter is necessary to estimate runup heights at oblique angles from the source region that may be significant, owing to the effect of edge waves (Lynett and Liu, 2005) and of secondary beaming from offshore bathymetric variations. With a larger model domain,

longer propagation durations can be simulated to determine at what time nearshore tsunami amplitudes start to decrease. In the vicinity of any particular site of interest, it is necessary to have a very high grid resolution ($\Delta x < 30$ m) to accurately model runup, rundown, and overland flow. It is expected that computational cost for this model would be high and that the parallel version of COULWAVE (pCOULWAVE) should be used. It would also be helpful in the future to modify the time evolution of the slide as it is implemented in COULWAVE to account for the initial high acceleration predicted from the mobility analysis.

Figures

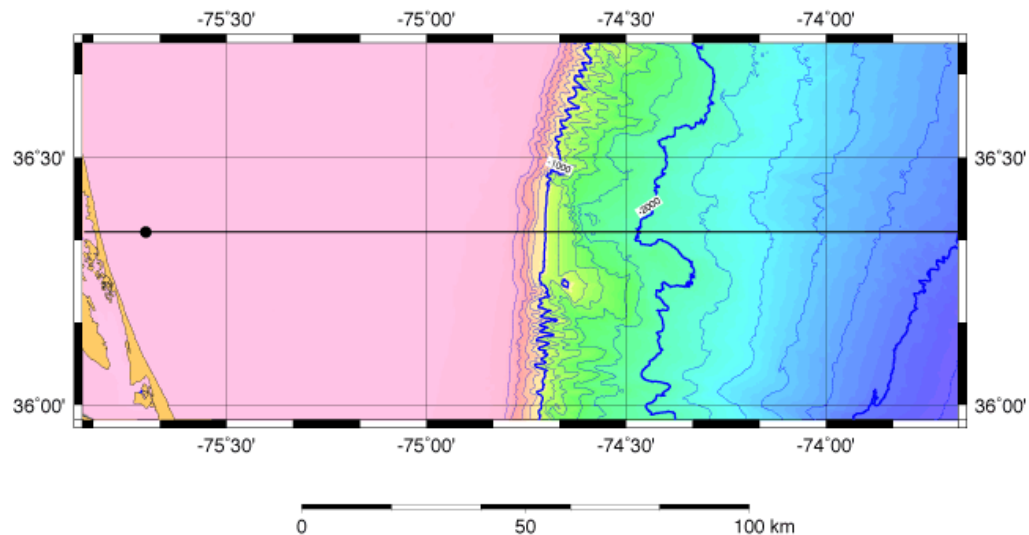


Figure 9-1: High resolution DEM of the Currituck landslide and nearshore region representing the model domain. Primary bathymetric contour interval 1,000 m; secondary contour interval 200 m. Black line shows location of profile where maximum tsunami amplitude is displayed in figures below; black dot, nearshore location where tsunami time series (marigram) is displayed.

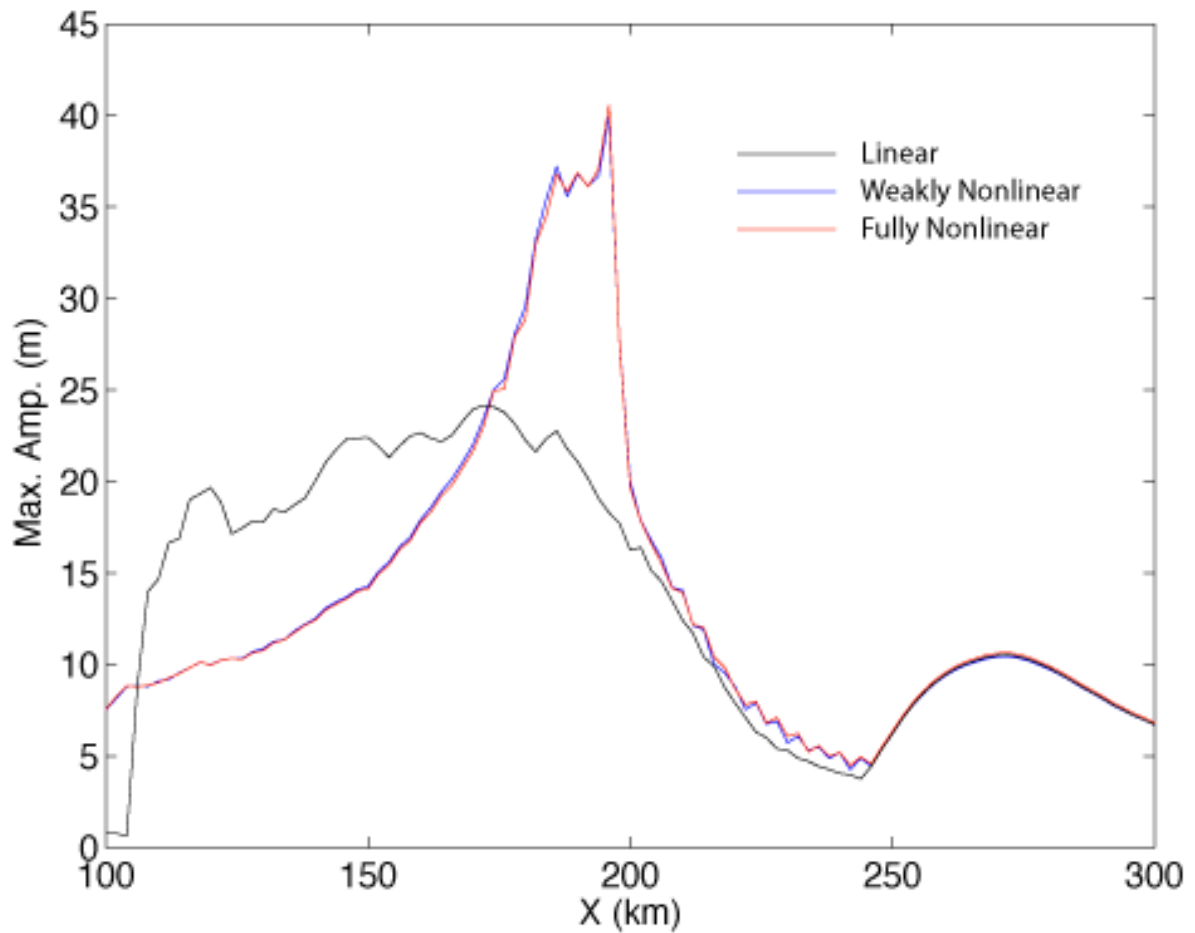


Figure 9-2: Comparison of maximum amplitude profiles aligned with slide axis for the linear, weakly nonlinear (WNL), and fully nonlinear (FNL) forms of the hydrodynamic equations. Simulation for highest amplitude composite slide (duration=7.2 min., $f = 1.0 \times 10^{-3}$) (cf., Figure 9-6 where duration=10 min.). The shoreline is at $x = 100$ km. The rapid amplitude drop off near shore is an artifact of the model.

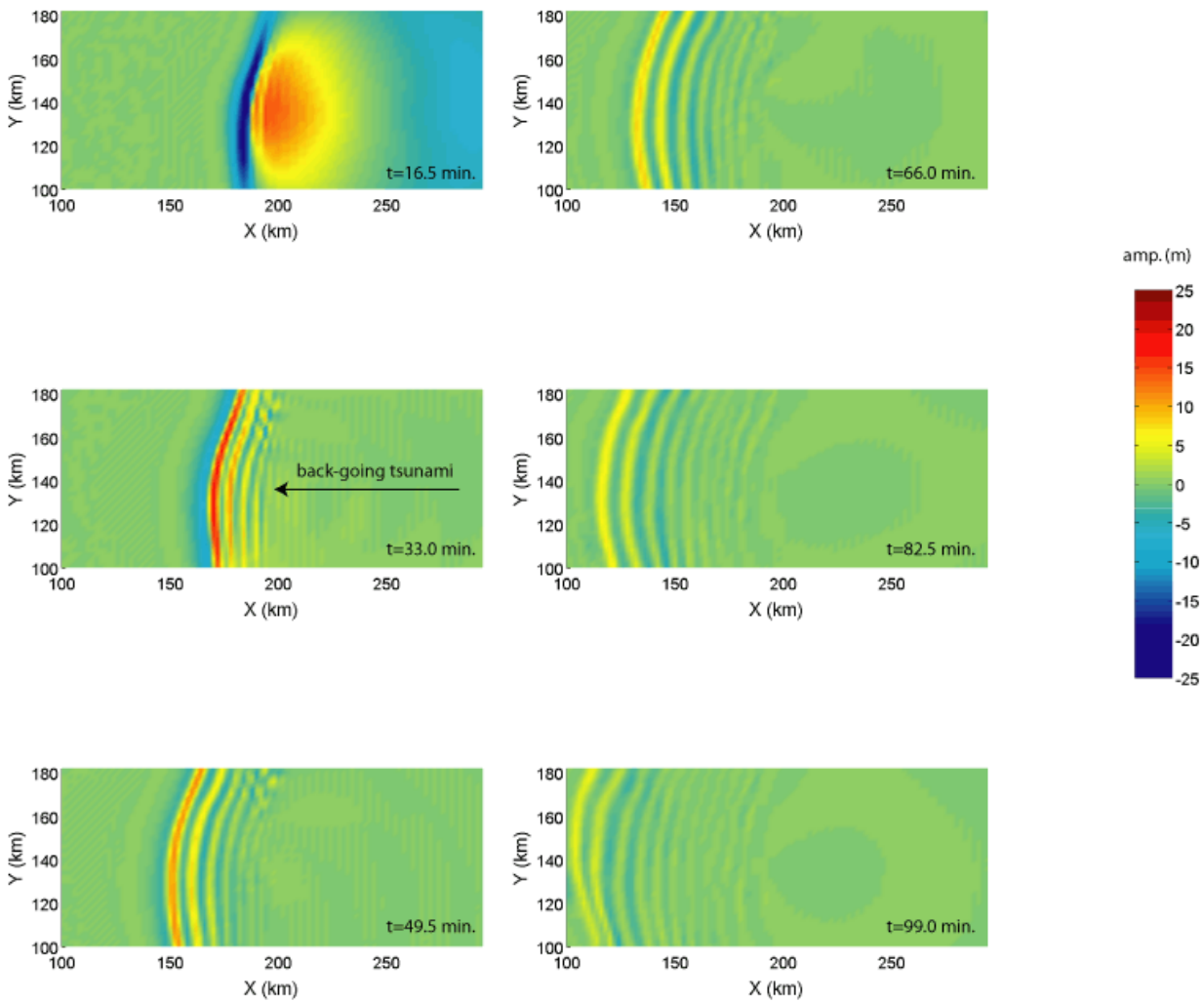


Figure 9-3: Evolution of tsunami wavefield for composite slide (failure duration 10 min.; $f = 2.5 \times 10^{-3}$) at time intervals of 16.5 minutes. Because out-going tsunami is propagating to the right at high speeds, primarily the back-going tsunami is illustrated as it propagates across the continental shelf (pink in Figure 9-1).

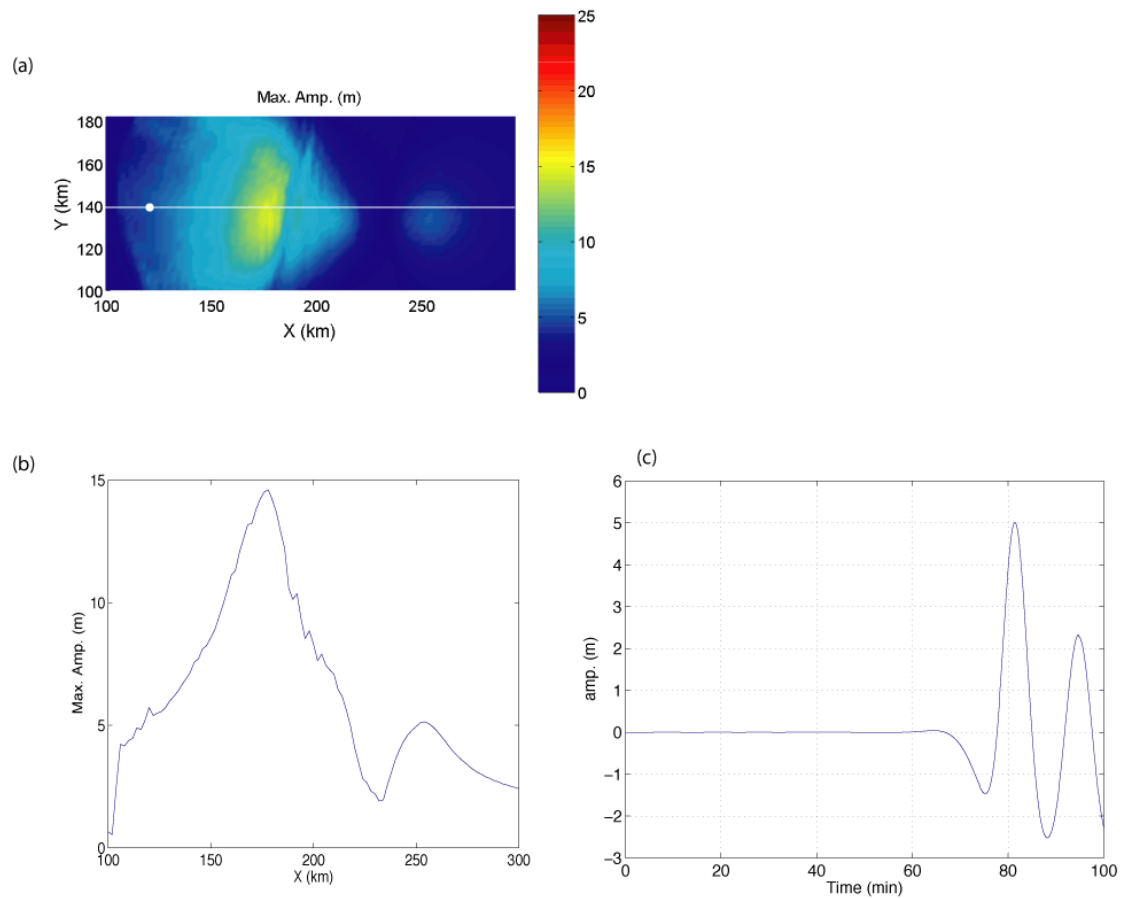


Figure 9-4: Results of hydrodynamic simulation for Slide 1 (duration=10 min., $f = 2.5 \times 10^{-3}$). (a) Maximum wave height during 100 min. of propagation time in map view. (b) Maximum wave height profile along centerline of landslide (white line in a). The shoreline is at $X = 100$ km. (c) Time series of tsunami amplitude at a water depth of 22 m nearshore (white dot in a) shoreward from the center of the landslide.

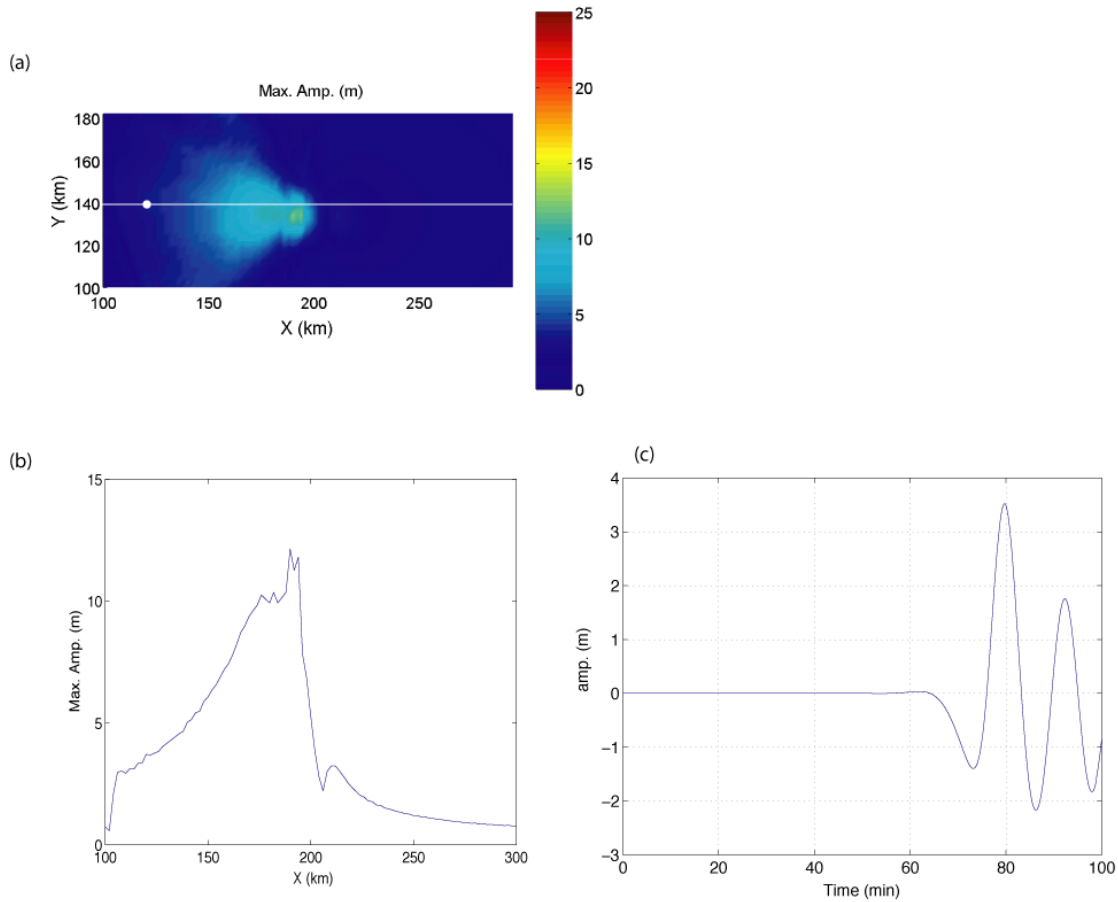


Figure 9-5: Results of hydrodynamic simulation for Slide 2 (duration=10 min., $f = 2.5 \times 10^{-3}$). (a) Maximum wave height during 100 min. of propagation time in map view. (b) Maximum wave height profile along centerline of landslide (white line in a). (c) Time series of tsunami amplitude at a nearshore location (white dot in a) broadside from the landslide in 22 m of water.

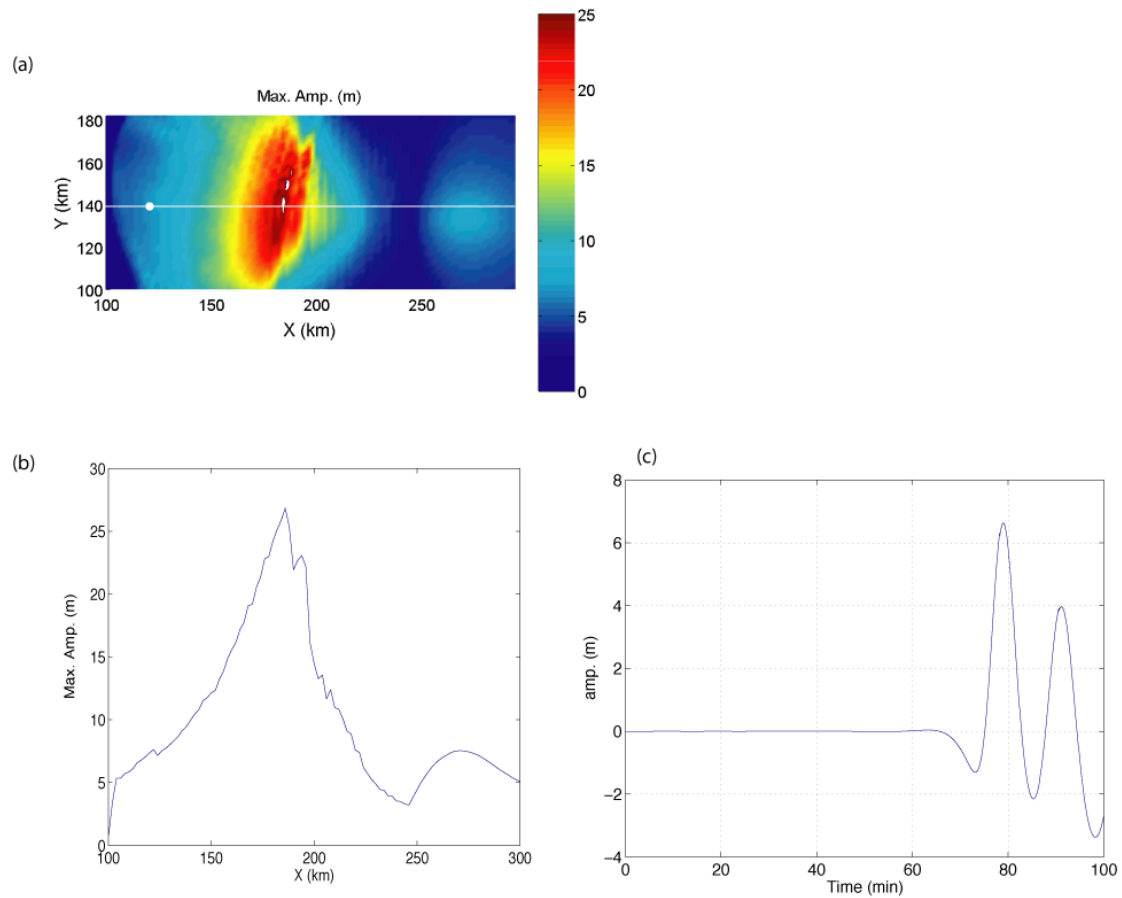
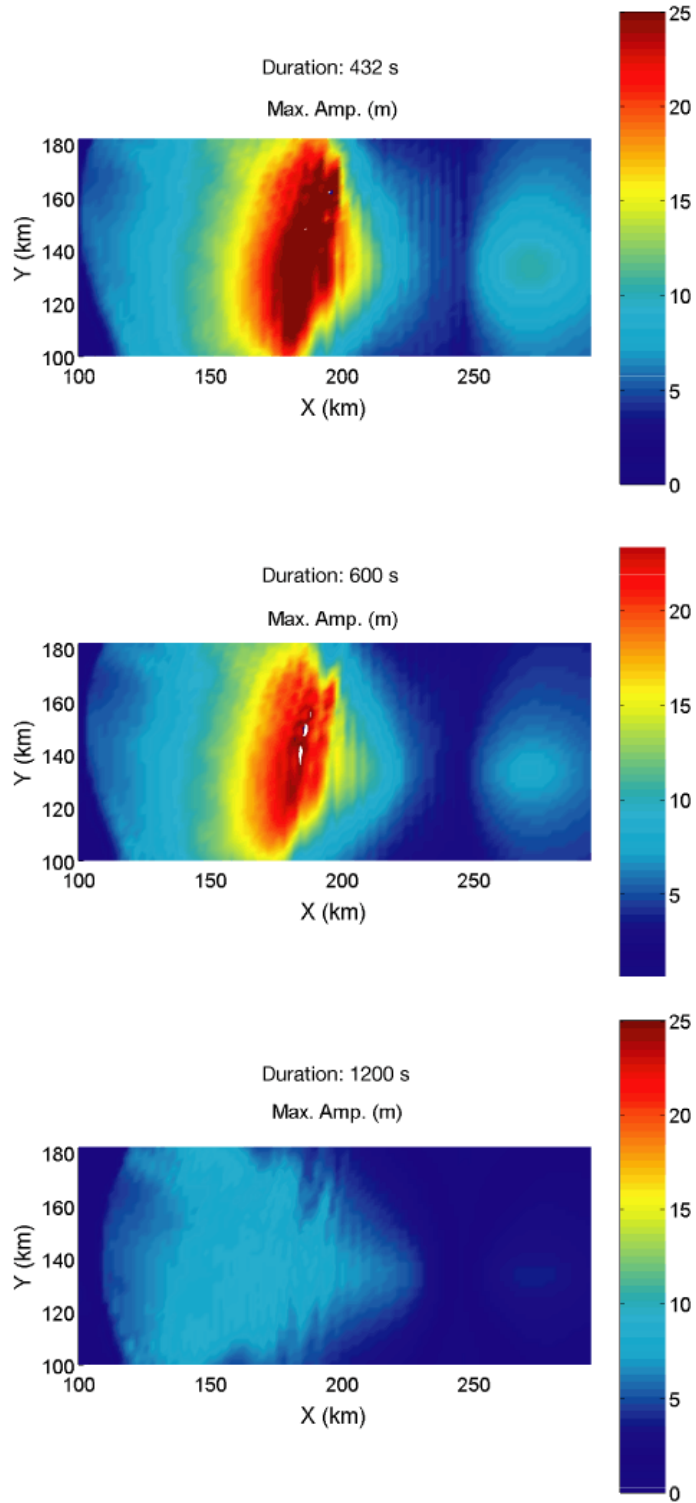


Figure 9-6: Results of hydrodynamic simulation for combined failure of both Slides 1 and 2 (duration=10 min., $f = 2.5 \times 10^{-3}$). (a) Maximum wave height during 100 min. of propagation time in map view. (b) Maximum wave height profile along centerline of landslide (white line in a). (c) Time series of tsunami amplitude at a nearshore location (white dot in a) broadside from the landslide in 22 m of water.



s

Figure 9-7: Comparison of maximum wave amplitude maps for the composite slide scenario (Slide 1 and Slide 2) using different values for failure duration in the excavation region.

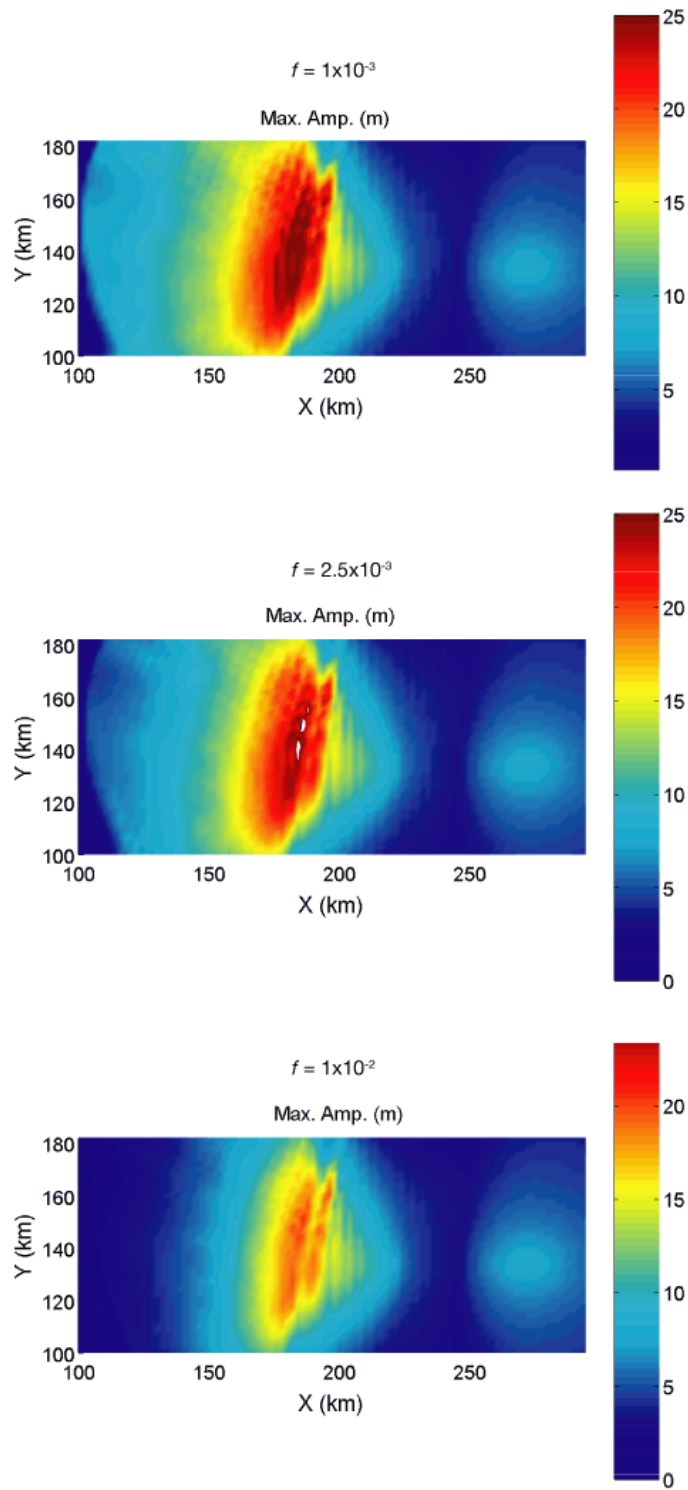


Figure 9-8: Comparison of maximum wave amplitude maps for the composite slide scenario (Slide 1 and Slide 2) using different values for the bottom friction coefficient.

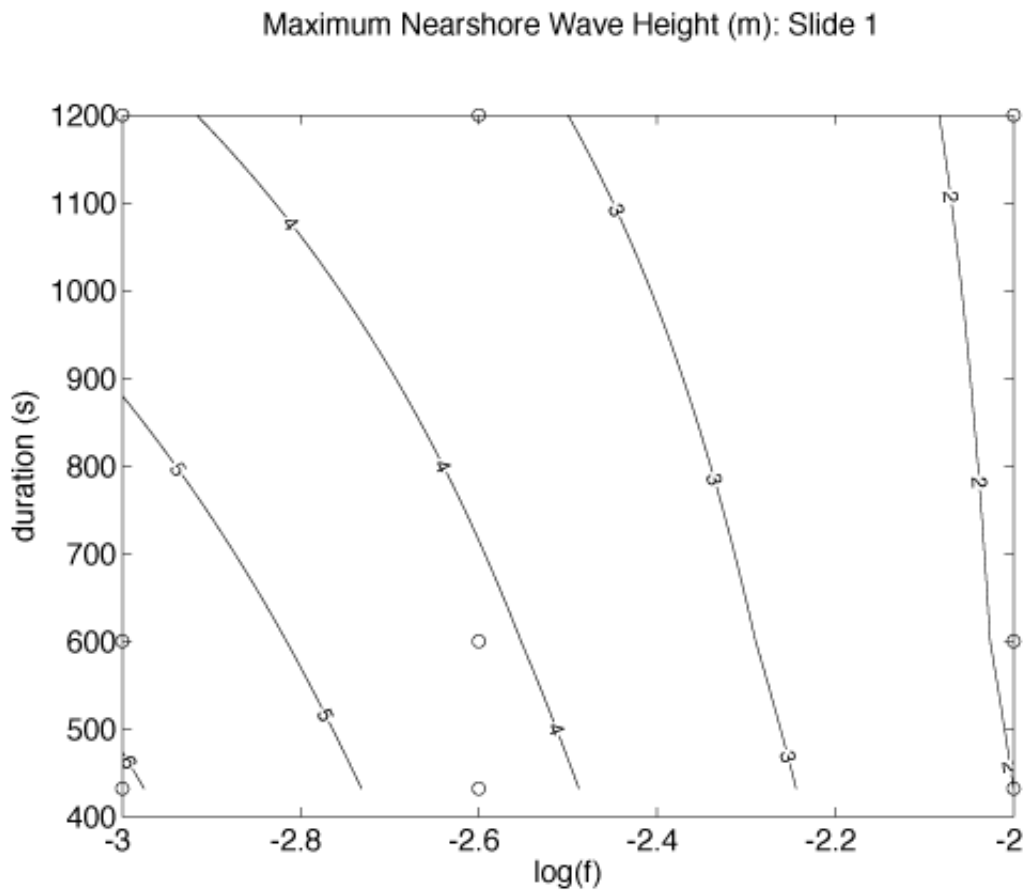


Figure 9-9: Bivariate analysis of the effect failure duration and bottom friction have on nearshore tsunami wave height for Slide 1. Water depth where maximum wave height is sampled is 18 m. Circles represent results from individual simulations. Maximum wave height contour interval: 1 m.

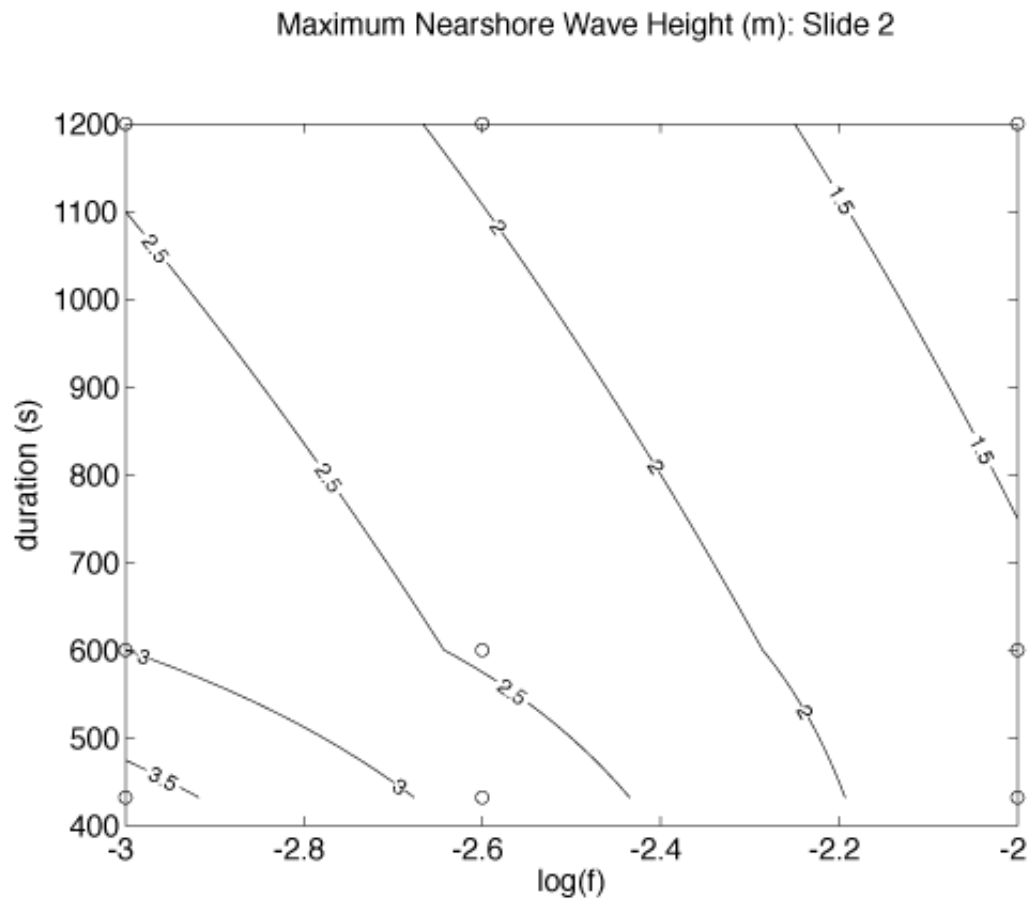


Figure 9-10: Bivariate analysis of the effect failure duration and bottom friction have on nearshore tsunami wave height for Slide 2. Water depth where maximum wave height is sampled is 18 m. Circles represent results from individual simulations. Maximum wave height contour interval: 0.5 m.

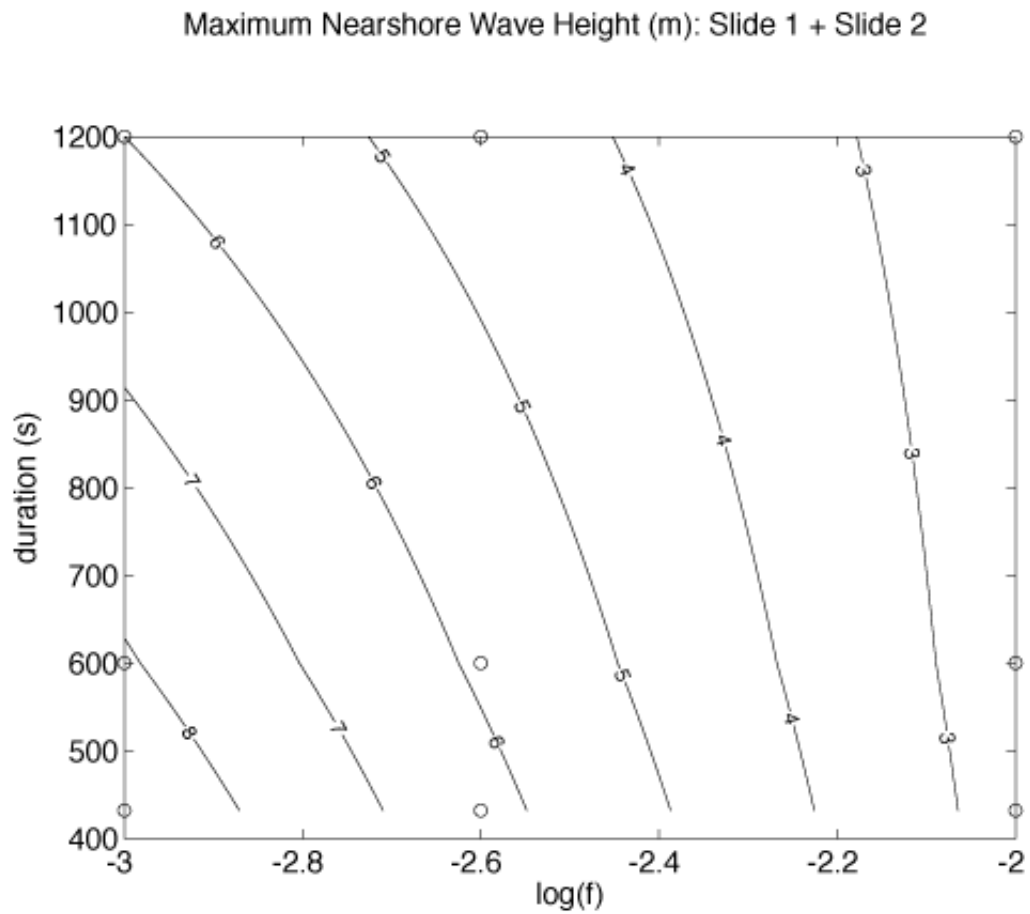


Figure 9-11: Bivariate analysis of the effect failure duration and bottom friction have on nearshore tsunami wave height for both Slides 1 and 2. Water depth where maximum wave height is sampled is 18 m. Circles represent results from individual simulations. Maximum wave height contour interval: 1 m.

References

- Carrier, G. F., 1971, The dynamics of tsunamis, *in* Reid, W. H. (Editor), *Mathematical Problems in the Geophysical Sciences*: American Mathematical Society, Providence, Rhode Island, p. 157-187.
- Chen, Y., and Liu, P. L.-F., 1995, Modified Boussinesq equations and associated parabolic model for water wave propagation: *Journal of Fluid Mechanics*, *v. 228*, p. 351-381.
- Grilli, S. T., and Watts, P., 1999, Modeling of waves generated by a moving submerged body: Applications to underwater landslides: *Engineering Analysis with Boundary Elements*, *v. 23*, p. 645-656.
- Heinrich, P., Piatanesi, A., and Hébert, H., 2001, Numerical modeling of tsunami generation and propagation from submarine slumps: the 1998 Papua New Guinea event: *Geophys. J. Int.*, *v. 145*, p. 97-111.
- Jiang, L., and Leblond P. H., 1992, The coupling of a submarine slide and the surface waves which it generates: *J. Geophys. Res.*, *v. 97*, p. 12,731-712,744.
- Jiang, L., and Leblond, P. H., 1993, Numerical modeling of an underwater Bingham plastic mudslide and the waves which it generates: *J. Geophys. Res.*, *v. 98*, p. 10,303-310,317.
- Jiang, L., and Leblond, P. H., 1994, Three-dimensional modeling of tsunami generation due to a submarine mudslide: *Journal of Physical Oceanography*, *v. 24*, p. 559-572.
- Lynett, P., and Liu, P. L. F., 2002, A numerical study of submarine-landslide-generated waves and run-up: *Proc. R. Soc. Lond. A*, *v. 458*, p. 2885-2910.
- Lynett, P. J., 2006, Nearshore wave modeling with high-order Boussinesq-type equations: *Journal of the Waterways and Harbors Division, A.S.C.E.*, *v. 132*, p. 348-357.
- Lynett, P. J., and Liu, P. L.-F., 2004, A two-layer approach to wave modeling: *Proc. R. Soc. Lond. A*, *v. 460*, p. 2637-2669.
- Lynett, P. J., and Liu, P. L.-F., 2005, A numerical study of run-up generated by three-dimensional landslides: *J. Geophys. Res.*, *v. 10*, doi:10.1029/2004JC002443.
- Lynett, P. J., Wu, T.-R., and Liu, P. L.-F., 2002, Modeling wave runup with depth-integrated equations: *Coastal Engineering*, *v. 46*, p. 89-107.
- Løvholt, F., Harbitz, C., and Haugen, K. B., 2005, A parametric study of tsunami generated by submarine slides in the Ormen Lange/Storegga area off western Norway: *Marine and Petroleum Geology*, *v. 22*, p. 219-231.
- Mei, C. C., 1989, *The Applied Dynamics of Ocean Surface Waves*, World Scientific, Singapore, 740 p.
- Nwogu, O., 1993, Alternative form of Boussinesq equations for nearshore wave propagation: *Journal of Waterway, Port, Coastal, and Ocean Engineering*, *v. 119*, p. 618-638.
- Rabinovich, A. B., Thomson, R. E., Bornhold, B. D., Fine, I. V., and Kulikov, E. A., 2003, Numerical modeling of tsunamis generated by hypothetical landslides in the Strait of Georgia, British Columbia: *Pure Appl. Geophys.*, *v. 160*, p. 1273-1313.

- Rubino, A., Pierini, S., and Backhaus, J. O., 1998, Dispersive mudslide-induced tsunamis: *Nonlinear Processes in Geophysics*, v. 5, p. 127-136.
- Satake, K., 1995, Linear and nonlinear computations of the 1992 Nicaragua earthquake tsunami: *Pure Appl. Geophys.*, v. 144, p. 455-470.
- Satake, K., Smith, J. R., and Shinozaki, K., 2002, Volume estimate and tsunami modeling for the Nuuanu and Wailau landslides, in Takahashi, E., *et al.* (Editors), Hawaiian Volcanoes: Deep Underwater Perspectives, Geophysical Monograph 128, American Geophysical Union, p. 333-348.
- Shibata, M., 1983, One-dimensional dispersive deformation of tsunami with typical initial profiles on continental topographies, in Iida K., and Iwasak, T. (Editors), Tsunamis: Their Science and Engineering, Terra Science Publication Company, Tokyo, p. 241-250.
- Sitanggang, K. I., and Lynett, P., 2005, Parallel computation of highly nonlinear Boussinesq equation model through domain decomposition: *International Journal for Numerical Methods in Fluids*, v. 49.
- Soulsby, R. L., 1983, The bottom boundary layer of shelf seas, in Johns, B. (Editor), Physical Oceanography of Coastal and Shelf Seas, Elsevier, Amsterdam, p. 189-266.
- Todorovska, M. I., Hayir, A., and Trifunac, M. D., 2002, A note on tsunami amplitudes above submarine slides and slumps: *Soil Dynamics and Earthquake Engineering*, v. 22, p. 129-141.
- Trifunac, M. D., Hayir, A., and Todorovska, M. I., 2002, A note on the effects of nonuniform spreading velocity of submarine slumps and slides on the near-field tsunami amplitudes: *Soil Dynamics and Earthquake Engineering*, v. 22, p. 167-180.
- Trifunac, M. D., Hayir, A., and Todorovska M. I., 2003, A note on tsunami caused by submarine slides and slumps spreading in one dimension with nonuniform displacement amplitudes: *Soil Dynamics and Earthquake Engineering*, v. 23, p. 223-234.
- Ward, S. N., 2001, Landslide tsunami, *J. Geophys. Res.*, v. 106, p. 11,201-211,215.
- Wei, G., Kirby, J. T., Grilli, S. T., and Subramanya, R., 1995, A fully nonlinear Boussinesq model for surface waves. Part 1: Highly nonlinear unsteady waves, *Journal of Fluid Mechanics*, v. 294, p. 71-92.

Chapter 10: Summary of the Current State of Knowledge Regarding Potential Tsunami Sources Affecting U.S. Atlantic and Gulf Coasts

The first phase of the assessment consisted of analysis of recently released detailed bathymetry along the Atlantic continental margin (Chapter 2), and review of previous work pertaining to landslides and earthquake sources (Chapters 3-6). Preliminary tsunami propagation models from earthquake sources in the Caribbean help identify sources, which are likely to present hazard to U.S. coasts (Chapter 7). A morphological, geotechnical and mobility analysis of the Currituck landslide offshore Virginia, and tsunami propagation models for this slide were performed as an example of more in-depth work that is necessary to quantify the tsunami hazard from submarine landslides along the U.S. Atlantic continental margin (Chapters 8-9). Following is a more detailed summary of each chapter.

Chapter 2

Although regional studies of the distribution and size of major submarine landslides along the U.S. Atlantic margin have been previously conducted, recently-collected high-resolution multibeam bathymetry enabled us to carry out a more accurate analysis of these features. As a result, although we report a smaller number of mass movement features than previously published, we have been able to better define the extent and thickness of individual and composite landslides, which in most cases incorporate a number of the singular features described by previous investigators.

The spatial distribution of landslides along the U.S. Atlantic margin is, in part, controlled by the underlying geology. The thickness of Quaternary sediment preserved on the outer shelf is closely associated with landslide distribution. Landslide areas are most common and tend to be largest offshore of these areas where Quaternary sediment is thickest. Nearly 60% of the area affected by landslides occurs offshore of the thick Quaternary shelf deposits of the Georges Bank, southern New England and Virginia areas. The thick Quaternary deposits presumably covered the upper slope as well and were the source material for many of the landslides. In these three areas,

the strata underlying the slope dip sub-parallel to the gradient of the present slope. Landslides covering the remainder of the continental margin, account for only 16% of the landslide area. They are associated with thin Quaternary deposits at the shelf edge and with nearly horizontal older strata underlying the slope. The two large landslide areas in the Carolina Trough are likely controlled by tectonic activity associated with the movement of salt domes. These two large salt-related landslides account for 24% of the area affected by landslides.

Landslides along the U.S. Atlantic margin initiate predominantly in two morphologic settings: canyon (heads and sidewalls) and on the open continental slope. The canyon-sourced failures commonly have several canyons feeding a single deposit, and the deposits are smaller than those derived from the open slope. Open-slope failures originate from scarps commonly on the middle and lower slope in 800-2,200 m depths, and not at the top of the gas hydrate stability zone, as previously suggested. These landslides extend farther offshore, are thicker, and have considerably larger volumes than their canyon derived counterparts. The dominant style of mass wasting identified along the Atlantic margin appears to be debris flows. In part, the reason for this may be because the bulk of the sediment that makes up the mass wasting deposits is Quaternary in age and sediment in the source areas was largely unconsolidated unlithified to semi-lithified, and could not be transported large distances without undergoing disintegration. The height of scarps in most landslide source areas is less than 75 m indicating that in most places only the Quaternary section is being removed.

Open slope sourced slides are larger both in the area of failure and overall volume, and as such, are the dominant means of rapid margin modification. Because of the large volumes of material that can fail during an individual or retrogressive open slope-sourced slide, these are considered to have the most potential to initiate tsunamis. From the modeling of source volumes of individual scarps along the margin, three regions (off Georges Bank, Currituck area, and in the Carolina Trough) appear to have had a history of, and therefore potential for, large volume failures. With the currently available data, it is difficult to determine if landslides on the southern New England slope involve large volumes of material per event, or if the region is dominated by smaller, but more numerous landslides.

Chapter 3

Landslides in the Gulf of Mexico occur in all three depositional provinces (carbonate, salt, and canyon/fan). The largest failures are found in the canyon/fan province. The largest failures filled the Bryant Canyon and covered the upper parts of the Mississippi and Eastern Mississippi Fans. Available information suggests they occurred during the early part of the Holocene (10,000-15,000 yr BP). The resumption of hemipelagic sedimentation in the head of Mississippi Canyon at 7,500 yr BP indicates that at least the largest of these landslide complexes had ceased being active by mid-Holocene time.

Landslides within the salt province are in general considerably smaller than those in the canyon/fan province, many of them are confined to the walls of mini-basins, but some occupy the Sigsbee escarpment. These landslides appear to be active and are driven by salt creep. Landslides in the carbonate provinces that fringe the eastern and southern Gulf of Mexico appear to have been derived from both the steep West Florida and Campeche Escarpments as well as from the gentler slope above the escarpments. The northern part of the Florida Escarpment has probably undergone little erosion since it originally formed during the Cretaceous, but the southern part of the Florida Escarpment shows sign of active erosion.

Chapter 4

Far-field submarine landslide sources have been quoted as potential sources for trans-oceanic tsunamis. The most widely known is the threat of a large-volume landslide caused by an imminent eruption of Cumbre Vieja volcano in the Canary Island. However, models of tsunami propagation, which take into account dispersion and non-linearity of the landslide-generated waves, show rapid amplitude decay with distance and predict <1 meter of flooding in Florida. In addition, the recurrence time of a major eruption-related landslide is 10^5 yr. The giant Storegga landslide offshore Norway caused large tsunami waves within 600 km radius in the northeast Atlantic, but the waves are not known to have propagate to the U.S. East Coast. Some large landslides have been identified along the Scotian margin north off New England. Most of them are Holocene and older in age and appear to be related to the expansion and contraction of the Laurentide ice sheet. The 1929 Grand Banks landslide generated a damaging tsunami locally, but not in New England. However, larger landslides than the 1929 Grand Banks landslide have been identified in the stratigraphic record.

Chapter 5

The Atlantic Ocean is generally devoid of subduction or convergent zones. Two exceptions are the area west of Gibraltar, the location of the 1755 Lisbon earthquake, and the Hispaniola-Puerto Rico-Lesser Antilles subduction zone. The 1755 Lisbon earthquake as well as an earthquake in 1761 in that area, generated a transoceanic tsunami recorded along the European and African coasts, islands in the Atlantic, and the Caribbean islands. The source of these earthquakes is still debatable, but recent papers suggest that it was perhaps caused by a small east-dipping subduction zone under the western Mediterranean.

The northern Caribbean subduction zone has the potential to cause a major tsunami similar to the 2004 Sumatra tsunami. However, detailed work in the Puerto Rico Trench indicates that slip there is highly oblique and the subducting lithosphere is very old, two indications that perhaps the subduction zone is not capable of generating very large earthquakes. The Hispaniola segment of this subduction zone, while perhaps capable of very

large earthquakes, is fringed to the north by an almost continuous line of islands and shallow banks that obstruct, but not completely block, propagating tsunami waves.

Chapter 6

Convergent or subduction zones in the southern Caribbean are reviewed and do not appear to be capable of generating very large earthquakes, and thus do not appear to pose a significant tsunami hazard to the Gulf of Mexico coastal zones.

Chapter 7

Tsunamis arising from the Caribbean earthquake sources outlined in Chapters 5 and 6, as well as from the transform faults along Cayman Trough were modeled using linear long-wave equation. Tsunami propagation was modeled only in deep water and up to a depth of 250 m in the continental margin of the Atlantic and the Gulf of Mexico. Tsunami propagation did not extend to shallower water, to avoid addressing energy dispersion, bottom friction, and non-linear attenuation. The models suggest that rupture of the Puerto Rico trench is the only Caribbean source capable of causing damaging tsunamis along U.S. coasts. High wave amplitude from rupture of the Puerto Rico trench is predicted to concentrate along the New England and New Jersey margin, and in the vicinity of Wilmington, N.C. and Myrtle Beach, S.C.

Chapter 8

The mobility of submarine mass movement Currituck slide offshore Virginia was analyzed using 1-D numerical model for muddy debris flows in order to provide input for a more precise analysis of tsunami wave generation and to validate the initial volume estimation. Input parameters for this analysis were derived from a morphological analysis of the landslide excavation and deposition areas, and from static slope stability analysis of the landslide. The Currituck landslide appears to have been comprised of 2 or perhaps 3 discrete slides. The results of the above analyses indicate that the Currituck slide was a lateral spread failure, much like the Storegga slide, which likely took place on low angle bedding planes (less than 4°) and involved a volume of sediment between 165 and 128 km³. The slide was triggered by a catastrophic event that must have required a sudden increase in pore pressure, likely due to an earthquake. According to the thickness of the slide deposit in the run out zone, the mobilized yield strength of the sediments was of the order of 2,000 Pa. The peak velocity may have been between 30 and 40 m/s and most of the acceleration phase was completed within 10 minutes. The acceleration of the flowing mass was not uniformly distributed with the shallowest elements having lower acceleration than the frontal element resulting in a very significant spreading (thinning) of the debris, over a distance of more than 200 km.

Chapter 9

Preliminary hydrodynamic modeling of a tsunami that could have been generated by the Currituck landslide, was conducted for the purpose of determining the range of possible near-shore wave heights directly shoreward from the landslide. The modeling indicates that the broad continental shelf off the U.S. Atlantic and Gulf coasts likely has a significant effect on tsunami propagation. It should be noted, however, that the continental shelf shoreward of the Currituck landslide is one of the narrowest along the U.S. Atlantic shelf. Tsunami simulations were computed for three landslide geometries discussed above: two discrete landslides with volumes of 108 km^3 and 57 km^3 , respectively, and a composite of Slides 1 and 2 (volume= 165 km^3). The modeling indicates that wave height is most sensitive to landslide volume, and bottom friction has a larger effect on wave height than failure duration. Using reasonable parameters for slide duration (10 minutes) and bottom friction (2.5×10^{-3}), the predicted maximum wave heights near shore (water depth of 18 m) are 4.3, 3.0, and 5.8 m, for Slide 1, Slide 2, and the composite slide, respectively. Although it is difficult to predict the exact runup on shore, if the wave height persists to shore, tsunamis from Slide 1 and the composite slide will overtop the barrier islands in the area.

Chapter 11: Future Directions to Increase the State of Knowledge

The systematic evaluation of tsunami sources that may impact the U.S. Atlantic Coast and the Gulf of Mexico has revealed gaps in our knowledge and the need for additional directions of investigations to help in a quantitative assessment of the hazard.

Probability analysis

- (1) Quantitative size distribution analysis of landslides on the U.S. Atlantic margin is needed to help determine the probability for landslides of certain volume to occur.
- (2) Better estimates are needed of the temporal distribution of landslides throughout the past 10,000 yr based on both a global compilation and on the collection of new cores in the region to help in probability hazard assessment.
- (3) Establishment of quantitative relationships between landslide area and earthquake magnitudes along the Atlantic continental margin to help in probability hazard assessment.
- (4) Probability hazard assessment of earthquakes along the Atlantic continental margin and the northern Caribbean plate boundary.

Understanding specific hazards

- (1) Analysis of the geomorphology, stability, and mobility of a slide off New England, which may reveal different characteristics than the Currituck slide.
- (2) Hydrodynamic modeling of the potential tsunami hazard from a slide offshore New England.
- (3) Testing different rupture sources for the 1755 Lisbon and comparing them with transoceanic tsunami records.
- (4) Quantitative analysis of large failures and their mobility in the Gulf of Mexico and modeling their potential tsunami hazard.

Data gaps

- (1) The source areas of the landslide complexes along the Georges Bank and southern New England margin need to be adequately imaged with multibeam sonar. This region houses the largest landslide complexes, and understanding the depth of the source area, relief and nature of the headwall scarps, would help explain the causes of these failures, and the volume of material removed in each failure episode.
- (2) Careful age dating on cores recovered from within and adjacent to several of the landslides in order to constrain the timing of the submarine landslides.
- (3) Compilation of database of multibeam bathymetry for the Gulf of Mexico from available sources.
- (4) Mapping of the Campeche Bank, Mexico. Potential landslides along the Campeche Bank margin may pose equal or higher threat to the U.S. Gulf coast than proximal landslides, but little has been published about them.
- (5) Further age dating to refine the timing of the landslides derived from the Mississippi Canyon area. These dates are needed to determine if they are associated with meltwater floods discharged into the Gulf of Mexico during the early part of the Holocene or whether they were triggered by other processes at a later time.
- (6) Increase our knowledge on the characteristics of coastal aquifers and their influence on slope stability.